MODELING AND CONTROL OF AUTOMATIC TRANSMISSION WITH PLANETARY GEARS FOR SHIFT QUALITY

by

PATINYA SAMANUHUT

Presented to the Faculty of the Graduate School of
The University of Texas at Arlington in Partial Fulfillment
of the Requirements
for the Degree of

DOCTOR OF PHILOSOPHY

THE UNIVERSITY OF TEXAS AT ARLINGTON

August 2011

Copyright © by Patinya Samanuhut 2011

All Rights Reserved

To my mother Pavinee and my father Suwan

who made me who I am.

ACKNOWLEDGEMENTS

I would like to thank my supervising professor Dr. Atilla Dogan for constantly motivating and encouraging me, and also for his invaluable advice during the course of my doctoral studies. I wish to thank my academic advisors Dr. David Hullender, Dr. Robert L. Woods, Dr. Panayiotis S. Shiakolas, and Dr. Brian Huff for their interest in my research and for taking time to serve in my dissertation committee.

I would also like to extend my appreciation to Royal Thai Goverment for providing financial support for my doctoral studies.

I am grateful to all the teachers who taught me during the years I spent in school, first in Thailand and in the Unites States.

Finally, I would like to express my deep gratitude to my parents who have encouraged and inspired me and sponsored my undergraduate and graduate studies. I also thank several of my friends who have helped me throughout my career.

April 13, 2011

ABSTRACT

MODELING AND CONTROL OF AUTOMATIC TRANSMISSION
WITH PLANETARY GEARS
FOR SHIFT QUALITY

Patinya Samanuhut, Ph.D.

The University of Texas at Arlington, 2011

Supervising Professor: Atilla Dogan

Automatic transmission is a major component in a vehicle that transmits the power source from the engine to the drive wheels of the vehicle. To improve fuel economy, reduce emission and enhance driving performance, many researchers have made tremendous efforts on new technologies for automatic transmission with planetary gear sets. Among these new technologies, system dynamics and control methodologies are extremely important tools to realizing the fuel economy, emission and driving performance. This research effort focuses on the modeling and control of an automatic transmission with planetary gear sets. A Lagrange-based method is developed to derive the equations of motion of planetary gear sets and applied to the development of a mathematical model for the automatic transmission GM Hydramatic 440. The other transmission subsystems such as torque converter, hydraulic system, friction elements and final drive are modeled based on the methods available in the open literature. Additionally, simple engine and vehicle models are included as the main focus of the research is on the transmission. Since the model of friction used in

clutches and bands are very important for studying shift quality, an improved friction model based on three modes is used. The hydraulic system is given particular attention as it is the primary source of actuation in performing shifts. The second part of the research focuses on developing feedback control mechanisms for improving shift quality. The implementation of feedback control helps avoid tedious process of pressure profile calibration to obtain satisfactory shift quality. Further, it provides a level of robustness in shift quality against the variation of vehicle properties and the changes in driving condition. One nonlinear and one linear feedback control design methods are implemented. The sliding mode control method is the nonlinear control approach. The implementation of this controller requires the knowledge of the clutch/band torque, which is not practical to measure. To overcome this difficulty, various observer solutions are investigated. Despite the difficulty in its implementation, the sliding mode controller is still useful to obtain required speed profiles for a satisfactory shift quality. As the linear feedback controller, the PID control design is employed. For each up and down shifts, a PID controller is tuned to generate the applied friction profile for the friction element involved. For the calculation of the error signal as the input to each PID controller, the most relevant speed measurements are used for feedback and the desired speed command is determined based on the status of the rotating elements in the desired gear. Despite its simplicity and ease of its implementation, the speed-measurement-based PID controllers are shown to provide satisfactory shift quality in terms of reduced jerk experienced during the shift and shorter duration of the shift. Further, a Monte Carlos analysis has shown the robustness of the PID controller against the model variation, specifically variation of the parameters in friction model.

TABLE OF CONTENTS

LIST OF FIGURES

LIST OF TABLES

CHAPTER 1

INTRODUCTION

1.1 Introduction and Motivation

An automatic transmission has a long history along with the development of a car [1]. The main purpose of the transmission is to provide, for any situation, the best gear ratio for the vehicle. Different gear ratios have different speeds. They trade engine output speed for torque multiplication to match the engine output to the vehicle and operator requirements at the drive wheels of the vehicle. Transmission also provides reverse gear ratio that permits the driver to back the vehicle up. Further, transmission provides "park"(P) and "neutral"(N), which disconnect the engine from the drivetrain, prevent the drive wheels from turning (P) and allow the drive wheels to turn freely (N), respectively. The transmission allows the driver to stop the vehicle with engine running (idle) without disengaging the gears. In addition, automatic transmission offers manual ranges which allow the engine to be used to slow the vehicle down (engine braking) without using the service brakes when descending steep grades. In some cases, the manual ranges also allow the driver to select higher gear to initiate the motion of the vehicle on a slippery surface (snow, ice, etc.). Among other benefits are reduced driver's distraction, better fuel-consumption, better performance and more comfortable ride.

Maximum torque at driving wheels (along with the maximum traction force at tireprints) limits the maximum achievable acceleration of a vehicle. The maximum attainable power of an internal combustion engine is a function of the engine angular speed and is approximated by a third-order polynomial as shown in Fig. 1.1. Fig.

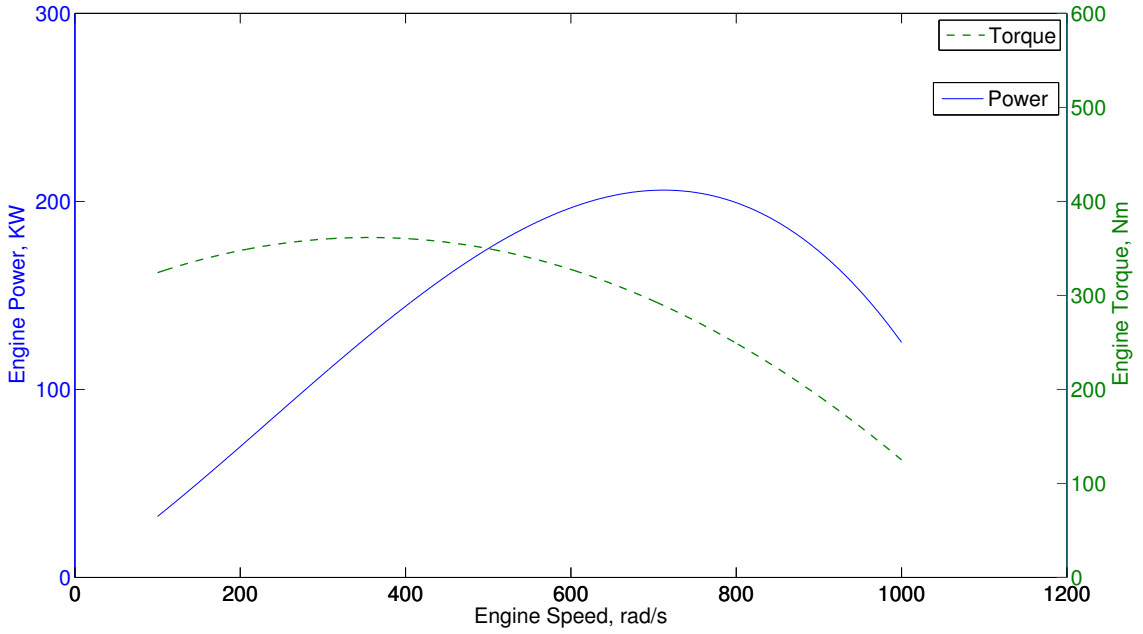

Figure 1.1. Real Engine Diagram.

1.1 indicates that the maximum attainable power increases to a peak and then starts dropping as the engine speed increases. The torque, $T = P/\omega$, also increases with engine angular speed but reaches a maximum point before the power peak. Thus, torque starts decreasing sooner than the power does. When the power starts decreasing, the torque is very far from its peak value.

Engine with the performance curve similar to Fig. 1.1 will provide the maximum torque at the drive wheels through a gear with the angular speed corresponding to the power peak. When the engine operates at the peak torque for a given drive wheel speed, the torque at the drive wheel will be the product of the the peak torque and the gear ratio required to go from the engine speed to the given drive wheel speed. By changing the gear ratio for the same drive wheel speed, the engine speed can be changed. If the gear ratio is selected such that the engine operates at the speed corresponding to the peak power, the torque at the drive wheels will be more than

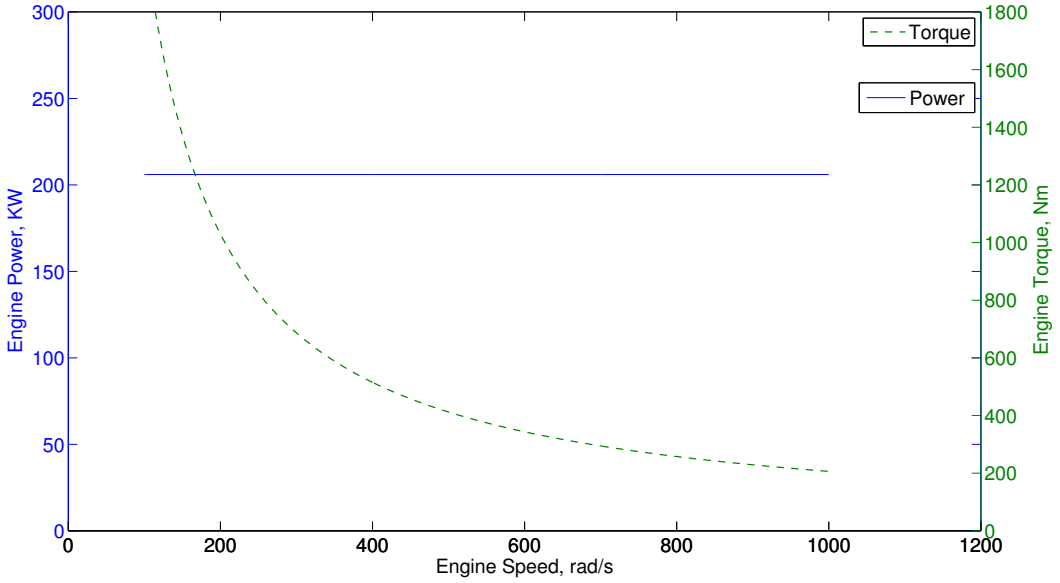

Figure 1.2. Ideal Engine Diagram.

the torque corresponding to the peak engine torque for the same drive wheel speed. For engines with performance curve similar to Fig. 1.1, any engine speed other than the peak power speed, at a given drive wheel speed, will provide a lower torque at the drive wheels.

An ideal engine is said to produce a constant power regardless of speed, as shown in Fig. 1.2. In vehicle dynamics, a gearbox is introduced to keep the engine running around the maximum power. In other words, the gearbox is used to keep the power of the engine constant at the peak value. Thus, the torque at the wheels should be similar to the torque of an ideal engine.

Figure 1.3 shows the wheel torque versus vehicle speed at six speeds (n_i refers to the i^{th} gear) [2]. Fig. 1.3 also presents the required wheel torque which includes wheel resistance, air drag, acceleration resistance and gradient resistance. Note that the envelop curve is similar to the torque curve of a constant power ideal engine.

Note that increasing the number of speed in a gearbox gives correspondingly better approximation to the ideal engine torque curve. Thus, with a transmission, the power potential of the engine can be better applied [1]. Theoretically, the best performance is obtained when the engine operates at its peak power. Thus, the automatic transmission is scheduled to shift gears to keep the engine speed close to the peak power speed. Other factors considered in shift scheduling are performance, fuel-efficient and driving comfort.

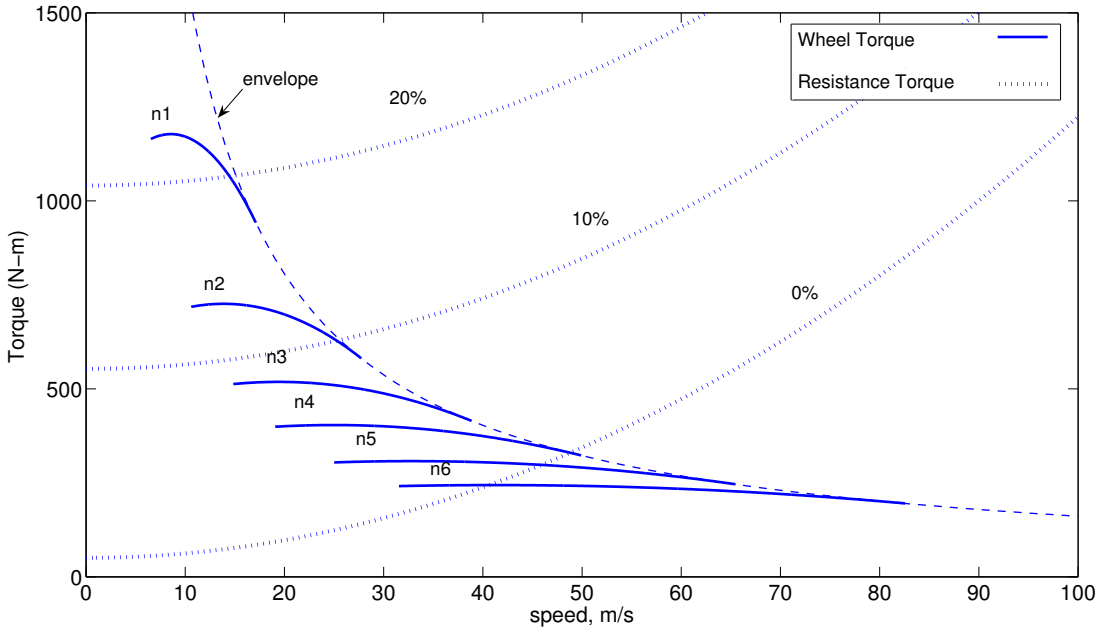

Figure 1.3. Traction Diagram.

1.1.1 Shift Schedule for Automatic Transmission

The main objective of a transmission is to keep the engine operating at an optimal condition in terms of engine speed for peak power as well as other factors such as fuel efficiency and driving comfort. This objective is formulated as a shift schedule to define when the transmission should change gear. The most common shift

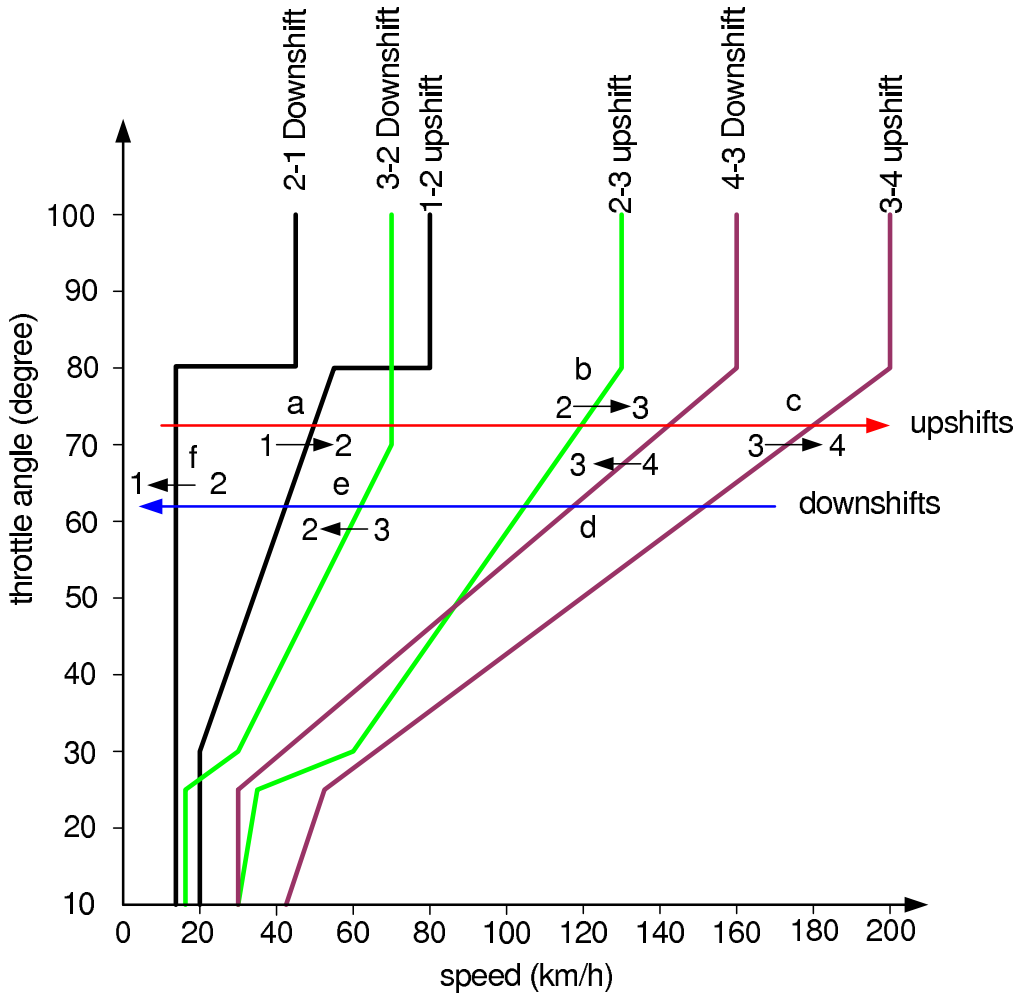

Figure 1.4. Shift Schedule.

scheduling is defined based on engine throttle position and engine or vehicle speed. Fig. 1.4 shows an example of a shift schedule chart for a four–speed transmission based on the throttle setting and vehicle speed. The chart consists of upshift and downshift curves that determines when to shift and which gear to shift to depending on the current gear, throttle setting and vehicle speed. The following is a sample scenario to demonstrate how the shift scheduling is done during the operation of a vehicle. The abc–line on the chart shows when the transmission is required to shift gears while the vehicle speed is increasing with a fixed throttle position. On the

other hand, with a different throttle setting, if the vehicle is slowing down, def–line demonstrates when the transmission should shift to a down gear. The focus of this research is not on the shift scheduling, but on the dynamics of a shift once the gear change command is issued based on the shift schedule chart.

1.1.2 Shift in Automatic Transmission by Planetary Gears

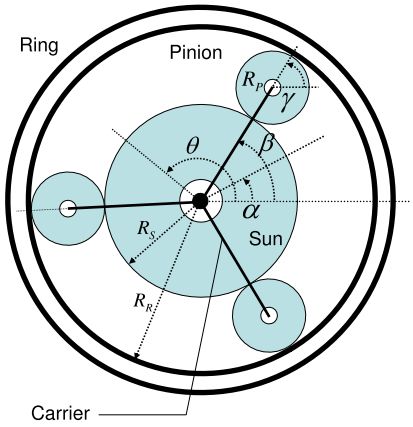

Figure 1.5. A single planetary gear set.

A conventional automatic transmission is composed of a torque converter, hydraulic system, planetary gear sets, friction elements and final drives. Planetary gear set is the most important component in an automatic transmission because it enables the variation of torque and speed ratios to match the vehicle and driver requirements. A planetary gear set, also known as epicyclic gear set, consists of a ring gear, a sun gear, a set of planet gears, and carrier as seen in Fig. 1.5 and is used to perform gear shifting. Different speed and torque ratios are easily achieved by alternating input, output, stationary components and holding elements. This is done by an electronic unit, engaging and/or disengaging various friction elements such as clutches and bands through the hydraulic system. The amount of hydraulic pressure applied

on a friction element determines the maximum amount of torque that the friction element can transmit, which is known as "the torque capacity of a friction element". To engage a friction element, its torque capacity should be increased, by increasing applied pressure on the friction element, more than the torque it needs to transmit in a given driving condition. The torque capacity is reduced to zero, by releasing its hydraulic pressure, to disengage a friction element.

1.1.3 Shift Quality

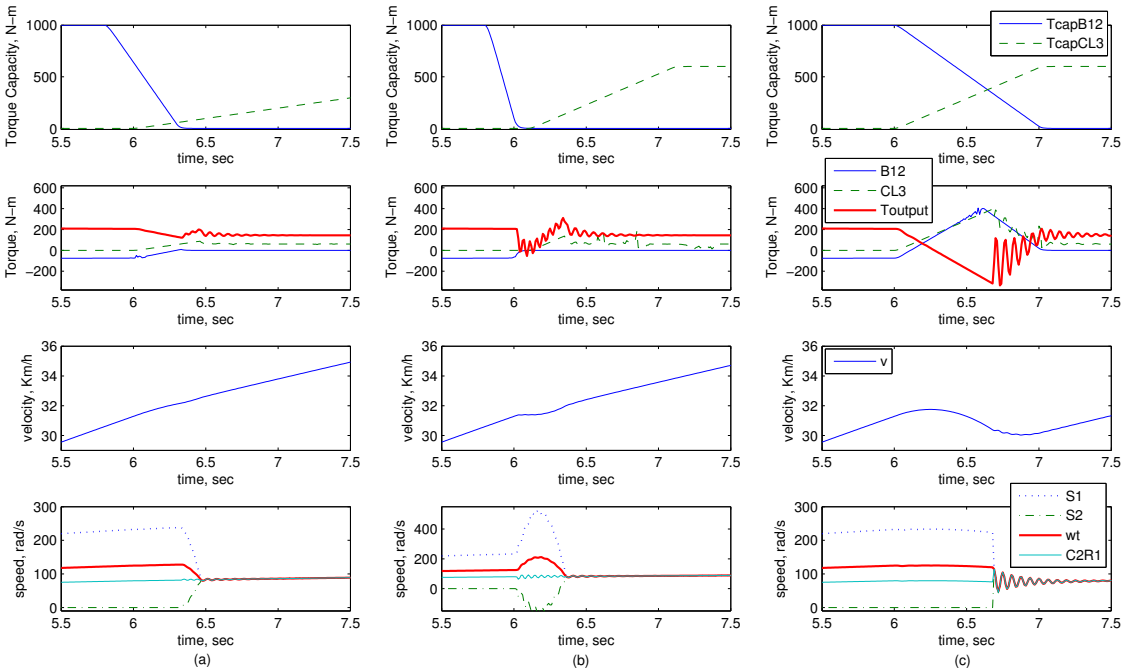

Figure 1.6. Shifting 2 to 3 (Note that: TcapB12 = torque capacity of band 12, TcapCL3 = torque capacity of clutch 3, B12 = applied torque at band 12 = applied torque at sun–2, CL3 = applied torque at clutch 3 = applied torque at sun–1, Toutput = Torque at output shaft before final drive, v = translational velocity of vehicle, S1 = angular velocity of sun–1, S2 = angular velocity of sun–2, wt = angular velocity of turbine, C2R1 = angular velocity of carrier–2 and ring–1).

The characteristics of a shift is determined by how the torque capacities are adjusted for the friction elements. Fig. 1.6 shows three different shift characteristics for the same shift, from 2^{nd} gear to 3^{rd} gear. In this particular transmission, band–12 (B12) should be released and clutch–3 (CL3) should be applied to conduct 2–3 shift. A shift that requires both an on–coming and off–going elements is called "a swap shift". The timing and the profiles of the torque capacity adjustment for B12 and CL3 are the defining factors for the shift characteristics. Fig. 1.6 shows two extreme shift characteristics and a "compromise" shift with the torque capacity profiles shown in Fig. 1.6.

Part (a) of Fig. 1.6 presents the "compromise" case with a good timing of the on-coming element (the clutch being applied) and the off-going element (the band being released). The shift is initiated by lowering the capacity of B12 and, after a short time, raising the capacity of CL3, as shown in the first plot of column (a) of Fig. 1.6. The increasing torque capacity of CL3 while B12 still has some torque capacity splits the torque transmission between CL3 and B12. This can be seen in the second plot of column (a) of Fig. 1.6. As more torque goes through CL3, less torque is carried by B12. Note that during this time, the output torque decreases. At the time when the torque capacity of B12 drops to zero and B12 no longer carries torque, CL3 starts carrying all the torque and the decrease in the output torque stops. This signifies the end of the "torque transfer phase" and the beginning of the "ratio change phase", or "inertia phase". During the inertia phase, the gear ratio is between the 2^{nd} gear and the 3^{rd} gear ratios. Since B12, which connects sun–2 to the transmission case, is fully released, sun–2 starts rotating. CL3 is used to connect sun–1 to the turbine shaft. As CL3 is engaged, the clutch slips until sun–1 and the turbine have the same speed. Once Sun–1 and the turbine rotate (zero slip in CL3) together with the sun–2 and they all have the same speed as carrier–2 (connected to the output shaft), the 3^{rd} gear

ratio (= 1) is obtained and the shift is completed (see the last plot of part (a) of Fig. 1.6). Then, the torque carried by CL3 is only the amount to prevent slipping. Once the shift is completed, the capacity on the clutch can be increased with no effect on the speeds or the torques. Note that the output torque drop stops at the beginning of the inertia phase and the output torque shows a transient in the inertia phase.

Part (b) of Fig. 1.6 presents 2–3 shift with a different B12 and CL3 torque capacity profiles. The torque capacity of B12 is reduced rapidly to zero before raising the torque capacity in CL3. This results in a very short torque transfer phase. In fact, since CL3 does not start carrying torque when B12 is fully released, no torque is transmitted from the turbine to the output shaft in the meantime, this causes the turbine speed and, as a result, the sun speeds to "flare up". Note that from the vehicle velocity plot that the vehicle acceleration stops during the "flare". Further, the output torque demonstrates a longer transient with longer oscillation relative to the "compromise" case. A longer inertia phase also results in a longer time of clutch slipping.

In part (c) of Fig. 1.6, another set of torque capacity profiles is used for 2–3 shift. In this case, CL3 torque capacity is started to raise while B12 still has significant torque capacity. By applying CL3 while CL2 is on, the whole planetary gear set becomes a rigid shaft. Since B12 still holds sun–2 stationary, CL3 acts like a brake for the vehicle, which can be clearly seen from vehicle velocity plot in part (c) as the vehicle speed starts decreasing. The braking–effect, called "tie-up", can also be seen in output torque dropping into the negative range. This continues until the torque capacity of B12 drops low enough for B12 to start slipping and thus for sun–2 to start spinning. After this point, the inertia phase lasts very short and turbine speed becomes equal to the output shaft (C2R1) speed as the third gear ratio is 1. Further, the vehicle starts accelerating again. However, even after the shift

is completed, a very long transient with large oscillations in the output torque and speed, called "jerking", is experienced.

These three examples, "flare", "tie-up" and "compromise" shifts, manifest the importance of the torque capacity or applied pressure profiles in shift quality. Better shift characteristics or better "shift quality" is desired for, first of all, driver and passenger comfort and easier driving conditions, especially in urban driving with frequent shifting. Shift quality is also sought for fuel efficiency, improved drivability and performance (maintained acceleration). Further, better shift quality leads to longer transmission and powertrain life and less maintenance cost.

The most common method of assessing shift quality is to rely on trained drivers to make a subjective judgement. Trained drivers and "calibrators", who calibrate torque capacity or applied pressure profiles to improve shift quality, rely on their experience and noise–vibration that they hear–sense during shifts. However, feedback control approaches for improving shift quality have to have measurable quantities. Methods are developed to provide objective description of shift characteristics [3, 4, 5]. Objective methods for measuring shift quality can rely on various characteristic such as torque at the output gear/shaft, acceleration or the derivative of acceleration of the output gear, or the shift duration, the time between the current gear ratio and the desired gear ratio. The torque at the output gear should have short transient with small amplitude during shifts. The acceleration of the output gear should also have small transient. Sudden change in output acceleration indicates poor shift quality. The derivative of acceleration is also used to measure shift quality.

1.2 Problem Statement

This research is aimed at investigating feasibility of robust feedback control laws that can lead to better shift quality. The emphasis of the control laws will be on

controlling the torque capacities or applied pressure of the friction elements involved in a given shift based on various feedback control signals. For the development, implementation and evaluation of feedback control laws, a mathematical model of a representative vehicle with the emphasis on planetary gear set should be developed. Further, the mathematical model should be implemented in a simulation environment for easy and accurate simulation of system response with the feedback control laws employed. Therefore, the objectives of this research effort are listed as follow:

(i) Development of dynamic models of transmission and other subsystems of a representative vehicle with a fidelity that the dynamic behavior of gear shifts can be described.

(ii) Development of a simulation environment that can be used for the analysis of dynamic system response in shift.

(iii) Development of quantitative measures that can describe "shift quality".

(iv) Definition of "good shift quality" in terms of quantitative measures.

(v) Development of feedback control laws for gear shift that can result in better shift quality.

(vi) Evaluation of feedback controllers by simulation of closed–loop system response in various test conditions.

1.3 Research Contributions

The following list summaries the contributions of this research.

- Development of a mathematical model of a planetary gear sets used in an automatic transmission.
  - Using Langrange's Method to derive the dynamics equations of planetary gear sets.

  - Develop the mathematical models of automatic transmissions for simulation of shift behaviors, including pinion effects.
  - A simple set of equations that are valid of any gear or shift.
  - A mathematical tool to easily determine steady-state speed relations of rotating elements in a given gear.
- Development of a hydraulic actuation system used in an automatic transmission.
- Development of friction elements model in an automatic transmission to increase the model's fidelity.
- Development of the control methodologies used to control gear shifting to achieve better shift quality.
- Evaluation of the control methodologies.

1.4 Organization of the Dissertation

A literature review of powertrain modeling including engine, transmission, and vehicle model is presented in Chapter 2. The planetary gear sets modeling is specially focused, since it is the key to understand the shift dynamics. The survey of control techniques implemented in a conventional automatic transmission is discussed and compared to find the control techniques that is suitable and available to improve the shift quality. A review of observers is also discussed to reconstruct the inaccessible variables in the automatic transmission.

In Chapter 3, the detailed powertrain model including engine, torque converter,final drive and vehicle mode is presented. The subsystems that are connected to the transmission have to be studied and developed properly to be able to obtain the shift dynamics.

In Chapter 4, the transmission modeling is described in details. The planetary gear sets is modeled by using Lagrange method. The equation of motion of the plan-

etary gear sets is presented. The hydraulic actuation system is modeled to determine the limitation of hydraulic actuation system to the shift dynamics. Further, new and more capable actuation mechanism for applying pressure on clutches and bands are presented. The friction elements are modeled by various friction models. The most suitable for the dynamics and control in the automatic transmission is selected and discussed.

In Chapter 5, the open–loop simulation results are presented. The powertrain model with classical friction model excluding hydraulic system is first discussed. Second, the powertrain model including the stiff drive shaft, hydraulic system and Woods static and dynamic friction model is discussed. Finally, the powertrain model including the non–stiff drive shaft, hydraulic system and Woods static and dynamic friction model is discussed.

In Chapter 6, the control objectives for good shift quality are discussed. The implementation of PID controllers and the evaluation of closed–loop simulations of various shifts are discussed. The PID controller is evaluated to determine its performance robustness against variation in friction characteristics. The robustness evaluation is performed using the Monte Carlo simulations and the results are presented as histograms. As a nonlinear control design method, sliding mode control design is presented. Since the sliding mode controller requires various variables that cannot be measured, various observer design methods are discussed.

Chapter 7 presents the summary and conclusion of the research work and discusses various future research directions.

CHAPTER 2

LITERATURE REVIEWS

This literature review has focused on modeling and control of automotive transmission with emphasis on planetary gear sets. The papers related to modeling methods are studied and compared to understand the prior work that have been done in this area. In addition to transmission, other subsystems in powertrain and vehicle models are also investigated. Other subsystems and vehicle dynamics models are needed for developing a simulation environment to study shift quality. The modeling techniques of the planetary gear sets are categorized as kinematics-based and dynamics-based, which are explained below. The friction model is studied and implemented to the clutch/band model. The friction plays a major role in the gear shift. With accurate friction models, the transmission model fidelity can be significantly improved. This gives us an insight into understanding shift behaviors and enables us to design and implement various control laws. The control techniques that are implemented to improve shift quality are proposed by many researchers. The control techniques are grouped into open–loop and closed–loop according to their dependency on feedback signals. Torque estimation is also investigated as one of the controllers investigated requires torque estimation.

2.1 Kinematics-Based Planetary Gear Modeling

1. Energy method [6] : This method utilizes the conservative energy law, where energy can be transferred from one system to other system. Then, a simple power flow equation within a planetary gear set is established in terms of torque

and velocity. Also, a gear geometry relationship is combined with the power flow equation. The results of the analysis are given in the formulas governing the speed and torque of the components in the planetary gear sets.

2. Lever analogy method [7] : In this method, an entire transmission is represented by a single vertical lever. The input, output and reaction torques are represented by horizontal forces on the lever, and the lever motion, relative to the reaction point, represents rotational velocities. The lever proportions are determined by the numbers of teeth (or the radii) on the sun and annulus.
3. Relative velocity method [8, 9] : It is based on simple principles of relative motion, the observation that a carrier can have four possible roles in a gear train, and concepts of mixed and fixed gear ratio. The velocities of gears relative to the carrier can be expressed as function of gear ratios. The derivation of the equations finally gives absolute velocity of all components in the planetary gear set.
4. Signal flow graph [10, 11] : By assuming the angular velocities as a collection of nodes, a full analogy between a planetary gear set and signal flow graph is established. This method considers a planetary gear set as a system processing inputs, outputs, and system transfer function. The system is then analyzed by means of block diagrams or flow graphs. Applying the Mason's rule, the governing equation of the dynamics of a planetary gear set is developed.
5. Tabular method [12] : The method provides computation of speeds and torques at each gear position. This is because gear geometry relations of its components are known. Utilizing the relations, formulas at specific conditions in the planetary gear set are formulated. This method, however, can not reveal power flow and action-reaction of each component in a planetary gear set.

6. Vector loop method [13, 14] : The equation of motion derived by this approach comes from a straightforward process of generating a sequence of vectors which sum to zero around a closed path. The velocity and acceleration are determined by differentiating the terms in the vector equations.
7. Velocity diagram method or graphical method [15] : This method presents the speed and torque relations of components in a planetary gear set based on the principle used for velocity analysis of other mechanism. This is by constructing the velocity diagram that exposes all related velocities of a planetary gear set. The formulas for a planetary gear set then are established by analyzing the velocity diagram. Since the method has the advantage of visualizing the effect of geometric variation on the kinematics of the planetary gear set, it could be used by a designer at an early stage of design.

2.2 Dynamics-Based Planetary Gear Modeling

1. Bond graph [3, 4, 16, 17] : This method analyzes a system by considering interactions between its components via ports having flow and effort variables as input-output. It helps visualize the whole system power flow as the subsystems are interacting. By using bond graph, a dynamic system of a planetary gear set that is analyzed with Newton's Law is established so that the flow variable (speed) and the effort variable (torque) interconnect to each component in the system via the input-output ports. In this way, the governing equations for the system are formed systematically.
2. Kinematics and static force analysis [5, 18, 19, 20, 21, 22, 23, 24, 25, 26, 27] : Kinematic analysis of a planetary gear train is established by applying Graph Theory. Static force and torque analysis is performed based on Newton's Law while analyzing the components in free-body diagram. Within free-body

diagram, the interaction of each component in a system can be visualized. It is a straightforward method in considering a multibody dynamics system.

3. Lagrange's method [28, 29, 30, 31, 32] : This method uses energy-based approaches to the derivation of the governing equations of planetary gears. If the focus is not on the structural mechanics of gears, then Lagrange methods are more appealing as the equations of motion can be derived without computing the reaction/contact forces and torques. Ref. [29] studies the dynamics of a robot wrist driven by motors. It uses the Lagrange method to derive the equations of motion for the gear-mechanism as well as the constraint forces and torques. In Ref. [30], the planetary gear sets in a transmission is analyzed by Lagrange equations under certain constraints. In this study, the shift dynamics is not studied while the transmission model along with the other subsystems is used to analyze vehicle dynamics. Ref. [31] starts with the general Lagrange equation, but derives only the speed relations. Ref. [32] applies the Lagrange method to derive torsional dynamic models to predict free vibration characteristics; no attempt is made for shift behavior or control. This research effort also uses the Lagrange method in deriving the dynamics equations of planetary gear sets [28]. In derivation, the assumption of ideal planetary gear is made. That is, no backlash occurs between gear meshing, gears and shafts are rigid, and friction is negligible. In this case, the Lagrange method is the most suitable because it provides a systematic and direct approach to derive the equations in terms of generalized coordinates and applied torques without dealing with vectors or constraint forces and torques. This method can easily take into consideration all rotating elements including pinions and their inertias in the derivation of the equations. This systematic approach can be easily applied to planetary gears of any configuration. The derived equations are used to study transient shift

behavior including the effects of the pinions and the torque capacity build up or release in friction elements. There is no need to switch from a set of equations to another when shifting gear ratio as the equations derived are valid in all gears and shifts.

2.3 Powertrain Modeling

Other subsystems in powertrain are crucial to obtaining high fidelity simulations for investigating shift quality. These subsystems are engine, torque converter, friction element, hydraulic system, final drive and vehicle model.

2.3.1 Engine Model

The engine models which is suitable for control design have been studied by many researchers. This type of the engine model is used in [3, 4, 5, 33], which also study shift dynamics for improving shift quality. Refs. [4, 33] works on improving shift quality by controlling the shift in the transmission. Ref. [5] controls both transmission and engine, while more emphasis is given to transmission. Ref. [3] tries to control both engine and transmission to improve shift quality as well as fuel consumption. Results presented in these references demonstrate that this engine model is adequate for capturing transient behaviors during all shifts as well as steady–state behavior.

The engine model used in Refs. [3, 4, 5, 33] is originated from Refs. [34, 35, 36, 37, 38], which study engine modeling and control. This model is a continuous time, three states engine model for a four–stroke engine. There are three states in the engine model – the mass of air in the intake manifold, the engine speed, and the fuel flow rate. Additionally, there are two transport delays in the model due to the discrete nature in a four–stroke engine – the intake–to–torque production delay and the spark–to–torque production delay. These engine models approximate all rotating

and oscillating masses inside the engine as a single engine mass with a polar moment of inertia [35]. Ref. [21] designs observer to estimate states of the whole powertrain model and also uses the same "single rotating mass" concept for engine modeling.

The mathematical model of an engine has long been developed for application to dynamic engine modeling and control [39, 34, 35, 36, 37, 38, 40, 41]. Physical phenomena that occur in an engine have been studied for many years. There are two main approaches to engine modeling [39, 40]. First one describes the combustion process, chemical reaction, pollution, exothermicity and phenomena involving the combustion in an engine [42, 43]. These models are rather complex and require issues related to heat transfer, thermodynamics, fluid mechanics and chemistry. Second one is for more control development oriented models. The models represent input-output behavior of the engine system with reasonable precision with low computational complexity, and includes, explicitly, all relevant transient (dynamics) effects. The engine model can be just, in some cases, a torque generation map whereas, in other cases, capture dynamics of the engine. Typically, in the latter approach, the engine models are represented by systems of nonlinear differential equations based on some physical principles. Further, data from engine experiments are used to identify the key parameters of these models. The engine models used in Refs. [4, 3, 21, 5, 33, 34, 35, 36, 37, 38] and adopted in this research are developed for control develop and design. These models are flexible and adjustable to different engines and operations without significant modification. Further, the engine models are validated with measurements taken on the vehicle of interest from wide-open throttle, standing start experiments.

2.3.2 Torque Converter

A torque converter generally consists of a pump (driving member or input member), a turbine (driven member or output member) and a stator (reaction member).

The converter pump is attached to the engine and turns at the same speed as the engine speed. The pump works as a centrifugal pump. It induces oil flow and transfers the engine torque/speed to the turbine. The detailed operational principles can be found in Refs [44, 45, 46]. The model of torque converter used in this study is adopted from Refs. [3, 4, 5, 44]. The model is a quadratic, regression-fit data from experiment to represent the static characteristics of a torque converter. The model has "torque converter/multiplier" and "fluid coupling" modes depending on engine or pump speed and turbine speed.

2.3.3 Friction Element

Clutches and bands in an automatic transmission are commonly represented with classical friction models. The friction is proportional to the normal force to the contact surfaces of two bodies. While this represents the ideal friction model, it gives rise to discontinuity problem in numerical solution in zero velocity region. To eliminate this problem, the steep curve in the neighborhood of zero velocity region is introduced. Additionally outside the small velocity neighborhood the friction is modeled as a function of the velocity, which is called "Stribeck effect" [47]. However, this model still has drawbacks including numerical simulation problem and physical fault representation [48], [49], [50].

There are many models developed to handle the problems in the classical friction model. These approaches known as dynamic friction model are studied and developed in various references including [47], [49], [51], [52], [53]. Dahl [51] developed his friction model from stress–strain characteristics in solid mechanics. The connection between two surfaces is modeled as spring and damper. Therefore, in this model, the friction force is proportional to displacement. An extension of Dahl friction model are Lugre and Bliman–Sorin friction models [54]. These models represent

many characteristics of friction phenomena. However, the models are quite difficult to apply to a complicated dynamic system such as in an automatic transmission. In [49], the bristle model and reset integrator model are presented. The models capture the behavior of the friction in microscopic level where the contact points between two surfaces are viewed as bonds between flexible bristles. As surfaces move, the strains in the bonds increase and the bristle acts as springs, which give rise to the friction force. Due to complexity, the bristle model consumes a lot of simulation time while the reset integrator model has a discontinuous function in the model that requires numerical algorithm to be carried carefully [55, 56].

2.3.4 Hydraulic System

An hydraulic system is an important component in gear shifting operation in an automatic transmission. The hydraulic system initiates the shifting operation by supplying pressure on the clutch surface where friction torque is generated. Then, the torque from the input shaft can be transmitted to the gear through the clutch. The hydraulic system in an automatic transmission consists of various components such as hydraulic pump, accumulators, valves and pressure regulators. This study focuses on a subsystem that is directly involved during shifting gears in an automatic transmission. Refs. [5] and [33] study the hydraulic system extensively in detail. However, the hydraulic system is complicated. Thus, for control purpose, a second order system is used to represent the hydraulic system without losing its characteristics. The hydraulic system in GM Hydramatic 440, used in this research, is similar to the hydraulic system in Refs. [5, 57, 58]. The hydraulic system consists of two main parts, “hydraulic supply” and “hydraulic load”. Hydraulic supply, consisting of a variable–displacement vane pump, a pressure regulator and control circuit, regulates the line pressure in the automatic transmission. The hydraulic load is either

leakage during fixed ratio condition or a combination of leakage, compliance and fluid resistance during shifting gear. The hydraulic load part consists of clutch actuators, accumulators and shift valve. This physics-based hydraulic model can be used to represent the dynamics of hydraulic system during fixed gear ratio and shifting gear.

In Ref. [33], more detailed models involved during shifting gear are studied including pressure regulation system, pressure control valve, solenoid valve and clutch and accumulator. The analysis in Ref. [33] is started with a physics–based model which is used for the purpose of design rather than control analysis. The detailed model, which is highly nonlinear and complex, is then simplified for the purpose of control design. In Ref. [33], the model includes a solenoid valve that operates under PWM signal. In PWM solenoid valve, the pressure is regulated by controlling duty cycle. There is another type of shift valve that is controlled by variable force solenoid (VFS). This types of valve directly attenuates the pressure more precisely than the PWM solenoid valve, since the pressure is a function of current. Ref. [59] developed a VFS model suitable for the purpose of control design. The model is simple, yet efficient enough to capture the essential dynamics.

From Refs. [57, 5, 58, 33], it is evident that the hydraulic system directly effects shift quality, since the friction torque at the clutch and bands are a function of the pressure generated by the hydraulic system. Thus, it is essential to realize the required pressure profile. During a fixed gear ratio, the assumption is that the transmission line pressure and pressure in clutch cavity are maintained constant. This means that the pressure control regulation of the hydraulic system can be neglected in this study. Thus, the hydraulic system in this study focuses on the components that involve with gear shifting operation. To obtain the shift characteristics, the major components must be included in the hydraulic model which are shift valve, supply transmission line pressure and clutch system. The solenoid valve is excluded from the hydraulic

model since the solenoid valve operates with high frequency comparing to the overall powertrain frequency. Excluding the solenoid valve from the hydraulic model reduces the degree of complexity due to the solenoid valve model. Currently automobile technology moves toward eliminating one-way clutches. The new technologies are in search for the clutch–to–clutch shifting which is achievable by using devices that handle the desired pressure profile directly [60].

2.3.5 Final Drive and Vehicle Model

Final drive gear is modeled as a simple torque/speed converter. Thus, the mathematical model of the final drive gear is a simple input/output proportional equation. The vehicle model used in this study considers longitudinal dynamics of the vehicle as a rotating shaft with a torsional spring constant and a lumped inertia. References [3, 4, 5, 33] also use this simplified vehicle model in studying shift dynamics and shift quality. With this type of vehicle model, power transferred from engine through transmission and finally from tires to road is analyzed in the form of torque and angular speed.

2.4 Description of Shift Quality

A poor quality shift appears in the form of jerking, inconsistent acceleration and output oscillation. In the literature, various metrics are reported that define and quantify shift quality. Such metrics are used to evaluate the performance of various open and closed loop control approaches to improving shift quality. The most common ones are listed below.

- Shift Duration [3, 5]: Shift duration is defined as the time from the start to the end of a shift process. A shift that takes a long time results in damages to the transmission, specifically to the friction elements of the transmission. Further,

a shift with long duration leads to loss of power transmission to the vehicle wheels. On the other hand, if the shift duration is too short, the shift may result in large overshoot and oscillation.

- Oncoming Clutch/Band Torque [3, 5]: Practically, it is difficult to measure clutch/band torque. However, this can be used to measure shift quality. Torque at the clutch/band are related to the fore/aft motion of the vehicle, since it is the torque that is transmitted to the planetary gear sets and finally to the driven wheel. Thus, the torque characteristic effects the driver and passenger comfort. The oscillation and overshoot in oncoming clutch/band torque are used to measure the shift quality.
- Output Torque at Planetary Gear Sets [3, 5]: Driver and passenger comfort during a shift depends on fluctuation of vehicle fore/aft motion. Torque is transmitted from the output gear of the planetary gear sets to the driven wheel, which drives the vehicle forward. Thus, it is directly related to with fore/aft motion. Maximum overshoot and oscillation in the torque at the output gear of the planetary gear sets are indications for the quality of a shift.
- Acceleration [3, 5]: The driver and passenger feel a sudden change of gear from the vehicle acceleration. Fore/aft acceleration is correlated with output torque of the planetary gear sets. It has been generally agreed that a shift quality metric should be a function of the fluctuation of vehicle fore/aft motion during a shift such as maximum overshoot and oscillation in the vehicle acceleration.
- Derivative of Acceleration (jerk) [3, 5]: The rate of change of acceleration with time has been used to evaluate shift quality. A good shift has small oscillation and overshoot in the jerk of the vehicle.
- Maximum Average Power (MAP) [3, 5, 61]: The power level of a shift is calculated from an algorithm called “Maximum Average Power” (MAP). It is an

objective measure directly related to the human perception of gear shift. A good shift has a low MAP, which implies comfortable ride. MAP is formulated as

$$MAP = max(10 \int_{t_{o-0.1}}^{t_o} [a - a_{mean}]^2 dt), 0 < t_o \leq T \tag{2.1}$$

where a is acceleration, a_{mean} is the mean acceleration during shift event, t_o is time of observation and T is shift duration.

- Vibration Dose Value (VDV) [62]: A particular function, the vibration dose value (VDV), has been used to quantify human reaction to numerous types of vibration in many fields including harsh/noise in automotive industrial. When applied to vehicle fore/aft acceleration during a transmission shift, this function produces a single output number proportional to the driver's sensation of the severity of the shift, regardless of the character of the acceleration signal. The VDV is calculated from a properly filtered vehicle acceleration signal as

$$VDV = \sqrt[4]{\int_{Ts}^{Tf} a(t)^4 dt}; \tag{2.2}$$

2.5 Control Techniques

In recent years, there are many attempts for improving shift quality either by open-loop or closed-loop control. Conventionally, automatic transmissions employ open–loop control to perform gear shift. Open–loop control requires tedious process of pressure profile calibration to obtain satisfactory shift quality. Further, open–loop control is susceptible to variation of vehicle properties and changes in driving conditions. Such issues with open–loop control motivates the investigation of the feasibility of feedback control in performing gear shifts.

2.5.1 Open-Loop Control

In a conventional automatic transmission, the transmission controller is pre–programmed by a tedious and complicated calibration procedure. The controller usually has the ability to perform gear shift when the desired shift point meets conditions pre–programmed in the transmission control module (TCM). The desire clutch pressure profile is generated by the hydraulic actuation system. The clutch pressure profile for each shift is pre–programmed in TCM. The open–loop controller in TCM is expected to perform well during the entire life of the transmission despite encountering various conditions. The fundamentals of passenger car automatic transmission can be found in Ref. [63]. The characteristics of torque and speed during gear shift with a specific pressure profile is analyzed. This pressure profile is commonly implemented in the conventional automatic transmission equipped with planetary gears.

The gear shift process as described in [63] is accomplished in open–loop manner. At the beginning of gear shift when conditions meet the preset shift point, the pre–programmed pressure profile commands are executed to generate a build up clutch pressure at the oncoming clutch while reducing offgoing clutch pressure. During gear shift, there are two phases, torque phase and inertia phase. In each phases, the pressure has to be properly regulated in a timely manner to maintain good shift quality.

In Ref. [64], the shift quality is accomplished by preset duty ratio map for the regulator valve to adjust the line pressure related to throttle position. A detailed description of the complete algorithms for power–on upshifts and downshifts is given in Refs. [65] and [66]. Variation in an automatic transmission such as clutch/band and hydraulic actuator, for instance, can lead to failure in gear shift operation. Optimal open-loop control and robustness analysis of the clutch-to-clutch shift in automatic transmission are studied in Ref. [67]. However, there are many criteria needed to ob-

tain the robust open–loop controller. Closed–loop control technique has an advantage over this problem, since it uses the feedback signal to compensate the error that occurs during gear shift. Therefore, it can yield the consistent performance during gear shift. Further, the transmission calibration procedure can be reduced significantly due to computer simulation and later field tested in realistic driving conditions.

2.5.2 Closed-Loop Control

The closed–loop control techniques can be used to overcome the difficulties with open–loop control such as those discussed above and to obtain consistent gear shift performance. During gear shift, there are many possible combinations of on/off clutches and bands involved such as ones called "clutch–to–clutch" and "overrunning clutch–to–clutch". In overrunning clutch–to–clutch, the oncoming clutch is controlled while the offgoing clutch which is one–way clutch or freewheeler assists gear shift process to obtain a satisfactory gear shift. Since there is only one clutch to be controlled, the process is less complicated but, on the other hand, there is no direct control on the engagement and the disengagement of the one–way clutch. Satisfactory execution of clutch–to–clutch control or swap shift is more challenging. In clutch–to–clutch control or swap shift, there is no freewheeler assisted shifting. The controller must be able to release offgoing clutch while engaging oncoming clutch in a compromising fashion. Any mismatch between the offgoing clutch and oncoming clutch can lead to "flare–up" or "tie–up". Flare–up happens when the offgoing clutch is released too early while the oncoming clutch is not engaged in time to carry the loads from the offgoing clutch. Tie–up happens when the offgoing clutch is released too late while the oncoming clutch has been engaged already. In the past decade, an automatic transmission relies on an acceleration detection to detect clutch pressure fill which prevents "tie–up" and "flare–up". Closed–loop control is executed after the clutch

pressure are detected [68]. Controller uses slip speed detection to ramp up the clutch pressure until it finishes gear shift by locking up the clutch. Thus, detecting the clutch pressure fill time is a key to the good shift quality.

In Ref. [68], the adaptive control strategies for power–on upshifts and downshifts are developed and tested in both simulation and vehicle. The adaptive control system is capable of compensating for the variation in the transmission. Adaptive control system focuses on the key parameters that influence the transmission over the life of the transmission. In the case of upshifts, oncoming clutch–fill time, oncoming and offgoing clutch pressures are adapted from one shift to the next, which will converge to a nominal shift in 3-5 shifts. In downshifts, only the clutch pressures are adapted, which will converge to a nominal shift in 1-2 shifts. Detecting the clutch fill is determined by the acceleration of input and output shafts. A Kalman filter technique is used to estimate the acceleration of the input and output shafts which are calculated from the measured speeds [69].

Reference [70] discusses the employment of computer simulation in the development of a transmission. Its hydraulic system has feedback control where the clutch pressure is controlled according to the rate of acceleration and compensated for dispersion to applied pressure, engine torque and the coefficient of friction of the clutch. The engine torque is also reduced by retarding ignition timing when the inertia phase is reached to obtain a smooth shift.

An example of closed-loop control of speed ratio is described in Ref. [71] along with computer control technique for a powertrain. The shift is controlled by electronic transmission control (ETC) through a clutch pressure modulation which is controlled via a PWM solenoid. The clutch controls the torque converter turbine speed such that the speed ratio is satisfied. The input of the PID controller is the difference

between the desired turbine speed and the feedback turbine speed. The performance of the controller is verified by various experiments.

In Ref. [5], a model-based control design is used for a 1-2 upshift and neutral idle control. The shift hydraulic system is controlled by a pulse–width–modulated (PWM) solenoid valve to perform gear shift. A simple linear second order model for this valve is developed and used to achieve good shift quality.

A new clutch–to–clutch shift control is reported in Ref. [72]. The new technology uses a hydraulic washout technique to control the synchronization of the oncoming and offgoing clutches. Regardless of detecting the end of the fill phase at the oncoming clutch as traditionally done, there are other ways to control gear shift.

A nonlinear sliding mode control technique for clutch–to–clutch is reported in Refs. [3]. The design controller is implemented to oncoming and offgoing clutch to be able to achieve a good shift quality. However, an ideal actuator is assumed. Thus, to be more realistic, a mathematical model representing the hydraulic actuation system must be developed to be able to implement the sliding mode controllers

In Ref. [73], using acceleration and an input/output speed ratio of the transmission, the controller can operate clutch–to–clutch shift with smooth shift quality and robustness. Ref. [73] also presents methods to estimate torque and calculate acceleration. The torque estimation uses the torque converter characteristics and an existing speed sensor. Clutch–to–clutch shift control has two parts, learning control and robust control. The learning control is applied to the engagement of the clutch in the upshift and the disengagement of the clutch in the downshift. The estimated torque is required to follow the target value. The H–∞ control theory is employed to restrain the torque fluctuation when shift characteristic changes in oil temperature range from 30 to 120 °C.

Reference [74] reports the development of a new very compact five-speed automatic transmission. The control during gear shift has three stages including servo activating control period, torque phase control period and inertia phase control period. In servo activating control period, the gear shift lag time due to hydraulic actuation system is reduced by detecting oil temperature and acceleration of input shafts. In the torque phase control period, the oncoming clutch pressure is determined based on transmission input torque calculated by the TCM using the engine torque signal input from the engine through CAN (Control Area Network) communication. In the inertia phase control period, the revolution change of oncoming element is detected and used to execute the controller while at the beginning of the inertia phase the engine torque is reduced to have a good smooth shift.

Reference [75] reports the development of a newer transmission with enhanced capabilities as compared to its predecessor [74]. Gear shift procedure is directly controlled by linear solenoids and compensation is executed using feedback control and self–learning control.

2.5.3 Integrated Powertrain Control

There are various simple methods to control the whole powertrain, instead of the engine and transmission separately. While it is more complicated, it can potentially provide better shift quality. Refs. [3] and [68] show that spark ignition retarding at the engine helps reduce the drop and high overshoot in the output torque and acceleration of the output shaft. As reported in [3] and [4], the sliding mode controller is capable of controlling the engine and the clutch pressure so that the gear shift process can be achieved smoothly. Many transmissions in the market control the engine during the gear shift by retarding the ignition timing [70, 74, 75, 76]. In Ref. [77], the anti-jerk control is developed using model-based control concepts. The controller designed by

root locus gives corrected torque. When it is compared to the assigned torque and feeded to the engine, the oscillation at the drive shafts are significantly reduced.

2.5.4 Observer

When a control law requires state or input information that are not measured, an observer can be designed and implemented to estimate the required information from the sensor measurements [78]. In this research, the system model is highly nonlinear. However, linear observer designs are investigated. A Luenberger observer based method, called Thau observer, is used to estimate states of a nonlinear system [79]. Ref. [80] investigates using an estimation technique for determining states for shift control.

CHAPTER 3

POWERTRAIN MODEL

Powertrain model is important to study shift dynamics. A powertrain consists of an engine, transmission, final drive and vehicle dynamics. As depicted in Fig. 3.1, the engine torque and speed are inputs to and the load torque and speed are outputs of the transmission. Thus, it is important to have appropriate models for the other subsystems in addition to the transmission model for the study of shift dynamics. This chapter gives the details of the models used to represent the engine, torque converter, final drive and vehicle.

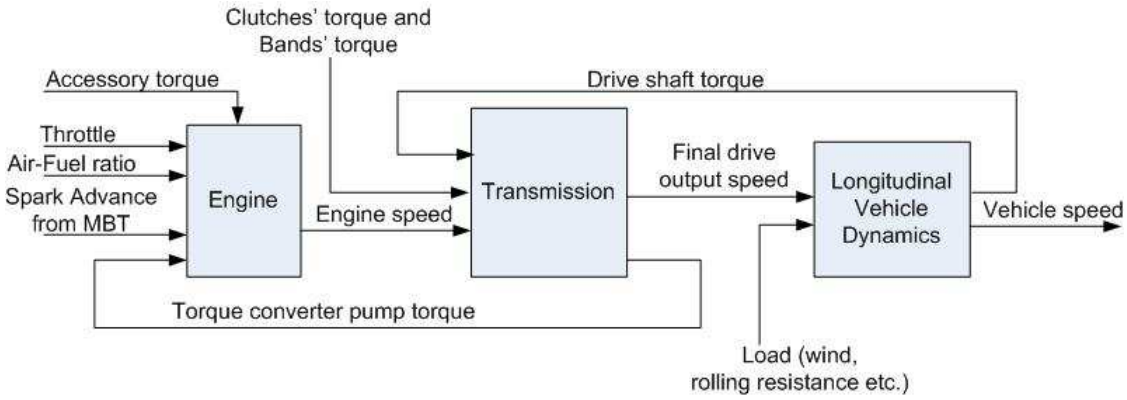

Figure 3.1. Powertrain System.

3.1 Engine

The engine model used in this research is adopted from [3, 4, 5, 33], which also study shift dynamics for improving shift quality. This engine model is a continuous time domain, three states engine model for a four–stroke engine. There are three

states in the engine model – the mass of air m_a in the intake manifold, the engine speed ω_e, and the fuel flow rate $\dot{m}_{fi}$. In addition, there are two transport delays in the model due to the discrete nature of a four–stroke engine – the intake–to–torque production delay, Δt_{it} and the spark–to–torque production delay, Δt_{st}. These engine models approximate all rotating and oscillating masses inside the engine as a single engine mass with a polar moment of inertia [35].

In the remainder of this section, specific models and mathematical expressions used for each subsystem of the engine model are presented. The numerical values of the parameters of the engine model, as implemented in simulation are given in Table 3.1.

3.1.1 Intake Manifold

By considering conservation of mass, air dynamics in the intake manifold is described by

$$\dot{m}_a = \dot{m}_{ai} - \dot{m}_{ao} \tag{3.1}$$

where $\dot{m}_a$ is mass flow rate of air in the intake manifold, $\dot{m}_{ai}$ is the mass flow rate of air entering the intake manifold and $\dot{m}_{ao}$ is the mass flow rate of air leaving the intake manifold and entering the combustion chamber.

The mass flow rate of air entering the intake manifold is modeled as

$$\dot{m}_{ai} = MAX \cdot TC \cdot PRI \tag{3.2}$$

where MAX is the maximum mass flow rate, obtained at a wide–open–throttle and chocked flow. TC is the normalized throttle area and, as shown in Fig. 3.2, charac-

terized by the following experimental curve–fit equation as a function of the throttle angle, α, as

$$TC = \begin{cases} 1 - \cos(1.14459 \cdot \alpha - 1.06) & for \quad \alpha \leq 79.46^\circ \\ 1 & for \quad \alpha > 79.46^\circ \end{cases} \tag{3.3}$$

PRI is the normalized pressure influence and characterizes the effect of the pressure ratio across the throttle body (ratio of the intake manifold plenum and upstream ambient pressure). The experimental curve fitting equation is developed (see Fig. 3.3) as

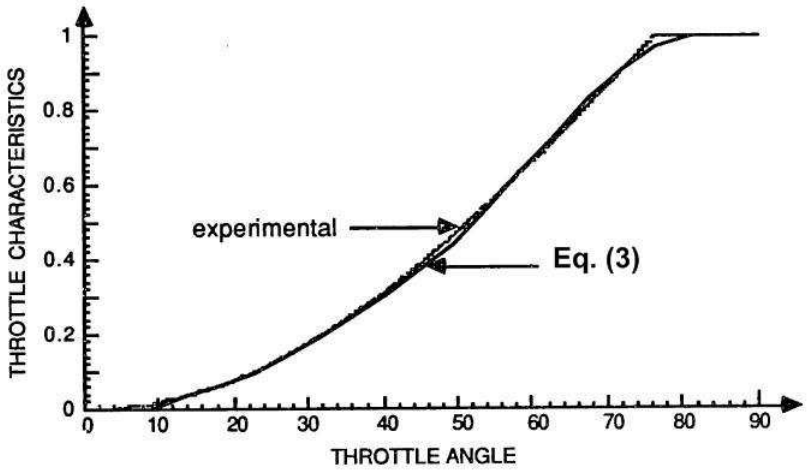

Figure 3.2. Normalized Throttle Characteristics [3].

$$PRI = 1 - \exp\left[9 \cdot \left(\frac{P_m}{P_{atm}} - 1\right)\right] \tag{3.4}$$

where P_{atm} is the atmospheric pressure and P_m, the intake manifold pressure under the assumption of uniform pressure distribution in the intake manifold, is

$$P_m = \frac{RT_m}{V_m} \cdot m_a \tag{3.5}$$

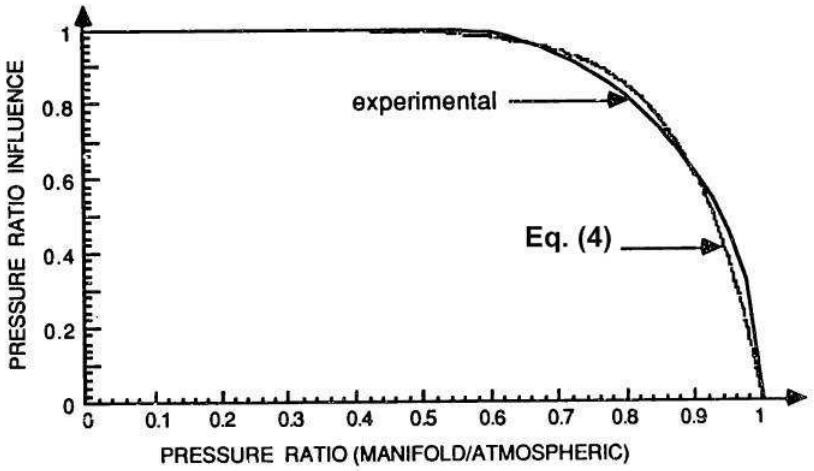

Figure 3.3. Normalized Pressure Ratio Influence Function [3].

where R is the universal gas constant for air, T_m is the intake manifold temperature, and V_m is the intake manifold volume. The mass flow rate of air entering the combustion chamber which is modeled as

$$\dot{m}_{ao} = c_1 \eta_{vol} m_a \omega_e \tag{3.6}$$

where ω_e is the engine speed, c_1 is a physical constant and η_{vol} is the engine volumetric efficiency. The physical constant is given by

$$c_1 = \frac{V_e}{4\pi \cdot V_m} \tag{3.7}$$

where V_e is the engine displacement. The volumetric efficiency, η_{vol}, is a measure of the effectiveness of an engine's induction process and defined as the volume flow rate of the air into an engine divided by the rate at which the volume is displaced by the piston. In this study, the following quadratic curve-fit from experiment data is used to characterize the volumetric efficiency.

$$\eta_{vol} = (24.5\omega_e - 3.1 \times 10^4)m_a^2 + (-0.167\omega_e + 222)m_a + (8.1 \times 10^{-4}\omega_e + 0.352) \tag{3.8}$$

3.1.2 Fueling Dynamics Model

According to Refs. [36, 37, 3], any fueling method results in a lag and a transportation delay. The transport delay is primarily a function of the timing of the injector firing interval and injector solenoid sizing rather than the characteristics of an engine. Thus, it is sufficient to model these two effects by a single first–order transfer function as

$$\tau_f \ddot{m}_{fi} + \dot{m}_{fi} = \dot{m}_{fc} \tag{3.9}$$

where $\dot{m}_{fc}$ is the commanded fuel rate, $\dot{m}_{fi}$ is the actual fuel rate entering the combustion chamber and τ_f is the effective fueling time constant. The fuel rate command is calculated to obtain the desired A/F as

$$\dot{m}_{fc} = \frac{\dot{m}_{ao}}{A/F} \tag{3.10}$$

While the effective time constant should be a function of engine speed, as done in Ref. [3], this study assumes τ_f to be constant. Otherwise, injector solenoid size and dynamics would need to be considered [3]. Refs. [4, 5, 33], which study shift dynamics, also assume the same.

3.1.3 Rotational Dynamics of Engine

The rotational motion of the engine crankshaft is given in terms of the engine polar moment of inertia, angular acceleration and the difference between the net torque generated by the engine and the load torque of the shaft. Such models are called constant inertia models [34, 35, 37, 21] since the effects from individuals events from the cylinders are not included. With this approach, the engine is modeled as a rotational shaft as

$$I_e \dot{\omega}_e = T_i - T_f - T_a - T_p \tag{3.11}$$

where I_e is the effective inertia of engine and pump, T_i is the engine indicated torque, which will be explained in detail in the next section, T_f is the engine friction torque, modeled by an experimental curve–fitting equation as

$$T_f = 0.1056\ \omega_e + 15.10 \tag{3.12}$$

where the constant term represents the static friction torque in N–m. T_p is the torque converter pump torque. T_a is from accessory components such as air condition compressor and steering power and assumed to be zero in this study.

The torque production is modeled as a steady–state phenomenon with the process delays associated with the four–stroke combustion process. The possible maximum torque is reduced by two reasons. First, AFI function represents the decreased torque when there is not enough fuel to utilize all of the air in the cylinders, or if there is insufficient air for fuel in the combustion chamber. Second, SI function decreases the engine indicated torque as a function of how far the spark/retard is from the MBT spark timing. The engine indicated torque is modeled by

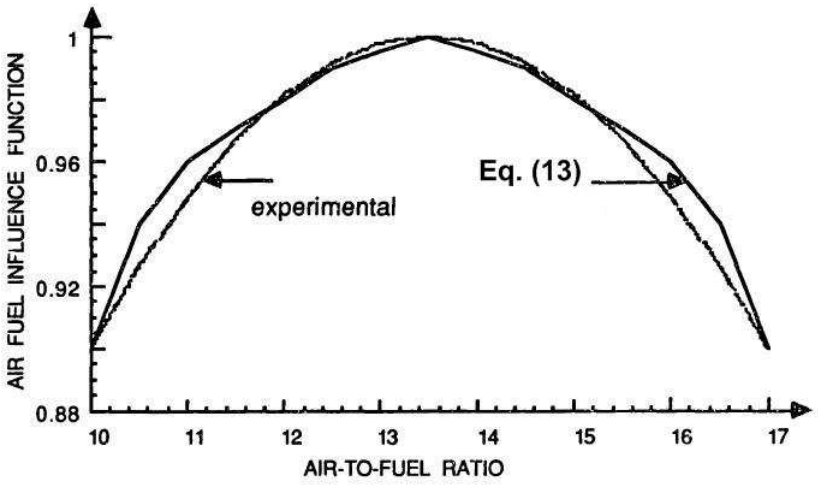

Figure 3.4. Normalized Air Fuel Influence Function [3].

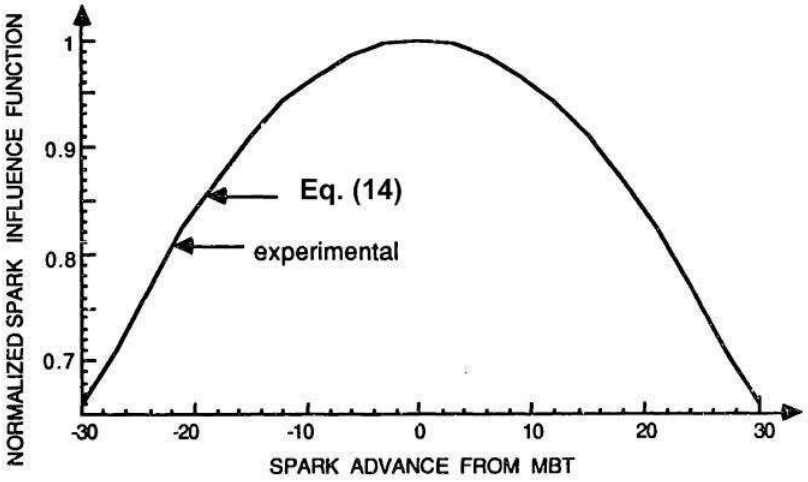

Figure 3.5. Normalized Spark Influence Function [3].

$$T_i = c_t \cdot \frac{\dot{m}_{ao}\left(t - \Delta t_{it}\right)}{\omega_e\left(t - \Delta t_{it}\right)} \cdot AFI\left(t - \Delta t_{it}\right) \cdot SI\left(t - \Delta t_{st}\right) \tag{3.13}$$

where c_T is torque constant representing the maximum torque capability of an engine for a given air mass. AFI is the normalized air fuel influence as a function of air–to–fuel ratio as illustrated in Fig. 3.4. It is a curve–fitted equation from the empirical data as shown

$$AFI = \cos\left(7.3834 \cdot (A/F - 13.5)\right) \tag{3.14}$$

SI is the normalized spark influence as a function of spark advance/retard from MBT as illustrated in Fig. 3.5. It is a curve–fitted equation from the empirical data as

$$SI = \left[\cos\left(SA - MBT\right)\right]^{2.875} \tag{3.15}$$

SA is the spark advance/retard from TDC (Top Dead Center) and MBT is the minimum spark advance for best torque. In this work, following the other references, $(SA - MBT)$ is taken as an input to the engine model. The cyclic nature of four–stroke engines is captured via the use of the intake to torque production delay, Δt_{it},

Table 3.1. Engine Model Parameters [4, 3, 5, 33]

Intake Manifold Model Parameters			
Symbol	Definition	Numerical Value	Unit
MAX	Maximum mass flow rate obtained at wide–open–throttle and choked flow	0.1843	Kg/s
P_{atm}	Atmospheric pressure	101.3	KPa
T_m	Intake manifold temperature	300	$Kelvin$
V_m	Intake manifold volume	0.0027	m^3
R	Universal gas constant	286	$J/Kg \cdot K$
V_e	Engine Displacement	0.0038	m^3
Fuel Dynamics Model Parameters			
τ_f	Fuel delivery time constant	0.05	$second$
Rotational Dynamics of Engine Model Parameters			
I_e	Engine inertia	0.087	$Kg \cdot m^2$
I_p	Pump inertia	0.058	$Kg \cdot m^2$
I_t	Turbine-Chain lumped inertia	0.05623	$Kg \cdot m^2$
c_T	Maximum torque constant	498,636	$N \cdot m/Kg/s$

and the spark to torque production delay, Δt_{st}, as express in Eq. (3.13). They are modeled as

$$\Delta t_{it} \approx \frac{5.48}{\omega_e} \tag{3.16}$$

$$\Delta t_{st} \approx \frac{1.30}{\omega_e} \tag{3.17}$$

In summary, the engine model adopted herein has three control variables, (i) throttle angle, α, (ii) air–to–fuel ratio, A/F, and (iii) spark advance from MBT, $(SA-MBT)$. Since the focus of this research is transmission control for shift quality, the engine model is set up to generate maximum possible torque for a given throttle angle. That is, A/F is set to 13.5 such that AFI is 1, based on Eq. (3.14) and $(SA - MBT)$ is set to 0 such that SI in Eq. (3.15) is 1.

3.2 Torque Converter

A torque converter generally consists of a pump (driving member or input member), a turbine (driven member or output member) and a stator (reaction member). The converter pump is attached to the engine and turns at the same speed as the engine speed. The pump works as a centrifugal pump. It induces oil flow and transfers the engine torque/speed to the turbine. The detailed operational principles can be found in Refs. [44, 45, 46]. The model of torque converter used in this study is adopted from Refs. [4, 3, 5, 44]. The model is a quadratic, regression-fit data from experiment to represent the static characteristics of a torque converter. The model has "torque converter/multiplier" and "fluid coupling" modes depending on engine or pump speed, ω_e, and turbine speed, ω_t. The input–output models for the torque converter of interest in these two modes are given below [4, 3, 5].

- For converter mode $\frac{\omega_t}{\omega_p} < 0.9$

$$\begin{aligned} T_p &= 3.4325 \times 10^{-3}\omega_e^2 + 2.2210 \times 10^{-3}\omega_e\omega_t - 4.6041 \times 10^{-3}\omega_t^2 \\ T_t &= 5.7656 \times 10^{-3}\omega_e^2 + 0.3107 \times 10^{-3}\omega_e\omega_t - 5.4323 \times 10^{-3}\omega_t^2 \end{aligned} \tag{3.18}$$

- For fluid coupling mode $\frac{\omega_t}{\omega_p} \geq 0.9$

$$T_p = T_t = -6.7644 \times 10^{-3}\omega_e^2 + 32.0084 \times 10^{-3}\omega_e\omega_t - 25.2441 \times 10^{-3}\omega_t^2 \tag{3.19}$$

The effect of the inertia of transmission fluid in torque converter is ignored in this study, as suggested in Refs. [4, 3, 5, 44].

Turbine shaft acts as the input shaft for the transmission, transmitting speed and torque from the torque converter to the planetary gear sets. As shown in Fig. 4.1 and Table 4.1, the turbine is coupled with the planetary gear set through combinations of C_1, C_2 and C_3, depending on the gear. Thus, the dynamics equation of the turbine shaft can be expressed as

$$I_t\ \dot{\omega}_t = T_t + T_{t,C_1} + T_{t,C_2} + T_{t,C_3} \tag{3.20}$$

where T_t is turbine torque and T_{t,C_i} is the applied torque due to C_i, where $i = 1, 2, 3$. T_{t,C_1}, T_{t,C_2} and T_{t,C_3} are given in Eqs. (4.105), (4.109) and (4.112), respectively.

3.3 Final Drive Gear and Vehicle Dynamics

The vehicle model used in this study considers longitudinal dynamics of the vehicle as a rotating shaft with a torsional spring constant and a lumped inertia. References [4, 3, 5, 33] also use this simplified vehicle model in studying shift dynamics and shift quality. The numerical values of the parameters of the final drive gear and vehicle models, as implemented in simulation are given in Table 3.3. The parameters are obtained from Refs. [4, 3, 5, 33]. With this type of vehicle model, power transferred from engine through transmission and finally from tires to road is analyzed in the form of torque and angular speed. The value of lumped inertia, which represents the equivalent moment of inertia of the vehicle, is computed as

$$I_V = (m_V + m_l) \cdot r^2 \tag{3.21}$$

where m_V is vehicle mass, m_l is passenger and luggage masses and r is tire radius. The rotational dynamics of the equivalent vehicle inertia is

$$\dot{\omega}_V = \frac{1}{I_V} (T_D - T_L) \tag{3.22}$$

where ω_V is the wheel angular speed, T_D is the torsional torque in the final drive shaft and T_L is the load torque due to external forces.

Final drive gear is modeled as a simple torque/speed converter. Thus, the simple mathematical model of the final drive gear is

$$\frac{T_{FD}}{T_{FD,in}} = \frac{\omega_{C2R1}}{\omega_{FD}} = R_{FD} \tag{3.23}$$

Table 3.2. Drivetrain–Vehicle Parameters [4, 3, 5, 33]

Drivetrain-Vehicle Parameters			
k	combined axle shaft stiffness	6742	N–m/rad
m_V	vehicle mass	1644	Kg
m_l	passenger and luggage	125	Kg
r	average front and rear wheel from ground to axle	0.31	m
R_{FD}	final gear ratio	2.84	

where note that the final drive input speed is $\omega_{C_2R_1}$ since C_2R_1 is directly connected to the input side of the final drive gear. Further, the free body diagram analysis of C_2R_1 and the final drive implies that $T_{C_2R_1,FD}$ in Eq. (4.69) is

$$T_{C_2R_1,FD} = -T_{FD,in} \tag{3.24}$$

The final drive shaft from the final drive gear to the vehicle is modeled as a torsional spring with spring coefficient k. Thus, the derivative of the torque in the final drive shaft is

$$\dot{T}_D = k\left(\omega_{FD} - \omega_V\right) \tag{3.25}$$

Note that when the final drive rotates faster than the wheel, $T_D > 0$ and the torsional torque should slow down the final drive. This implies that the output torque of the final drive gear in Eq. (3.23) is

$$T_{FD} = -T_D \tag{3.26}$$

The load torque due to the motion of the vehicle is due to the external forces such as aerodynamic drag force, gravitational force, longitudinal tire force and rolling resistance force at tires. T_L is modeled as a function of the vehicle translational speed as [4, 3, 5, 33]

$$T_L = \left(158.2 + 4.479 \times 10^{-2} V_{Kmh}^2\right) \cdot r \tag{3.27}$$

where V_{Kmh} is the vehicle velocity in kilometer per hour.

Torsion in the drive shaft models the oscillation in a powertrain, caused by bad quality shifts. To understand the effect of torsional spring in shift modeling and simulation, the shaft compliance is set to be stiff and the simulation with stiff and torsional spring drive shafts are compared. In the case of stiff shaft, the dynamic equations reduce to Eq. 3.22 only. The shaft is rigid which implies that

$$\omega_{FD} = \omega_V \tag{3.28}$$

$$\dot{\omega}_{FD} = \dot{\omega}_V \tag{3.29}$$

By this assumption, the simulation results reveal that the oscillation due to the drive shaft is omitted from the simulation results. The drive shaft inertia only effects the powertrain model. The simulation results are discussed in Chapter 5.

CHAPTER 4

TRANSMISSION MODEL

Transmission consists of torque converter, planetary gear sets, friction elements, hydraulic system and final drive. The transmission model used in the simulation represents GM Hydramatic 440. This transmission is selected for this study because the numerical values of its parameters are available in Refs. [3, 4, 5, 28]. As shown in its stick diagram in Fig. 4.1, this transmission has two coupled planetary gear sets, controlled with four clutches and two bands. This transmission has a torque converter, a planetary gear set, four clutches and two bands and a final drive. The torque converter is connected to an engine at the pump side. It transmits torque and speed to the planetary gear set at the turbine side through clutch–1 and clutch–2 which are activated by the hydraulic system corresponding to the gear shifting schedule from the transmission control unit (TCU). Clutch C_1 and C_3 are modeled as one–way clutches due to the accompanying sprag clutches. The torque converter model is adopted from Ref. [44]. Table 4.1 shows the clutch engagement schedule and gear ratios. The subsystems of the transmission are described in following sections.

4.1 Planetary Gear Sets

A new approach to deriving a mathematical model for the dynamics of rigid planetary gear sets is developed. This approach that uses Lagrange method is applied to the planetary gear set configuration of GM Hydramatic 440 [28]. The details of this

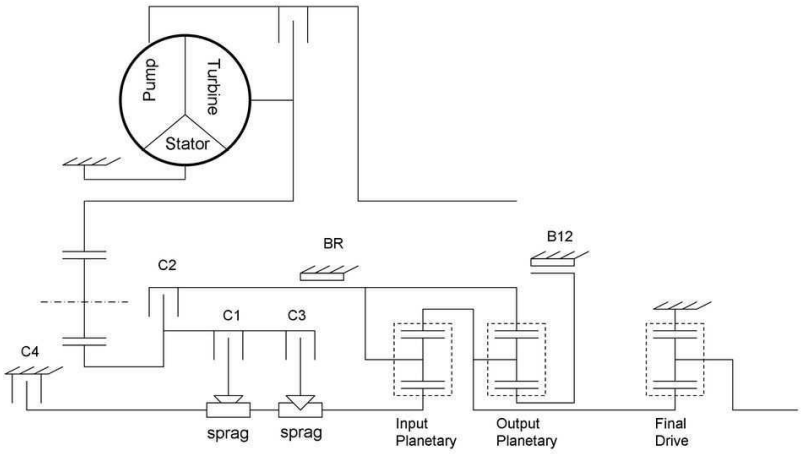

Figure 4.1. Stick Diagram for GM Hydramatic 440.

Table 4.1. Clutch Engagement Schedule

Range	**Clutches Engaged**						**Gear**
	C_1	C_2	C_3	C_4	B_{12}	B_R	**Ratio**
1^{st}	X				X		2.93
2^{nd}	$\bigotimes$	X			X		1.57
3^{rd}		X	X				1
4^{th}		X	$\bigotimes$	X			0.70
Rev	X					X	2.38
	X $\sim$ Clutch on		$\bigotimes \sim$ sprag over-running				

method is given below starting with a simple system of two gears and then applied to the planetary gear set of the transmission.

A single planetary gear set consists of a ring gear, a sun gear, a set of planet gears (or pinions) and a carrier. GM Hydramatic 440 transmission has two single planetary gear sets, which are coupled as follows. The carrier of the first planetary gear set is rigidly connected to the ring of the second set and the ring of the first set is rigidly connected to the carrier of the second one, as depicted in Fig. 4.2.

In automatic transmissions, different speed and torque ratios are achieved by alternating input, output and stationary components of the planetary gear sets. Table

4.1 summarizes which friction elements are used to obtain different gear ratios. For the first gear in Hydramatic 440, C_1 and B_{12} should be engaged. B_{12} is engaged to stop the sun of the second planetary gear set. Note from Fig. 4.1 that, in the first gear, the torque is transmitted from the turbine through C_1 to the sun of the first planetary gear set. To shift to the second gear, C_2 should be applied. When C_2 is engaged, C_1 starts over-running and the torque is transmitted through C_2 to the carrier of the first planetary gear set. To shift to the third gear, C_3 should be applied while B_{12} is released. Note that shift to the 3^{rd}–gear requires the synchronization of C_3 engagement and B_{12} disengagement. Shifts requiring such synchronization of multiple friction elements are called "swap" or "clutch–to–clutch" shifts and most challenging for shift quality. In the third gear, C_2 and C_3 are both engaged, which indicates that the sun and carrier of the first planetary gear set are connected. In planetary gear sets, when two elements are connected, i.e. forced to rotated together, then the other elements also have to rotate with the two elements, making the planetary gear set rotate like a single shaft, with 1–to–1 speed ration between its input and output shafts. Similarly, planetary gear configurations and the required clutch/band engagements for other shifts and gears can be seen from Fig. 4.1 and Table 4.1.

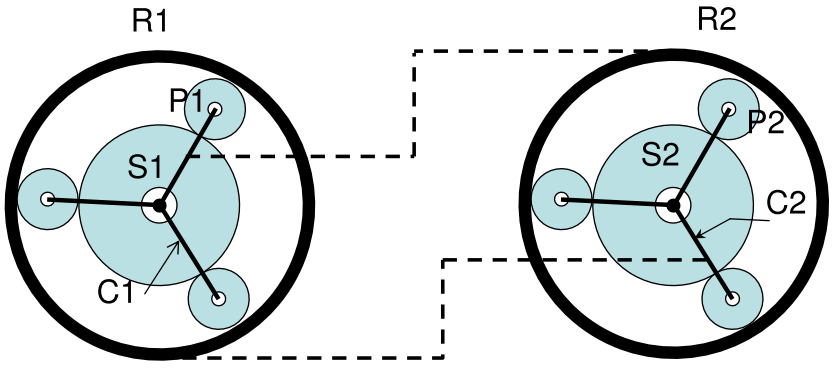

Figure 4.2. GM Hydramatic 440 Gear Set.

4.1.1 Lagrange Method Applied to Gear Dynamics :

A general form of $\mathcal{L}$agrange's equation used to derive the equations of motion of a system with generalized coordinates, q_i, $(i = 1, 2, \ldots, n)$ is [81]

$$\frac{d}{dt}\left(\frac{\partial \mathcal{L}}{\partial \dot{q}_i}\right) - \frac{\partial \mathcal{L}}{\partial q_i} = Q_i \quad (i = 1, 2, \ldots, n) \tag{4.1}$$

where Q_i are generalized forces not derivable from a potential function. Examples of typical Q forces are frictional forces, time-variant forcing functions, and nonholonomic constraint forces. Note that although Q_i is called generalized "force", it can also be a "moment" if the corresponding generalized coordinate is a rotational position, i.e. "angle" instead of a translational position, i.e. "distance". $\mathcal{L}$ is called "Lagrangian function"

$$\mathcal{L} = \mathcal{K} - \mathcal{V} \tag{4.2}$$

where $\mathcal{K}$ and $\mathcal{V}$ are the total kinetic and potential energy of the system, respectively.

In order to introduce the basic concepts used in the application of $\mathcal{L}$agrange Method on gear sets, the equations of motion of a simple system of two gears (see Fig.4.3) is derived. First, the coordinates which are used to specify the configuration of the system are selected. In this example, α, angular position of Gear–1, and β, angular position of Gear–2, are the coordinates of this system. Positive direction for this coordinate system is counter–clockwise. Positive torque is also in the counter-clockwise direction. Second, the constraint equations of the system are written. Since the two gears are meshed together by teeth, no sliding occurs between. That is, the translational velocities of the two gears are equal at the contact point

$$-\dot{\beta} r_2 = \dot{\alpha} r_1 \tag{4.3}$$

where $\dot{(\ )}$ stands for time derivative of $(\ )$, e.g. $\dot{\alpha}$ is the time derivative of α or angular velocity of Gear–1, r_1 and r_2 are the radia of Gears–1 and –2, respectively. Then, the

total kinetic and potential energies of the whole system is formulated in term of the coordinates of choice. Since the potential energy of the system is constant, we can say that the total potential energy of the system is zero, i.e.,$\mathcal{V} = 0$. The system has only rotational kinetic energy due to the rotation of each gear as

$$\mathcal{K} = \frac{1}{2} I_1 \dot{\alpha}^2 + \frac{1}{2} I_2 \dot{\beta}^2 \tag{4.4}$$

where I_1 and I_2 are the moments of inertia of Gears–1 and –2, respectively.

Note that the system has only one independent constraint (Eq.4.3) in terms of the coordinates of choice, (α, β). Since the system has two coordinates and one constraint equation, its DOF (Degree–Of–Freedom) is 1. Since the system is holonomic, we can describe the configuration of the system by one independent coordinate.

In order to apply the $\mathcal{L}$agrange's equation (4.1), we choose α as the generalized or independent coordinate. Then, we need to write the $\mathcal{L}$agrangian and the generalized force in terms of the generalized coordinate. Eq.(4.3) implies

$$\dot{\beta} = -\frac{r_1}{r_2} \dot{\alpha} \tag{4.5}$$

Substituting $\dot{\beta}$ into Eq.(4.4) and recalling that the total potential energy is zero, we obtain, from Eq.(4.2), the $\mathcal{L}$agrangian in terms of the generalized coordinate, α as

$$\mathcal{L} = \frac{1}{2} \left[I_1 + \left(\frac{r_1}{r_2} \right)^2 I_2 \right] \dot{\alpha}^2 \tag{4.6}$$

In the $\mathcal{L}$agrange's equation (4.1), generalized moment Q_α should be determined in terms of the generalized coordinate. A convenient way to obtain generalized forces is to write the virtual work of the system in terms of the generalized coordinates. Since N, the normal forces at the contact point (see Fig.4.3), are constraint forces and F, tangential forces at the contact point, are "frictionless" forces, only forces or moments that do virtual work in a virtual displacement are the applied torques T_1

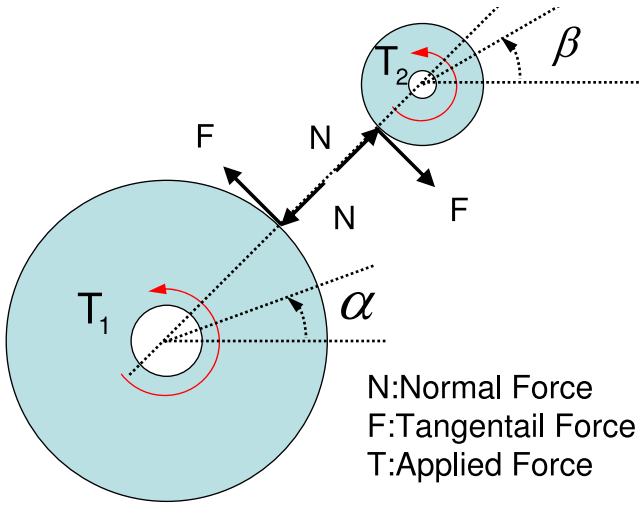

Figure 4.3. Free Body Diagram of Two Gear.

and T_2 on Gear–1 and –2, respectively. Thus, the virtual work of the system in terms of the virtual displacements, $\delta\alpha$ and $\delta\beta$ is

$$\delta W = T_1\delta\alpha + T_2\delta\beta \tag{4.7}$$

The constraint in Eq.(4.5) implies $\delta\beta = -\frac{r_1}{r_2}\delta\alpha$. Substituting $\delta\beta$ into Eq.(4.7), yields the virtual work in terms of virtual displacement of the generalized coordinate as

$$\delta W = \left(T_1 - \frac{r_1}{r_2}T_2\right)\delta\alpha \tag{4.8}$$

where the coefficient of $\delta\alpha$ is the generalized moment corresponding to the generalized coordinate, α. Thus,

$$Q_\alpha = T_1 - \frac{r_1}{r_2}T_2 \tag{4.9}$$

$\mathcal{L}$agrange's equation for the system is

$$\frac{d}{dt}\left(\frac{\partial\mathcal{L}}{\partial\dot{\alpha}}\right) - \frac{\partial\mathcal{L}}{\partial\alpha} = Q_\alpha \tag{4.10}$$

which requires the partial derivatives of the $\mathcal{L}$agrangian with respect to $\dot{\alpha}$ and α. The partial derivative of $\mathcal{L}$ with respect to α is zero, since $\mathcal{L}$ does not explicitly depend

on α. Taking the partial derivative of $\mathcal{L}$ in Eq.(4.6), substituting its time derivative along with Eq. (4.9) into Eq.(4.10), the equation of motion of the system in terms of the angular position of Gear–1 is obtained as

$$\left[I_1 + \left(\frac{r_1}{r_2}\right)^2 I_2\right] \ddot{\alpha} = T_1 - \frac{r_1}{r_2} T_2 \tag{4.11}$$

Note that if the inertias of the gears are ignored (i.e. $I_1 = I_2 = 0$) or the motion of the system is at steady-state (i.e. $\dot{\alpha} = constant$), then Eq.(4.11) yields

$$\frac{T_1}{r_1} = \frac{T_2}{r_2} \tag{4.12}$$

which is the well-known gear torque relation.

4.1.2 Single Planetary Gear Set :

This section follows the procedure established in the previous section to derive the equations of motion of a single planetary gear set.

The four coordinates to specify the configuration of the system are $(\alpha, \beta, \gamma, \theta)$, the angles of the sun, carrier, pinions and ring, respectively (see Fig.4.4). Note, however, that they are not independent because the system has some constraints in terms of these coordinates. No sliding can occur between the sun and the pinions, or between the pinions and the ring since they are meshed by teeth. This implies

$$\dot{\beta} R_S - \dot{\gamma} R_P = \dot{\alpha} R_S \tag{4.13}$$

$$\dot{\beta}(R_S + 2R_P) + \dot{\gamma} R_P = \dot{\theta} R_R \tag{4.14}$$

where R_S, R_P, and R_R are the radia of the sun, pinions, and ring, respectively. By the geometry, we have the following relation between the radia :

$$R_R = R_S + 2R_P \tag{4.15}$$

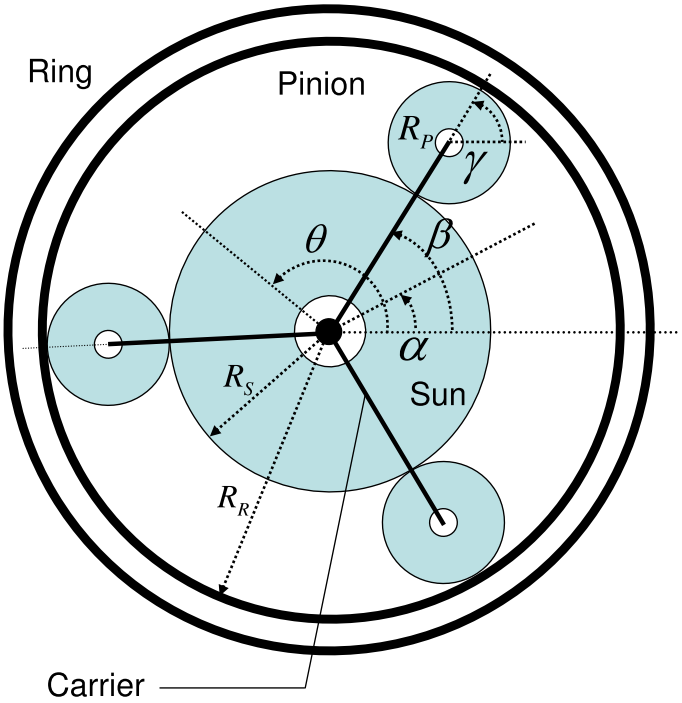

Figure 4.4. A Single Planetary Gear Set.

The potential energy of the system may vary due to the rotational motion of the pinions around the sun. However, in this work, this variation is neglected due to the fact that the vertical motion of the pinions is small and they are positioned around the sun by equal angles between each other. Furthermore, note that many planetary gear sets use 4 pinions. In this case, there is no potential energy change due to the rotation of the pinions around the sun. Thus, $\mathcal{V} = 0$. The kinetic energies of the sun and the carriers, respectively, are

$$\mathcal{K}_S = \frac{1}{2} I_S \dot{\alpha}^2 \tag{4.16}$$

$$\mathcal{K}_C = \frac{1}{2} I_C \dot{\beta}^2 \tag{4.17}$$

where I_S and I_C are the moment of inertia of the sun and the carrier, respectively, and everything rigidly connected to them. The kinetic energy of the pinions :

$$\mathcal{K}_P = n\left[\frac{1}{2}I_P\dot{\gamma}^2 + \frac{1}{2}m_P\left(R_S + R_P\right)^2\dot{\beta}^2\right] \tag{4.18}$$

where I_P is the moment of inertia of one of the pinions, and m_P is the mass of one of the pinions. The second term is due to the fact that each pinion can rotate around the sun while rotating around its center and n is the number of pinions in this single planetary gear box. The kinetic energy of the ring :

$$\mathcal{K}_R = \frac{1}{2}I_R\dot{\theta}^2 \tag{4.19}$$

where I_R is the moment of inertia of the carrier and everything rigidly connected to it.

The system has 4 coordinates and 2 equations of constraint in terms of these coordinates. Thus, the DOF of the system is 2. This means that the configuration of system can be specified by two independent generalized coordinates. We choose (β, γ) as the set of independent coordinates.

As can be seen in Fig.4.5, F and N forces do not do virtual work due to the reasons explained in Section 4.1.1. Only the applied torques, T_S, T_C, T_R do virtual work. Thus, the virtual work of the system in a virtual displacement is

$$\delta W = T_S\delta\alpha + T_C\delta\beta + T_R\delta\theta \tag{4.20}$$

The virtual displacements $\delta\alpha$ and $\delta\theta$ can be written, from Eqs.(4.13) and (4.14), in terms of the virtual displacements of the generalized coordinates (β, γ) as

$$\delta\alpha = \delta\beta - \frac{R_P}{R_S}\delta\gamma \tag{4.21}$$

$$\delta\theta = \delta\beta + \frac{R_P}{R_R}\delta\gamma \tag{4.22}$$

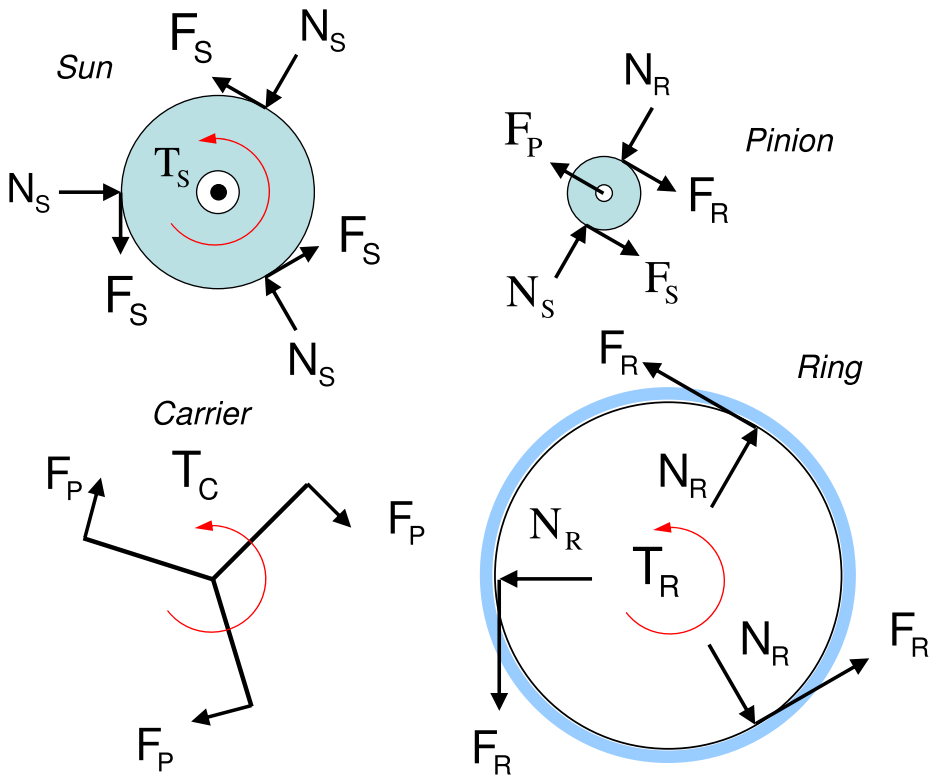

Figure 4.5. Free Body Diagram of Single Planetary Gear Set.

where in the $\delta\theta$–equation we use the relation from Eq.(4.15). Substituting $\delta\alpha$ and $\delta\theta$ into Eq.(4.20) yields the virtual work in terms of the generalized coordinates as

$$\delta W = (T_S + T_C + T_R)\,\delta\beta + R_P \left(\frac{T_R}{R_R} - \frac{T_S}{R_S}\right)\delta\gamma \tag{4.23}$$

From Eqs.(4.13) and (4.14), $\dot{\alpha}$ and $\dot{\theta}$ can also be written in terms of the time derivative of the generalized coordinates (β, γ)

$$\dot{\alpha} = \dot{\beta} - \frac{R_P}{R_S}\dot{\gamma} \tag{4.24}$$

$$\dot{\theta} = \dot{\beta} + \frac{R_P}{R_R}\dot{\gamma} \tag{4.25}$$

Using the constraint equations in Eqs.(4.16)–(4.19), the kinetic energies are rewritten in terms of the time derivative of the generalized coordinates as

$$\mathcal{K}_S = \frac{1}{2} I_S \left(\dot{\beta} - \frac{R_P}{R_S} \dot{\gamma} \right)^2 \tag{4.26}$$

$$\mathcal{K}_C = \frac{1}{2} I_C \dot{\beta}^2 \tag{4.27}$$

$$\mathcal{K}_P = n \left[\frac{1}{2} I_P \dot{\gamma}^2 + \frac{1}{2} m_P \left(R_S + R_P \right)^2 \dot{\beta}^2 \right] \tag{4.28}$$

$$\mathcal{K}_R = \frac{1}{2} I_R \left(\dot{\beta} + \frac{R_P}{R_R} \dot{\gamma} \right)^2 \tag{4.29}$$

$\mathcal{L}$agrange's equations for this system, from Eq.(4.1), are

$$\beta\text{–equation :} \quad \frac{d}{dt} \left(\frac{\partial \mathcal{L}}{\partial \dot{\beta}} \right) - \frac{\partial \mathcal{L}}{\partial \beta} = Q_\beta \tag{4.30}$$

$$\gamma\text{–equation :} \quad \frac{d}{dt} \left(\frac{\partial \mathcal{L}}{\partial \dot{\gamma}} \right) - \frac{\partial \mathcal{L}}{\partial \gamma} = Q\gamma \tag{4.31}$$

where, from Eq.(4.23),

$$Q_\beta = T_S + T_C + T_R \tag{4.32}$$

$$Q_\gamma = R_P \left(\frac{T_R}{R_R} - \frac{T_S}{R_S} \right) \tag{4.33}$$

Since the potential energy is constant, $\mathcal{L} = \mathcal{K}$, which is the total kinetic energy, i.e., sum of $\mathcal{K}_S$, $\mathcal{K}_C$, $\mathcal{K}_P$ and $\mathcal{K}_R$. Since $\mathcal{K}$ does not explicitly depend on β or γ, the partial derivatives with respect to β and γ are zero. Taking the partial derivative of $\mathcal{L}$ with respect to $\dot{\beta}$, substituting it and Eq.(4.32) into Eq.(4.30), and rearranging, β–equation of motion is obtained as

$$\left[I_S + I_C + n\ m_P \left(R_S + R_P \right)^2 + I_R \right] \ddot{\beta} + R_P \left(\frac{I_R}{R_R} - \frac{I_S}{R_S} \right) \ddot{\gamma} = T_S + T_C + T_R \tag{4.34}$$

Taking the partial derivative of $\mathcal{L}$ with respect to $\dot{\gamma}$, substituting it and Eq.(4.33) into Eq.(4.31), and rearranging, γ–equation of motion is obtained as

$$\left[\frac{I_R}{R_R} - \frac{I_S}{R_S} \right] \ddot{\beta} + R_P \left[\frac{I_S}{R_S^2} + n \frac{I_P}{R_P^2} + \frac{I_R}{R_R^2} \right] \ddot{\gamma} = \frac{T_R}{R_R} - \frac{T_S}{R_S} \tag{4.35}$$

In summary, the dynamics of a single planetary gear set is represented by two differential equations, Eqs.(4.34) and (4.35), in terms of the angles of the carrier and pinions. The equations are second order regarding the angles, (β, γ), but first order regarding the angular velocities, $(\dot{\beta}, \dot{\gamma})$. Also note that we have a linear set of equations in terms of the accelerations. Additionally, we have two algebraic equations, Eqs.(4.24) and (4.25) for the other coordinates, i.e. angle/velocity/acceleration of the sun and ring.

4.1.3 Coupled Planetary Gear Set in GM Hydramatic 440

This section applies the Lagrange method to the coupled planetary gear set used in GM Hydramatic 440. In this planetary gear configuration, there are two sets of planetary gears. The carrier of the first planetary gear set is rigidly connected to the ring of the second set and the ring of the first set is rigidly connected to the carrier of the second one.

The coordinates to specify the configuration of the system are (see Fig.4.2) α_1 as the angle of the sun–1, θ_2 as the angle of carrier–1 and ring–2, γ_1 as the angle of pinions–1, θ_1 as the angle of ring–1 and carrier–2, α_2 as the angle of the sun–2, and γ_2 as the angle of pinions–2. There are 4 constraint equations for the above set of coordinate system. No sliding occurs between (i) the sun–1 and pinions–1,(ii) pinions–1 and ring–1 , (iii) the sun–2 and pinions–2, and (iv) pinions–2 and ring–2. These imply

$$R_{S_1}\dot{\theta}_2 - R_{P_1}\dot{\gamma}_1 = R_{S_1}\dot{\alpha}_1 \tag{4.36}$$

$$\left(R_{S_1} + 2R_{P_1}\right)\dot{\theta}_2 + R_{P_1}\dot{\gamma}_1 = R_{R_1}\dot{\theta}_1 \tag{4.37}$$

$$R_{S_2}\dot{\theta}_1 - R_{P_2}\dot{\gamma}_2 = R_{S_2}\dot{\alpha}_2 \tag{4.38}$$

$$\left(R_{S_2} + 2R_{P_2}\right)\dot{\theta}_1 + R_{P_2}\dot{\gamma}_2 = R_{R_2}\dot{\theta}_2 \tag{4.39}$$

The system has 6 coordinates and 4 equations of constraint in terms of these coordinates. Thus, the DOF of the system is 2. We choose (θ_1, θ_2) as the set of independent coordinates. Then, we solve the constraint equations for the remaining coordinates in terms of the generalized ones.

$$\dot{\alpha}_1 = A_1\dot{\theta}_2 - A_2\dot{\theta}_1 \tag{4.40}$$

$$\dot{\gamma}_1 = A_3\left(\dot{\theta}_1 - \dot{\theta}_2\right) \tag{4.41}$$

$$\dot{\alpha}_2 = A_4\dot{\theta}_1 - A_5\dot{\theta}_2 \tag{4.42}$$

$$\dot{\gamma}_2 = A_6\left(\dot{\theta}_2 - \dot{\theta}_1\right) \tag{4.43}$$

where

$$A_1 = 1 + A_2\ , \quad A_2 = \frac{R_{R_1}}{R_{S_1}}\ , \quad A_3 = \frac{R_{R_1}}{R_{P_1}}\ ,$$
$$A_4 = 1 + A_5\ , \quad A_5 = \frac{R_{R_2}}{R_{S_2}}\ , \quad A_6 = \frac{R_{R_2}}{R_{P_2}}\ .$$

As in the case of the single planetary gear set, we assume that the potential energy variation is small enough to neglect. The kinetic energy of carrier–1 and ring–2 is represented as a single quantity since they are rigidly attached. Similarly, the combined kinetic energy of carrier–2 and ring–1 is formulated. The kinetic energies of all the components are :

$$\mathcal{K}_{S_1} = \frac{1}{2}I_{S_1}\dot{\alpha}_1^2 \tag{4.44}$$

$$\mathcal{K}_{C_1R_2} = \frac{1}{2}I_{C_1R_2}\dot{\theta}_2^2 \tag{4.45}$$

$$\mathcal{K}_{P_1} = n_1\left[\frac{1}{2}I_{P_1}\dot{\gamma}_1^2 + \frac{1}{2}m_{P_1}\left(R_{S_1} + R_{P_1}\right)^2\dot{\theta}_2^2\right] \tag{4.46}$$

$$\mathcal{K}_{S_2} = \frac{1}{2}I_{S_2}\dot{\alpha}_2^2 \tag{4.47}$$

$$\mathcal{K}_{C_2R_1} = \frac{1}{2}I_{C_2R_1}\dot{\theta}_1^2 \tag{4.48}$$

$$\mathcal{K}_{P_2} = n_2\left[\frac{1}{2}I_{P_2}\dot{\gamma}_2^2 + \frac{1}{2}m_{P_2}\left(R_{S_2} + R_{P_2}\right)^2\dot{\theta}_1^2\right] \tag{4.49}$$

Substituting Eqs.(4.40)–(4.43) into Eqs.(4.44)–(4.49), yields the kinetic energies in terms of the generalized coordinates, (θ_1, θ_2)

$$\mathcal{K}_{S_1} = \frac{1}{2} I_{S_1} \left(A_1 \dot{\theta}_2 - A_2 \dot{\theta}_1 \right)^2 \tag{4.50}$$

$$\mathcal{K}_{C_1 R_2} = \frac{1}{2} I_{C_1 R_2} \dot{\theta}_2^2 \tag{4.51}$$

$$\mathcal{K}_{P_1} = n_1 \left[\frac{1}{2} I_{P_1} A_3^2 \left(\dot{\theta}_1 - \dot{\theta}_2 \right)^2 + \frac{1}{2} m_{P_1} \left(R_{S_1} + R_{P_1} \right)^2 \dot{\theta}_2^2 \right] \tag{4.52}$$

$$\mathcal{K}_{S_2} = \frac{1}{2} I_{S_2} \left(A_4 \dot{\theta}_1 - A_5 \dot{\theta}_2 \right)^2 \tag{4.53}$$

$$\mathcal{K}_{C_2 R_1} = \frac{1}{2} I_{C_2 R_1} \dot{\theta}_1^2 \tag{4.54}$$

$$\mathcal{K}_{P_2} = n_2 \left[\frac{1}{2} I_{P_2} A_6^2 \left(\dot{\theta}_2 - \dot{\theta}_1 \right)^2 + \frac{1}{2} m_{P_2} \left(R_{S_2} + R_{P_2} \right)^2 \dot{\theta}_1^2 \right] \tag{4.55}$$

The virtual work of the system in terms of the virtual displacements of the original coordinates is written as

$$\delta W = T_{S_1} \, \delta\alpha_1 + T_{C_1 R_2} \, \delta\theta_2 + T_{C_2 R_1} \, \delta\theta_1 + T_{S_2} \, \delta\alpha_2 \tag{4.56}$$

Eqs.(4.40)–(4.43) can be written in terms of the virtual displacement of the coordinates instead of their time derivatives. Substituting these equivalent equations into Eq. (4.56) and rearranging, the virtual work is written in terms of the virtual displacements of the generalized coordinates, $(\delta\theta_1, \delta\theta_2)$ as

$$\delta W = \left(-A_2 T_{S_1} + T_{C_2 R_1} + A_4 T_{S_2} \right) \delta\theta_1 + \left(A_1 T_{S_1} + T_{C_1 R_2} - A_5 T_{S_2} \right) \delta\theta_2 \tag{4.57}$$

which indicates the generalized forces (torques) for the generalized coordinates as

$$Q_{\theta_1} = \left(-A_2 T_{S_1} + T_{C_2 R_1} + A_4 T_{S_2} \right) \tag{4.58}$$

$$Q_{\theta_2} = \left(A_1 T_{S_1} + T_{C_1 R_2} - A_5 T_{S_2} \right) \tag{4.59}$$

For the same reasons explained in the previous sections, the $\mathcal{L}$agrange's equations for this system are reduced to

$$\theta_1\text{–equation}: \quad \frac{d}{dt}\left(\frac{\partial \mathcal{K}}{\partial \dot{\theta}_1}\right) = Q_{\theta_1} \tag{4.60}$$

$$\theta_2\text{–equation}: \quad \frac{d}{dt}\left(\frac{\partial \mathcal{K}}{\partial \dot{\theta}_2}\right) = Q_{\theta_2} \tag{4.61}$$

where the total kinetic energy, $\mathcal{K}$, is

$$\mathcal{K} = \mathcal{K}_{S_1} + \mathcal{K}_{C_1R_2} + \mathcal{K}_{P_1} + \mathcal{K}_{S_2} + \mathcal{K}_{C_2R_1} + \mathcal{K}_{P_1} \tag{4.62}$$

Taking the partial derivatives of the kinetic energy in Eq.(4.62) with respect to $\dot{\theta}_1$ and $\dot{\theta}_2$ and substituting them into Eqs.(4.60) and (4.61) along with the generalized moments from Eqs.(4.58) and (4.59) yield the θ_1– and θ_2–equations of dynamics for the planetary gear set of GM Hydramatic 440 as

$$B_{11}\ddot{\theta}_1 + B_{12}\ddot{\theta}_2 = -A_2T_{S_1} + T_{C_2R_1} + A_4T_{S_2} \tag{4.63}$$

$$B_{21}\ddot{\theta}_1 + B_{22}\ddot{\theta}_2 = A_1T_{S_1} - A_5T_{S_2} + T_{C_1R_2} \tag{4.64}$$

where

$$\begin{aligned}
B_{11} &= A_2^2 I_{S_1} + n_1 A_3^2 I_{P_1} + I_{C_2R_1} + A_4^2 I_{S_2} \\
&\quad + n_2\left[A_6^2 I_{P_2} + m_{P_2}\left(R_{S_2} + R_{P_2}\right)^2\right] \\
B_{12} &= B_{21} = -A_1A_2I_{S_1} - n_1A_3^2I_{P_1} - A_4A_5I_{S_2} - n_2A_6^2I_{P_2} \\
B_{22} &= A_1^2 I_{S_1} + n_2 A_6^2 I_{P_2} + I_{C_1R_2} + A_5^2 I_{S_2} \\
&\quad + n_1\left[A_3^2 I_{P_1} + m_{P_1}\left(R_{S_1} + R_{P_1}\right)^2\right]
\end{aligned}$$

4.1.4 Matrix Representation of the Equations of Motion

In this section, the equations of dynamics and constraint for GM Hydramatic 440 are written in matrix form. This produces a concise representation of the equations and enables an efficient implementation in simulation.

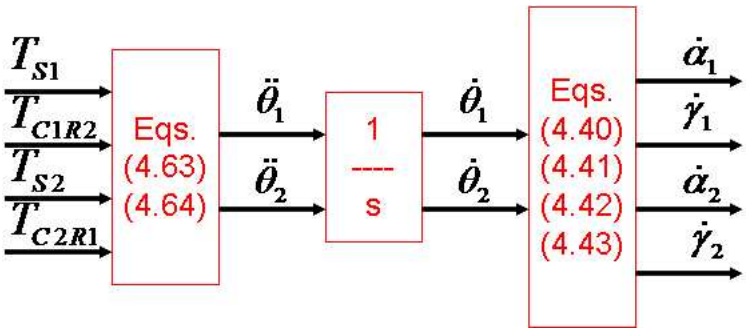

Figure 4.6. Block Diagram Representation.

Figure 4.6 shows the block diagram representation of the planetary gear set of GM Hydramatic 440. Eqs.(4.63) and (4.64), in matrix form, are

$$\mathbf{E}_G \begin{bmatrix} \ddot{\theta}_1 \\ \ddot{\theta}_2 \end{bmatrix} = \mathbf{B}_G \begin{bmatrix} T_{S1} \\ T_{C1R2} \\ T_{S2} \\ T_{C2R1} \end{bmatrix} \tag{4.65}$$

where $\mathbf{E_G}$ is a 2×2 and $\mathbf{B_G}$ is a 2×4 matrices. The entries of the matrices are determined easily by inspection of Eqs.(4.63) and (4.64). By inspection, it can be seen that $\mathbf{E_G}$ is almost always non-singular. Pre–multiplied by the inverse of $\mathbf{E}_G$, Eq.(4.65) gives the equations of motion in state-space form for implementation in simulation. The constraint equations in Eqs.(4.40)–(4.43), in matrix form, are

$$\begin{bmatrix} \dot{\alpha}_1 \\ \dot{\gamma}_1 \\ \dot{\alpha}_2 \\ \dot{\gamma}_2 \end{bmatrix} = \mathbf{C}_G \begin{bmatrix} \dot{\theta}_1 \\ \dot{\theta}_2 \end{bmatrix} \tag{4.66}$$

where $\mathbf{C_G}$ is a 4×2 matrix and its entries are determined by inspection of Eqs.(4.40)–(4.43).

Note that all the matrices $\mathbf{E}_G{}^{-1}, \mathbf{B}_G, \mathbf{C}_G$, are constant with respect to time once radia and the moments of inertia of the gears are given. The dynamic model of the coupled planetary gear sets in GM Hydramatic 440 is Eqs. (4.63) and (4.64) where T_{S_1} is the applied torque on sun–1, T_{S_2} is the applied torque on sun–2, $T_{C_2R_1}$ is the applied torque on carrier–2, which is ring–1, and $T_{C_1R_2}$ is the applied torque on carrier–1, which is ring–2. The numerical values of the parameters of the planetary gear sets model, as implemented in simulation are given in Table 4.2. The coefficients in Eqs. (4.63) and (4.64) depend on the moment of inertia of all the gears, the mass and number of pinions, and the inertia of all the gears. These coefficients are constant for a given transmission and can be calculated as follows.

The applied torques included in Eqs. (4.63) and (4.64) are moments that are the results of the engagements of the clutches and bands, or the connection to the final drive. The reaction forces between the gears do not appear in the equations because they are constraint forces and the constraint equations are handled by the Lagrange method [28].

Note that, C_i and B_j refer to the i^{th} clutch and j^{th} band, respectively. From Fig. 4.1, it can be seen that sun–1 is connected to C_1, C_3 and C_4. Thus, the applied torque on sun–1 is

$$T_{S_1} = T_{S_1,C_1} + T_{S_1,C_3} + T_{S_1,C_4} \tag{4.67}$$

where $T_{i,j}$ is the torque acting on gear–i due to friction element–j, e.g., T_{S_1,C_1} is the torque acting on sun–1 due to clutch C_1. Note that torque due to friction elements are zero when they are not applied and will be discussed in detail in a subsequent section. Similarly, Fig. 4.1 shows that sun–2 is connected only to B_{12}. Thus,

$$T_{S_2} = T_{S_2,B_{12}} \tag{4.68}$$

Again, from Fig. 4.1, carrier–2 and ring–1, as one single rotating element, are connected to the final gear set only, which implies that

$$T_{C_2R_1} = T_{C_2R_1,FD} \tag{4.69}$$

Finally, carrier–1 and ring–2, together, are connected to C_2 and B_R. Thus,

$$T_{C_1R_2} = T_{C_1R_2,C_2} + T_{C_1R_2,B_R} \tag{4.70}$$

Table 4.2. Planetary Gear Set Parameters [3, 4, 5, 33]

Inertia Values			
Symbol	Definition	Numerical Value	Unit
I_{S_1}	Sun–1 lumped inertia	0.00102	$Kg \cdot m^2$
I_{S_2}	Sun–2 lumped inertia	0.00452	$Kg \cdot m^2$
$I_{C_1R_2}$	Carrier–1/Ring–2 lumped inertia	0.00902	$Kg \cdot m^2$
$I_{C_2R_1}$	Carrier–2/Ring–1 lumped inertia	0.005806	$Kg \cdot m^2$
I_{P_1}	Pinion–1 inertia	$6.7295 \cdot 10^{-6}$	$Kg \cdot m^2$
I_{P_2}	Pinion–2 inertia	$4.7637 \cdot 10^{-6}$	$Kg \cdot m^2$
Number of Teeth			
N_{S_1}	No. of teeth in sun–1 gear	26	
N_{R_1}	No. of teeth in ring–1 gear	62	
N_{P_1}	No. of teeth in pinion–1 gear	18	
N_{S_2}	No. of teeth in sun–2 gear	42	
N_{R_2}	No. of teeth in ring–2 gear	74	
N_{P_2}	No. of teeth in pinion–2 gear	16	
$N_{R_i} = N_{S_i} + 2 \cdot N_{P_i}\ , i = 1, 2$			
Radius			
R_{S_1}	Radius of sun–1 gear	0.019786	m
R_{R_1}	Radius of ring–1 gear	0.047182	m
R_{P_1}	Radius of pinion–1 gear	0.013698	m
R_{S_2}	Radius of sun–2 gear	0.031962	m
R_{R_2}	Radius of ring–2 gear	0.056314	m
R_{P_2}	Radius of pinion–2 gear	0.012176	m
$R_{R_i} = R_{S_i} + 2 \cdot R_{P_i}\ , i = 1, 2$			
Pinions			
m_{P_1}	mass of pinion–1 gear	0.060967	Kg
m_{P_2}	mass of pinion–2 gear	0.053199	Kg
n_1	Number of pinion–1 gear	4	
n_2	Number of pinion–2 gear	4	

4.2 Hydraulic System in Automatic Transmission

An hydraulic system in an automatic transmission consists of various components such as hydraulic pump, accumulators, valves and pressure regulators. This study focuses on a subsystem that is directly involved during shifting gears in an automatic transmission. As shown in Fig. 4.7, the simple hydraulic system for clutch C_2 consists of 1–2 upshift valve, supply transmission line pressure and clutch actuator. Supply transmission line pressure is assumed to have constant pressure and thus the transmission fluid inductance is neglected. The resistance in shift valve accounts for all the resistance including the resistance in the supply transmission line pressure. Shift valve is opened very fast and operating at high frequency. Thus, the solenoid is not considered in this study. Under these assumptions, the dynamic model of the simple hydraulic system is derived as follows.

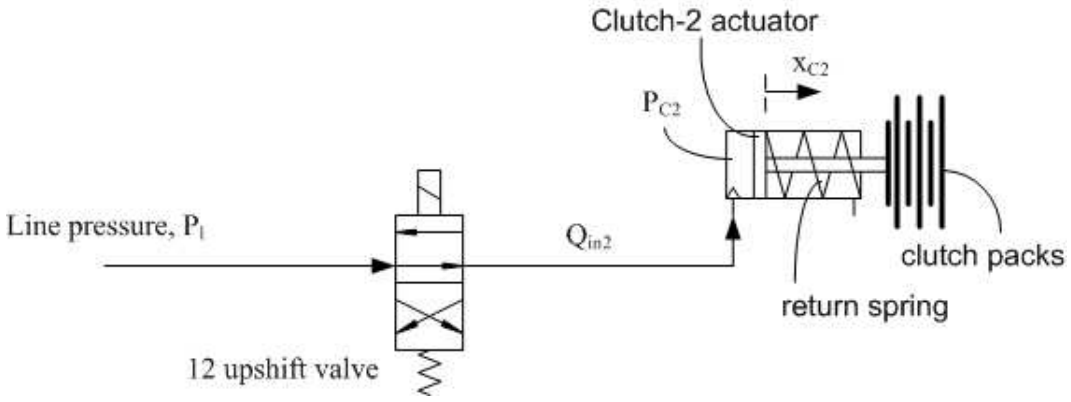

Figure 4.7. Simple Hydraulic System including 1–2 upshift valve, fluid line, clutch C_2 actuator and clutch packs.

The transmission fluid flowing through 1–2 upshift valve is assumed to have incompressible flow. The volumetric flow rate equation is

$$Q_{in} = C_d A \sqrt{\frac{2|P_l - P_C|}{\rho}} sign(P_l - P_C) \quad \text{for} \quad 0 \leq u \leq 1 \tag{4.71}$$

where

$$A = A_v^o u$$

when u is positive, the inlet port is opened while the exhaust port is fully closed.

$$Q_{out} = C_d A \sqrt{\frac{2|P_C - P_r|}{\rho}} sign(P_C - P_r) \quad \text{for} \quad -1 \leq u < 0 \tag{4.72}$$

when u is negative, the exhaust port is opened while the inlet port is fully closed.

The transmission fluid flows, with rate Q_{in}, from transmission line into the clutch cavity through the upshift valve orifice, A_v^o. The build–up pressure, P_C, in the clutch cavity compresses the spring in the clutch actuator. The transmission fluid flows, with rate Q_{out}, from the clutch cavity to transmission reservoir or transmission oil pan.

The net flow into and out of clutch is conserved. With the assumption that the transmission fluid bulk modulus is very large, the continuity of clutch cavity for incompressible flow implies

$$Q_{in} = A_C \ \dot{x}_C \tag{4.73}$$

Clutch actuator force balance equation, neglecting inertial and friction, is

$$P_C = \frac{k_C}{A_C} x_C + \frac{F}{A_C} \tag{4.74}$$

The pressure has to be adequate to overcome the clutch return spring and the clutch pack. The clutch pack including a number of clutches and a wave spring behaves like

Table 4.3. Hydraulic Actuator System Parameters

Symbol	Description	Value
k_C	clutch return spring rate	$111,400\ N/m$
$x_{C_{stk}}$	clutch return spring stroke	$2.941 \times 10^{-3}\ m$
$x_{C_{max}}$	the maximum deflection of clutch return spring	$4.611 \times 10^{-3}\ m$
k_w	wave spring rate	$5408 \times 10^3\ N/m$
A_C	clutch actuator area	$9.5411 \times 10^{-}3\ m^2$
A_v^o	orifice area of the shift valve	2.6273×10^{-6}
ρ	transmission fluid density	$840\ kg/m^3$
Cd	Orifice discharge coefficient	0.61
P_l	Transmission line pressure	$100\ kPa$

a spring. This spring will exert force, F, on the actuator after the force due to the fluid pressure exceeds the return spring which has deflection including preload, x_C, and clutch return spring rate, k_C. The clutch pack model is described as follow.

$$F = \begin{cases} 0 & if \quad 0 < x_C \leq x_{C_{stk}} \\ k_w(x_C - x_{C_{stk}}) & if \quad x_{C_{stk}} < x_C \leq x_{C_{max}} \end{cases} \tag{4.75}$$

When the clutch packs are pushed together and wave spring starts to stroke, F is determined by the second expression in Eq. (4.75). Wave spring rate accounts for all effects of the clutch pack and the wave spring between the clutch packs. The clutch actuator area is calculated by

$$A_C = \pi D_C^2/4 \tag{4.76}$$

4.3 Fast Hydraulic Actuation Technologies

The desired control pressure profile is generated by the hydraulic actuation system of the transmission. Traditional shift control systems manipulate the oil pressure on the clutch actuator by a control pressure valve, which is controlled by PWM (Pulse Width Modulation) solenoid valve. Traditional hydraulic actuation systems cannot

regulate pressure profile for a successful implementation of feedback control systems. It is obvious that faster actuation system are needed for feedback control. This section will demonstrate in detail the need for fast hydraulic actuation systems and discuss some new technologies that can potentially provide fast pressure regulation.

For traditional control systems in an automatic transmission with clutch-to-clutch shifts, the oncoming clutch fill process is a major source of uncertainty and it makes the clutch coordination during the shift a difficult task. The fill time of the oncoming clutch varies due to many factors, such as fluid temperature, solenoid valve characteristics, line pressure variations and elapsed time between shifts. The commanded fill pressure and the commanded fill time are critical to achieving a good fill and a smooth start to the shift process. Even small errors in these two parameters could lead to an overfill or an underfill, as shown schematically in Fig. 4.8. In Ref. [69], the speed and acceleration of the input and output shafts in a powertrain is used to detect the fill time. Some algorithms have been developed to detect the end of fill using speed signals but none of them has proven reliable and fast enough to prevent overfill spikes. An example of an oncoming clutch overfill during an upshift is shown in Fig. 4.9. The high oil pressure and high flow rate is applied to the oncoming clutch. With the improper detection of the end of fill, this event makes the transmission oil overfill. On the under hand, the oil underfill occurs when the detection misinterprets signals and leads to slow filling in oil pressure. In the past, an automatic transmission was equipped with a proportional PWM valve. A PWM valve operates on a duty cycle that comprises a percentage of time within a period of time during which the valve is open. The PWM valves are able to output the flow and pressure, by opening and closing during the duty cycle. PWM valves are more efficient to operate, but require greater bandwidth. It has delay in response to commanded signal due to physical interaction between pressure supply device and

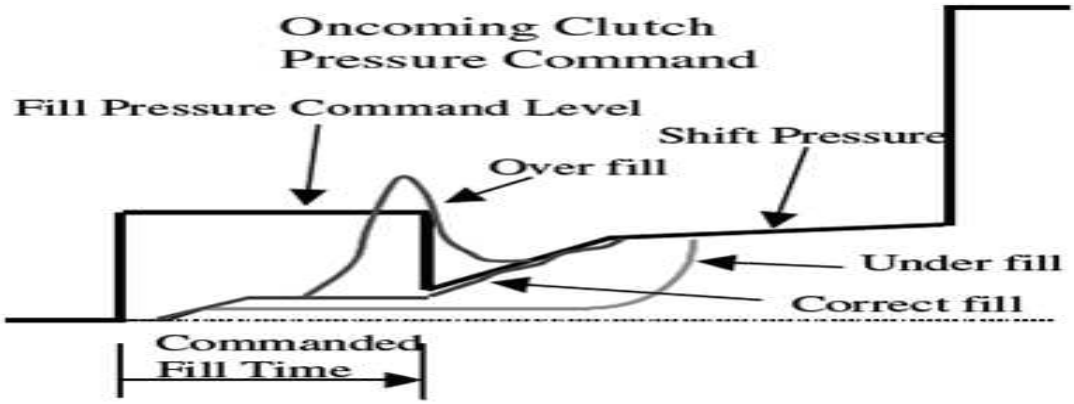

Figure 4.8. Variation in Clutch Fill Process [60].

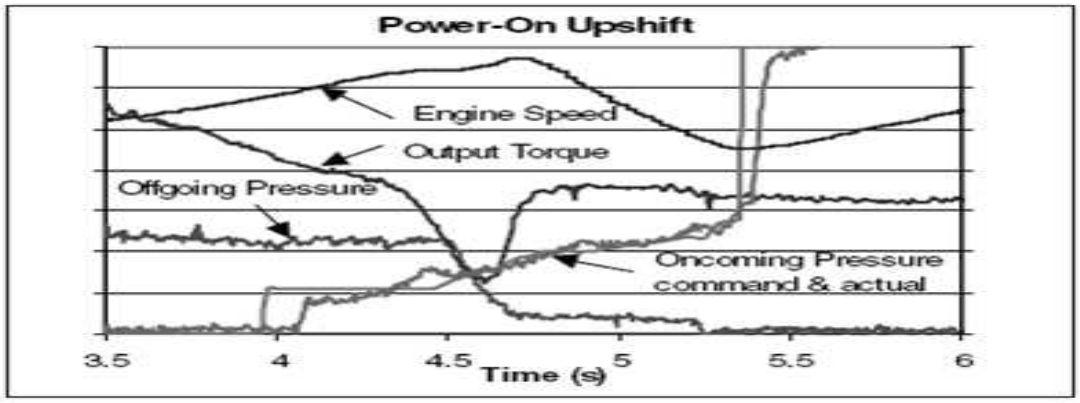

Figure 4.9. Effect of Clutch Overfill on an Upshift [60].

control device. The automatic transmission equipped with a PWM valve appears to have limitation in solenoid part which limits the hydraulic actuation system. Thus, alternative technologies are required to reduce the delay in response to commanded signals so that precise control pressure generated on the clutch/band surface can be achieved.

In the past decade, the proportional PWM valve was replaced by two faster valves for clutch actuation in an automatic transmission. Variable bleed solenoid (VBS) valves and variable force solenoid (VFS) valves are widely used now for better controllability. The VBS valve or proportional control solenoid valve attenuates the

pressure as a function of input current. Analytical modeling of proportional control solenoid valves was conducted using system identification theory in [82]. The PCSV characteristics is analyzed as illustrated in Fig. 4.10. It has bandwidth around 10 Hz. Ref. [82] concludes that the valve bandwidth was limited by the bandwidth of the electromagnetic portion of the solenoid. This implies that the valve can be fully opened approximately in 100 ms. Variable force solenoid (VFS) valves are also used in some transmissions. VFS is studied in Refs. [59] and [83]. In Ref. [59], it is shown that the VFS valve can be fully opened in 100 ms when it is tested with a step input from 0 to 50 psi as shown in Fig. 4.12. Its natural frequency is around 10 Hz as shown in Fig. 4.11. In Ref. [83], VFS valve is studied with a different set–up which shows that the valve can be fully opened in 16 ms. VBS and VFS valves are also known as proportional valves because they regulate pressure based on the valve being open or partially open. However, VBS valves suffer from hysteresis and variations due to temperature. To further enhance system performance, fast and precise valve actuation devices are needed. A new concept for an on/off valve with rotary actuator was proposed to handle flow rate greater than 10 lpm with less than 5 ms response time [84], as illustrated in Fig. 4.13. A key feature of this concept is that the valve has a single stage construction, but performs as a two-stage valve. Figure 4.14 shows the schematics and cross section view of this valve.

Alternative clutch actuation technologies were also pursued to replace the electro-hydraulic actuators in automatic transmissions to improve fuel economy and performance. Motor driven clutch actuation has been investigated by a number of researchers [85]. The major challenges for the electromechanical actuators are the low power density and available electrical power inside the vehicle. Usually, some kind of gearing is required to amplify the torque capacity of the motor.

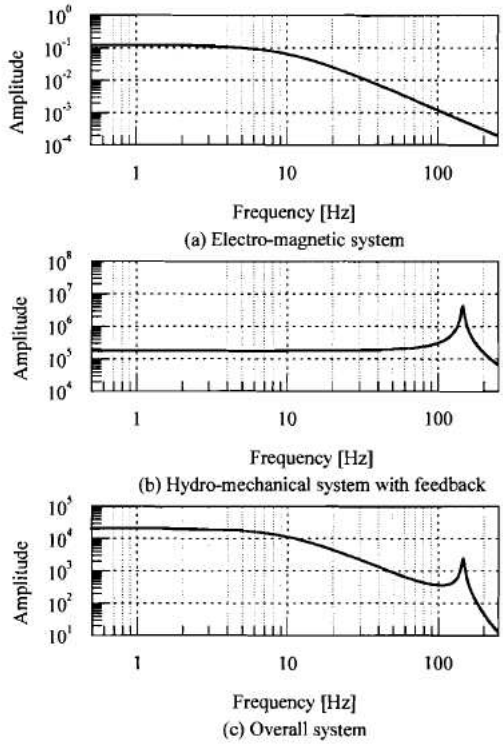

Figure 4.10. Frequency Response of the Overall System for PCSV [82].

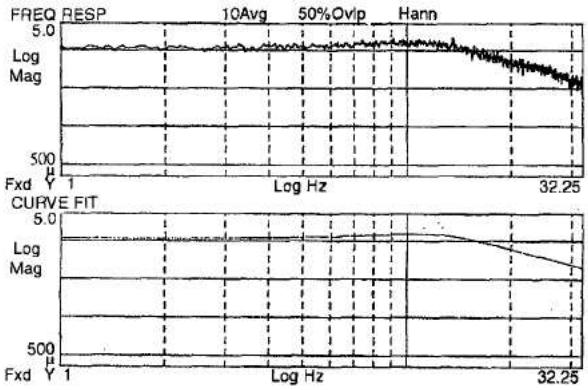

Figure 4.11. Frequency Response and the Identified Function Plot for VFS Solenoid [59].

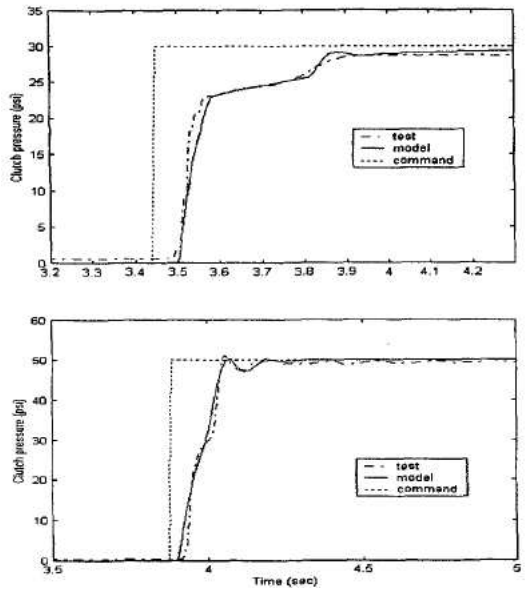

Figure 4.12. VFS Valve Validation Data for Solenoid and Clutch [59].

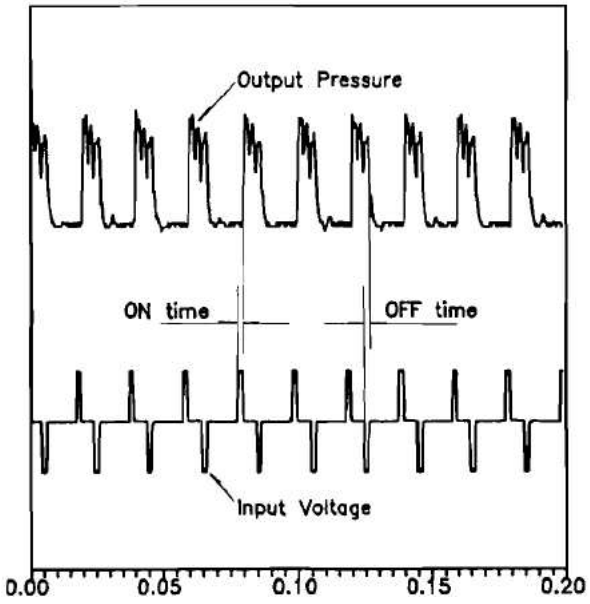

Figure 4.13. Illustration of ON/OFF Time calculation [84].

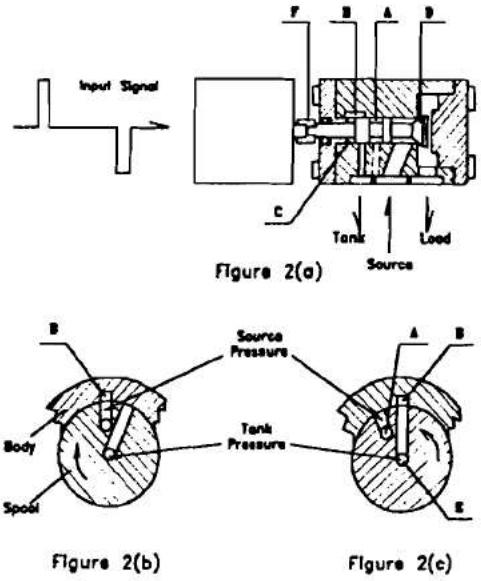

Figure 4.14. High Speed On/Off Valve Schematic and Cross Sectional Views [84].

Smart material based clutch actuation devices were also developed by a number of researchers. Feasibility of using electrorheological (ER) fluid clutch inside automotive transmission was investigated and desirable properties of ER fluid were proposed for future research [86]. Magnetic powder clutch was used as a starting clutch for a CVT equipped vehicle [87]. Potential applications of magnetorheological (MR) fluid clutch were discussed [88].

There are many research and development studies in both control algorithm and hardware to improve the actuation technology in the automotive transmission. The key to any successful development is the integration of software and hardware systems.

4.4 Friction Elements

Basically, the clutches and bands in an automatic transmission are represented as classical friction model. The characteristic of this model is as shown in Fig. 4.15. The friction is proportional to the normal force to the contact surfaces of two bodies. While this represents the ideal friction model, it gives rise to discontinuity problem in numerical solution in zero velocity region. To eliminate this problem, the steep curve in the neighborhood of zero velocity region is introduced as shown in Fig. 4.16. Additionally, outside the small velocity neighborhood, the friction is modeled as a function of the velocity, which is called "Stribeck effect" [47]. However, this model still has drawbacks including numerical simulation problem and physical fault representation [48, 49, 50].

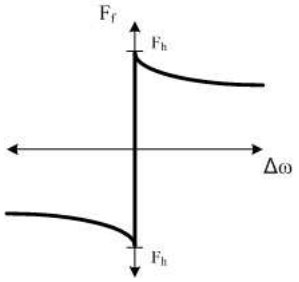

Figure 4.15. Classical Friction Model.

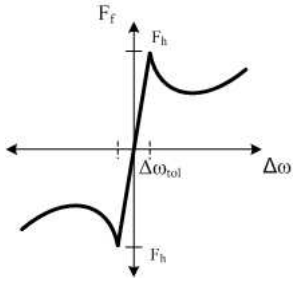

Figure 4.16. Stribeck Friction Model.

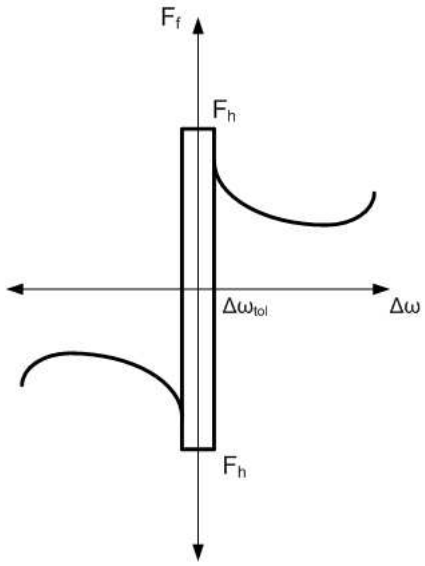

Figure 4.17. Karnopp's Friction Model.

There are many models developed to handle the problems in the classical friction model. These approaches are known as dynamic friction models, which are studied and developed in various references including [47, 49, 51, 52, 53]. Dahl friction model primarily reported in [51] develops the friction model from stress–strain characteristics in solid mechanics. The connection between two surfaces is modeled as spring and damper. Therefore, in this model, the friction force is proportional to displacement. An extension of Dahl friction model is Lugre friction and Bliman–Sorin model [54]. These models represent many characteristics of friction phenomena. However, the models are quite difficult to apply to a complicated dynamic system such as in an automatic transmission. In [49], the bristle model and reset integrator model are presented. The models capture the behavior of the friction in microscopic level where the contact points between two surfaces are viewed as bonds between flexible bristles. As surfaces move, the strains in the bonds increase and the bristles act as springs, which give rise to the friction force. Due to complexity, the bristle model consumes a

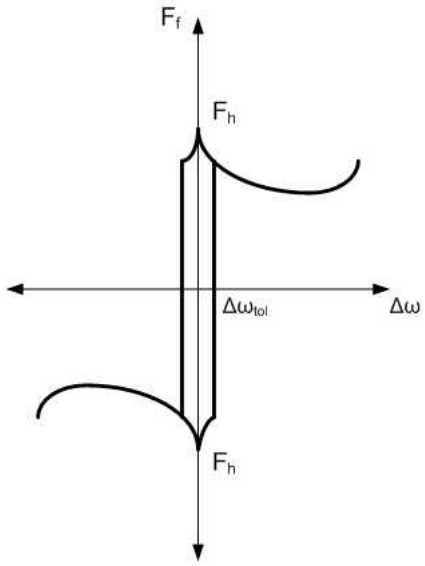

Figure 4.18. Modified Woods Static and Dynamic Friction Model.

lot of simulation time while the reset integrator model has a discontinuous function in the model that requires numerical algorithm to be carried carefully [55, 56]. Karnopp's model eliminates the discontinuity in ideal Coulomb friction model while be able to implicate stick-slip behavior of a system with friction[48].

Woods static and dynamic friction model is based on the Coulomb friction model for dry friction [89]. This model is a three–state logic function of the differential velocity and the forces that could pass through it as shown in Fig. 4.19. If the forces are larger than the torque capacity of the friction element or if there is a velocity difference already, then the friction force is constant and the normal differential equations governing the analyzed system are in effect. However, if the velocity difference is near zero and the forces applied to the friction element are smaller than the torque capacity, then there is a "capture" of the motion such that there is no velocity difference in the element. The element can come out of capture when the forces applied to it exceed the friction value. When the element is in capture, the velocity difference is zero and the acceleration of the masses connected by the friction

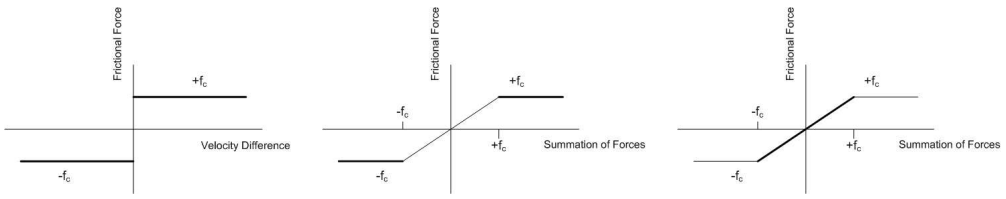

Figure 4.19. Woods Static and Dynamic Friction Model.

element should be identical. In such a case, the number of states of the system drops by one and a new set of reduced–order differential equations should be defined. There are three distinct operational states for Coulomb friction: in motion, in capture but about to accelerate out of capture, in capture but insufficient forces to accelerate into motion. Notice that we need to know the definitions of velocity difference and the summation of forces to get the proper signs for the logic function. Also, the minimum velocity difference should be defined. This minimum velocity determines when the velocity difference will go to zero, which prevents any computer simulation error due to any non–zero speed difference.

Even through there are many accurate friction models in the literature, Woods static and dynamic friction model is the preferred one in this study over other friction models when it comes to stick–slip behavior prediction and simulation accuracy. Therefore, in this research the clutches and bands are modeled by Woods static and dynamic friction model to overcome the numerical difficulties in zero velocity neighborhood, which would happen when the classical friction model is used.

4.5 Classical and Woods Static and Dynamic Friction in Clutch and Band

In this section, the implementation of the friction models in modeling friction elements of automatic transmission is explained, using a simple system of two shafts connected through a clutch. The hydraulic system described in Section 4.2 is used

to generate the pressure on the clutch. The clutch is modeled by Woods static and dynamic friction model.

Coulomb friction or dry friction model describes friction force that occurs between two connecting surfaces when a moving body slips over another body or a stationary body has a tendency to slip over another body. Coulomb friction model approximates the friction force as a coefficient of friction, μ, multiplied by the normal force, N, which is the contacting force between the two surfaces. The coefficient of friction, μ, depends on the material properties and surface characteristics. For two bodies with relative speed on the contacting surfaces, the coefficient of friction is determined as the coefficient of kinetic friction, μ_k. For two bodies with zero relative speed, the coefficient of friction is determined as the coefficient of static friction, μ_s. In general, the coefficient of static friction, μ_s, is greater than or equal to the coefficient of kinetic friction, μ_k. Therefore, the two bodies begin to move apart when the applied force exceeds the friction forces $\mu_s N$ or the breakaway force level, F_h as seen in Fig. 4.15. Once the bodies start moving, the friction force becomes $\mu_k N$. Figure 4.15 illustrates this ideal friction model. However, this friction model has discontinuity at zero relative speed. This causes numerical problems in computer simulation. As seen in Fig. 4.15, at zero relative speed, the friction force is not unique. In simulation of discontinuous dynamic system such as this one, the simulation software such as Matlab/Simulink will experience sudden appearance of an eigenvalue located far out to the left in the complex plane due to very steep gradient in the discontinuous differential equations. In a numerical software with variable step size, its step-size control algorithm will try to reduce the step-size. However, the new eigenvalue cannot be easily solved. The algorithm finally quits solving for the new eigenvalue, as its step size is either reduced to the smallest tolerance value or the step size control is fooled. The integration algorithm recognizes the discontinuity as a singular point

of stiffness. As a consequence, the discontinuity is passed through with a very small step size. The algorithm judges the solution to be correct, even though the solution might be incorrect. Other possible phenomena is that the algorithm might not be able to recognize the discontinuity and pass over the point of discontinuity [55, 56].

To deal with this problem, the classical friction model or generalized Stribeck friction model is introduced [47, 48, 49, 50, 90]. In this model, as shown in Fig. 4.16, a steep straight line in small relative speed region replaces the friction curve around the zero relative speed. The friction force, now, is a unique function of the relative speed.

As stated earlier, different speed and torque ratios in a transmission are easily achieved by alternating input, output, stationary components and holding elements. This is done by an electronic unit, engaging and/or disengaging various friction elements such as clutches and bands through the hydraulic system. The amount of hydraulic pressure applied on a friction element determines the maximum amount of torque that the friction element can transmit, which is known as "the torque capacity of a friction element". To engage a friction element, its torque capacity should be increased more than the torque it needs to transmit in a given driving condition. The torque capacity is reduced to zero, by releasing its hydraulic pressure, to disengage a friction element.

Using the classical friction model, the friction elements are modeled as Coulomb friction torque where the amount of friction torque is a function of contact area, friction coefficient, and pressure applied to the friction elements. To avoid the singularity

present in the Coulomb friction model, torque friction is represented as a two–folded saturation function, $T = f_{TC}(\Delta\omega, T_{cap^+}, T_{cap^-})$ as (see Fig. 4.20 for the depiction)

$$f_{TC}(\Delta\omega, T_{cap^+}, T_{cap^-}) = \begin{cases} T_{cap^+} & , \quad \Delta\omega > \omega_{tol} \\ \frac{T_{cap^+}}{\omega_{tol}}\Delta\omega & , \quad 0 \leq \Delta\omega \leq \omega_{tol} \\ \frac{T_{cap^-}}{\omega_{tol}}\Delta\omega & , \quad -\omega_{tol} \leq \Delta\omega \leq 0 \\ T_{cap^-} & , \quad \Delta\omega < -\omega_{tol} \end{cases} \tag{4.77}$$

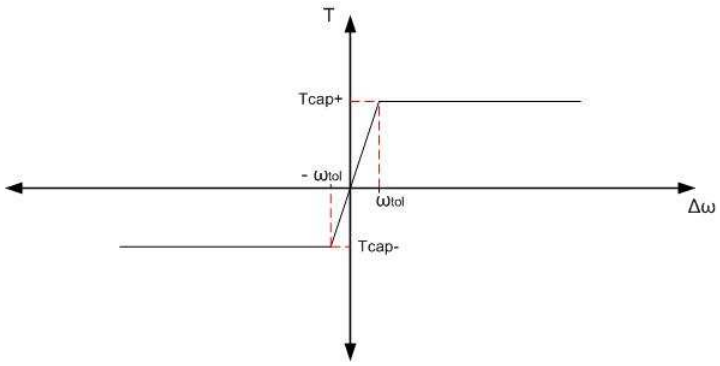

Figure 4.20. Friction element torque.

where T_{cap^+} and T_{cap^-} are the torque capacities adjusted by pressure increase or decrease through the hydraulic system, $\Delta\omega$ is the relative speed and ω_{tol} is a simulation parameter set to a very small number as the relative speed tolerance, for example, ω_{tol} is 0.001 rad/s in the simulations that use this friction model. For clutches, $T_{cap^+} = T_{cap^-}$ while $T_{cap^+} \neq T_{cap^-}$ for bands as bands may have more torque friction capacity in one direction than the other. For one–way clutches, either T_{cap^+} or T_{cap^-} is zero depending on the sprag direction.

There are still some issues in the implementation of this friction model in simulation. Improper simulation results may occur when the bodies move into the small relative speed region. This model allows the bodies to move even though the net

sum of external force is less than the breakaway force level, F_h. As a result, it cannot predict the static behavior. Therefore, this model cannot predict limit cycle or other effects associated with stick-slip phenomena. Additionally, the simulation time is increased if a larger slope is used in the small relative speed region. Karnopp's model eliminates the discontinuity in ideal Coulomb friction model while be able to implicate stick-slip behavior of a system with friction. As illustrated in Fig. 4.17, this model introduces a finite neighborhood of zero velocity where static friction occurs. Outside the neighborhood, the kinetic friction is a function of velocity. Inside the neighborhood, velocity is set to zero and the static friction force is determined by the other elements in the system. If the friction force exceeds the breakaway force level, F_h, then the friction switches to slipping mode [48].

The friction model adopted here is modified from Woods static and dynamic friction model, as shown in Fig. 4.18. This model inherits stick-slip behavior within the finite neighborhood of zero velocity. Outside the neighborhood where the friction is in slipping mode, the friction is a function of the velocity which happens according to Stribeck effect. However, to account for Stribeck effect, this friction model uses a function from [57], instead of the function used in Refs. [50] and [47]. As illustrated in Fig. 4.22, the coefficient of friction is a function of the relative speed.

In this model, dynamic torque, T_d is defined as Coulomb friction torque occurring between two contacting surfaces that are rotating relatively to each other. The magnitude of the dynamic torque is proportional to axial force across the clutch surface and the fiction coefficient which is a function of velocity [57]. The direction of the dynamic torque opposes the relative motion of the rotating objects.

Throughput or static torque, T_{tp} is defined as friction torque occurring between two contacting surfaces that have zero relative speed. Two objects rotate together, with the equal speed in the same direction. The throughput or static torque in

this case no longer depends on the friction coefficient and normal force. The static torque is calculated from all the external torques applied to the system with the direction against the rotation. The throughput torque is limited to the value of breakaway toque, T_h. However, in this study, the value of the dynamic torque, T_d, when the relative speed goes to zero, is used instead of T_h. To account for the stiction event which is greater than the friction torque/force during in–motion mode, the approximation is made by using the friction coefficient function available in Ref. [58]. Thus, the value of T_d and T_h are approximately the same value in the region of zero relative speed. Using T_d as the value of breakaway torque does not cause the error in the simulation result, but it enhances the transition event when the friction modes are changed. The available data for coefficient of friction for wet clutch that is needed to calculate for T_d can be obtained from Ref. [58]. For a single-mass system, the static torque is equal to the value of applied torque to the mass with the opposite direction [89]. For a multi–mass and multi–friction system, the procedure is demonstrated in the next section.

Woods static and dynamic friction model for dry friction is a three–state logic function of the relative speed and torque that could pass through the friction element. Three distinct operational modes are “In–Motion”, “Captured but Accelerating” and “Captured and Static” as shown in Fig. 4.21.

4.5.1 In–Motion Mode

When two contacting objects have relative speed, they are considered to be in “in–motion mode”. In this mode, Coulomb friction torque is proportional to clutch pressure, piston area, effective radius of clutch plates or band drum, number of clutch surfaces and the coefficient of friction. The coefficient of friction is dependent of the

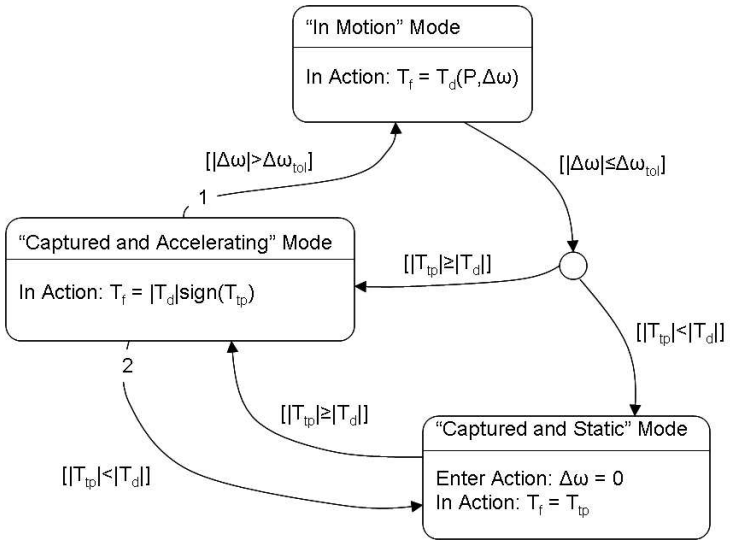

Figure 4.21. New Friction Model Modes.

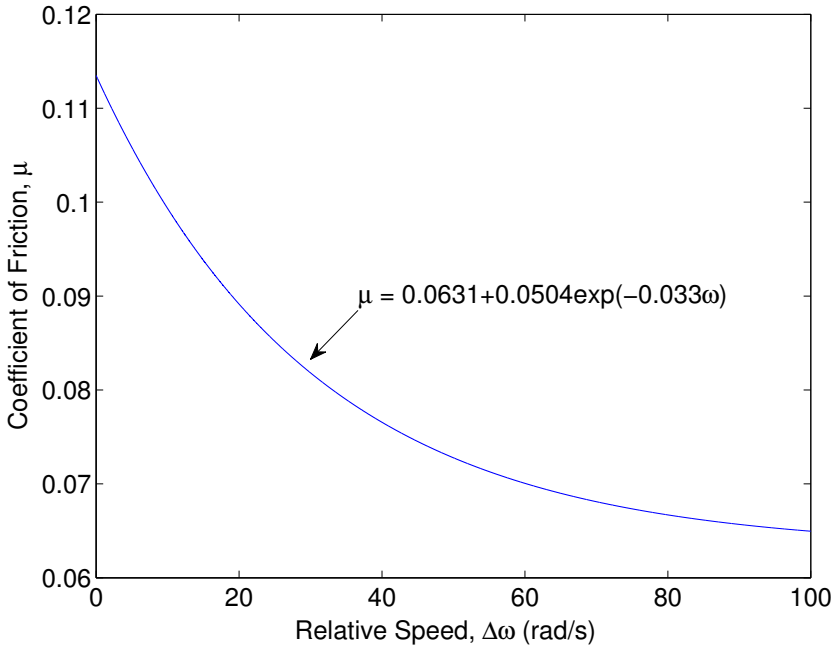

Figure 4.22. Coefficient of Friction Versus Relative Speed for Wet Clutches [58].

relative angular velocity, as shown in Fig. 4.22, and has a direction against the motion of the objects. In this state, the coulomb friction torque is given by

$$\begin{aligned} \text{If} \quad |\Delta\omega| &> \Delta\omega_{tol} \ , \qquad \text{then} \\ T_f &= T_d \end{aligned} \tag{4.78}$$

where

$$T_d = \begin{cases} P_C \ A \ r \ n \ \mu \ sign\Delta\omega & for \ clutch \\ P_C \ A \ r \ n \ (\exp^{\mu\alpha} - 1) \ sign(\Delta\omega) & for \ band \end{cases} \tag{4.79}$$

where

T_f = friction torque

T_d = dynamic torque

P_C = hydraulic pressure applied to clutch actuator

A = actuator area

r = effective radius of clutch plate and band drum

n = number of clutch surfaces

μ = coefficient of friction

α = effective wrap angle of the band around a drum

$\Delta\omega$ = relative angular velocity

4.5.2 Captured and Accelerating Mode

This mode occurs when the relative speed between two contacting objects is less than or equal to $\Delta\omega_{tol}$ but the throughput torque is greater than the breakaway

torque. Therefore, the objects are accelerating out of capture. In this mode, the friction torque is given by

$$\begin{aligned} \text{If} \quad |\Delta\omega| &\leq \Delta\omega_{tol} \quad \text{and} \quad |T_{tp}| \geq |T_d|, \quad \text{then} \\ T_f &= T_{ca} \end{aligned} \tag{4.80}$$

where

$$T_{ca} = |T_d| \; sign \; (T_{tp}) \tag{4.81}$$

4.5.3 Captured and Static Mode

In this mode, two contacting objects have relative speed equal to zero, the friction torque is exactly the same magnitude and direction as the throughput torque, T_{tp}. When the throughput torque, T_{tp} exceeds the breakaway friction torque while the relative speed is still in the zero velocity region, the system leaves "Captured and Static" mode and moves into "Captured and Accelerating" mode. When the relative speed is greater than $\Delta\omega$ and the surfaces of the two objects start moving relative to each other, the Coulomb friction switches to "In–Motion" mode.

$$\begin{aligned} \text{If} \quad |\Delta\omega| &\leq \Delta\omega_{tol} \quad \text{and} \quad |T_{tp}| < |T_d|, \quad \text{then} \\ \Delta\omega &= 0 \end{aligned} \tag{4.82}$$

$$T_f = T_{cs} \tag{4.83}$$

where

$$T_{cs} = T_{tp} \tag{4.84}$$

In Captured and Static mode, the friction is independent from the normal forces applied to the clutch plates. For a single-rotating inertia system, the friction in the captured and static condition has the same magnitude as the applied torque to the shaft, but it has the opposite direction. For the multi-mass and multi-friction systems

such as planetary gear sets, the calculation of the throughput torque is more involved and will be explained in Sections 4.6, 4.7 and 4.8.

4.6 Application to a System of Two Shafts

Figure 4.23 depicts a system of two shafts connected together by a clutch. This system analyzed using a lumped-parameter model. The clutch in this system consists of two plates that are used to transmit torque between shaft–1 and shaft–2. The clutch is modeled as explained in Section 4.5.

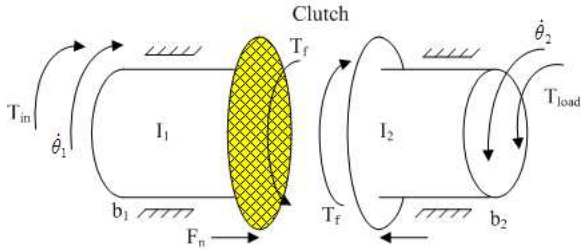

Figure 4.23. Two shafts connected by a clutch.

The differential equations representing the dynamics of two shafts coupled by the clutch are

$$\ddot{\theta}_1 = -\frac{b_1}{I_1}\dot{\theta}_1 + \frac{1}{I_1}T_{in} - \frac{1}{I_1}T_f \tag{4.85}$$

$$\ddot{\theta}_2 = -\frac{b_2}{I_2}\dot{\theta}_2 + \frac{1}{I_2}T_f - \frac{1}{I_2}T_{load} \tag{4.86}$$

where T_{in} is the input torque at the shaft–1, T_{load} is the load at the shaft–2 and T_f is the Coulomb friction torque on the clutch. Shaft–1 and Shaft–2 have the moments of inertia, I_1 and I_2, respectively. Both shafts have rotational damping constant, b_1 and b_2, respectively.

In addition to the relative angular velocity, the throughput torque is a factor determining transitions between the modes. In Captured and Static mode, the two

shafts coupled by the clutch rotate together, and thus have the same speed and acceleration. This implies, along with, Eqs. (4.85) and (4.86), that

$$\ddot{\theta}_1 - \ddot{\theta}_2 = -\frac{b_1}{I_1}\dot{\theta}_1 + \frac{b_2}{I_2}\dot{\theta}_2 + \frac{1}{I_1}T_{in} - (\frac{1}{I_1} + \frac{1}{I_2})T_f + \frac{1}{I_2}T_{load} = 0. \tag{4.87}$$

This is a simple algebraic equation, which can be solved for the only unknown, T_f. In this mode, the friction torque, T_f, is equal to the throughput torque, T_{tp}, which is used, along with the relative angular speed, to determine the friction modes.

$$T_f = \frac{I_2 T_{in} + I_1 T_{load} + (I_1 b_2 - I_2 b_1)\dot{\theta}_1}{I_1 + I_2} \tag{4.88}$$

$$T_{tp} = T_f \tag{4.89}$$

As shown in Fig. 4.23, shaft–1 and shaft–2 are connected via a clutch. Input torque, T_{in}, is the applied torque on Shaft–1 and load torque, T_{load}, is the applied torque on shaft–2. T_{in} and T_{load} are assigned as a function of time as shown in Fig. 4.24. T_{in} and T_{load} are applied at the beginning of simulation. However, T_{in} is reduced to zero at 6 seconds while T_{load} stays acting on shaft–2. The load torque on shaft–2 has slightly change which is enough to move shaft–2 from shaft–1.

At the initial time, the upshift valve is opened, as seen in Fig. 4.25. The transmission fluid is passed into the clutch cavity, as shown in Fig. 4.26. The pressure that builds up in the clutch cavity pushes the clutch plates together. At this moment, the relative speed at the clutch is still grater than the speed tolerance, $\Delta\omega_{tol}$. Coulomb friction is in "In–Motion" mode where flag number, i, is 1. Note that flag number in Fig. 4.27 indicates the friction mode. The friction torque in this mode depends on the applied pressure, which is being raised to about the magnitude of the line pressure. After the pressure on the clutch increases, as shown in Fig. 4.26, the input shaft and the output shafts are accelerating to have the synchronous angular velocity as shown in Fig. 4.27. When the relative angular velocity between two shaft are less than or

equal to the relative speed tolerance, $\Delta\omega_{tol}$, the friction mode would change to either "captured and acceleration" or "captured and static" modes. Once the throughput torque, T_{tp}, is equal to or greater the breakaway torque T_h, the friction mode is in "Capture and Accelerating" mode where flag number in Fig. 4.27 is 2. Note that in this friction model, the breakaway torque, T_h is approximated by the dynamic friction torque, T_d, which is computed by the available data in [58]. The friction torque, T_f is the same amount as the breakaway torque, T_h, but with the same direction as the throughput torque, T_{tp}. When the throughput torque, T_{tp}, is less than the breakaway torque, T_h, the friction is in "Captured and Static" mode where flag number in Fig. 4.27 is 3. The friction torque, T_f, is equal to the throughput torque, T_{tp}. Figs. 4.28 and 4.29 show a close–up view of the shaft speeds when the shafts couple and break away, respectively.

Figure 4.30 shows the friction torque, the torque capacity and the throughput torque at the clutch. It is the breakaway level of friction torque, T_h, that defines the maximum amount of the friction torque that a clutch/band can hold. Thus, it is called as "torque capacity, T_C" which is the maximum possible friction toque that can occur on the clutch surface. In our research, T_h is assumed to have the same value as dynamic torque, T_d. During "In–Motion" mode, the friction torque is dynamic torque, T_d, which has the same direction and magnitude as the torque capacity. During "Captured and Accelerating" mode, the friction torque T_f is the same amount as the torque capacity, T_C, but with the same direction as the calculated static torque, T_{tp}. During "Captured and Static" mode, the friction torque, T_f, is equal to the throughput torque, T_{tp}. Notice from Fig. 4.30 also that, the magnitude of the friction torque drops from the higher value supplied during "In–Motion" mode to a value that is necessary to keep the two shafts rotating at the same rate. Note

Table 4.4. Coulomb Friction Logic Function

Mode	**Flag,i**	**logic function**	**differential equation**
In–Motion	1	If $\|\Delta\omega\| > \|\Delta\omega_{tol}\|$, then $T_f = T_d$ $T_d = P(t)\ A\ r\ n\ \mu\ sign\ (\Delta\omega)$	$\ddot{\theta}_1 = -\frac{b_1}{I_1}\dot{\theta}_1 + \frac{1}{I_1}T_{in} - \frac{1}{I_1}T_f$ $\ddot{\theta}_2 = -\frac{b_2}{I_2}\dot{\theta}_2 + \frac{1}{I_2}T_f - \frac{1}{I_2}T_{load}$
Captured and Accelerating	2	If $\|\Delta\omega\| \leq \|\Delta\omega_{tol}\|$, then and $\|T_{tp}\| \geq \|T_d\|$ $T_f = \|T_d\|\ sign\ (T_{tp})$	$\ddot{\theta}_1 = -\frac{b_1}{I_1}\dot{\theta}_1 + \frac{1}{I_1}T_{in} - \frac{1}{I_1}T_f$ $\ddot{\theta}_2 = -\frac{b_2}{I_2}\dot{\theta}_2 + \frac{1}{I_2}T_f - \frac{1}{I_2}T_{load}$
Captured and Static	3	If $\|\Delta\omega\| \leq \|\Delta\omega_{tol}\|$,then and $\|T_{tp}\| < \|T_d\|$ $T_f = T_{tp}$	$\ddot{\theta}_1 = -\frac{b_1}{I_1}\dot{\theta}_1 + \frac{1}{I_1}T_{in} - \frac{1}{I_1}T_f$ $\ddot{\theta}_2 = \ddot{\theta}_1$ $\dot{\theta}_2(t_k) = \dot{\theta}_1(t_k)$ where t_k=time instant of transition to this mode

that for a two–way clutch, the torque capacity has both positive and negative values due to the capability to resist the rotation in both direction.

A significant moment of the simulation is when the friction model changes mode. The differential equations representing the system dynamics switch from one to another as shown in Table 4.4. When the system is in captured and static mode, the angular velocity of the output shaft in next step time should be exactly the same as the angular velocity of the input shaft. In order to have the both shafts rotate with same speed in the next step time, the integral state (angular velocity) of the output shaft is reset to the angular velocity of the input shaft as shown closely in Fig. 4.28. The output shaft has less moment of inertia. Thus, the angular speed in next step time of the output shaft is assumed to be the same as the angular speed

of the input shaft, which has larger moment of inertia. The clutch starts to slip when the throughput torque, T_{tp}, at the clutch exceeds the breakaway level or the torque capacity as shown in Figure 4.29. The friction mode switches to "Captured and Accelerating" mode and later to "In–Motion" mode due to the releasing of the pressure in the clutch cavity as shown in Fig. 4.26.

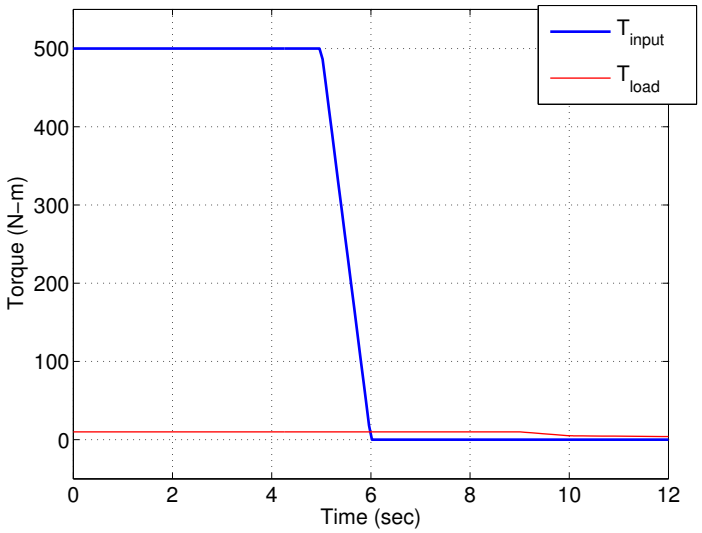

Figure 4.24. Input Torque at Shaft–1 and Load Torque at Shaft–2.

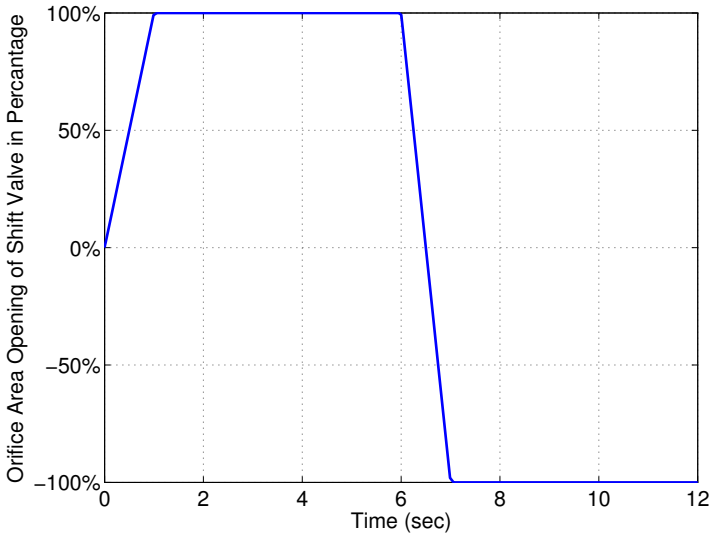

Figure 4.25. Orifice Area Opening of Shift Valve in Percentage.

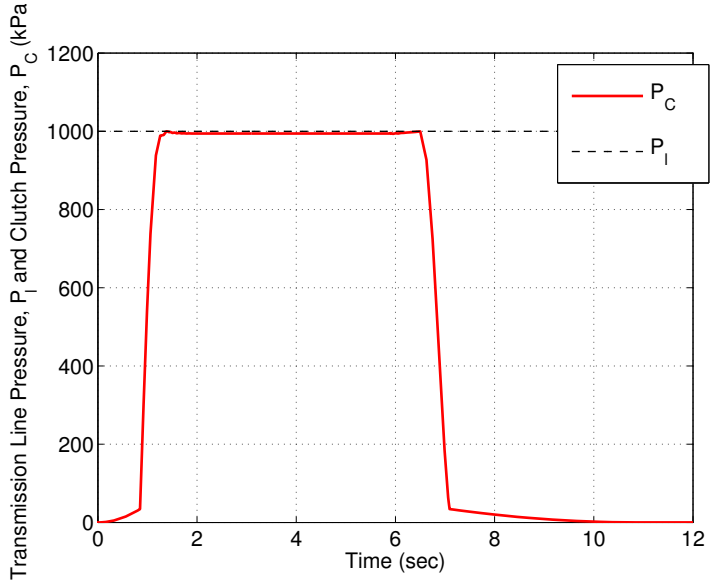

Figure 4.26. Line Pressure and Pressure applied on the Clutch.

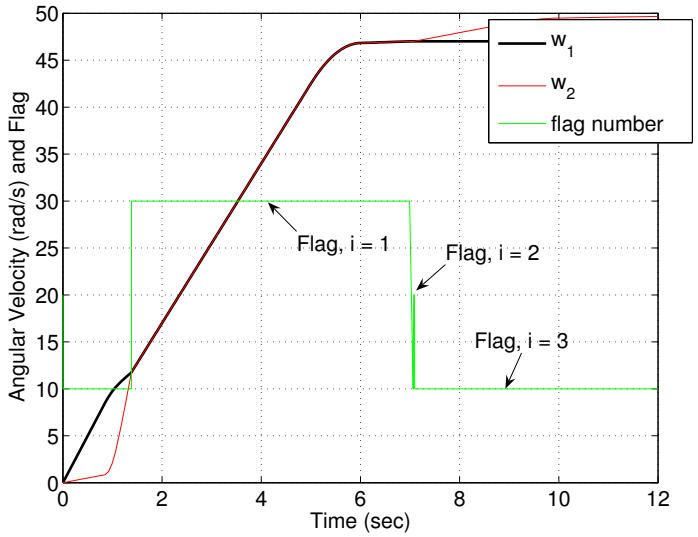

Figure 4.27. Input Shaft and Output Shaft Angular Velocities.

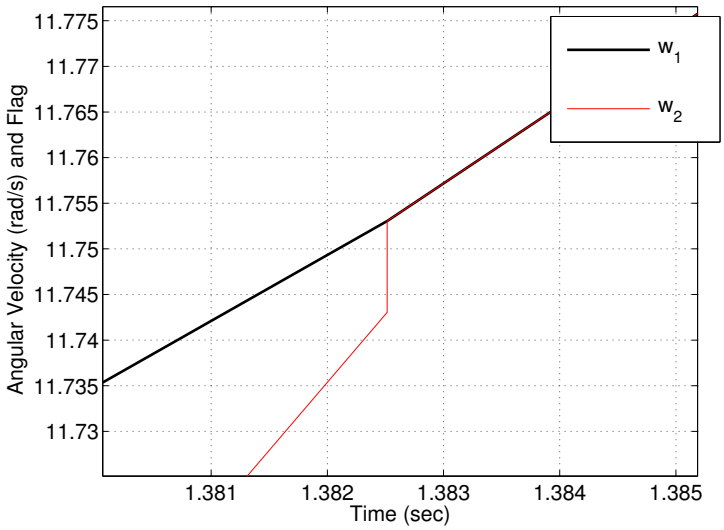

Figure 4.28. Enlarged View when the Shaft–1 and Shaft–2 become the Synchronous Angular Velocity.

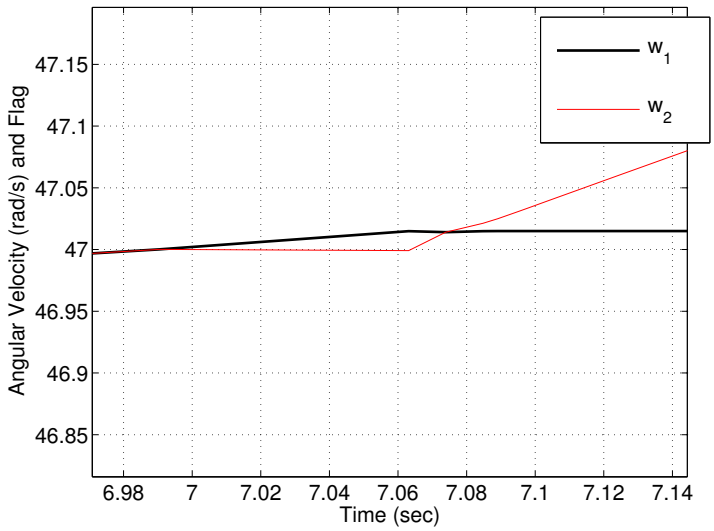

Figure 4.29. Enlarged View when the Shaft–1 and Shaft–2 break apart.

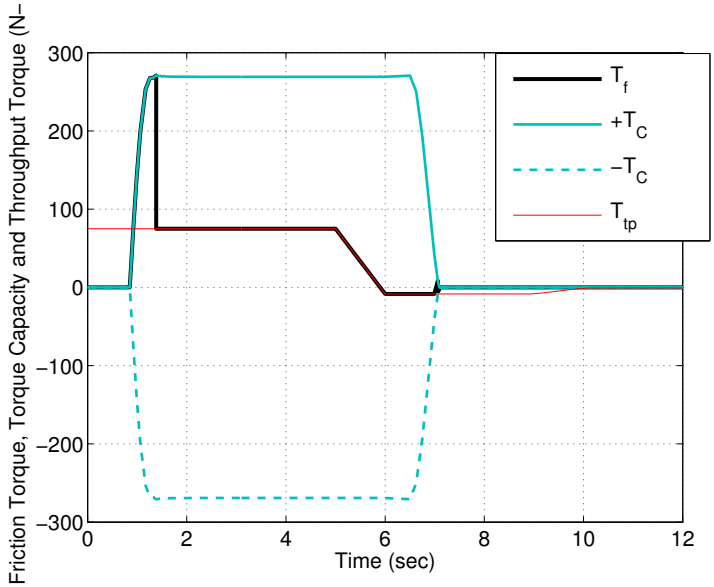

Figure 4.30. Torque Capacity and Coulomb Friction Torque at the Clutch.

4.7 Three Shafts Connected by Two Clutches

A system of three shafts connected by two clutches, as illustrated in Fig. 4.31, is analyzed. Analysis of this system will facilitate transitioning to the analysis of planetary gear set, which consist of multiple shafts connected through multiple friction elements. Similar to the system of two shafts, the coulomb friction model with three distinct modes is used at clutch–1 and clutch–2.

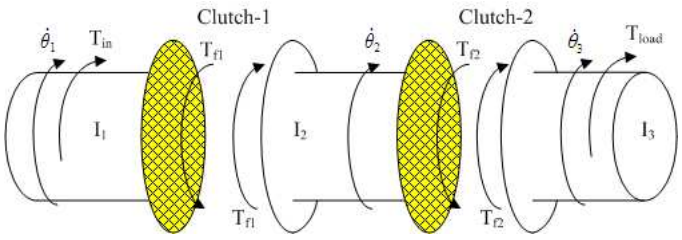

Figure 4.31. Three shafts connected by two clutches.

The differential equations representing the dynamics of three shafts connected by two clutch are

$$\ddot{\theta}_1 = \frac{1}{I_1}T_{in} - \frac{1}{I_1}T_{f1} \tag{4.90}$$

$$\ddot{\theta}_2 = \frac{1}{I_2}T_{f1} - \frac{1}{I_2}T_{f2} \tag{4.91}$$

$$\ddot{\theta}_3 = \frac{1}{I_3}T_{f2} + \frac{1}{I_3}T_{load} \tag{4.92}$$

where T_{in} is the input torque at the shaft–1, T_{load} is the load at the shaft–3, T_{f1} is the Coulomb friction torque on the clutch–1 and T_{f2} is the Coulomb friction torque on the clutch–2. The shaft–1, –2 and –3 have the moments of inertia, I_1, I_2 and I_3, respectively. For simplicity, torsional spring and rotational damper in these three shafts are neglected.

According to the coulomb friction model, each clutch can be in one of the three different modes, “in–motion”, “capture and accelerating” and “captured and static”.

Therefore, there are $3^2 = 9$ possible cases for this system of two clutches, as shown in Table 4.5. The case number, i, indicates which friction mode each clutch is as follows. When i is 1, the clutch is in dynamic mode. When i is 2, the clutch is in captured and accelerating. When i is 3, the clutch is in captured and static. Angular velocity of the shaft with less inertia is reset to that with more inertia when both shaft should have the same velocity after the relative speed is less than $\Delta\omega_{tol}$. It always happens when the clutch goes into "captured and static" mode.

Note from Table 4.5 that the differential equations in Eqs. (4.90)–(4.92) representing the dynamic system switch from 3–DOF to 2–DOF or 1–DOF depending on the coulomb friction mode of the clutches. Similar to the system of two shafts coupled by a clutch, throughput or static torque, the T_{tp} is another condition used to determine the mode of the Coulomb friction in additional to the relative angular velocity at the clutch.

The throughput or static torque, T_{tp} is more involved as the system has more friction elements. Depending on the modes of each clutch, the number of the unknowns, namely the static torques to compute, changes. In general, the equations used to solve for the unknown static torque(s) are obtained from the dynamic equations, Eqs. (4.90)–(4.92). Since the static torque on a friction element needs to be calculated when the friction element is in "captured and static mode", i.e., relative speed and acceleration are zero, the relative accelerations are calculated from Eqs. (4.90)–(4.92) as

$$\ddot{\theta}_1 - \ddot{\theta}_2 = \frac{1}{I_1}T_{in} - (\frac{1}{I_1} + \frac{1}{I_2})T_{f1} + \frac{1}{I_2}T_{f2} \tag{4.93}$$

$$\ddot{\theta}_2 - \ddot{\theta}_3 = \frac{1}{I_2}T_{f1} - (\frac{1}{I_2} + \frac{1}{I_3})T_{f2} - \frac{1}{I_3}T_{load} \tag{4.94}$$

Table 4.5. Possible Modes of Two Clutches

Case	**C1**	**C2**	**differential equation**	**friction torque**
1	1	1	$\ddot{\theta}_1 = \frac{1}{I_1}T_{in} - \frac{1}{I_1}T_{f1}$ $\ddot{\theta}_2 = \frac{1}{I_2}T_{f1} - \frac{1}{I_2}T_{f2}$ $\ddot{\theta}_3 = \frac{1}{I_3}T_{f2} + \frac{1}{I_3}T_{load}$	$T_{f1} = T_{C_1,d}$ $T_{f2} = T_{C_2,d}$
2	1	2	$\ddot{\theta}_1 = \frac{1}{I_1}T_{in} - \frac{1}{I_1}T_{f1}$ $\ddot{\theta}_2 = \frac{1}{I_2}T_{f1} - \frac{1}{I_2}T_{f2}$ $\ddot{\theta}_3 = \frac{1}{I_3}T_{f2} + \frac{1}{I_3}T_{load}$	$T_{f1} = T_{C_1,d}$ $T_{f2} = T_{C_2,ca}$
3	1	3	$\ddot{\theta}_1 = \frac{1}{I_1}T_{in} - \frac{1}{I_1}T_{f1}$ $\ddot{\theta}_2 = \frac{1}{I_2+I_3}T_{f1} + \frac{1}{I_2+I_3}T_{load}$ $\ddot{\theta}_3 = \frac{1}{I_2+I_3}T_{f1} + \frac{1}{I_2+I_3}T_{load}$	$T_{f1} = T_{C_1,d}$ $T_{f2} = T_{C_2,cs}$ reset $\dot{\theta}_3(t_k) = \dot{\theta}_2(t_k)$
4	2	1	$\ddot{\theta}_1 = \frac{1}{I_1}T_{in} - \frac{1}{I_1}T_{f1}$ $\ddot{\theta}_2 = \frac{1}{I_2}T_{f1} - \frac{1}{I_2}T_{f2}$ $\ddot{\theta}_3 = \frac{1}{I_3}T_{f2} + \frac{1}{I_3}T_{load}$	$T_{f1} = T_{C_1,ca}$ $T_{f2} = T_{C_2,d}$
5	2	2	$\ddot{\theta}_1 = \frac{1}{I_1}T_{in} - \frac{1}{I_1}T_{f1}$ $\ddot{\theta}_2 = \frac{1}{I_2}T_{f1} - \frac{1}{I_2}T_{f2}$ $\ddot{\theta}_3 = \frac{1}{I_3}T_{f2} + \frac{1}{I_3}T_{load}$	$T_{f1} = T_{C_1,ca}$ $T_{f2} = T_{C_2,ca}$
6	2	3	$\ddot{\theta}_1 = \frac{1}{I_1}T_{in} - \frac{1}{I_1}T_{f1}$ $\ddot{\theta}_2 = \frac{1}{I_2+I_3}T_{f1} + \frac{1}{I_2+I_3}T_{load}$ $\ddot{\theta}_3 = \frac{1}{I_2+I_3}T_{f1} + \frac{1}{I_2+I_3}T_{load}$	$T_{f1} = T_{C_1,ca}$ $T_{f2} = T_{C_2,cs}$ reset $\dot{\theta}_3(t_k) = \dot{\theta}_2(t_k)$
7	3	1	$\ddot{\theta}_1 = \frac{1}{I_1+I_2}T_{in} - \frac{1}{I_1+I_2}T_{f2}$ $\ddot{\theta}_2 = \frac{1}{I_1+I_2}T_{in} - \frac{1}{I_1+I_2}T_{f2}$ $\ddot{\theta}_3 = \frac{1}{I_3}T_{f2} + \frac{1}{I_3}T_{load}$	$T_{f1} = T_{C_1,cs}$ $T_{f2} = T_{C_2,d}$ reset $\dot{\theta}_2(t_k) = \dot{\theta}_1(t_k)$
8	3	2	$\ddot{\theta}_1 = \frac{1}{I_1+I_2}T_{in} - \frac{1}{I_1+I_2}T_{f2}$ $\ddot{\theta}_2 = \frac{1}{I_1+I_2}T_{in} - \frac{1}{I_1+I_2}T_{f2}$ $\ddot{\theta}_3 = \frac{1}{I_3}T_{f2} + \frac{1}{I_3}T_{load}$	$T_{f1} = T_{C_1,cs}$ $T_{f2} = T_{C_2,ca}$ reset $\dot{\theta}_2(t_k) = \dot{\theta}_1(t_k)$
9	3	3	$\ddot{\theta}_1 = \frac{1}{I_1+I_2+I_3}T_{in} + \frac{1}{I_1+I_2+I_3}T_{load}$ $\ddot{\theta}_2 = \frac{1}{I_1+I_2+I_3}T_{in} + \frac{1}{I_1+I_2+I_3}T_{load}$ $\ddot{\theta}_3 = \frac{1}{I_1+I_2+I_3}T_{in} + \frac{1}{I_1+I_2+I_3}T_{load}$	$T_{f1} = T_{C_1,cs}$ $T_{f2} = T_{C_2,cs}$ reset $\dot{\theta}_2(t_k) = \dot{\theta}_1(t_k)$ and $\dot{\theta}_3(t_k) = \dot{\theta}_1(t_k)$

Note that : t_k is time instant of transition to the specific mode
$T_{C_i,d} = P_i(t)\ A_i\ r_i\ n_i\ \mu_i\ sign\ (\Delta\omega_i)$
$T_{C_i,ca=T_{d,i}\ sign\ (T_{tp,i})}$
$T_{C_i,cs=T_{tp,i}}$

Writing Eqs. (4.93) and (4.94) in matrix form yields

$$\begin{bmatrix} \ddot{\theta}_1 - \ddot{\theta}_2 \\ \ddot{\theta}_2 - \ddot{\theta}_3 \end{bmatrix} = \mathcal{A} \begin{bmatrix} T_{in} \\ T_{load} \end{bmatrix} + \mathcal{B} \begin{bmatrix} T_{f1} \\ T_{f2} \end{bmatrix}. \tag{4.95}$$

where

$$\mathcal{A} = \begin{bmatrix} \frac{1}{I_1} & 0 \\ 0 & -\frac{1}{I_3} \end{bmatrix}, \tag{4.96}$$

and

$$\mathcal{B} = \begin{bmatrix} -(\frac{1}{I_1} + \frac{1}{I_2}) & \frac{1}{I_2} \\ \frac{1}{I_2} & -(\frac{1}{I_2} + \frac{1}{I_3}) \end{bmatrix}. \tag{4.97}$$

Since the relative accelerations are zero in "captured and static" mode, Eq. (4.95) becomes a set of linear algebraic equations with the unknown T_{f1} and T_{f2} as

$$\begin{bmatrix} 0 \\ 0 \end{bmatrix} = \mathcal{A} \begin{bmatrix} T_{in} \\ T_{load} \end{bmatrix} + \mathcal{B} \begin{bmatrix} T_{f1} \\ T_{f2} \end{bmatrix}. \tag{4.98}$$

The modes of the clutches will indicate which one(s), if any, of these equations should be solved for the static torque(s). For example, when both clutches are fully engaged, i.e., in "captured and static" mode, the static torques for both the clutches should be solved. Thus, Eq. (4.98) is considered as a set of two algebraic equations with two unknowns and can analytically be solved as

$$\begin{bmatrix} T_{f1} \\ T_{f2} \end{bmatrix} = -\mathcal{B}^{-1}\mathcal{A} \begin{bmatrix} T_{in} \\ T_{load} \end{bmatrix}. \tag{4.99}$$

Eq. (4.98) can also be solved numerically by a numerical solver such as "linsolve" in [91].

Another example is when clutch–1 is in "captured and static" mode while clutch–2 is in one of the other two modes. In this case, the second equation in Eq.

(4.98) is not valid as the relative acceleration is nonzero. Then, only for clutch–1, the static torque is calculated from the solution of the first equation in Eq. (4.98). Note that, in this case, T_{f2} is known from the dynamic friction calculation. The numerical solver can be used to solve the first equation in Eq.(4.98). In this case, the analytic solution can easily be obtained as

$$T_{f1} = \frac{I_2}{I_1 + I_2} T_{in} + \frac{I_1}{I_1 + I_2} T_{f2}. \tag{4.100}$$

Similarly, when clutch–2 is in "captured and static" mode while clutch–1 is not, the second equation in Eq. (4.98) can numerically or analytically solved as

$$T_{f2} = \frac{I_3}{I_2 + I_3} T_{f1} - \frac{I_2}{I_2 + I_3} T_{load}. \tag{4.101}$$

When none of the clutches is in "captured and static" mode, Eq. (4.98) becomes irrelevant and dynamic friction calculation is used for T_{f1} and T_{f2}. Table 4.5 presents all possible cases and summarizes the differential equations and friction calculations in every cases.

The system consists of three shafts and two clutches as shown in Fig. 4.31. The pressure, applied on the clutch, is controlled by the hydraulic system during connecting and disconnecting the shafts. Shaft–1 is connected to shaft–2 via clutch–1. Input torque, T_{in}, is applied on shaft–1, causing it to rotate. Friction torque, T_{f1}, acts on shaft–1 to resist its rotation while pushes shaft–2 to rotate against the friction torque T_{f2} applied on shaft–2, as illustrated in Fig. 4.31. Shaft–2 is connected to shaft–3 via clutch–2. Load torque, T_{load}, is applied on shaft–3. Friction torque, T_{f2}, acts on the direction that resists the rotation of shaft–3.

At the initial time, the three shafts system is at ease. When the input torque is applied to shaft–1, as shown in Fig. 4.32, and shift valve–1 is opened, as illustrated in Fig. 4.33, shaft–1 starts rotating while clutch–1 connects it to shaft–2. The pressure

build up in clutch–1, as shown in Fig. 4.34, generates the friction on the clutch surface. As a result, shaft–2 is pushed to rotate by the clutch. Both shafts are rotating with different speeds as seen in Fig. 4.35. The friction at clutch–1 is in "in–motion" mode. When the pressure in clutch–1 reaches the highest value around 1000 kPa, the friction torque is build up enough to make shaft–2 to have the same speed as shaft–1. When they reach the synchronous velocity, this is where the friction is in "Captured and Static" mode. At this moment, the differential equations of shaft–1, shaft–2 are changed, as seen in Table 4.5. Also, the angular velocity states are reset to the same angular velocity to be integrated to obtain the same angular velocity in the next time step, as shown in Fig. 4.36. Once the friction is switched mode to "captured and accelerating", the friction torque is reduced to the magnitude that is enough to maintain both shafts at the same speed. As seen in Fig. 4.38, the friction torque at clutch–1 drops significantly from the beginning even though the pressure at clutch–1 remains at 1000 kPa.

When releasing shift valve–1, the pressure in clutch–1 drops as seen in Fig. 4.33 and 4.34. Consequently, the friction in clutch–1 drops, as shown in Fig. 4.38. Shaft–1 and shaft–2 start rotating with different speeds. As seen in Fig. 4.35, the speed of shaft–1 departs from the speed of shaft–2. After a few seconds, shift valve–2 is opened and the pressure in clutch–2 is built up. The friction in clutch–2 is generated as seen in Fig. 4.39. This causes shaft–2 and shaft–3 to rotate together with different speeds. Once the friction is enough to make both shafts to rotate at the same speed, the friction drops to the magnitude that is enough to maintain both shafts at the same speed. The differential equations of shaft–1 and shaft–2 are changed as seen in Table 4.5. Also, the angular velocity states are reset to the same angular velocity, as done previously at clutch–1.

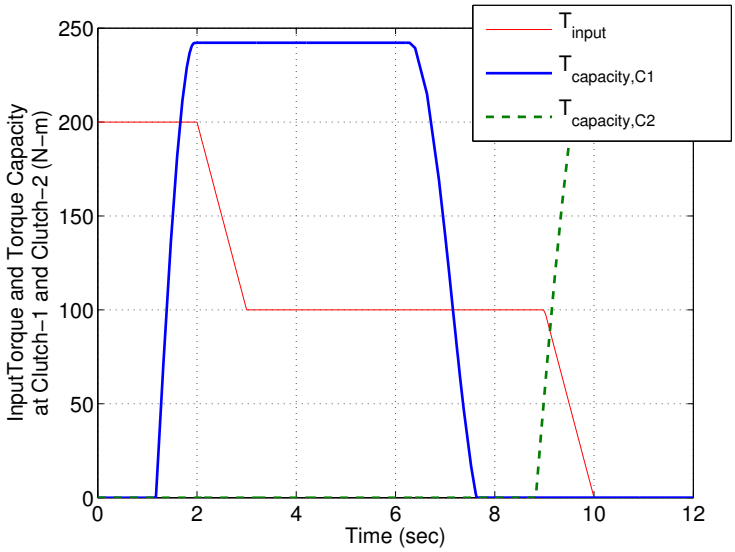

Figure 4.32. Input Torque and Torque Capacity at Clutch–1 and Clutch–2.

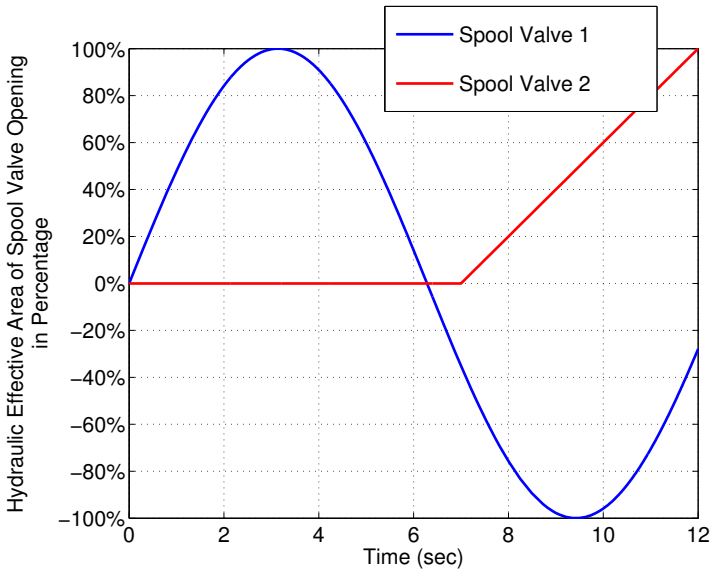

Figure 4.33. Hydraulic Effective Area of Spool Valve 1 and 2 in Percentage.

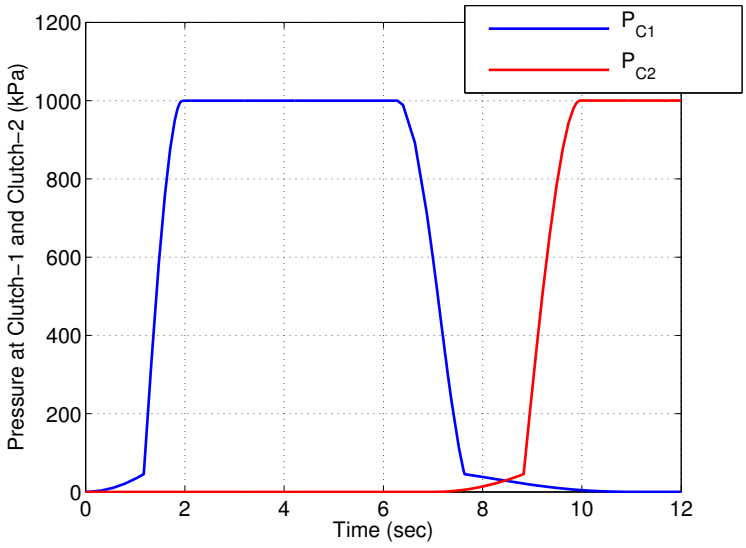

Figure 4.34. Pressure at Clutch–1 and Clutch–2.

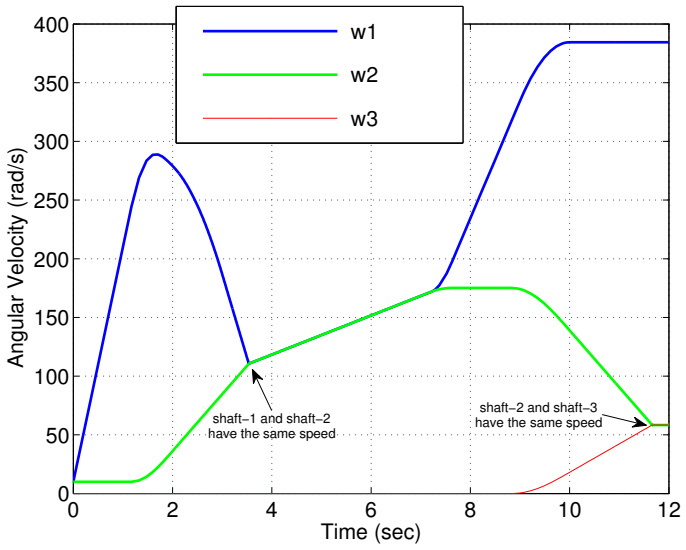

Figure 4.35. Angular Velocities of Shaft–1, Shaft–2 and Shaft–3.

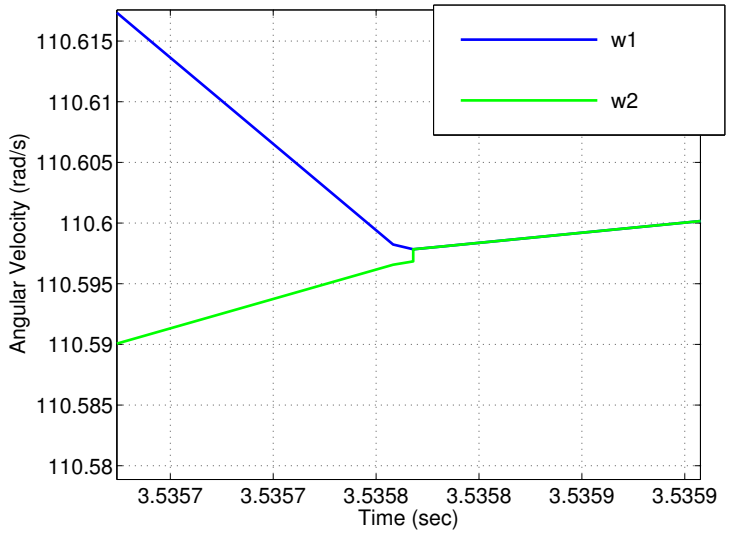

Figure 4.36. Angular Velocities of Shaft–1 and shaft–2 at the moment when they become the same.

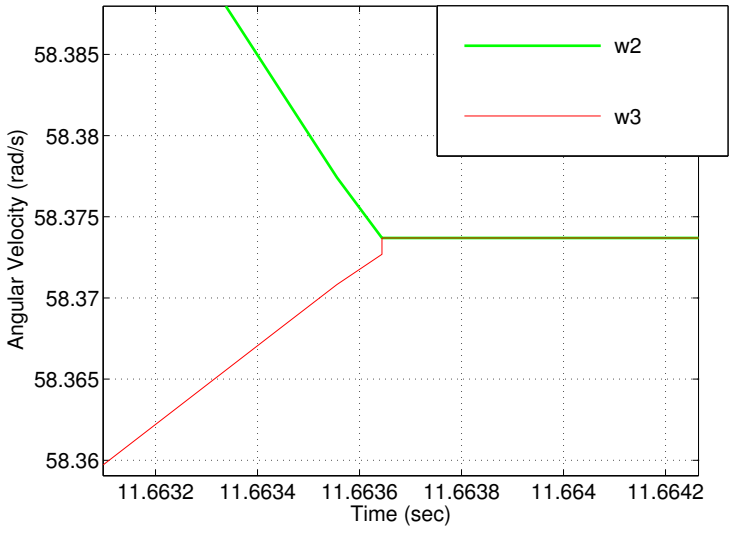

Figure 4.37. Angular Velocities of Shaft–2 and shaft–3 at the moment when they become the same.

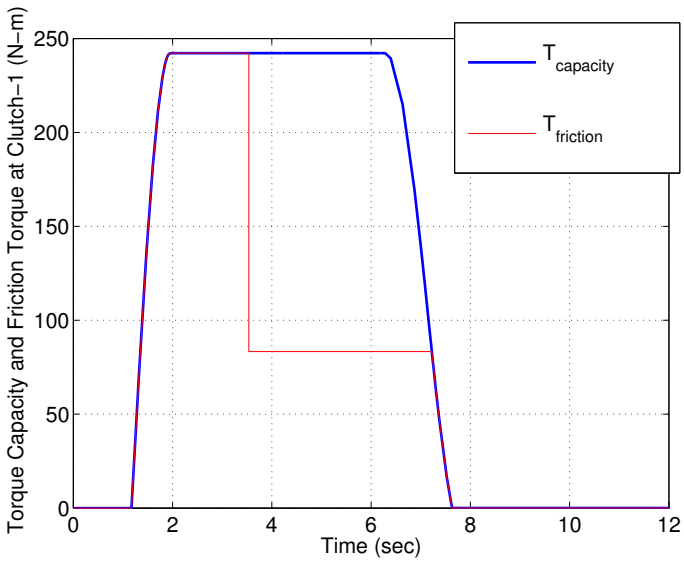

Figure 4.38. Torque Capacity and Friction Torque at Clutch–1.

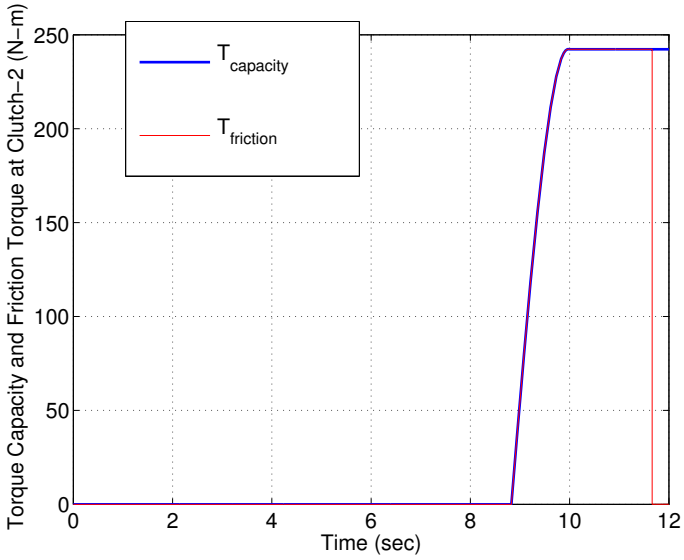

Figure 4.39. Torque Capacity and Friction Torque at Clutch–2.

4.8 Hydramatic 440 Automatic Transmission Clutch and Band with Classical Friction Models

To apply the classical friction model in Section 4.5 to the friction elements in GM Hydramatic 440, the relative speed for each clutch and band should be defined. C_1 couples the turbine with sun–1 and the relative speed is defined as

$$\Delta\omega_{C_1} = \omega_t - \omega_{S_1} \tag{4.102}$$

Further, the sprag is set up such that this one–way–clutch allows S_1 to rotate freely faster than the turbine, or the turbine to rotate freely slower than S_1. This implies $T_{cap^-} = 0$. Thus, the torque carried through C_1, based on Eq. 4.5, is expressed as

$$T_{C_1} = f_{TC}(\omega_t - \omega_{S_1}, T_{C_1,cap^+}, 0) \tag{4.103}$$

Note that when T_{C_1} is applied (i.e. T_{C_1,cap^+} is increased) while the turbine rotates faster than S_1, $T_{C_1} > 0$, which should accelerate S_1. Positive torque should accelerate a rotating element in the positive direction. Thus,

$$T_{S_1,C_1} = T_{C_1} \tag{4.104}$$

Consequently,

$$T_{t,C_1} = -T_{C_1} \tag{4.105}$$

C_2 couples the turbine with carrier–1/ring–2 and the relative speed is defined as

$$\Delta\omega_{C_2} = \omega_t - \omega_{C_1R2} \tag{4.106}$$

Thus, the torque carried through C_2 is

$$T_{C_2} = f_{TC}(\omega_t - \omega_{C_1R_2}, T_{C_2,cap^+}, T_{C_2,cap^-}) \tag{4.107}$$

Based on the definition of $\Delta\omega_{C_2}$, when C_2 is applied while $\omega_t > \omega_{C_1R_2}$, $T_{C_2} > 0$. In this case, either the turbine will slow down, or C_1R_2 will speed up. Thus,

$$T_{C_1R_2,C_2} = T_{C_2} \tag{4.108}$$

$$T_{t,C_2} = -T_{C_2} \tag{4.109}$$

C_3 couples the turbine with sun–1 and the relative speed is defined as

$$\Delta\omega_{C_3} = \omega_t - \omega_{S_1} \tag{4.110}$$

Recall that C_3 is a one–way clutch like C_1. However, its sprag is set up to rotate freely in the opposite direction of C_1. That is, S_1 can rotate freely slower than the turbine, or the turbine can rotate freely faster than S_1. This implies $T_{C_3,cap^+} = 0$

$$T_{C_3} = f_{TC}(\omega_t - \omega_{S_1}, 0, T_{C_3,cap^-}) \tag{4.111}$$

Based on the definition of $\Delta\omega_{C_3}$, when C_3 is applied while S_1 rotates faster than the turbine, $T_{C_3} < 0$. In this case, either S_1 slows down or the turbine speeds up. Thus, the applied torque on the turbine due to C_3 should be positive but $T_{C_3} < 0$, which implies

$$T_{t,C_3} = -T_{C_3} \tag{4.112}$$

Since S_1 slows down

$$T_{S_1,C_3} = T_{C_3} \tag{4.113}$$

C_4 couples S_1 with the transmission case, whose rotational speed is assumed to be zero. Then, the relative speed is defined as

$$\Delta\omega_{C_4} = -\omega_{S_1} \tag{4.114}$$

Thus, the torque carried through C_4 is

$$T_{C_4} = f_{TC}(-\omega_{S_1}, T_{C_4,cap^+}, T_{C_4,cap^-}) \tag{4.115}$$

Based on the definition of $\Delta\omega_{C_4}$, when C_4 is applied while S_1 rotates in the positive direction, $T_{C_4} < 0$ and S_1 will slow down. Thus, Since S_1 slows down

$$T_{S_1,C_4} = T_{C_4} \tag{4.116}$$

B_{12} couples S_2 with the transmission case. The relative speed is defined as

$$\Delta\omega_{B_{12}} = -\omega_{S_2} \tag{4.117}$$

The torque carried through B_{12} is

$$T_{B_{12}} = f_{TC}(-\omega_{S_2}, T_{B_{12},cap^+}, T_{B_{12},cap^-}) \tag{4.118}$$

when B_{12} is applied while S_2 rotates in the positive direction, $T_{B_{12}} < 0$ and S_2 will slow down. Thus,

$$T_{S_2,B_{12}} = T_{B_{12}} \tag{4.119}$$

When the shift valve responds to a shifting signal, it directs the hydraulic pressure to the designated clutch or band that causes the shift to occur. The hydraulic pressure enters the cylinder-housing cavity behind the piston. As the pressure in the cavity increases, the piston is forced against the return spring, drive plates and driven clutch plates. The drive plates are splined to the drum. The driven clutch plates are splined to the hub connected to a planetary gear member. The return spring reaches full compression as the piston reaches the end of its travel in the drum. At the same time the drive plates and the clutch plates are compressed together, torque is transmitted via the clutch from the input shaft torque to a component of the planetary gear sets. Consequently, the input shaft and the planetary gear set member rotate with the same speed. When hydraulic fluid is "cut–off" to the piston by the shift valve due to the shift signal, the circuit is exhausted and vented to atmosphere through the valve body, and the return spring forces the piston to its"off position". When

the clutch pressure decays to the check ball apply pressure, the check ball drops from its seat, thereby relieving residual centrifugal pressure. The drive and driven clutch plates are separated.

4.9 Hydramatic 440 Automatic Transmission Clutch and Band with Woods Static and Dynamic Friction Models

The hydraulic system in Section 4.2 and Woods static and dynamic friction model are applied to GM Hydramatic 440 transmission model in this section. The equations of motion of the planetary gear set model are given in Eqs. (4.63) and (4.64).

Based on Eq. (4.65), the dynamics equation of the planetary gear sets can be represented in matrix form. Rearranging Eq. (4.65) to have the angular acceleration, $\dot{\omega}_{C_2R_1}$ and $\dot{\omega}_{C_1R_2}$ in the right hand–side of the equation yields

$$\begin{bmatrix} \dot{\omega}_{C_2R_1} \\ \dot{\omega}_{C_1R_2} \end{bmatrix} = \mathbf{E}_G^{-1}\mathbf{B}_G \begin{bmatrix} T_{S_1} \\ T_{C_1R_2} \\ T_{S_2} \\ T_{C_2R_1} \end{bmatrix} \tag{4.120}$$

where $\mathbf{E_G^{-1}}$ is a 2×2 and $\mathbf{B_G}$ is a 2×4 matrices which can be obtained by inspection from Eqs. (4.63) and (4.64). From Eqs. (4.40) and (4.42) the angular acceleration of sun–1 and sun–2 are expressed in matrix form as

$$\begin{bmatrix} \dot{\omega}_{S_1} \\ \dot{\omega}_{S_2} \end{bmatrix} = \mathbf{H}_G \begin{bmatrix} \dot{\omega}_{C_2R_1} \\ \dot{\omega}_{C_1R_2} \end{bmatrix} \tag{4.121}$$

where $\mathbf{H_G}$ is a 2×2 which can be obtained by inspection. From Eqs.(4.120) and (4.121), the derivative of speeds of sun–1, carrier–1 ring–2, sun–2, and carrier–2 ring–1 can be written as

$$\begin{bmatrix} \dot{\omega}_{C_2R_1} \\ \dot{\omega}_{C_1R_2} \\ \dot{\omega}_{S_1} \\ \dot{\omega}_{S_2} \end{bmatrix} = \mathbf{D} \begin{bmatrix} T_{S_1} \\ T_{C_1R_2} \\ T_{S_2} \\ T_{C_2R_1} \end{bmatrix} \tag{4.122}$$

where

$$\mathbf{D} = \begin{bmatrix} \mathbf{E}_G^{-1}\mathbf{B}_G \\ \mathbf{H}_G\mathbf{E}_G^{-1}\mathbf{B}_G \end{bmatrix} \tag{4.123}$$

The dynamics equation of the turbine shaft gives the derivative of the turbine speed which is expressed as

$$\dot{\omega}_t = \frac{1}{I_t}(T_t + T_{t,C_1} + T_{t,C_2} + T_{t,C_3}) \tag{4.124}$$

where T_t is turbine torque and T_{t,C_i} is the applied torque due to C_i, where $i = 1, 2, 3$.

In Woods static and dynamic friction model, the relative speed and the throughput torque determine the friction mode. The relative speed and its derivative at the clutches and bands are found from Eq. (4.122). The relative speed derivatives at the clutches and bands can be written in terms of turbine, sun, carrier, ring and transmission case speeds.

$$\begin{bmatrix} \Delta\dot{\omega}_{C_1} \\ \Delta\dot{\omega}_{C_2} \\ \Delta\dot{\omega}_{C_3} \\ \Delta\dot{\omega}_{C_4} \\ \Delta\dot{\omega}_{B_{12}} \end{bmatrix} = \begin{bmatrix} \dot{\omega}_t - \dot{\omega}_{S_1} \\ \dot{\omega}_t - \dot{\omega}_{C_1R_2} \\ \dot{\omega}_t - \dot{\omega}_{S_1} \\ -\dot{\omega}_{S_1} \\ -\dot{\omega}_{S_2} \end{bmatrix} \tag{4.125}$$

Substituting Eq. (4.124), and 2^{nd}, 3^{rd} and 4^{th} rows of Eq. (4.122) with corresponding gear positions into Eq. (4.125) yields following equation. Note that the gear positions determine whether there are friction torques at sun–1, carrier–1 ring–2, sun–2, and carrier–2 ring–1.

$$\begin{bmatrix} \Delta\dot{\omega}_{C_1} \\ \Delta\dot{\omega}_{C_2} \\ \Delta\dot{\omega}_{C_3} \\ \Delta\dot{\omega}_{C_4} \\ \Delta\dot{\omega}_{B_{12}} \end{bmatrix} = \mathbf{K} \begin{bmatrix} T_t \\ T_{C_2R_1,FD} \\ T_{S_1,C_1} \\ T_{C_1R_2,C_2} \\ T_{S_1,C_3} \\ T_{S_1,C_4} \\ T_{S_2,B_{12}} \end{bmatrix} \tag{4.126}$$

where

$$\mathbf{K} = \begin{bmatrix} \frac{1}{I_t} & -D_{34} & -(\frac{1}{I_t}+D_{31}) & -(\frac{1}{I_t}+D_{32}) & 0 & 0 & -D_{33} \\ \frac{1}{I_t} & -D_{24} & -(\frac{1}{I_t}+D_{21}) & -(\frac{1}{I_t}+D_{22}) & -(\frac{1}{I_t}+D_{21}) & -D_{21} & -D_{23} \\ \frac{1}{I_t} & -D_{34} & 0 & -(\frac{1}{I_t}+D_{32}) & -(\frac{1}{I_t}+D_{31}) & -D_{31} & -D_{33} \\ 0 & -D_{34} & 0 & -D_{32} & -D_{31} & -D_{31} & 0 \\ 0 & -D_{44} & -D_{41} & -D_{42} & 0 & 0 & -D_{43} \end{bmatrix} \tag{4.127}$$

where D_{ij} can be obtained from matrix D in Eq. (4.123).

The throughput torque is solved from Eq. (4.126). In Eq. (4.126), whenever a clutch or a band is in "captured and static" mode, the corresponding relative speed at the clutch or the band $\Delta\omega$ and its derivative $\Delta\dot{\omega}$ are equal to zero. Rearranging those rows from Eq. (4.126) which relate to the clutches and bands that are in "capture

and static" mode yields the throughput torque at those clutches and bands. This is written in matrix form as

$$T_{tp} = Z \cdot T_{applied} \tag{4.128}$$

where Z is a product of matrices after rearrange Eq. (4.126) at the clutch and band that are in "captured and static" mode. $T_{applied}$ is the applied torque to the turbine and the friction torque at the other clutches and bands that are not in "captured and static" mode. The procedure to find the throughput torque is demonstrated in the following example.

Table 4.6. Total events that would happen in 1^{st} gear

case	C_1	B_{12}
1	1	1
2	2	1
3	3	1
4	1	2
5	2	2
6	3	2
7	1	3
8	2	3
9	3	3

In the first gear, clutch C_1 and band B_{12} are engaged. The clutch and band can be in one of the three friction modes. Thus, there are $3^2 = 9$ possible cases. Table 4.6 shows all the cases regarding clutch C_1 and band B_{12}.

In case 9, the clutch C_1 and the band B_{12} are in "captured and static" mode, which represents the first gear. From Eq. (4.126), the first and the fifth rows are

separated and rewritten as

$$\begin{aligned}\Delta\dot{\omega}_{C_1} &= \frac{1}{I_t}T_t - D_{34}T_{C_2R_1,FD} - (\frac{1}{I_t} + D_{31})T_{C_1,tp} \\ &\quad -(\frac{1}{I_t} + D_{32})T_{C_2} - D_{33}T_{B_{12},tp} \qquad (4.129)\\ \Delta\dot{\omega}_{B_{12}} &= -D_{44}T_{C_2R_1,FD} - D_{41}T_{C_1,tp} - D_{42}T_{C_2} \\ &\quad -D_{43}T_{B_{12},tp} \qquad (4.130)\end{aligned}$$

T_{C_1} and $T_{B_{12}}$ are the throughput torques that needs to be calculated. The corresponding derivative of the relative speed at the clutch C_1, $\Delta\dot{\omega}_{C_1}$, and the band B_{12}, $\Delta\dot{\omega}_{B_{12}}$ both equal to zero. T_{C_2} is zero because clutch C_2 is not activated in first gear. Thus, Eqs. (4.129) and (4.130) is reduced to

$$\begin{aligned}0 &= \frac{1}{I_t}T_t - D_{34}T_{C_2R_1,FD} - (\frac{1}{I_t} + D_{31})T_{C_1,tp} \\ &\quad -D_{33}T_{B_{12},tp} \qquad (4.131)\\ 0 &= -D_{44}T_{C_2R_1,FD} - D_{41}T_{C_1,tp} - D_{43}T_{B_{12},tp} \qquad (4.132)\end{aligned}$$

From Eqs. (4.131) and (4.132), the throughput frictions at the clutch C_1 and the band B_{12} in matrix form are

$$\begin{bmatrix} T_{C_1,tp} \\ T_{B_{12},tp} \end{bmatrix} = \mathbf{Z}_3 \begin{bmatrix} T_t \\ T_{C_2R_1,FD} \end{bmatrix} \qquad (4.133)$$

where

$$\begin{aligned}\mathbf{Z_3} &= MK_3^{-1}MD_3 \qquad (4.134)\\ MK_3 &= \begin{bmatrix} (\frac{1}{I_t} + D_{31}) & D_{33} \\ D_{41} & D_{43} \end{bmatrix} \qquad (4.135)\\ MD_3 &= \begin{bmatrix} \frac{1}{I_t} & -D_{34} \\ 0 & -D_{44} \end{bmatrix} \qquad (4.136)\end{aligned}$$

For other gears and shifting, a similar procedure can be applied to determine the throughput torque at the corresponding clutches and bands. For the specific transmission studied, the total number of the possible friction modes needed to be determined for shifting gear and fixed gear operation is $3^6 = 729$. In this study, however, the simulation for the 1^{st} gear, $1-2-1$ up/downshift, 2^{nd} gear, $2-3-2$ up/downshift, 3^{rd} gear, $3-4-3$ up/downshift, 4^{th} gear are studied. Thus, the total possible friction modes is 81 modes. The comparison of the simulation results with the classical friction model and with Woods static and dynamic friction model is presented in Chapter 5 and [28].

CHAPTER 5

OPEN LOOP SIMULATION RESULTS

This chapter presents the simulation of various shifts using open–loop control. Depending on the type of the friction model used, a pre–set torque capacity or clutch/band pressure profile is applied to execute a desired shift. A significant amount of time is spent in each case in calibrating the torque capacity or pressure profile in order to obtain a good shift. As stated in Section 1.1.3, the shift quality can be characterized by various specifications of a shift. The ones used in this research are listed below.

1. Torque at the output gear/shaft: The torque at the output gear/shaft should have small amplitude and low frequency of oscillation during the shift transient.
2. Vehicle Acceleration: The magnitude and frequency of oscillation of the vehicle acceleration should be small during the time the gear ratio is changed.
3. Derivative of acceleration of the output gear: This is also called "Jerk". The magnitude and oscillation should be small during the shift transient.
4. Shift duration: The time between the current gear ratio and the desired gear ratio should be as short as possible.

Through this exercise, it has become clear that manual calibration is a very tedious and ineffective process to obtain good shifts. There are three different simulation cases presented in this chapter. In all three cases, the powertrain model has the same subsystems, except the friction, hydraulic and drive shaft models. The first case uses the classical friction model, which takes torque capacity as the control variable and uses only a first–order filter as the representation of the hydraulic system. In

the first case, a non–stiff drive shaft model is used. The second and the third cases have the Woods friction model with a traditional hydraulic actuation system. The difference between these two cases is that the second case uses a stiff drive shaft while the third case uses a non–stiff one. The initial conditions of the simulation are set as below.

1. The engine is set up to run at 60 rad/s, 13.5 air-fuel ratio and 90 degree throttle angle.
2. The turbine shaft has speed of zero rad/s.
3. The gear position is in neutral.
4. Gears in the planetary gear sets have speeds of zero rad/s.
5. The vehicle speed is at zero km/h.

5.1 Powertrain with the Classical Friction Model

First, the overall simulation results are discussed. The overview of the simulation results of the powertrain from start to finish of the simulation are illustrated in Figs. 5.1–5.9. This is followed by two subsections focusing on two specific upshifts. Figs. 5.10 - 5.18 present the characteristics of the shift dynamics during 1–2 upshift. Figs. 5.19–5.27 present the characteristics of the shift dynamics during 2–3 upshift. At the initial time, the simulation starts while the transmission is in neutral, but immediately shift to the first gear is initiated. At 2.5 s, 1–2 shift is started. Upshift 2–3 starts at 6 s. Shift to the fourth gear from the third starts at 14.0 s. As discussed in Section 4.5, the clutch and band models with the classical friction model takes "torque capacity" as the input. Torque capacity indicates the maximum amount of torque a friction element can hold and is adjusted by applied pressure in real implementations. Since the hydraulic system is not modeled with this friction model, torque capacities of the friction elements will be adjusted to initiate a shift

and control its quality. To engage a friction element, its torque capacity should be increased to exceed the amount of torque that the friction element needs to hold in the target gear in the driving condition. If the torque capacity is less than the torque that the friction element is required to carry, the friction element will slip. To fully disengage a friction element, its torque capacity should be reduced to zero. Fig. 5.1 shows the torque capacities adjusted based on Table 4.1 to achieve the desired shifts.

The engine torque and speed plots representing the dynamics of the engine are shown in Figs. 5.2 and 5.3. Note that the engine and the pump in the torque converter are lumped together as explained in Chapter 3. Fig. 5.2 shows the turbine torque and pump torque in the torque converter. The large torque multiplication can be seen in Fig. 5.2. The turbine torque is greater than the engine torque. On the other hand, the engine has higher speed than that of the turbine as shown in Fig. 5.3. This results from the torque converter characteristics. Changing gear results in torque and speed changes in the engine and the torque converter. As seen in Fig. 5.2, both torques repeatedly spike up. The two shift phases, "torque phase" and "inertia phase" can be easily seen. "Torque phase" is initiated when the oncoming clutch torque starts to increase. In the "torque phase", the engine and turbine torques remain unchanged. In the "inertia phase" or "speed phase", which starts after "torque phase", the offgoing clutch/band torques are zero. Also, sudden increases occur in the engine and turbine torques. After the peaks in magnitudes, the torques start to decrease. Fig. 5.3 shows that large drops occur in the engine and turbine speeds due to the gear ratio charge during the inertia phase of each shift. The oscillations seen in Figs. 5.2 and 5.3 are due to poor shift quality and will be addressed via feedback control.

Fig. 5.4 shows the clutch torques in the clutches and bands. Fig. 5.5 shows applied torques on gears in the planetary gear sets from the first gear to the forth gear. Fig. 5.6 shows the speed of gears in the planetary gear sets. The output shaft

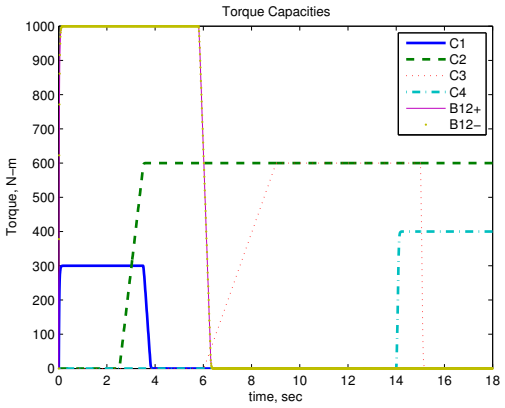

Figure 5.1. Torque Capacities.

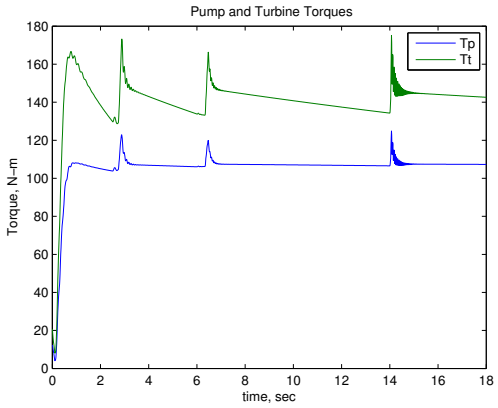

Figure 5.2. Pump and Turbine Torque.

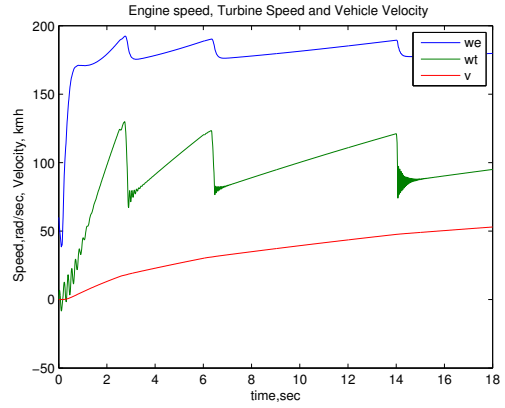

Figure 5.3. Engine Speed, Turbine Speed and Vehicle Velocity.

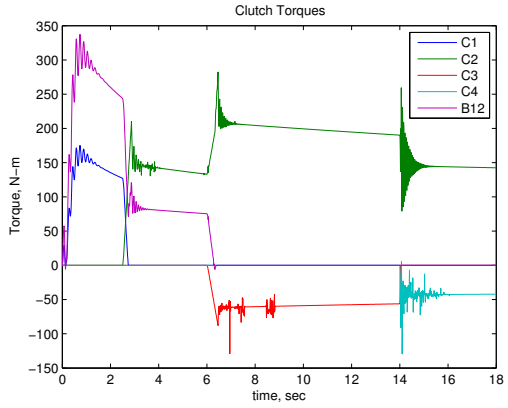

Figure 5.4. Clutch Torques.

torque at final drive is illustrated in Fig. 5.7. The simulation results of the vehicle model are also illustrated in Figs. 5.3, 5.8 and 5.9. The vehicle velocity is shown in Fig. 5.3. The vehicle moves from starting point at zero km/h and reaches the velocity about 50 km/h in 18 sec. The vehicle acceleration is shown in Fig. 5.8. The peak and transient during upshifts can be seen. In Fig. 5.9, the derivative of acceleration is shown. The derivative of acceleration or jerk indicates unpleasant ride caused by poor shifting.

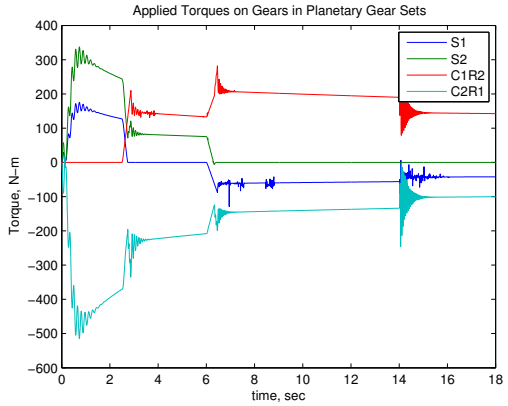

Figure 5.5. Applied Torques on Gears in Planetary Gear Sets.

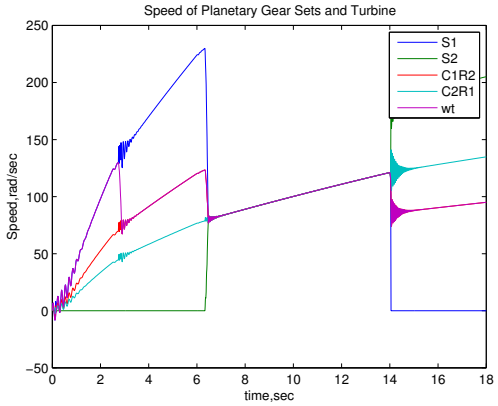

Figure 5.6. Speed of Planetary Gear Sets and Turbine.

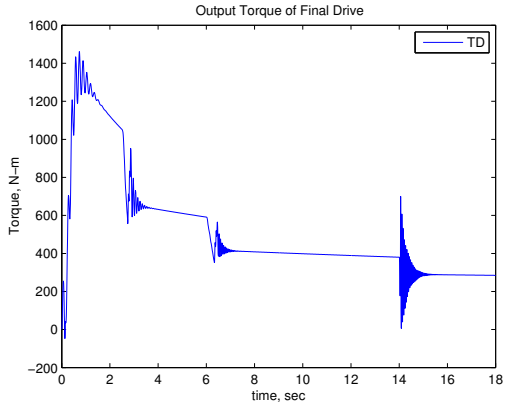

Figure 5.7. Output Torque of Final Drive.

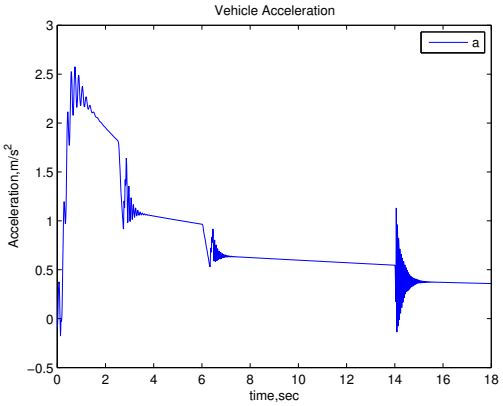

Figure 5.8. Vehicle Acceleration.

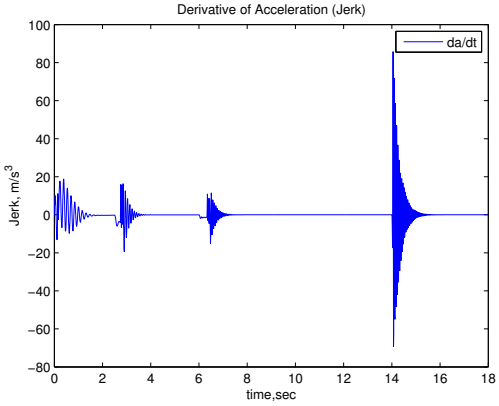

Figure 5.9. Derivative of Acceleration.

5.1.1 1–2 Upshift

The characteristic of 1–2 upshift is analyzed in this section through Figs. 5.10 to 5.18. The characteristic of shift is influenced by torque capacities on the clutches and bands. In practice, the torque capacities is determined by calibration until the shift quality is acceptable. The results of improper applied torque capacities are "tie up" or "flare up" as discussed in Chapter 1. In this section, the torque capacities are adjusted to obtain the best results as much as possible without any help from control techniques. In 1–2 upshift, the on–coming clutch is clutch C_2 and off–going clutch is clutch C_1 as indicated in Table 4.1. The shift happens when clutch C_2 is engaging to connect the turbine with carrier–1. Even though clutch C_1 is off-going clutch in this upshift, the characteristic of shift is solely influenced by torque capacity profile of the on–coming clutch C_2. As shown in Fig. 5.10, the torque capacity profile of clutch C_1 remains constant during 1–2 upshift. Band B_{12} remains engaged through 1–2 upshift with the constant torque capacity. C_1 is one–way clutch which has a mechanism called "sprag" that makes upshift happens automatically when on-coming clutch engages without adjusting the clutch C_1 pressure profile.

The torque phase of 1–2 upshift starts when clutch C_2 torque capacity starts to increase at time 2.5 sec as shown in Figs. 5.10 and 5.11. The output shaft torque drops as seen in Fig. 5.18, because some parts of turbine torque start to be transmitted via sun–1 while carrier–1 still transmits the other part of turbine torque. This drop is undesirable, since the output torque to the drive shaft is interrupted and the passengers may feel this. However, it is unavoidable, since changing the size of gear ratio is not a continuous event in the step gear automatic transmission. Intuitively, the drop in the output torque should be around the neighborhood of the output torque when the shift is completed at the next gear. During this torque phase, the speed of turbine is still equal to the speed of sun–1. Even tough clutch C_2

is engaging and clutch torque on clutch C_2 is increasing, the turbine and sun–1 speed are still increasing. The torque at turbine remains unchanged, thus it still speeds up. This happens because torque on clutch C_1 is decreasing while torque on clutch C_2 is increasing as seen in Fig. 5.11. Turbine torque is transmitted from sun–1 to carrier–1 as seen in Fig. 5.12.

At the beginning of inertia phase which is the end of torque phase at 2.75 sec, the turbine speed decelerates to a new synchronous speed. As seen in Fig. 5.13, turbine is apart from sun–1. At this moment, the sprag is overrun by sun–1, since the speed of sun–1 is faster than the speed of turbine. Clutch C_1 fully disengages due to the sprag. Even though the hydraulic actuator at clutch C_1 is still on, as shown in Fig. 5.10, there is no clutch torque at clutch C_1 as seen in Fig. 5.11. Applied torque on sun–1 is zero as seen in Fig. 5.12. In the speed phase, turbine and carrier–1 are slipping until clutch C_2 is slowing down the turbine and speeding up carrier–1. The speed of the turbine is reduced because the turbine torque is reduced by increasing clutch torque at clutch C_2 as seen in Fig. 5.14 and 5.15. The decrease in turbine speed results in a higher slip across the the converter, which yields a higher pump torque as seen in Fig. 5.14. Consequently, the engine speed is reduced. During this phase, the speed of turbine is dropping to the new synchronized speed to be equal to the speed of carrier–1 as seen in Fig. 5.13. At the end of speed phase, turbine and carrier–1 have the same speed and there is no slipping in clutch C_2. Also, the clutch C_2 and applied torque on carrier–1 reach highest magnitude as seen in Figs. 5.11 and 5.12, respectively.

At the end of 1–2 upshift carrier–1's torque drops to the level of the turbine torque in Fig. 5.12. The output shaft torque has a large transient as seen in Fig. 5.18. Following the drop, the output torque increases until it reaches the peak and later oscillates with high frequency. Again, the maximum output torque should be

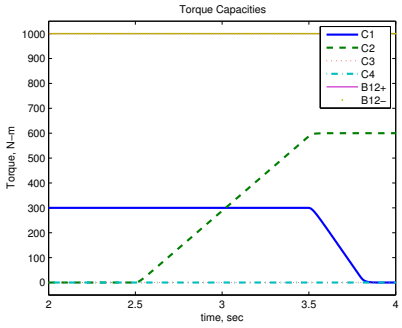

Figure 5.10. Torque Capacities During 1–2 Upshift.

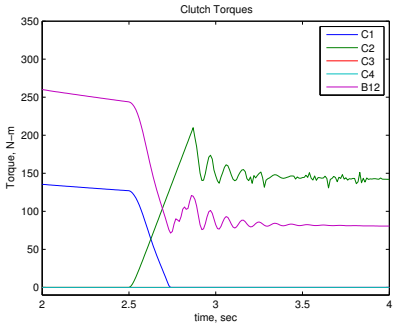

Figure 5.11. Clutch Torques During 1–2 Upshift.

the same level as the output torque in the next gear. The frequency of the oscillation should be as small as possible. The vehicle acceleration is shown in Fig. 5.16 and the derivative of the acceleration in Fig. 5.17. The high frequency and amplitude in the output torque and vehicle acceleration indicate the poor shift quality. To a passenger of the vehicle, this rapid change in the vehicle acceleration is felt as a jerk. Jerk is derivative of acceleration as shown in Fig. 5.17 used to measure the quality of the shift. High frequency and amplitude in jerk indicates the poor shift quality.

The transient will be damped out by torque converter once 1–2 upshift completes where the turbine rigidly connects to output shaft. While in speed phase during 1–2 upshift, the slipping clutch decouples the output shaft from the torque converter. The shift duration is about 1 sec. Even though this short duration seems to be acceptable, there are torque and speed oscillations with high amplitude and frequency as shown in the figures, which indicates poor shift quality.

5.1.2 2–3 Upshift

The characteristics of 2–3 upshift is determined by how the torque capacities are adjusted for band B_{12} and clutch C_3. In this particular transmission, band B_{12} should be released and clutch C_3 should be applied to conduct 2–3 shift. A shift

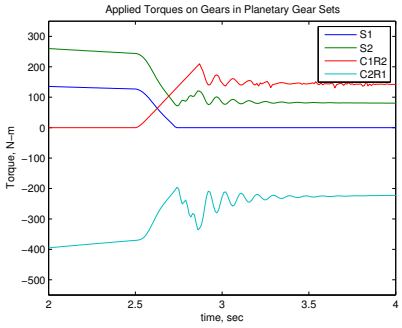

Figure 5.12. Applied Torques on Gears in Planetary Gear Sets During 1–2 Upshift.

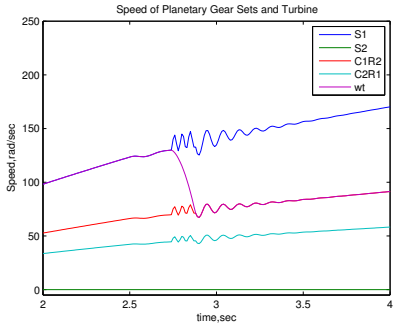

Figure 5.13. Speed of Planetary Gear Sets and Turbine During 1–2 Upshift.

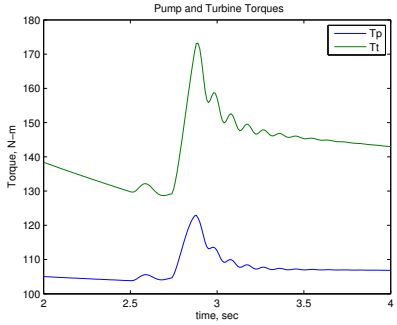

Figure 5.14. Pump and Turbine Torque During 1–2 Upshift.

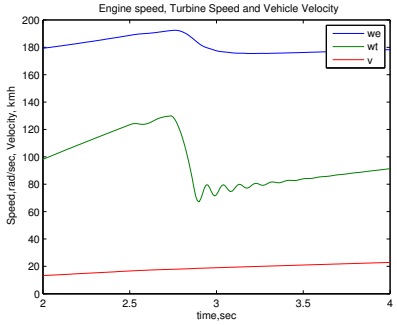

Figure 5.15. Engine Speed, Turbine Speed and Vehicle Velocity During 1–2 Upshift.

that requires both an on-coming and off-going elements is called “a swap shift”. The timing and the profiles of the torque capacity adjustment for B_{12} and C_3 are the defining factors for the shift characteristics. If C_3 is applied before B_{12} is release, a tie–up will occur while a flare will take place if B_{12} released before C_3 is applied. Fig. 5.20–5.27 shows shift behavior during 2–3 upshift with the torque capacity profiles shown in Fig. 5.19.

In this upshift the timing of the on–coming element (the clutch being applied) and the off–going element (the band being released) are tuned up to obtain the better

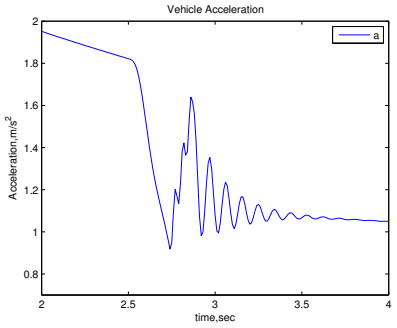

Figure 5.16. Vehicle Acceleration During 1–2 Upshift.

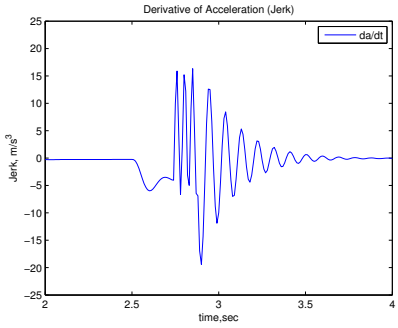

Figure 5.17. Derivative of Acceleration During 1–2 Upshift.

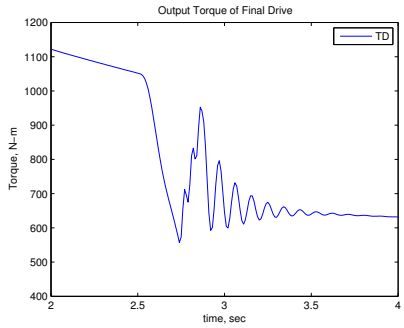

Figure 5.18. Output Torque of Final Drive During 1–2 Upshift.

upshifting results. The shift is initiated by lowering the torque capacity of band B_{12} and, after a short time, raising the torque capacity of clutch C3, as shown in Fig. 5.19. The increasing torque capacity of C_3 while B_{12} still has some torque capacity splits the torque transmission between C_3 and B_{12}. This can be seen in Fig. 5.20. The transmission torque is carried through carrier–1 and sun–1 as seen in Fig. 5.21. The turbine torque remains unchange during this torque phase as shown in Fig. 5.23. As more torque goes through C_3, less torque is carried by B_{12}. The sharp drops in the output shaft torque and the vehicle acceleration indicate the beginning of torque phase as seen in Figs. 5.25 and 5.27. This drop happens since the output torque to the drive shaft is interrupted due to changing gear ratio size. The passengers feel

this event. However, it is unavoidable, since changing the size of gear ratio is discrete event in the step gear automatic transmission. Intuitively, the drop in the output torque should be approximately around the vicinity of the output torque when the shift is completed at the next gear. At the time when the torque capacity of B_{12} drops to zero and B_{12} no longer carries torque, C_3 starts carrying all the torque and the decrease in the output torque stops. This signifies the end of the "torque transfer phase" and the beginning of the "ratio change phase", or "inertia phase". During the inertia phase, the gear ratio is between the 2^{nd} gear and the 3^{rd} gear ratios. Since B_{12}, which connects sun–2 to the transmission case, is fully released, sun–2 starts rotating as seen in Fig. 5.22. C_3 is used to connect sun–1 to the turbine shaft. As C_3 is engaged, the clutch slips until sun–1 and the turbine have the same speed. Once Sun–1 and the turbine rotate (zero slip in C_3) together with the sun–2 and they all have the same speed as carrier–2 (connected to the output shaft), the 3^{rd} gear ratio ($= 1$) is obtained and the shift is completed as shown in Fig. 5.22. Then, the torque carried by C_3 is only the amount to prevent slipping. Once the shift is completed, the capacity on the clutch can be increased with no effect on the speeds or the torques. Note that the output torque drop stops at the beginning of the inertia phase and the output torque shows a transient in the inertia phase.

The speed of the turbine is reduced because the turbine torque is reduced by increasing clutch torque at C_2 and C_3 as seen in Figs. 5.22 and 5.24. The decrease in turbine speed results in a higher slip across the converter, which yields a higher pump torque as seen in Fig. 5.23. Consequently, the engine speed is reduced.

At the end of 2–3 upshift the magnitude of carrier–2/ring–1 torque drops to the level of the turbine torque in Fig. 5.21 and 5.23. The output shaft torque begins to oscillate as seen in Fig. 5.27. The output shaft torque has a large transient as seen in Fig. 5.27. Following the drop, the output torque increases until it reaches the

peak and later oscillates with high frequency. Again, the maximum output torque should be the same level as the output torque in the next gear. The frequency of the oscillation should be as small as possible. The high amplitude and frequency of the oscillation in the vehicle acceleration can be seen in Fig. 5.25 and derivative of acceleration in Fig. 5.26. The high frequency and amplitude in the output torque and vehicle acceleration indicate the poor shift quality.

The transient in Figs. 5.20 – 5.27 will be damped out by torque converter once 2–3 upshift completes when the turbine rigidly connects to the output shaft. While in the speed phase during the 2–3 upshift, the slipping clutch decouples the output shaft from the torque converter. Torque converter provides good damping characteristics to the powertrain similar to the 1–2 upshift.

5.1.3 3–4 Upshift

The characteristic of 3–4 upshift is analyzed in this section. The characteristic of shift is determined by how the torque capacities are adjusted for clutch $C4$. The torque capacities are adjusted by calibration until an acceptable shift quality is obtained. In 3–4 upshift, the on–coming clutch is clutch C_4 and off–going clutch is clutch C_3 as stated in Table 4.1. The shift is initiated when clutch C_4 starts to engage. Even though clutch C_3 is off-going clutch in this upshift, the characteristic of shift is determined by the torque capacity of the on–coming clutch C_4. The torque capacity profile of clutch C_3 does not affect 3–4 upshift because C_3 is a one–way clutch. C_3 like any other one-way clutch has a mechanism called "sprag" that enables the clutch spin freely when the on–coming clutch engages. Note that C_2 remains engaged through the 3–4 upshift. The operational principles of the clutch C_3 during 3–4 upshift is identical to those of clutch C_1 during 1–2 upshift. The 3–4 upshift process is similar to 1–2 upshift since the shift is accomplished with one–way clutch. The shift behavior

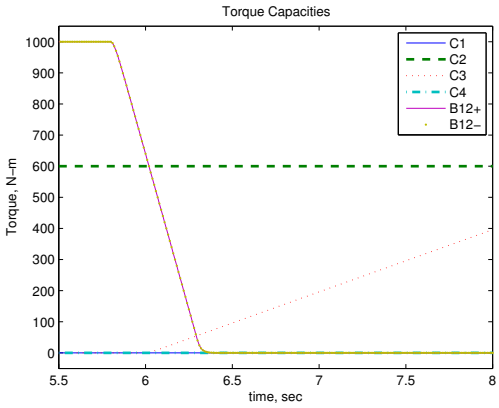

Figure 5.19. Torque Capacities During 2–3 Upshift.

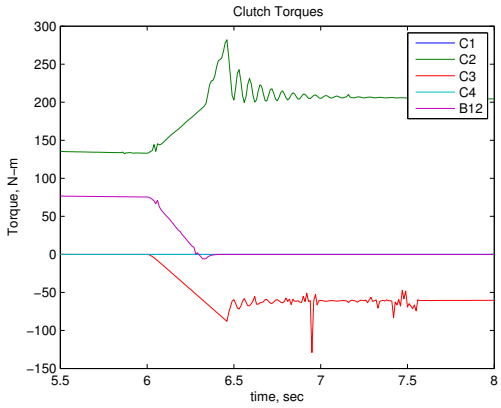

Figure 5.20. clutch Torques During 2–3 Upshift.

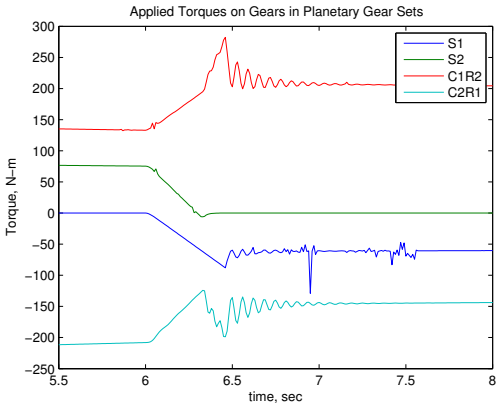

Figure 5.21. Applied Torques on Gears in Planetary Gear Sets During 2–3 Upshift.

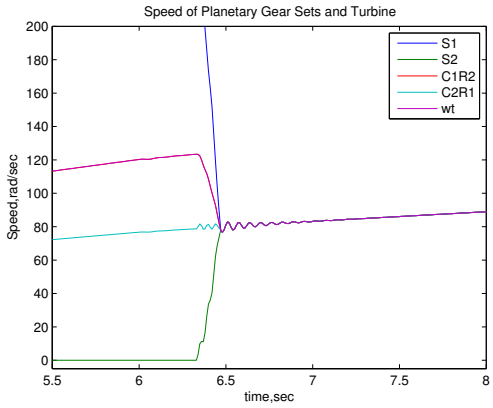

Figure 5.22. Speed of Planetary Gear Sets and Turbine During 2–3 Upshift.

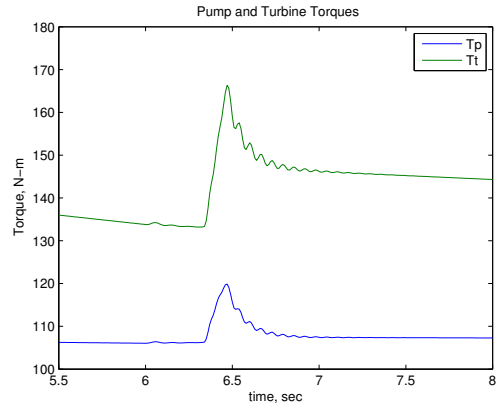

Figure 5.23. Pump and Turbine Torque During 2–3 Upshift.

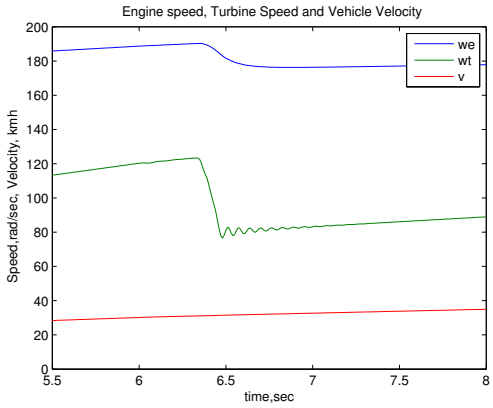

Figure 5.24. Engine Speed, Turbine Speed and Vehicle Velocity During 2–3 Upshift.

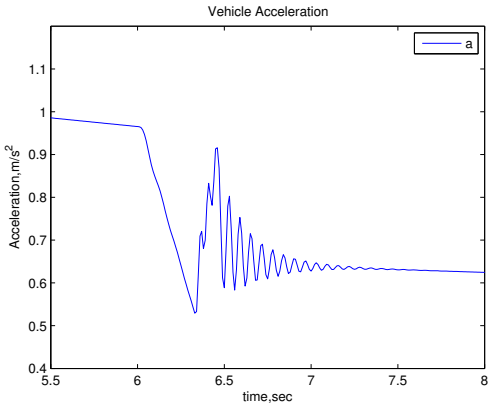

Figure 5.25. Vehicle Acceleration During 2–3 Upshift.

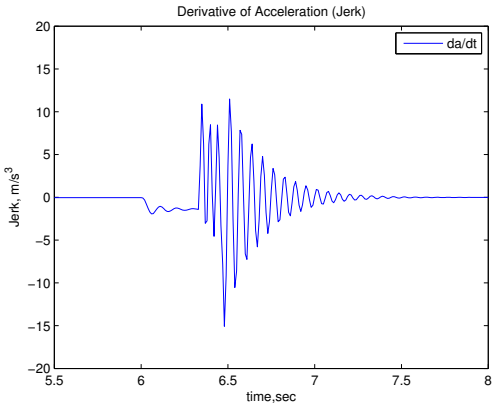

Figure 5.26. Derivative of Acceleration During 2–3 Upshift.

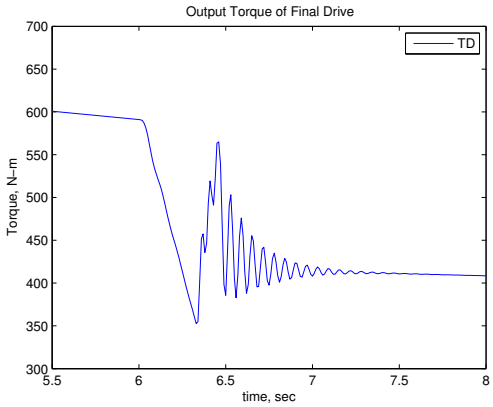

Figure 5.27. Output Torque of Final Drive During 2–3 Upshift.

has similar characteristics as discussed in 1–2 upshift section. However, the magnitude and frequencies of the oscillations are higher. Since during this 3–4 upshift the torque converter is not locked up as usually done, the torque multiplication is large as seen in Fig. 5.32. However, the torque converter lock–up is not studied in this research. This phenomena is considered as one of the bad shift quality indications and eliminated by feedback control in Chapter 6.

The 3–4 upshift starts with the torque phase of 3–4 upshift when clutch C_4 starts to engage as shown in Figs. 5.28 and 5.29. The output shaft torque drops as shown

in Fig. 5.36 because some parts of the turbine torque starts to go through carrier–1 while sun–1 still transmits the other part of turbine torque. This drop is undesirable, since the output torque to the drive shaft is interrupted and the passengers may feel this disturbance. During this torque phase, the speed of the turbine is still equal to the speed of sun–1 and carrier–1. Even though clutch C_4 is engaging and clutch torque on clutch C_4 is increasing, the turbine, carrier–1 and sun–1 speeds are still increasing. The torque at the turbine remains unchanged, thus it still speeds up. This happens because torque on clutch C_3 is decreasing while torque on clutch C_4 is increasing as seen in Fig. 5.29. Turbine torque is transmitted to sun–1 and carrier–1 as seen in Fig. 5.30.

At the beginning of inertia phase which is the end of torque phase, the turbine speed decelerates to a new synchronous speed. As seen in Fig. 5.31, the turbine is apart from sun–1 but still connected to carrier–1. At this moment, the sprag in clutch C_3 is overrun by sun–1, since the speed of sun–1 is slower than the speed of the turbine. Clutch C_3 becomes fully disengaged due to the sprag. Even though the hydraulic actuator at clutch C_3 is still on, as shown in Fig. 5.28, there is no clutch torque at clutch C_3 as seen in Fig. 5.29. Applied torque on sun–1 is equal to the clutch torque from clutch C_4 as seen in Fig. 5.30. In the speed phase, sun–1 is slipping until clutch C_4 is slowing down sun–1 to stop. The speed of the turbine inertia is reduced because the turbine torque is reduced by increasing clutch torque at clutch C_4 as seen in Fig. 5.32 and 5.33. The decrease in turbine speed results in a higher slip across the the converter, which yields a higher pump torque as seen in Fig. 5.32. Consequently, the engine speed is reduced. During this phase, the speed of turbine is dropping to the new synchronized speed to have the same speed as that of carrier–1 as seen in Fig. 5.31. At the end of speed phase, sun–1 has the zero speed

and there is no slipping in clutch C_4. Also, the clutch C_4 and applied torque on sun–1 reach their highest magnitude as seen in Figs. 5.29 and 5.30, respectively.

The output shaft torque has a large transient as seen in Fig. 5.36. Following the drop, the output torque increases until it reaches the peak and later oscillates with high frequency. Again, the maximum output torque should be the same level as the output torque in the next gear. The frequency of the oscillation should be as small as possible. Also high amplitude and frequency of the oscillations can be seen in the vehicle acceleration in Fig. 5.34 and derivative of acceleration in Fig. 5.35. As shown in Fig. 5.35, high frequency and amplitude in jerk indicates poor shift quality. Similarly, the high frequency and amplitude in the output torque and vehicle acceleration indicate poor shift quality.

The transient will be damped out by torque converter once 3–4 upshift completes when the turbine rigidly connects to the output shaft. During the speed phase, the slipping clutch decouples the output shaft from the torque converter. The shift duration is about 1 sec. Even with this short duration, but there are torque and speed oscillations with high amplitude and frequency as shown in the figures. These imply poor shift quality.

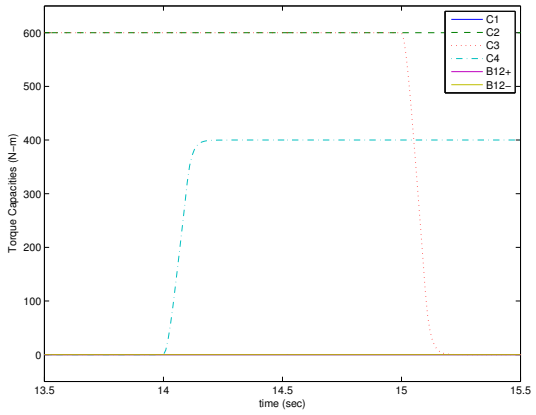

Figure 5.28. Torque Capacities During 3–4 Upshift.

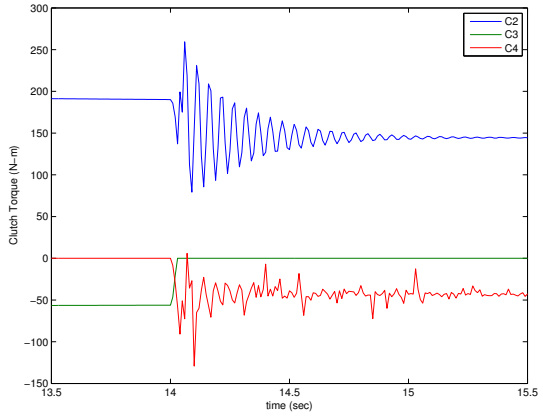

Figure 5.29. clutch Torques During 3–4 Upshift.

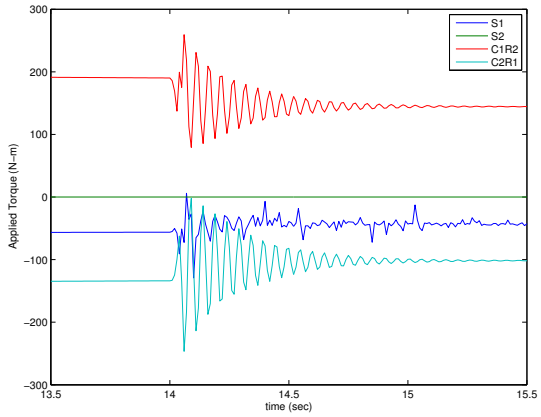

Figure 5.30. Applied Torques on Gears in Planetary Gear Sets During 3–4 Upshift.

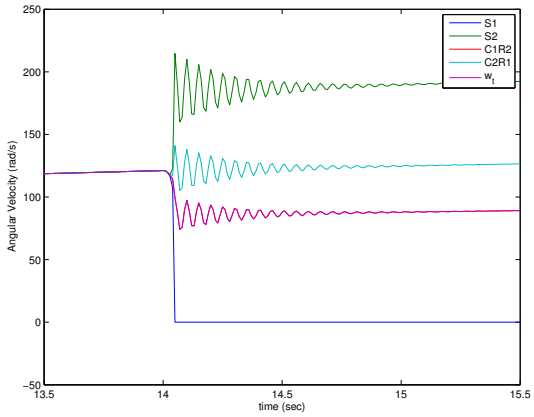

Figure 5.31. Speed of Planetary Gear Sets and Turbine During 3–4 Upshift.

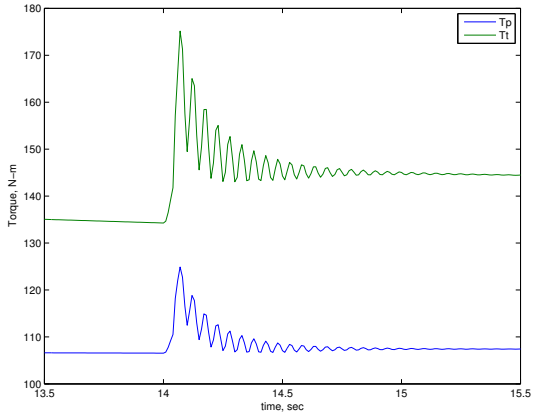

Figure 5.32. Pump and Turbine Torque During 3–4 Upshift.

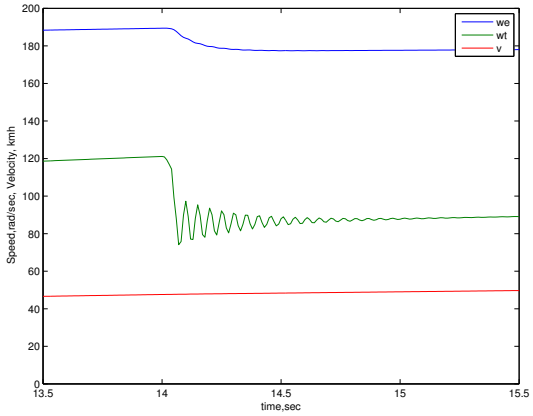

Figure 5.33. Engine Speed, Turbine Speed and Vehicle Velocity During 3–4 Upshift.

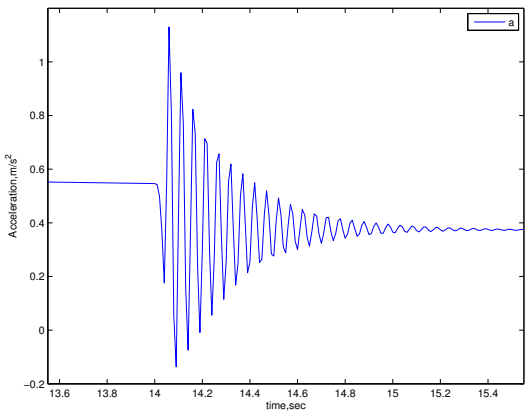

Figure 5.34. Vehicle Acceleration During 3–4 Upshift.

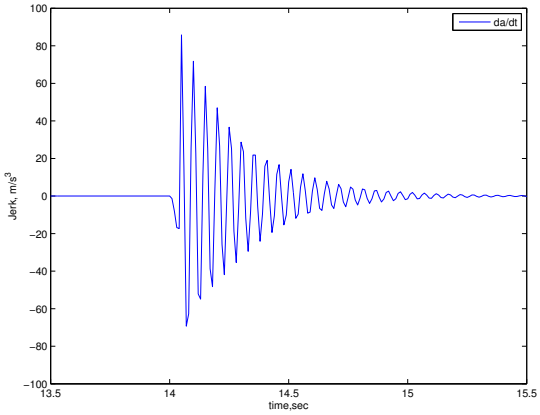

Figure 5.35. Derivative of Acceleration During 3–4 Upshift.

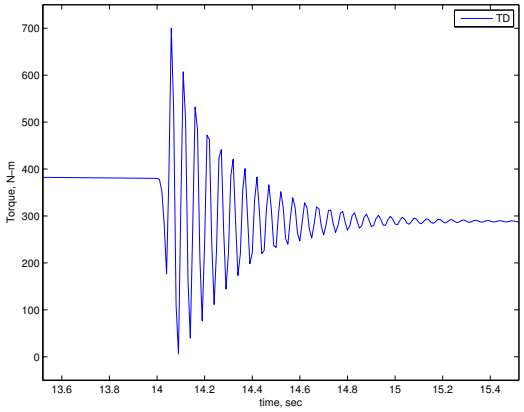

Figure 5.36. Output Torque of Final Drive During 3–4 Upshift.

5.2 Powertrain with Stiff Drive Shaft Using Woods Friction Model

The powertrain in this section had a hydraulic actuation system, Wood friction model used for the clutches and bands and the drive shaft modeled as a stiff one. The hydraulic actuation system is added to have pressure as the control variable. This way, the limitations of current hydraulic systems are investigated in regulating friction element pressures for enhancing shift quality. Employment of Wood friction model is to improve accuracy of the models of the friction elements. The output shaft is modeled as a torsional spring in the previous section, Section 5.1. While this is a common modeling approach in shift dynamics research, in this section, the output shaft is assumed to be stiff. This will help investigate whether the shift quality can be studied without the oscillations in torque and speed variables, as observed in Section 5.1.

Figure 5.37 shows the pressure profiles at clutches and bands adjusted for 1–2 and 2–3 upshifts. The speed of turbine and engine are illustrated in Fig. 5.38. The speed of planetary gear sets are shown in Fig. 5.39. Figure 5.40 shows that the vehicle accelerates from about 10 km/h to 50 km/h. In first gear, clutch C_1 and band B_{12} are engaged. The pressure at the clutch and band is at 1000 kPa. In first gear, the turbine speed and sun–1 speed are equal while sun–2 speed is zero as shown in Fig. 5.38. During 1^{st}–2^{nd} upshift, clutch C_2 is engaged while the pressure on clutch C_1 and band B_{12} stay on as shown in Fig. 5.37. This is because clutch C_1 is a one–way clutch and allows sun–1 to rotate faster than the turbine even when it is engaged. During this shift, the turbine speed decreases while carrier–1 accelerates to have a synchronized speed at the end of the shift. In second gear, clutch C_2 is locked up and the turbine speed is equal to carrier–1 speed. Clutch C_1 is disengaged after the shift is completed. During 2^{nd}–3^{rd} upshift, band B_{12} is released and clutch C_3 is engaged, as shown in Fig. 5.37. Fig. 5.39 shows that sun–2 is accelerated while sun–1 and

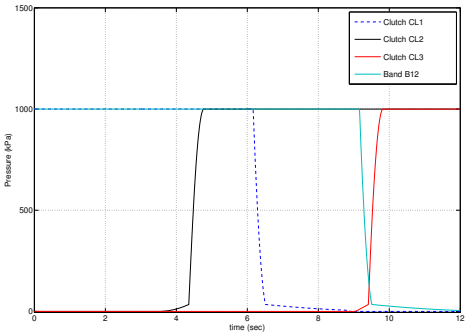

Figure 5.37. Pressure at Clutch and Band During 1–2, 2–3 upshifts.

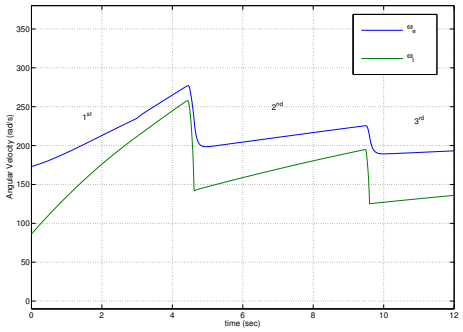

Figure 5.38. Turbine and Engine Speeds During 1–2, 2–3 upshifts.

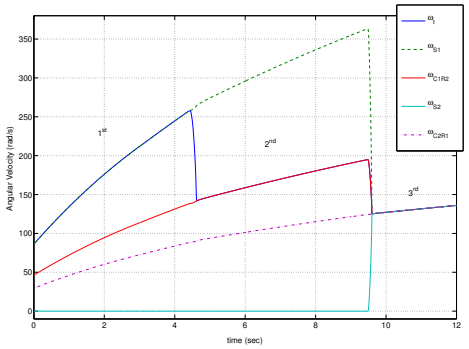

Figure 5.39. Turbine and Subassembly Speeds During 1–2, 2–3 upshifts.

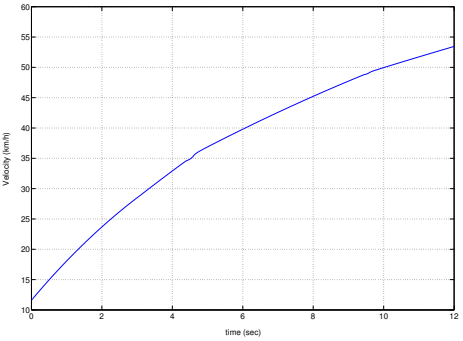

Figure 5.40. Vehicle Speed.

carrier–1 are decelerated to have the synchronized speed at the end of 2^{nd}–3^{rd} upshift. Planetary gear sets rotate with the the same speed as the turbine in third gear.

Figure 5.41 shows the transmission output shaft torque, which is transmitted to the drive shaft. The output torque spikes during the 1^{st}–2^{nd} and 2^{nd}–3^{rd} upshifts. The on–coming clutch causes the high magnitude transient in the output torque during the upshifts. As the pressure is raised on the on–coming clutch, the friction torque is increased. The on–coming clutch friction torque resists the rotation of the turbine while it pushes the gear that is connected to the another side of the clutch.

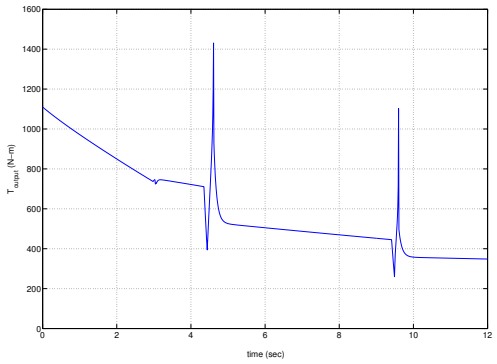

Figure 5.41. Transmission Output Shaft Torques T_s.

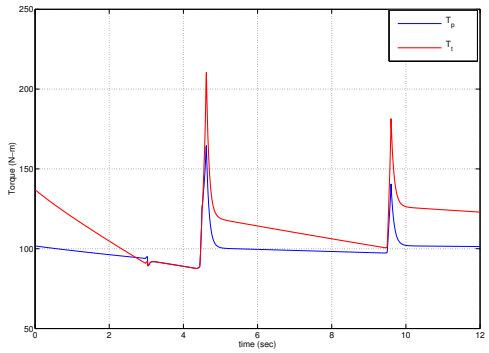

Figure 5.42. Turbine and Pump Torques T_t and T_p.

The similar transients appear in the vehicle acceleration and its derivative. These transients depend on the clutch pressure profile. In this case, the pressure is applied to the clutch rapidly and causes the shorter and sever transients than it should be in a normal operation.

During torque phase in upshift, the turbine speed continues to increase. The output torque remains unchanged. This is because torque is transmitted through the on–coming clutch and off–going clutch. During the speed phase, the off–going clutch is fully released. The on–coming clutch friction torque is increased to connect turbine to the new component in the planetary gear set. This results in a turbine speed decreases as shown in Figs. 5.38 and 5.39. This decrease in turbine speed results in a high slip over across the converter, which yields a higher pump torque. This causes the engine inertia to decelerate. Figure 5.42 shows the torque converter pump and turbine torque. The torque converter operates in the torque multiplying mode most of the time. Figure 5.40 shows the vehicle speed during the 1–2 and 2–3 shifts.

5.2.1 1–2 Upshift

The characteristics of 1–2 upshift for the powertrain model with stiff drive shaft is analyzed in this section. The characteristics of the shift is influenced by the hydraulic pressure profile and the friction model of the clutches and bands. The pressure profile is determined by calibration until an acceptable shift quality is obtained. An improper pressure profile results in "tie up" or "flare up". In 1–2 upshift, the on–coming clutch is clutch C_2 and off–going clutch is clutch C_1 as listed in Table 4.1. The shift happens when clutch C_2 starts to engage, which connects the turbine with carrier–1. Since the off-going clutch C_1 is a one-way clutch, the characteristics of the shift is solely influenced by the pressure profile and the friction model of the on–coming clutch C_2. As shown in Fig. 5.37, the pressure profile of clutch C_1 remains constant during 1–2 upshift. Band B_{12} remains engaged through the 1–2 upshift with constant pressure.

The torque phase of 1–2 upshift starts when clutch C_2 engages by applied pressure as shown in Figs. 5.37. The friction torque on clutches C_1, C_2 and band B_{12} are shown in Fig. 5.48. The output shaft torque drops as shown in Fig. 5.46 because part of turbine torque starts to transmit via carrier–1 while sun–1 still transmits the other part of turbine torque. This drop is undesirable since the output torque to the drive shaft is interrupted and the passengers may feel this disturbance. During this torque phase, the speed of turbine is still equal to the speed of sun–1. Even tough clutch C_2 is engaged and clutch torque on clutch C_2 is increasing, the turbine and sun–1 still speed up. The torque at the turbine remains unchanged, thus it still speeds up. This happens because torque on clutch C_1 is decreasing while torque on clutch C_2 is increasing as seen in Fig. 5.48. Turbine torque is transmitted from sun–1 to carrier–1 as seen in Fig. 5.47.

At the beginning of inertia phase, the turbine speed decreases to a new synchronous speed. As seen in Fig. 5.44, the turbine rotates apart from sun–1. At this moment, the sprag is overrun by sun–1 since the speed of sun–1 is faster than the speed of the turbine. Clutch C_1 fully disengages due to the sprag. Even though the hydraulic actuator at clutch C_1 is still on as shown in Fig. 5.37, there is no clutch torque at clutch C_1 as seen in Fig. 5.48. In the speed phase, the turbine and carrier–1 are slipping until clutch C_2 slows down the turbine and speeds up carrier–1. The turbine inertia slows down as shown in Fig. 5.43 because the turbine torque is reduced by increased clutch torque at clutch C_2 as seen in Fig. 5.48. The decrease in turbine speed results in a higher slip across the the converter, which yields a higher pump torque as seen in Fig. 5.47. Consequently, the engine speed is reduced. During this phase, the speed of turbine drops to a new synchronized speed with carrier–1 as shown in Figs. 5.43 and 5.44. At the end of the speed phase, turbine and carrier–1 have the same speed and there is no slipping in clutch C_2. Also, the clutch C_2 torque reaches its maximum as seen in Fig. 5.48.

At the end of 1–2 upshift, clutch C_2 torque drops to the level of the turbine torque as can be seen in Figs. 5.48 and 5.47. The output shaft torque has a large interruption as seen in Fig. 5.46. Following the large drop, the output torque increases until it reaches its peak. There are large variations in the vehicle acceleration and in the derivative of the acceleration (jerk) as seen in Figs. 5.49 and 5.50, respectively. These variations indicate poor shift quality. The transient is damped out by the torque converter once the 1–2 upshift is complete when the turbine rigidly connects to the output shaft.

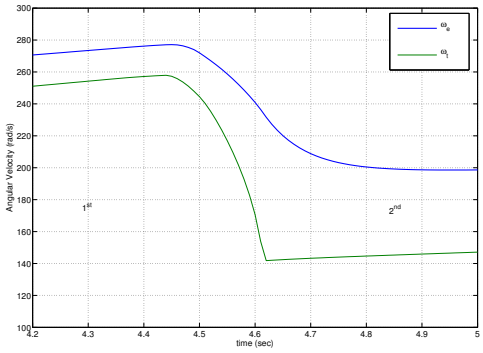

Figure 5.43. Turbine and Pump Speed During 1–2 Upshift for Stiff Drive Shaft.

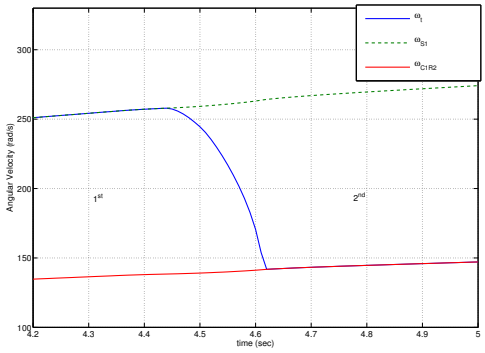

Figure 5.44. Speed of Planetary Gear Sets and Turbine During 1–2 Upshift for Stiff Drive Shaft.

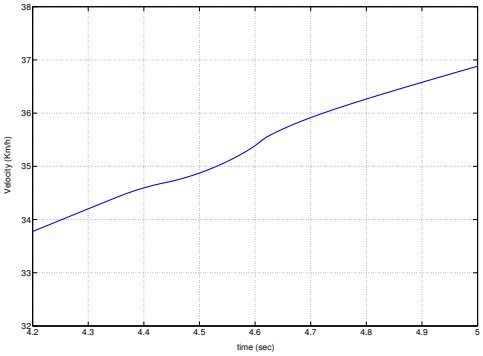

Figure 5.45. Vehicle Speed During 1–2 Power–On Upshift.

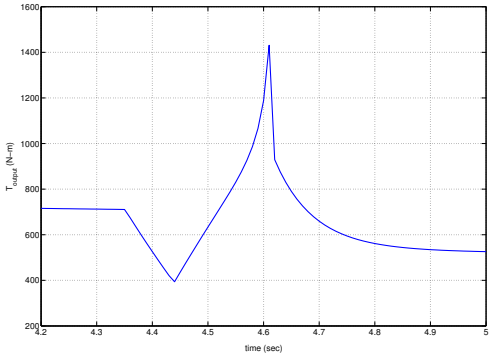

Figure 5.46. Output Torque of Stiff Drive Shaft During 1–2 Upshift.

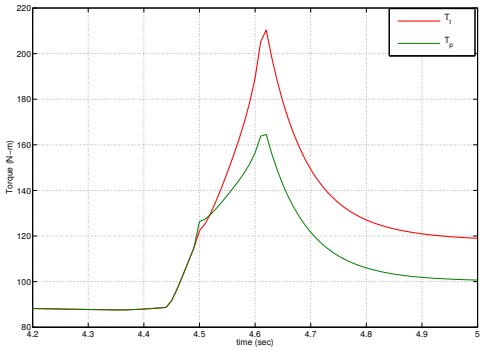

Figure 5.47. Pump and Turbine Torque During 1–2 Upshift for Stiff Drive Shaft.

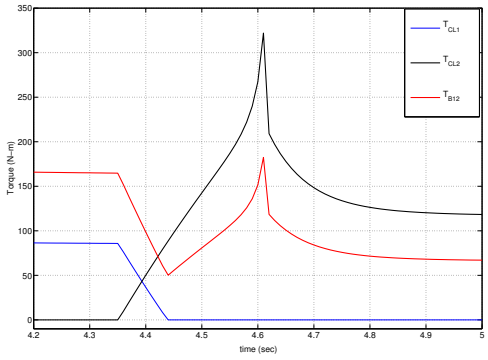

Figure 5.48. Clutch Torques During 1–2 Upshift for Stiff Drive Shaft.

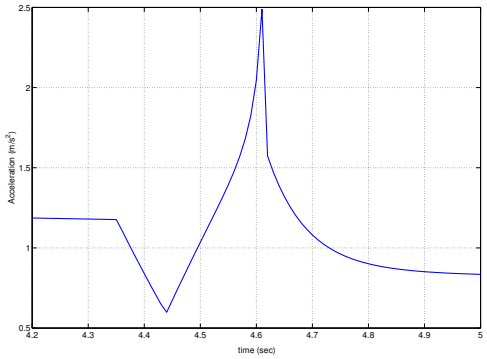

Figure 5.49. Vehicle Acceleration During 1–2 Upshift.

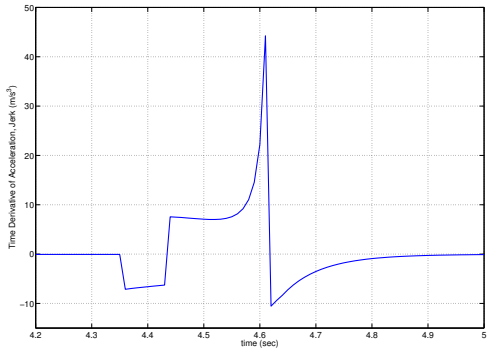

Figure 5.50. Derivative of Acceleration During 1–2 Upshift.

5.2.2 2–3 Upshift

The characteristics of 2–3 upshift is determined by the pressure profiles on band B_{12} and clutch C_3. Band B_{12} should be released and clutch C_3 should be applied to have 2–3 shift. A shift that requires both an on-coming and off-going elements is called "a swap shift". The timing as well as the pressure profiles for B_{12} and C_3 are very important for shift quality. If C_3 is applied before B_{12} is release, a tie–up will occur while a flare will take place if B_{12} released before C_3 is applied. The pressure profiles for clutch C_3 and band B_{12} are shown in Fig. 5.37.

The shift is initiated by lowering the pressure on band B_{12} and, after a short time, raising the pressure of clutch C3, as shown in Fig. 5.37. The increasing pressure on C_3 while B_{12} still has some pressure splits the torque transmission between C_3 and B_{12}. This can be seen in Figs. 5.56 and 5.55. The transmission torque is carried through carrier–1 and sun–1 as seen in Fig. 5.56. The turbine torque remains unchanged during the torque phase as shown in Fig. 5.55. The more torque goes through C_3, the less torque is carried by B_{12}. The sharp drops in the output shaft torque and the vehicle acceleration indicate the beginning of torque phase as seen in Figs. 5.54 and 5.57. This drop happens since the output torque to the drive shaft is

interrupted due to the gear ratio change. At the time when the torque capacity of B_{12} drops to zero and B_{12} no longer carries torque, C_3 starts carrying all the torque and the decrease in the output torque stops. This signifies the end of the "torque transfer phase" and the beginning of the "ratio change phase", or "inertia phase". During the inertia phase, the gear ratio is between the 2^{nd} gear and the 3^{rd} gear ratios. Since B_{12}, which connects sun–2 to the transmission case, is fully released, sun–2 starts rotating as seen in Fig. 5.52. C_3 is used to connect sun–1 to the turbine shaft. As C_3 is engaged, the clutch slips until sun–1 and the turbine have the same speed. Once Sun–1 and the turbine rotate together with the sun–2 (zero slip in C_3) and they all have the same speed as carrier–2 (connected to the output shaft), the 3^{rd} gear ratio ($= 1$) is obtained and the shift is completed as shown in Fig. 5.52. Then, the torque carried by C_3 is only the amount to prevent slipping. Once the shift is completed, the pressure on the clutch is increased to prevent the slipping with no effect on the speeds or the torques. Note that the output torque drop stops at the beginning of the inertia phase and the output torque shows a transient in the inertia phase.

The speed of turbine is reduced because the turbine torque is reduced by the increase in the clutch torque at C_2 and C_3 as seen in Figs. 5.51. The friction torque on the clutches and band are illustrated in Fig. 5.56. The decrease in the turbine speed results in a higher slip across the converter, which yields a higher pump torque as seen in Fig. 5.55. Consequently, the engine speed is reduced.

At the end of 2–3 upshift, the output shaft torque has a large transient as shown in Fig. 5.54. As a result, the vehicle acceleration and its derivative (jerk) show large transients, as can be seen in Figs. 5.57 and 5.58, respectively. These are indications of poor shift quality.

The transient will be damped out by the torque converter once the 2–3 upshift is complete when the turbine is rigidly connected to the output shaft. During the

speed phase of the 2–3 upshift, the slipping clutch decouples the output shaft from the torque converter. Torque converter provides good damping characteristics to the powertrain as also seen in 1–2 upshift.

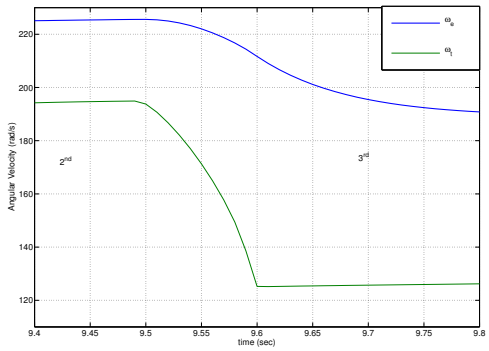

Figure 5.51. Turbine and Pump Speed During 2–3 Upshift for Stiff Drive Shaft.

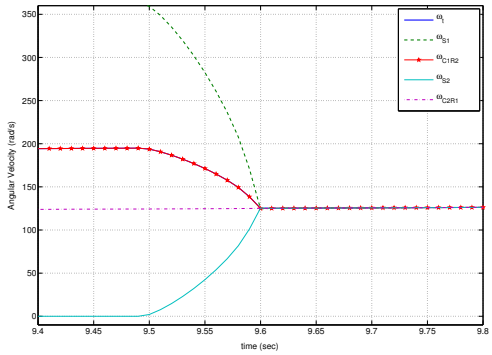

Figure 5.52. Speed of Planetary Gear Sets and Turbine During 2–3 Upshift for Stiff Drive Shaft.

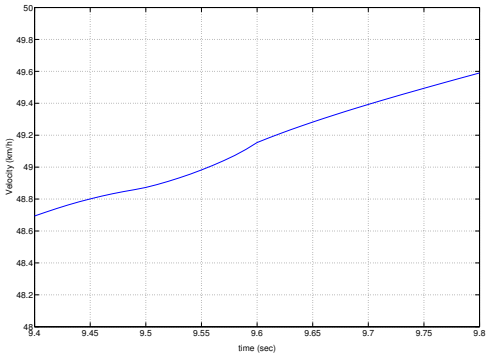

Figure 5.53. Vehicle Speed During 2–3 Power–On Upshift.

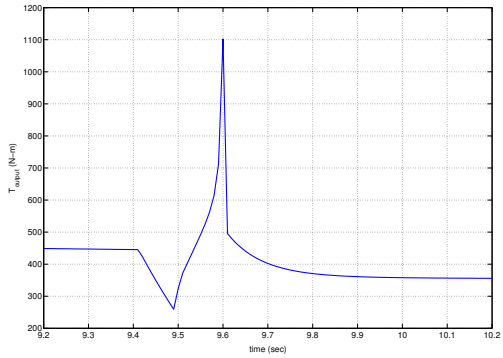

Figure 5.54. Output Torque of Stiff Drive Shaft During 2–3 Upshift.

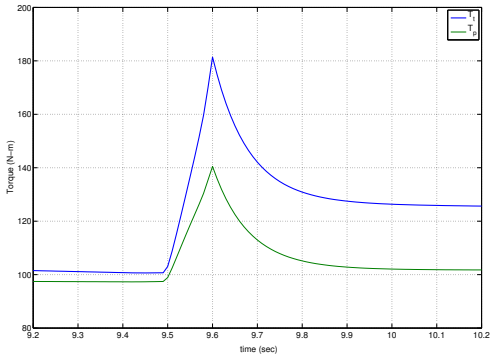

Figure 5.55. Pump and Turbine Torque During 2–3 Upshift for Stiff Drive Shaft.

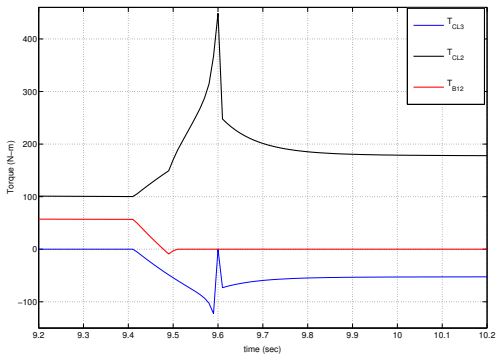

Figure 5.56. Clutch Torques During 2–3 Upshift for Stiff Drive Shaft.

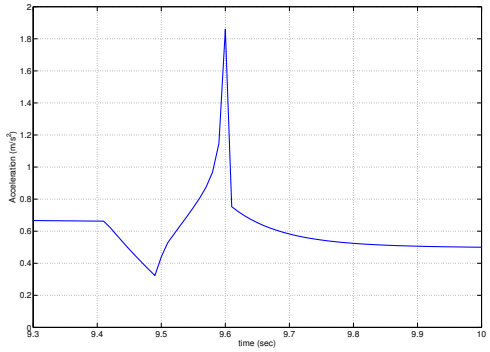

Figure 5.57. Vehicle Acceleration During 2–3 Upshift.

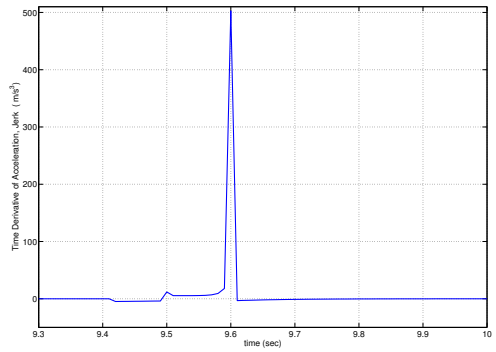

Figure 5.58. Derivative of Acceleration During 2–3 Upshift.

5.3 Powertrain with Non–stiff Drive Shaft Using Woods Friction Model

The simulation results in this section corresponding to the powertrain model with the drive shaft modeled as a compliant shaft. The conditions used here are the same as in the previous section, where the drive shaft is assumed to be a non–stiff shaft.

Figures 5.59–5.62 show an overview of the simulation results when shifts 1–2, 2–3 and 3–4 are conducted. The oscillations are excited by the shifts are observed as a results of the drive shaft compliant effect. The details of the 1–2 upshift are

shown in Figs. 5.66 to 5.73 and the details of the 2–3 upshift are given in Figs. 5.74 to 5.81. The torque phase and speed phase occur while the on–coming clutch engages and off–going clutch disengages. The shift characteristics observed in this case are similar to those in the stiff shaft simulation. However, this case shows high frequency oscillations can be observed due to the compliant shaft model included in the powertrain. Figure 5.73 and 5.81 show the jerks during the 1–2 and 2–3 upshifts.

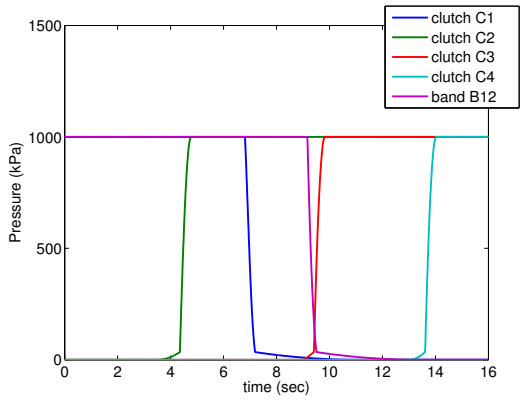

Figure 5.59. Pressure at Clutch and Band During 1^{st}–4^{th} gear upshifts.

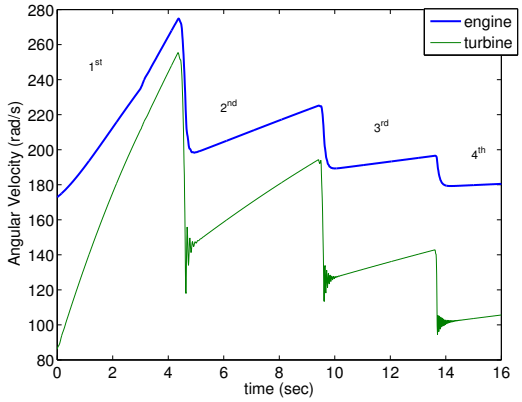

Figure 5.60. Turbine and Engine Speeds During 1^{st}–4^{th} gear upshifts.

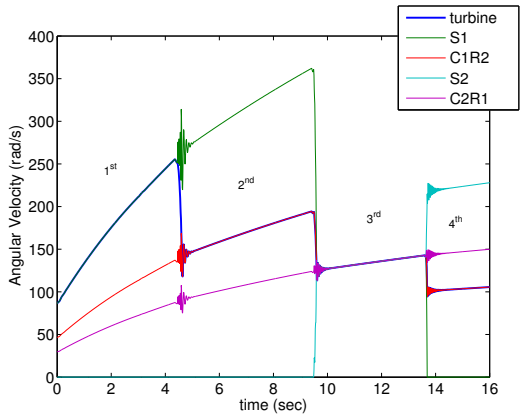

Figure 5.61. Turbine and Subassembly Speeds During 1^{st}–4^{th} gear upshifts.

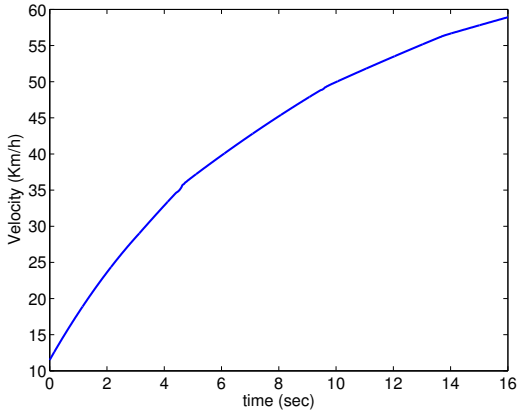

Figure 5.62. Vehicle Velocity.

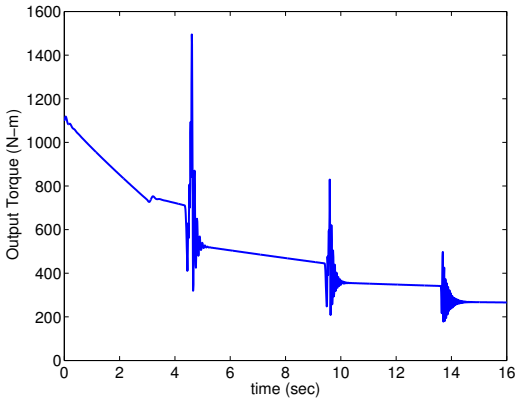

Figure 5.63. Transmission Output Shaft Torque.

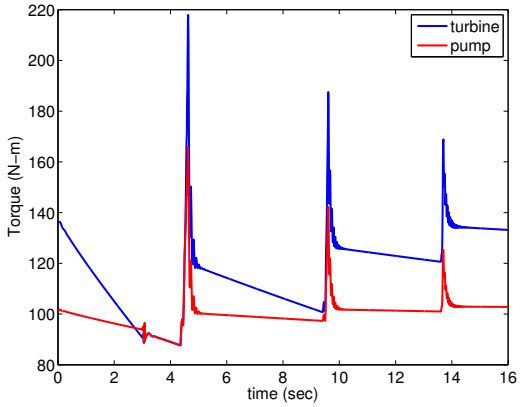

Figure 5.64. Turbine and Pump Torques T_t and T_p.

5.3.1 1–2 Upshift

The characteristics of the 1–2 upshift is analyzed in this section. The characteristics of the shift is defined by the pressure profile on the clutches and bands. In the 1–2 upshift, the on–coming clutch is clutch C_2 and off–going clutch is clutch C_1 as listed in Table 4.1. The shift is initiated with connecting the turbine with carrier–1 by engaging clutch C_2. Even though clutch C_1 is off-going clutch in this upshift, the characteristics of the shift is solely influenced by pressure profile of the on–coming clutch C_2 because clutch C_1 is a one-way clutch. As shown in Fig. 5.59, the pressure profile of clutch C_1 remains constant during 1–2 upshift. Band B_{12} remains engaged during the 1–2 upshift with the constant torque capacity.

The 1–2 upshift stars with the torque phase when clutch C_2 engages as shown in Figs. 5.59 and 5.71. The output shaft torque drops as seen in Fig. 5.69 because some parts of turbine torque start to transmit via carrier–1 while sun–1 still transmits the other part of the turbine torque. During this torque phase, the speed of turbine is still equal to the speed of sun–1. Even tough clutch C_2 is engaged and clutch torque on clutch C_2 is increasing, the turbine and sun–1 speeds still increase. The torque at the turbine remains unchanged, thus it still speeds up. This is because torque on

clutch C_1 decreases while torque on clutch C_2 increases as seen in Fig. 5.71. Turbine torque is transmitted from sun–1 to carrier–1.

At the beginning of the inertia phase, the turbine speed decelerates to a new synchronous speed. As seen in Fig. 5.67, turbine detaches from sun–1. At this moment, the sprag is overrun by sun–1 since the speed of sun–1 is faster than the speed of turbine while the hydraulic actuator at clutch C_1 is still on as shown in Fig. 5.59. Once the clutch overruns, the clutch torque at clutch C_1 goes to zero as seen in Fig. 5.71. In the speed phase, turbine and carrier–1 are slipping until clutch C_2 slows down the turbine and speeds up carrier–1. The turbine speed decreases because the turbine torque is reduced by increased clutch torque at clutch C_2 as seen in Figs. 5.66 and 5.70. The decrease in turbine speed results in a higher slip across the the converter, which yields a higher pump torque as seen in Fig. 5.66. Consequently, the engine speed is reduced. During this phase, the turbine speed drops to a new synchronized speed with the speed of carrier–1 as shown in Fig. 5.67. At the end of the speed phase, turbine and carrier–1 speed difference goes to zero and there is no slipping in clutch C_2. Also, the clutch C_2 torque on carrier–1 reach its highest magnitude as seen in Figs. 5.71.

At the end of the 1–2 upshift, carrier–1 torque drops to the level of the turbine torque as shown in Figs. 5.70 and 5.71. The output shaft torque has a large transient as seen in Fig. 5.69. Following the drop, the output torque increases until it reaches its peak and then oscillates with high frequency. Similar oscillation can also be seen in the vehicle acceleration in Fig. 5.72 and the derivative of the acceleration in Fig. 5.73. The high frequencies and large transients in the output torque, vehicle acceleration and jerk indicate poor shift quality.

The transient will be damped out by the torque converter once the 1–2 upshift is complete when the turbine rigidly connects to the output shaft. During the speed

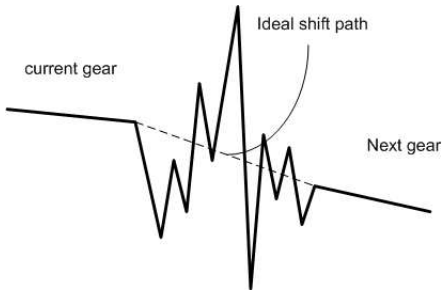

Figure 5.65. Ideal Path During Shift for Non–Stiff Drive Shaft.

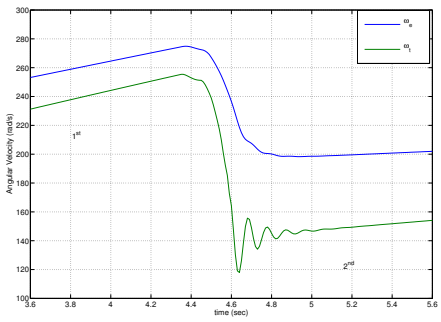

Figure 5.66. Turbine and Pump Speed During 1–2 Upshift for Non–Stiff Drive Shaft.

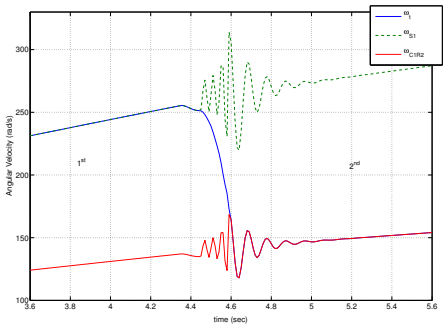

Figure 5.67. Speed of Planetary Gear Sets and Turbine During 1–2 Upshift for Non–Stiff Drive Shaft.

phase of the 1–2 upshift, the slipping clutch decouples the output shaft from the torque converter. The shift duration is about 1 sec. Even though the shift takes a short amount of time of 1 sec, the high frequencies and large transients indicate poor shift quality. As depicted in Fig. 5.65, in an ideal case, the transient from one gear to another in a shift should be very smooth for a good shift quality as opposed to what is observed with 1–2 upshift analyzed in this section.

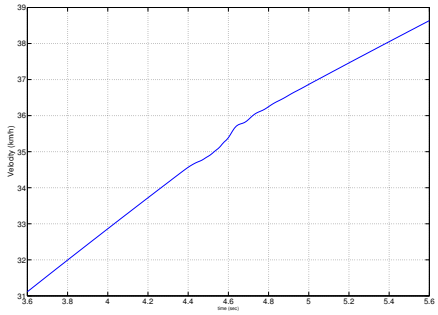

Figure 5.68. Vehicle Speed During 1–2 Power–On Upshift.

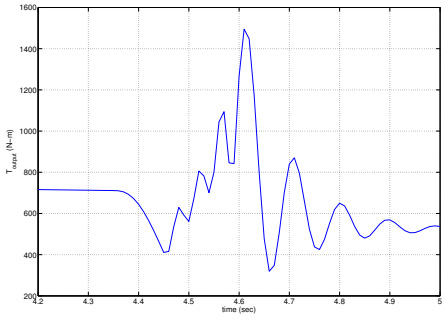

Figure 5.69. Output Torque of Stiff Drive Shaft During 1–2 Upshift.

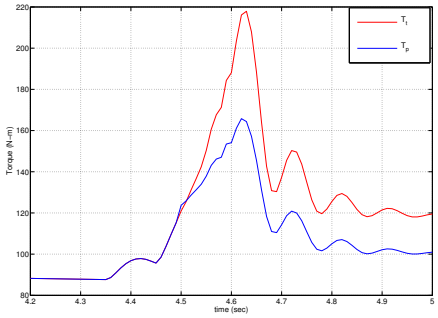

Figure 5.70. Pump and Turbine Torque During 1–2 Upshift for Non–Stiff Drive Shaft.

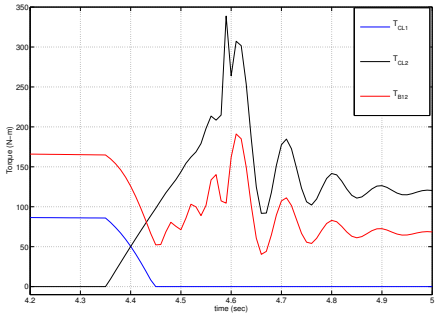

Figure 5.71. Clutch Torques During 1–2 Upshift for Non–Stiff Drive Shaft.

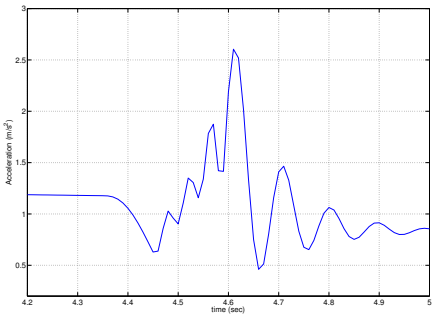

Figure 5.72. Vehicle Acceleration During 1–2 Upshift.

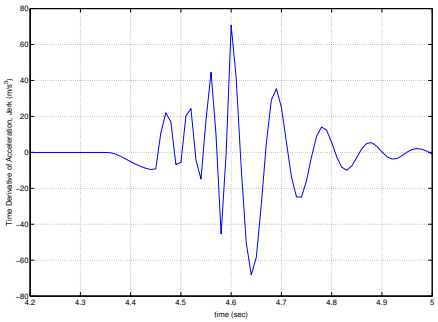

Figure 5.73. Derivative of Acceleration During 1–2 Upshift.

5.3.2 2–3 Upshift

The characteristics of the 2–3 upshift are determined by the torque capacity profiles of band B_{12} and clutch C_3. Band B_{12} should be released and clutch C_3 should be applied to conduct 2–3 shift. A shift that requires both an on-coming and off-going elements is called "a swap shift". The timing and the profiles of the torque capacity adjustment for B_{12} and C_3 are the defining factors for the shift characteristics. In this upshift the timing of the on–coming element (the clutch being applied) and the off–going element (the band being released) are tuned up to obtain better upshifting results.

The shift is initiated by lowering the pressure on band B_{12} and, after a short time, raising the pressure on clutch C3, as shown in Fig. 5.59. The increasing pressure on C_3 while B_{12} still has some pressure splits the torque transmission between C_3 and B_{12}. This can be seen in Fig. 5.79. The transmission torque is carried through carrier–1 and sun–1. The turbine torque remains unchanged during this torque phase as shown in Fig. 5.78. The more torque goes through C_3, the less torque is carried by B_{12}. The sharp drops in the output shaft torque and the vehicle acceleration indicate the beginning of torque phase as seen in Figs. 5.77 and 5.80. This drop happens since the output torque to the drive shaft is interrupted due to changing gear ratio. At the time when the torque capacity of B_{12} drops to zero and B_{12} no longer carries torque, C_3 starts carrying all the torque and the decrease in the output torque stops. This signifies the end of the "torque transfer phase" and the beginning of the "ratio change phase", or "inertia phase". During the inertia phase, the gear ratio is between the 2^{nd} gear and the 3^{rd} gear ratios. Since B_{12}, which connects sun–2 to the transmission case, is fully released, sun–2 starts rotating as seen in Fig. 5.75. C_3 is used to connect sun–1 to the turbine shaft. As C_3 is engaged, the clutch slips until sun–1 and the turbine have the same speed. Once Sun–1 and the turbine rotate together with the

sun–2 (zero slip in C_3) and they all have the same speed as carrier–2 (connected to the output shaft), the 3^{rd} gear ratio (= 1) is obtained and the shift is complete as shown in Fig. 5.75. Then, the torque carried by C_3 is only the amount to prevent slipping. Once the shift is completed, the pressure on the clutch can be increased with no effect on the speeds or the torques. Note that the output torque drop stops at the beginning of the inertia phase and the output torque shows a transient in the inertia phase.

The turbine torque is reduced by increasing clutch torque at C_3 as seen in Fig. 5.79, which results in reduction in the turbine speed as seen in Fig. 5.74. The decrease in turbine speed leads to a higher slip across the converter, which yields a higher pump torque as seen in Fig. 5.78. Consequently, the engine speed is reduced.

At the end of the 2–3 upshift, the magnitude of carrier–2/ring–1 torque drops to the level of the turbine torque as shown in Figs. 5.79 and 5.78. The output shaft torque begins to oscillate as can be seen in Fig. 5.77 and has a large transient. Following the drop, the output torque increases until it reaches its peak and then oscillates with high frequency. Figs. 5.80 and 5.81 show that the vehicle acceleration and its derivative (jerk) go through large transients with high frequencies, which are indicators of poor shift quality.

The transients shown in Figs. 5.74 – 5.81 are damped out by the torque converter once the 2–3 upshift is over when the turbine rigidly connects to the output shaft. During the speed phase of the 2–3 upshift, the slipping clutch decouples the output shaft from the torque converter.

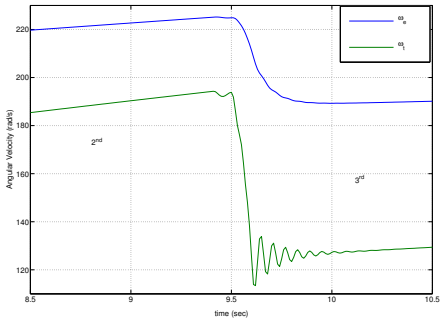

Figure 5.74. Turbine and Pump Speed During 2–3 Upshift for Non–Stiff Drive Shaft.

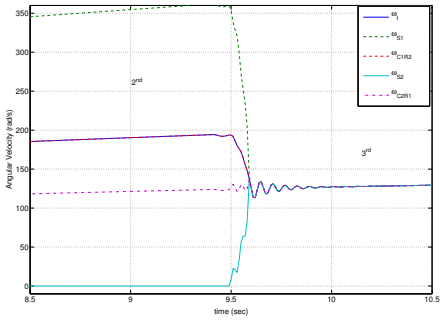

Figure 5.75. Speed of Planetary Gear Sets and Turbine During 2–3 Upshift for Non–Stiff Drive Shaft.

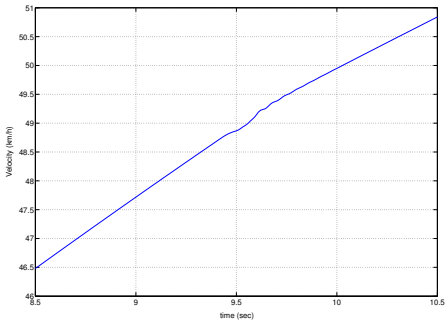

Figure 5.76. Vehicle Speed During 2–3 Power–On Upshift.

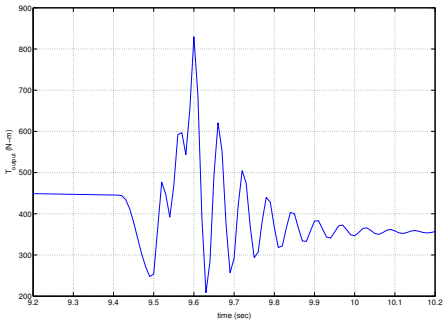

Figure 5.77. Output Torque of Stiff Drive Shaft During 2–3 Upshift.

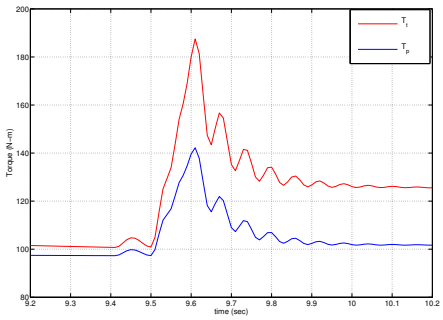

Figure 5.78. Pump and Turbine Torque During 2–3 Upshift for Non–Stiff Drive Shaft.

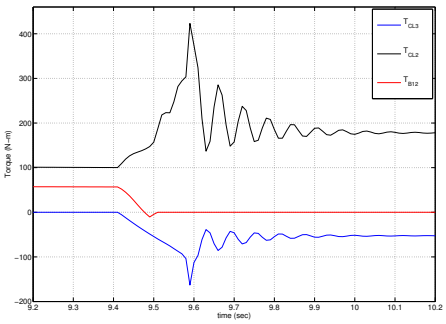

Figure 5.79. Clutch Torques During 2–3 Upshift for Non–Stiff Drive Shaft.

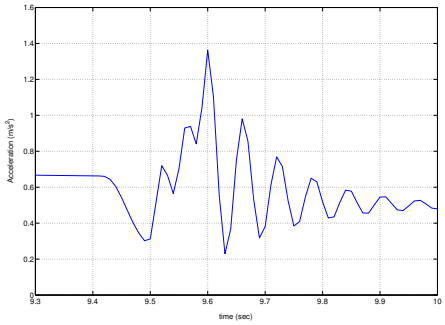

Figure 5.80. Vehicle Acceleration During 2–3 Upshift.

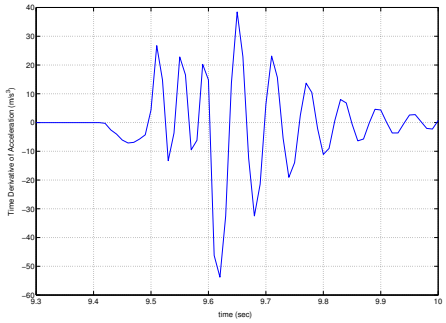

Figure 5.81. Derivative of Acceleration During 2–3 Upshift.

5.3.3 3–4 Upshift

The characteristics of the 3–4 upshift are analyzed in this section. In the 3–4 upshift, the on–coming clutch is clutch C_4 and off–going clutch is clutch C_3 as listed in Table 4.1. The shift starts when clutch C_4 is engaging to stop sun–1. Even though clutch C_3 is off-going clutch in this upshift, the shift quality is solely influenced by the pressure profile of the on–coming clutch C_4 since C_3 is a one-way clutch with constant pressure profile as shown in Fig. 5.59.

The 3–4 upshift starts with the torque phase when clutch C_4 starts to engage as shown in Figs. 5.59 and 5.87. The output shaft torque drops as seen in Fig. 5.86 because some parts of turbine torque starts to transmit via carrier–1 while sun–1 still transmits the rest of the turbine torque. During the torque phase, the speed of turbine remains equal to the speed of carrier–1. Clutch C_4 is engaging and clutch torque on clutch C_4 is increasing. Consequently, the turbine and carrier–1 speed decrease. The turbine torque remains unchanged. This is because the torque on clutch C_3 is decreasing while torque on clutch C_4 is increasing as seen in Fig. 5.87. Turbine torque is transmitted from sun–1 to carrier–1.

At the beginning of inertia phase, the turbine speed decelerates to a new synchronous speed. As seen in Fig. 5.83, turbine detaches from sun–1. At this moment,

the sprag is overrun by sun–1 since the speed of sun–1 is slower than the turbine speed. Clutch C_3 fully disengages due to the sprag while the pressure is kept as shown in Fig. 5.59. Once clutch C_3 overruns, the throughput torque drops to zero as seen in Fig. 5.87. In the speed phase, the turbine and carrier–1 have the same speed. The turbine speed decreases because the turbine torque is reduced by increasing clutch torque at clutch C_4 as seen in Figs. 5.82 and 5.85. The decrease in the turbine speed results in a higher slip across the the converter, which yields a higher pump torque as seen in Fig. 5.82. Consequently, the engine speed is reduced. During this phase, the turbine speed drops to a new synchronized speed with carrier–1 in Fig. 5.83. At the end of the speed phase, sun–1 comes to a stop and there is no slipping in clutch C_4. At the same time, the clutch C_2 torque on carrier–1 reaches its highest magnitude as seen in Figs. 5.87.

At the end of 3–4 upshift, carrier–1 torque drops to the level of the turbine torque as shown in Figs. 5.85 and 5.87 and the sun–1 stops. The output shaft torque has a large transient as seen in Fig. 5.86. Following the drop, the output torque increases until it reaches its peak and then oscillates with high frequency. Similar transients are seen in the vehicle acceleration and its derivative (jerk) as shown in Figs. 5.88 and 5.89, respectively. These indicate poor shift quality.

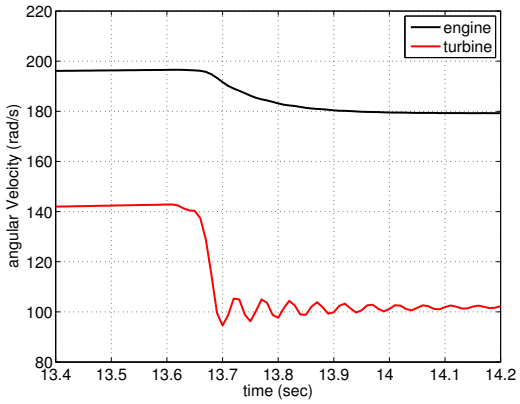

Figure 5.82. Turbine and Engine Speed During 3–4 Upshift for Non–Stiff Drive Shaft.

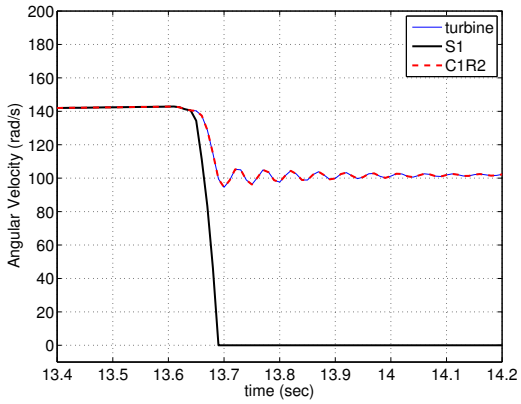

Figure 5.83. Speed of Planetary Gear Sets and Turbine During 3–4 Upshift for Non–Stiff Drive Shaft.

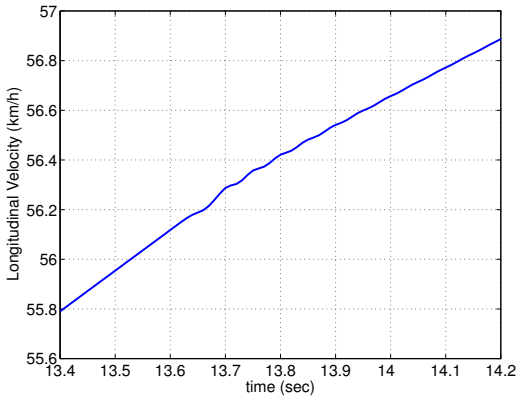

Figure 5.84. Vehicle Speed During 3–4 Power–On Upshift.

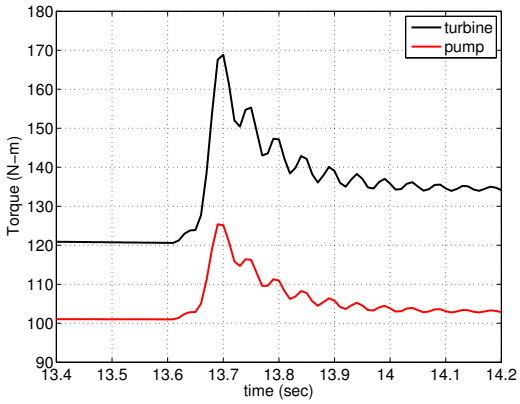

Figure 5.85. Pump and Turbine Torque During 3–4 Upshift for Non–Stiff Drive Shaft.

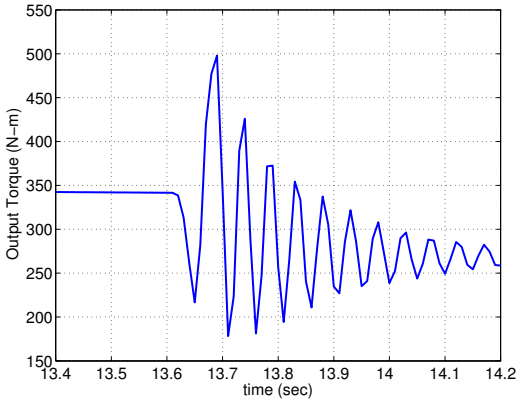

Figure 5.86. Output Torque of Stiff Drive Shaft During 3–4 Upshift.

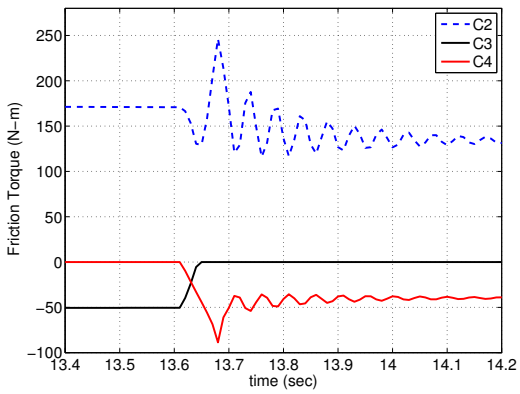

Figure 5.87. Clutch Torques During 3–4 Upshift for Non–Stiff Drive Shaft.

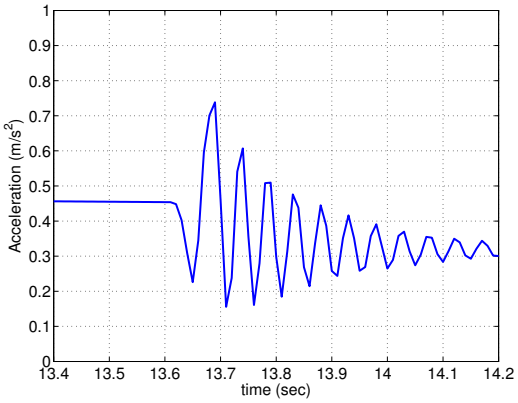

Figure 5.88. Vehicle Acceleration During 3–4 Upshift.

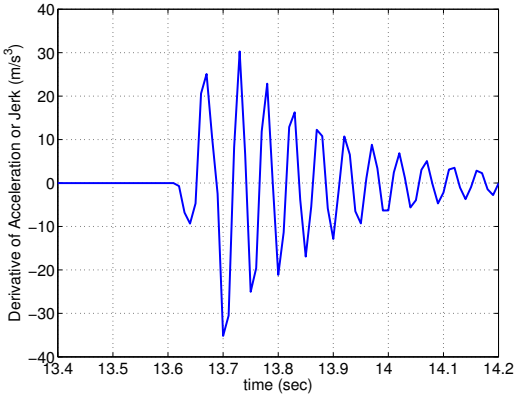

Figure 5.89. Derivative of Acceleration During 3–4 Upshift.

CHAPTER 6

FEEDBACK CONTROL FOR SHIFT QUALITY

This chapter investigates the feasibility of feedback control for shift quality. The previous chapter describes in detail the importance of calibrating proper pressure profiles on the relevant friction elements for good shift quality. The previous chapters also demonstrate the difficulty in finding such a satisfactory pressure profile for open loop execution of a shift. This chapter presents the application of feedback control methods to shift dynamics, which eliminates the need for calibrating pressure profile and generates a satisfactory pressure profile based on a formulation of a shift objective. First, a linear feedback control method is employed. Then, the feasibility of a nonlinear feedback control approach is investigated.

6.1 PID Controller and its Evaluation

The Proportional–Integral–Derivative (PID) control approach is employed for the feedback control of shift due to its simplicity in design and implementation. Fig. 6.1 depicts the feedback structure. Angular speed is used in the feedback since speed measurements are available from the speed sensors. The choice of the reference speed signal differs depending on the rotating elements involved in a given shift. In the target gear after a shift, the speed ratios of the rotating elements are known, thus, the desired speed is chosen based on the speed that the rotating element (whose speed is used in the feedback) should have after the shift is complete. As depicted in Fig. 6.1, the input to the PID controller is the error in speed and the output is the pressure

command, P_d, the desired pressure for the friction element involved in the shift. The equation of a PID controller in time domain in terms of this input–output pair is

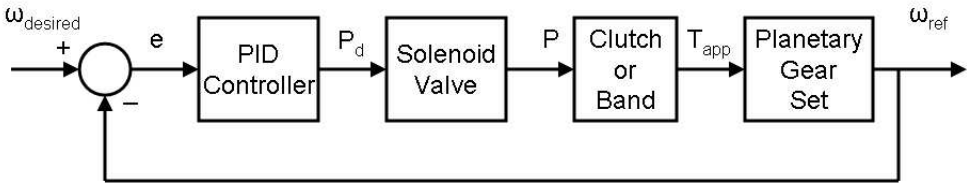

Figure 6.1. PID Feedback Control Structure.

$$u(t) = K_P\, e(t) + K_I \int e(t)dt + K_D\, \dot{e}(t) \tag{6.1}$$

where e(t) is the speed error, K_P is the proportional gain, K_I is the integral gain, K_D is the derivative gain. Once computed by the PID controller, the desired pressure on the clutch or band involved should be realized by a hydro–electric solenoid valve, described in Section 4.2. The dynamics of such a solenoid valve that generates the applied pressure on a clutch or band based on the desired pressure is modeled by a first order transfer function.

$$G_{valve} = \frac{1}{\tau s + 1} \tag{6.2}$$

where τ is set to be 0.02 sec based on the response characteristics of fast hydraulic actuation technologies discussed in Section 4.3.

For each up and down shift, the reference and the desired speeds as well as the clutch/band involved are different. Thus, each shift requires a different PID control design. However, the objectives of the control design are the same: (i) minimum drop around 50% reduction when comparing to the open loop both in the output shaft torque and accelerations and (ii) if not avoided completely, short transient with about 50% reduction in overshoot and oscillation in clutch/band torques and planetary gear speeds. Based on these objectives, the PID gains are tuned to obtain a satisfactory shift response by hand. The tuning procedure consists of the following steps.

1. Analyze the open–loop response in Chapter 5 to determine what aspects of the shift needs to be improved.
2. Add the proportional gain to reduce the rise time and steady–state error.
3. Add the integral gain to eliminate the steady–state error without degrading the transient response. The speed error goes to zero eventually when the clutch/band is locked up.
4. Add the derivative gain to reduce overshoot and improve transient response.
5. Adjust each gain until a satisfactory response is achieved.

Table 6.1 lists the important aspects of PID controller designed for each shift in terms of the reference angular speed, desired angular speed, desired pressure output and the gains. The performances of the upshift and the downshift sequences achieved by the PID controllers are shown in Figs. 6.2 and 6.3, respectively. The details of each PID controller and the closed–loop performance of the corresponding shift are discussed in the following sections.

Table 6.1. Reference and Desired Speeds, Output Pressure and Gains of the PID Controllers

Shift	**Reference Speed**	**Desired Speed**	**Output Pressure**	**Gains**		
				$K_P(\frac{kPa}{rad/s})$	$K_I(\frac{kPa}{rad})$	$K_D\ (\frac{kPa}{rad/s^2})$
1–2	ω_{C1R2}	ω_t	Clutch C_2	100	400	10
2–3	ω_{S2}	ω_t	Band B_{12}	100	10	10
	ω_{S1}	ω_t	Clutch C_3	100	10	10
3–4	ω_{S1}	0	Clutch C_4	0.01	1	1
4–3	ω_{S1}	ω_t	Clutch C_4	100	10	10
3–2	ω_{S1}	$1.863 \cdot \omega_t$	Clutch C_3	0.1	1	0.1
	ω_{S2}	0	Band B_{12}	0.3	0.4	0.1
2–1	ω_{S1}	ω_t	Clutch C_2	10,000	40,000	10,000

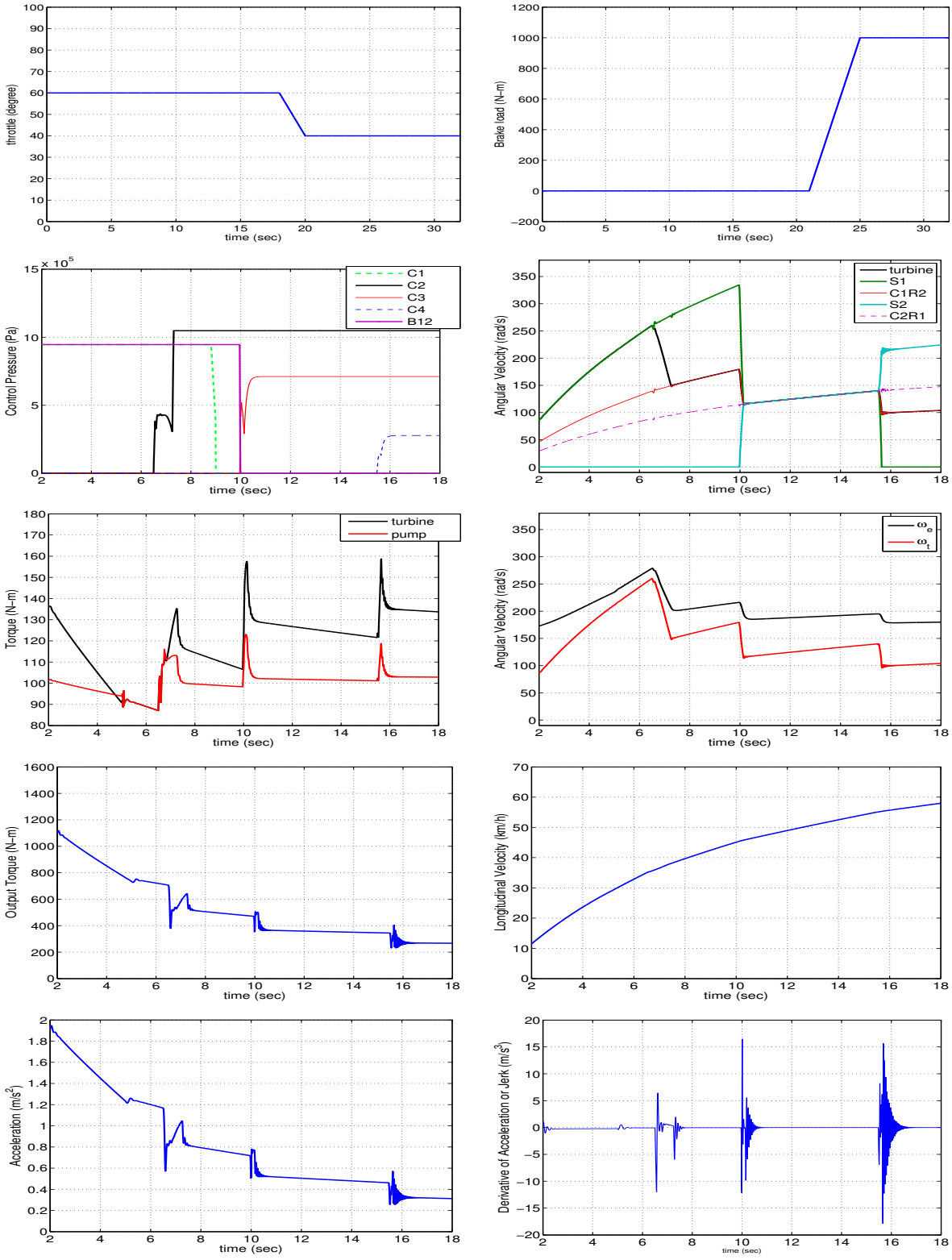

Figure 6.2. Overview 1–2, 2–3 and 3–4 Sequence of the Upshifts.

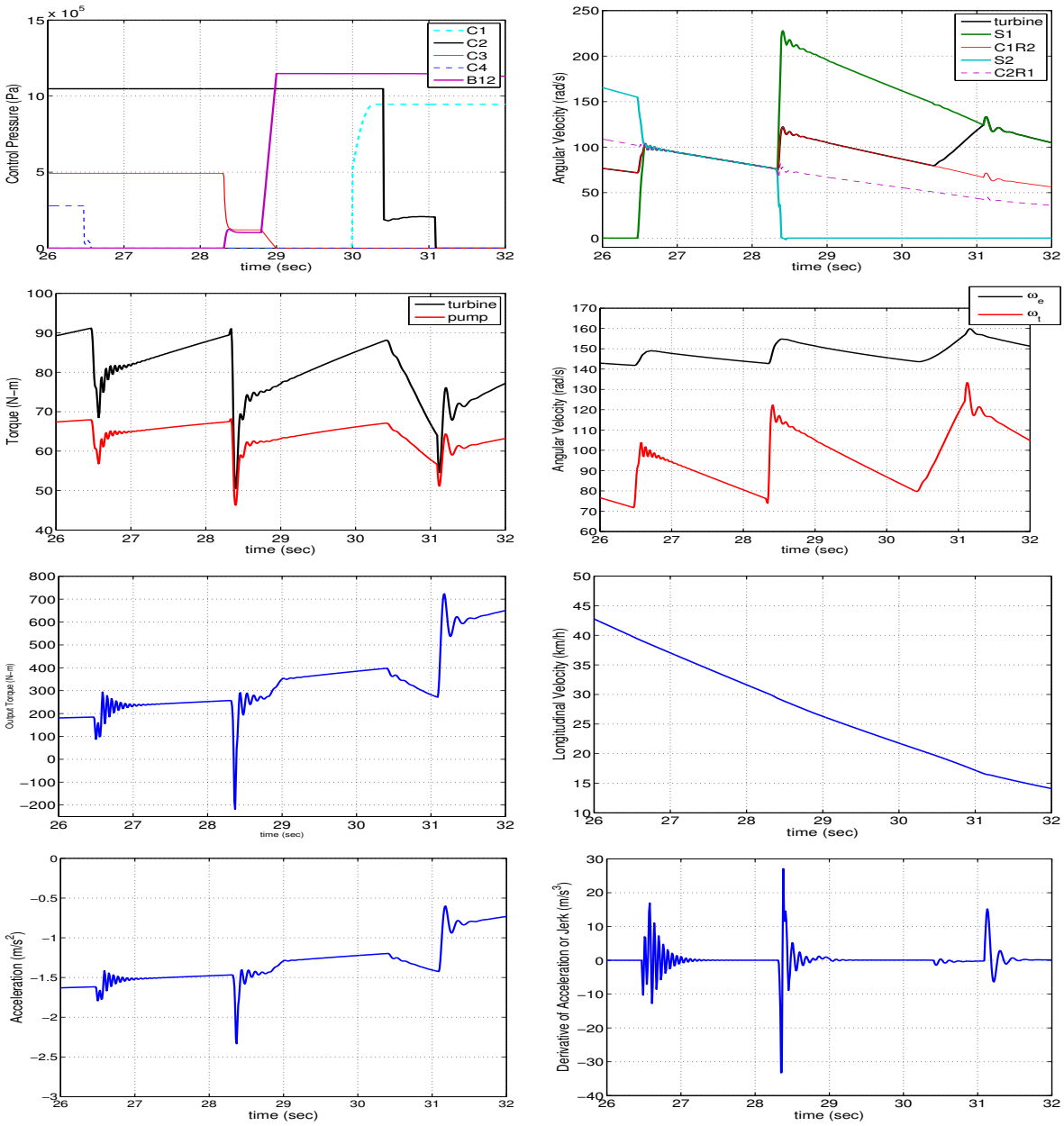

Figure 6.3. Overview 4–3, 3–2 and 2–1 Sequence of Downshifts.

6.1.1 1–2 upshift

A 1–2 upshift requires the engagement of clutch C_2 since the one–way clutch C_1 will overrun in the second gear, as listed in Table 4.1. Once engaged, clutch C_2 will connect the carrier of the front planetary gear set to the turbine. Thus, the reference angular speed is ω_{C1R2}, the speed of carrier–1 and ring–2, which are rigidly connected, and the desired speed is the turbine speed. This means the error signal for the PID controller for this shift is

$$e_{12}(t) = \omega_t - \omega_{C1R2} \tag{6.3}$$

The PID controller, with this error input, generates the desired pressure profile for the hydro-electric solenoid valve of clutch C_2.

The PID gains are tuned based on the simulation results of the velocity, the acceleration, the jerk and the output shaft torque. Increasing K_P results in smaller speed error. First, K_P is set to be 1, suggested as the PID tuning method [92]. Gain K_P is increased until excessive oscillation is seen in both speed and torque plots, which indicate poor shift quality. Then, the gains are reduced by half. The re-tuning of the gains is repeated until a satisfactory change of the pressure in the torque phase is observed as shown in Fig. 6.4. Adding K_I eliminates the steady state error, but worsens the transient response with high overshoot and slow settling time. Finally, adding K_D improves the transient response by reducing overshoot and achieves tracking the desired speed. K_I and K_D are used to shape the pressure profile as shown in Fig. 6.4, since increasing K_P only can not eliminate the steady-state error. Gains K_I and K_D are initially started as 1 and increased gradually until acceptable results are obtained. The final values of the gains are given in Table 6.1, which result in satisfactory shift response. A comparison is made between the open loop pressure profiles as illustrated in Fig. 5.59 with the closed loop pressure profile

in Fig. 6.4. Fig. 6.4 shows that the control pressure is built up in the beginning of the torque phase to about 400 kPa. In the inertia phase, the pressure slightly drops before it increases to about 1000 kPa where the clutch is locked up to prevent the clutch slipping. This pressure profile generated by the PID controller leads to a good shift quality. The open loop response has high overshoot and oscillation at the carrier–1 speed as illustrated in Fig. 5.67. Once the PID controller is used to generate the pressure profile, Fig. 6.5 shows that the overshoot and oscillation are eliminated significantly. Fig. 6.5 shows that the speed of carrier–1 is successfully raised to match the turbine speed without any unacceptable transient. Note that the steady-state error is reduced to zero after two rotating elements are matched. The friction torque at clutch C_2 applied to carrier–1 is controlled to have small overshoot and oscillation. The open loop response has high overshoot and oscillation as shown in Fig. 5.71. Compared with the open loop response, PID controller, as shown in Fig. 6.6, almost completely eliminates the overshoot and oscillation. The output torque of the planetary gear sets also has low overshoot and oscillation, as shown in Fig. 6.7. Recall from Fig. 5.69 that the open loop response has higher overshoot and oscillation. In the closed loop response, the vehicle acceleration and jerk show small overshoot and oscillation, as seen in Figs. 6.8 and 6.9, respectively, in comparison to the open loop response with high overshoot and oscillation as can be seen in Figs. 5.72 and 5.73. Maximum Average Power is reduced from 0.2419 in the open loop to 0.0083 in the closed loop control. Vibration Dose Value (VDV) is reduced from 1.2546 in the open loop to 0.942 in the closed loop control. Table 6.2 summarizes the shift characteristics of the closed–loop response compared with the open–loop and clearly demonstrates the significant improvements in shift quality with the employment of the PID controller.

Table 6.2. Comparison of 1–2 Upshift Characteristics between the Open–Loop and Closed–Loop Simulations

	open	closed	percent reduction
Carrier–1 speed			
overshoot	$\sim 14\%$	none	
frequency (cycle/shift duration)	8	none	
Clutch Torque at clutch C_2			
overshoot	$\sim 183\%$	25.65%	88%
frequency (cycle/shift duration)	8	4	50%
Output Torque			
overshoot	$\sim 172\%$	25.6%	85.1%
frequency (cycle/shift duration)	8	5	37.5%
Acceleration			
overshoot	$\sim 237\%$	29.97%	87.35%
frequency (cycle/shift duration)	8	5	37.5%
Jerk			
overshoot	$7 \times 10^6\%$	6800%	100%
frequency (cycle/shift duration)	8	8	0%
Max. Average Power (MAP)	0.2419	0.0083	96.6%
VDV	1.2546	0.942	24.9%

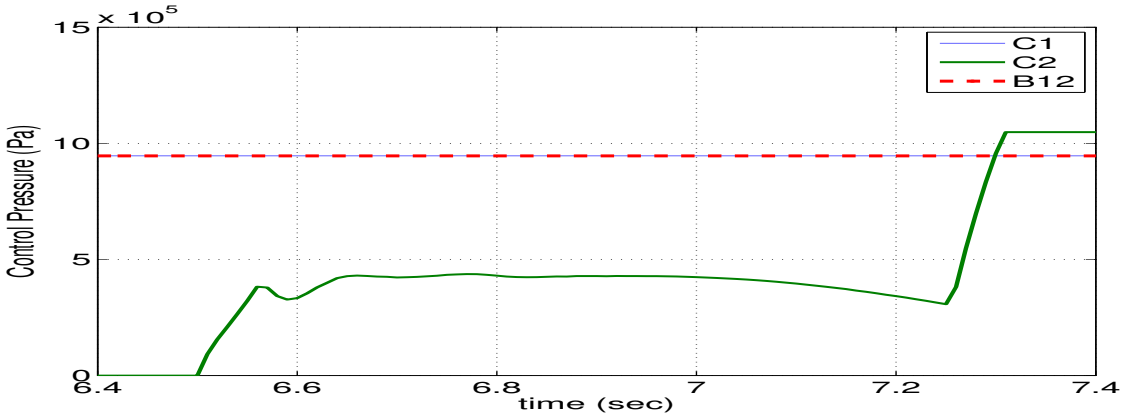

Figure 6.4. Closed–Loop Control Pressure Profile for 1^{st}–2^{nd} Upshift.

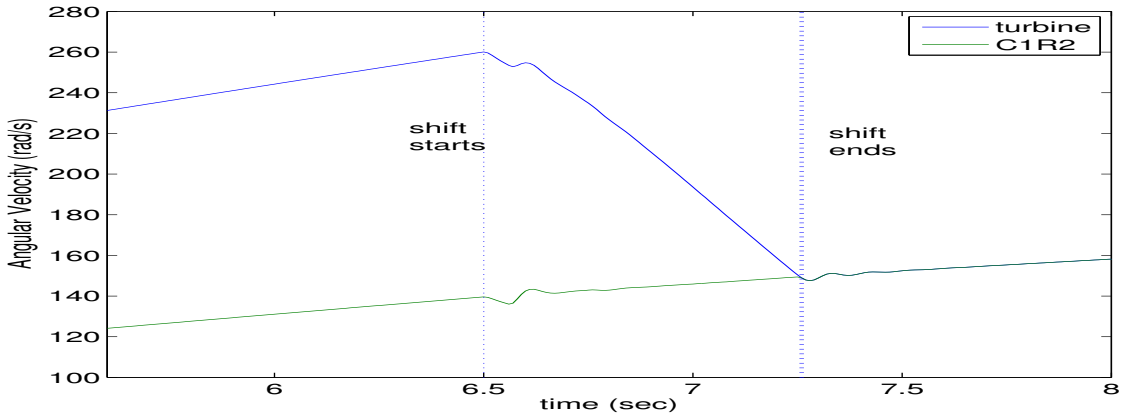

Figure 6.5. Closed–Loop Speed Results for 1^{st}–2^{nd} Upshift.

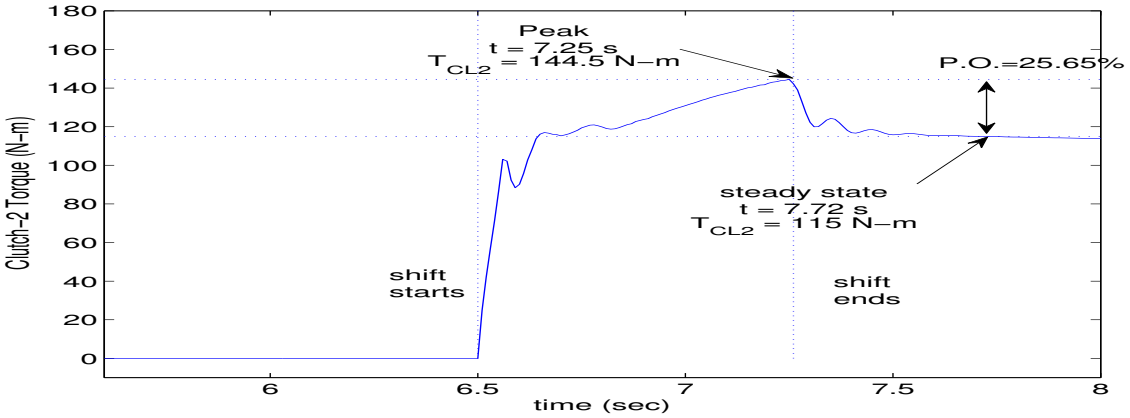

Figure 6.6. Closed–Loop Friction Torque at Clutch C_2 during 1^{st}–2^{nd} Upshift.

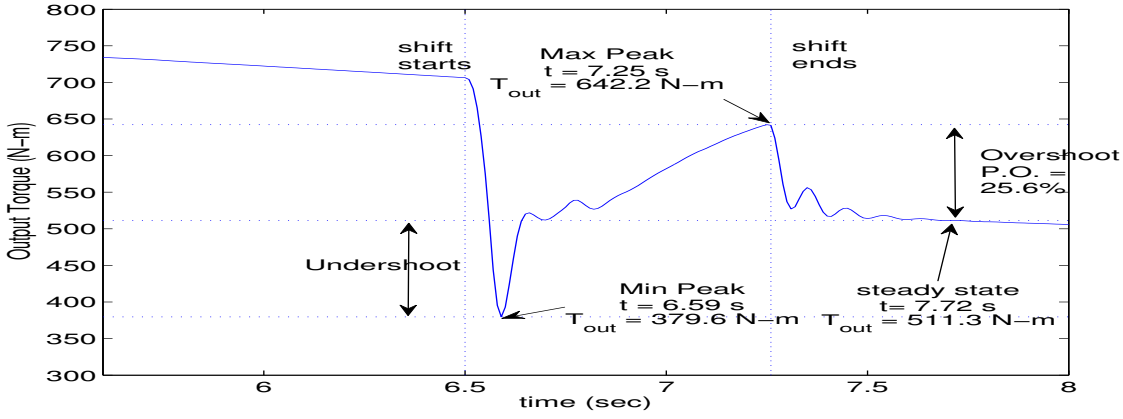

Figure 6.7. Closed–Loop Output Torque during 1^{st}–2^{nd} Upshift.

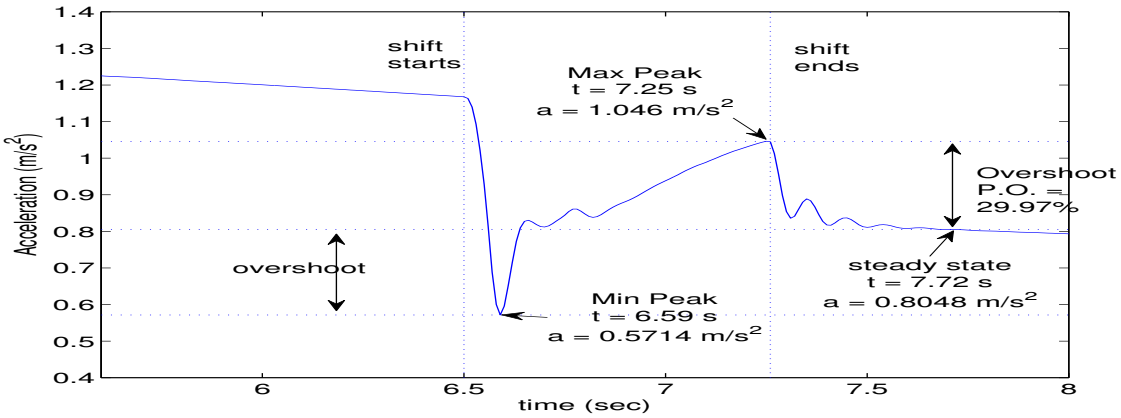

Figure 6.8. Closed–Loop Vehicle Acceleration during 1^{st}–2^{nd} Upshift.

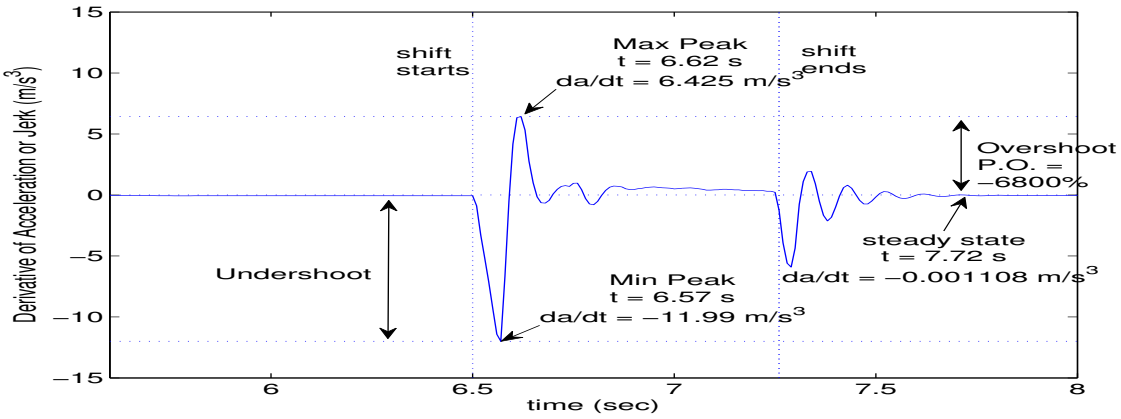

Figure 6.9. Closed–Loop Derivative of Acceleration or Jerk during 1^{st}–2^{nd} Upshift.

6.1.2 2–3 upshift

A 2–3 upshift requires the engagement of clutch C_3 and the disengagement of band B_{12}, as listed in Table 4.1. Once engaged, clutch C_3 will connect the sun of the front planetary gear set to the turbine. Thus, the reference angular speed is ω_{S1}, the speed of sun–1, and the desired speed is the turbine speed. This means the error signal for the PID controller for clutch C_3 is

$$e_{23,C3}(t) = \omega_t - \omega_{S1} \tag{6.4}$$

Band B_{12} will disconnect the sun of the rear planetary gear set from the transmission case. Thus, the reference angular speed is ω_{S2}, the speed of sun–2, and the desired speed is the turbine speed. This means the error signal for the PID controller for band B_{12} is

$$e_{23,B12}(t) = \omega_t - \omega_{S2} \tag{6.5}$$

The PID controllers, with these error inputs, generate the desired pressure profiles for the hydro-electric solenoid valves of clutch C_3 and band B_{12}.

The PID gains are tuned based on the simulation results of the velocity, the acceleration, the jerk and the output shaft torque. Increasing K_P results in smaller speed error. First, K_P is set to be 1 for both C_3 and B_{12}. Gains K_P are increased until excessive oscillation is seen in both speed and torque plots, which indicate poor shift quality. Then, the gains are reduced by half. The re-tuning of the gains is repeated until a satisfactory change of the pressure in the torque phase is observed as shown in Fig. 6.10. The control pressure is built up in the beginning of the torque phase for clutch C_3 while band B_{12} pressure is reduced significantly. Adding K_I eliminates the steady state error, but worsens the transient response with high overshoot and slow settling time. Finally, adding K_D improves the transient response by reducing overshoot and achieves tracking the desired speed. K_I and K_D are used to shape the pressure profile as shown in Fig. 6.10, since increasing K_P only can not eliminate the steady-state error. Gains K_I and K_D are initially started as 1 and increased gradually until acceptable results are obtained. The final values of the gains are given in Table 6.1, which result in satisfactory shift response. A comparison is made between the open loop pressure profiles as illustrated in Fig. 5.59 with the closed loop pressure profile in Fig. 6.10. Fig. 6.10 shows that the control pressure on clutch C_3 is built up in the beginning of the torque phase to about 400 kPa. In the inertia phase, the

pressure slightly drops before it increases to about 800 kPa where the clutch is locked up to prevent the clutch slipping. The control pressure on band B_{12} is reduced to zero at the end of the torque phase. These pressure profiles generated by the PID controllers leads to a good shift quality. The open loop response has high overshoot and oscillation at the sun–1 and sun–2 speeds as illustrated in Fig. 5.75. Once the PID controllers are used to generate the pressure profiles, Fig. 6.11 shows that the overshoot and oscillation are eliminated significantly. Fig. 6.11 shows that the speed of sun–1 is successfully reduced to match the turbine speed without any unacceptable transient. Also, the speed of sun–2 is raised to match the turbine speed without any unacceptable transient. Note that the steady-state error is reduced to zero after two rotating elements are matched. The friction torque at clutch C_3 applied to sun–1 is controlled to have small overshoot and oscillation. Similarly, the friction torque at band B_{12} applied to sun–2 is controlled to have small overshoot and oscillation. The open loop response has high overshoot and oscillation as shown in Fig. 5.79. Compared with the open loop response, PID controllers, as shown in Figs. 6.12 and 6.13, almost completely eliminate the overshoot and oscillation. The output torque of the planetary gear sets also has low overshoot and oscillation, as shown in Fig. 6.14. Recall from Fig. 5.77 that the open loop response has higher overshoot and oscillation. In the closed loop response, the vehicle acceleration and jerk show small overshoot and oscillation, as seen in Figs. 6.15 and 6.16, respectively, in comparison to the open loop response with high overshoot and oscillation as can be seen in Figs. 5.80 and 5.81. Maximum Average Power is reduced from 0.0632 in the open loop to 0.0029 in the closed loop control. Vibration Dose Value (VDV) is reduced from 0.6297 in the open loop to 0.5712 in the closed loop control. Table 6.3 summarizes the shift characteristics of the closed–loop response with the open–loop and clearly

demonstrates the significant improvements in shift quality with the employment of the PID controller.

Table 6.3. Comparison of 2–3 Upshift Characteristics between the Open–Loop and Closed–Loop Simulations

	open	closed	percent reduction
Sun–1 speed			
overshoot	$\sim 5\%$	none	
frequency (cycle/shift duration)	5	none	
Sun–2 speed			
overshoot	$\sim 7\%$	none	
frequency (cycle/shift duration)	5	none	
Clutch Torque at clutch C_3			
overshoot	$\sim 200\%$	50%	75%
frequency (cycle/shift duration)	7	5	28.6%
Clutch Torque at Band B_{12}			
overshoot	none	none	0%
frequency (cycle/shift duration)	none	none	0%
Output Torque			
overshoot	$\sim 130\%$	38.34%	70.5%
frequency (cycle/shift duration)	12	8	33.33%
Acceleration			
overshoot	$\sim 176\%$	49.64%	71.8%
frequency (cycle/shift duration)	12	8	33.33%
Jerk			
overshoot	$5.5 \times 10^5\%$	$1.2 \times 10^5\%$	78%
frequency (cycle/shift duration)	14	9	35.7%
Max. Average Power (MAP)	0.0632	0.0029	95.41%
VDV	0.6297	0.5712	9.3%

6.1.3 3–4 upshift

A 3–4 upshift requires the engagement of clutch C_4 since the one–way clutch C_3 will overrun in the second gear, as listed in Table 4.1. Once engaged, clutch C_4 will connect the sun of the front planetary gear set the transmission case. Thus, the

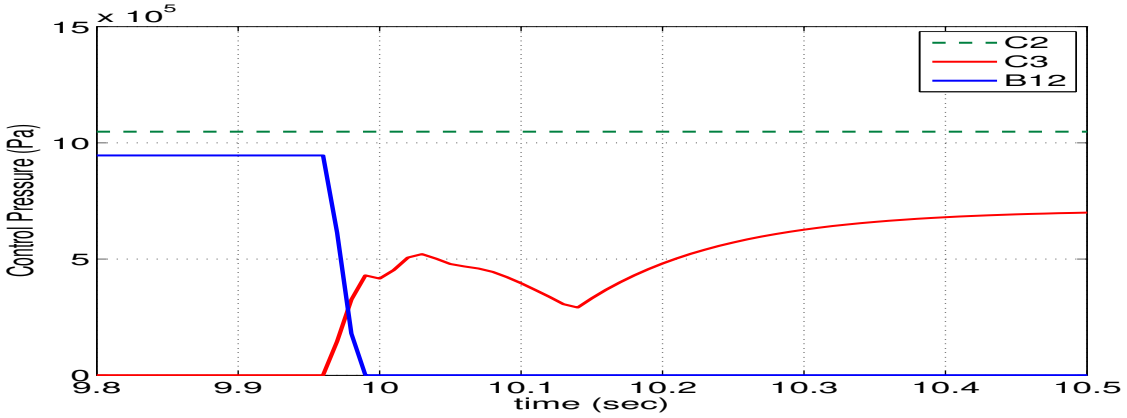

Figure 6.10. Closed–Loop Control Pressure Profile for 2^{nd}–3^{rd} Upshift.

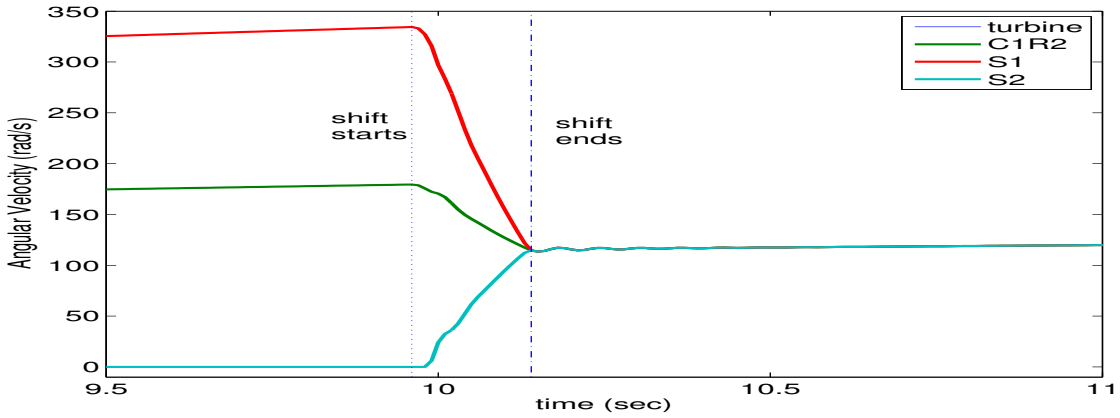

Figure 6.11. Closed–Loop Speed Results for 2^{nd}–3^{rd} Upshift.

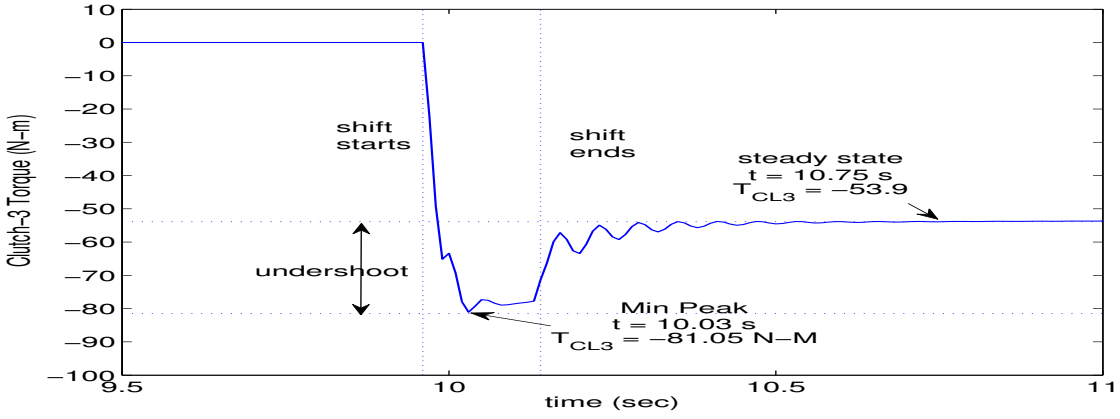

Figure 6.12. Closed–Loop Friction Torque at Clutch C_3 during 2^{nd}–3^{rd} Upshift.

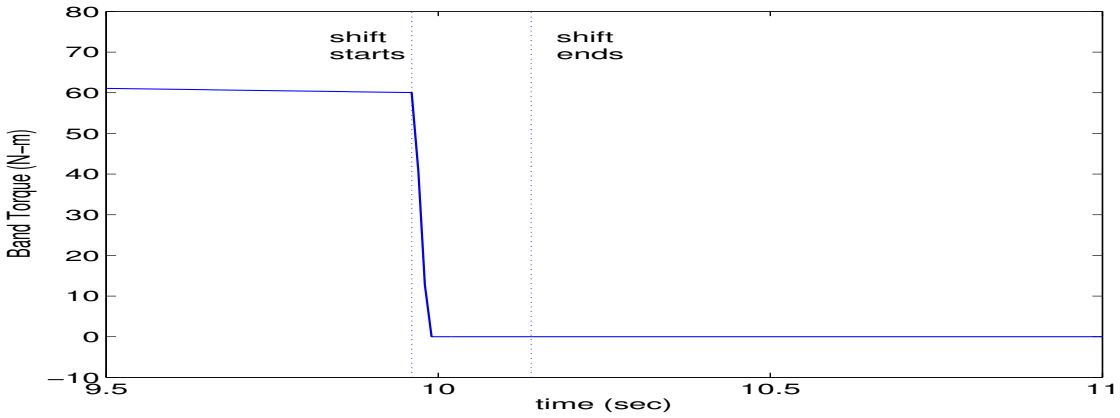

Figure 6.13. Closed–Loop Friction Torque at Band B_{12} during 2^{nd}–3^{rd} Upshift.

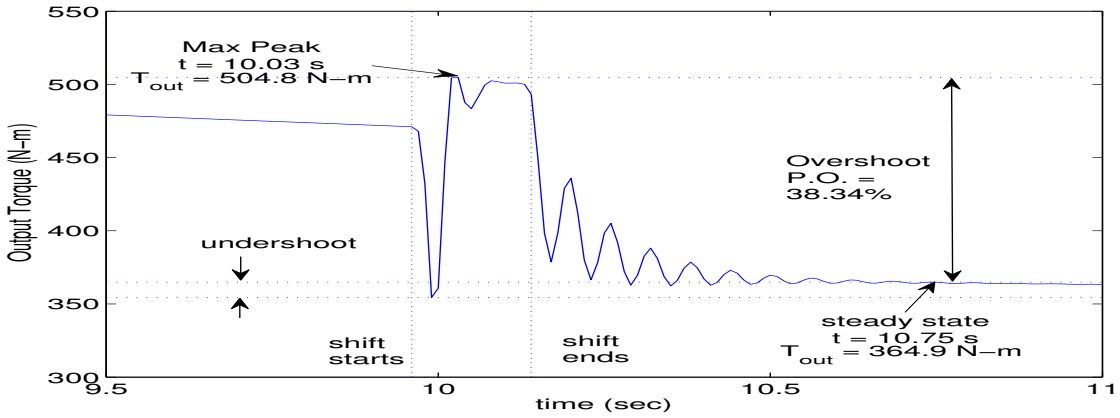

Figure 6.14. Closed–Loop Output Torque during 2^{nd}–3^{rd} Upshift.

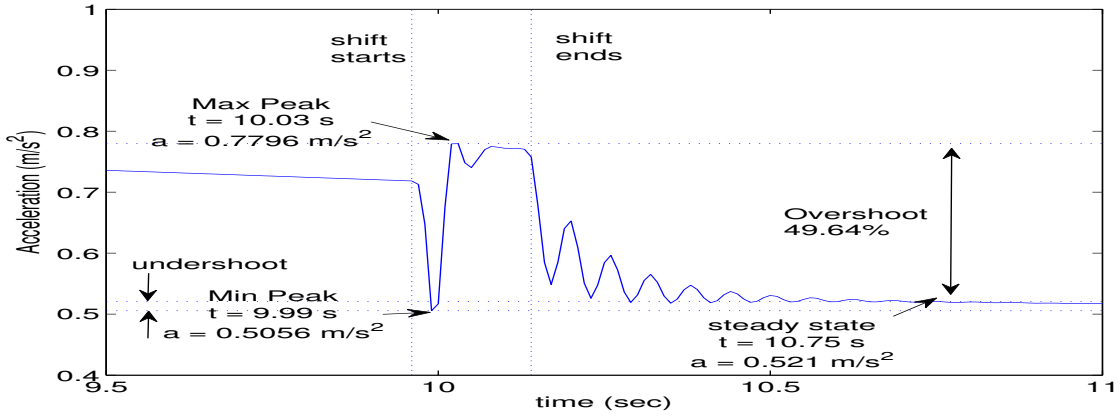

Figure 6.15. Closed–Loop Vehicle Acceleration during 2^{nd}–3^{rd} Upshift.

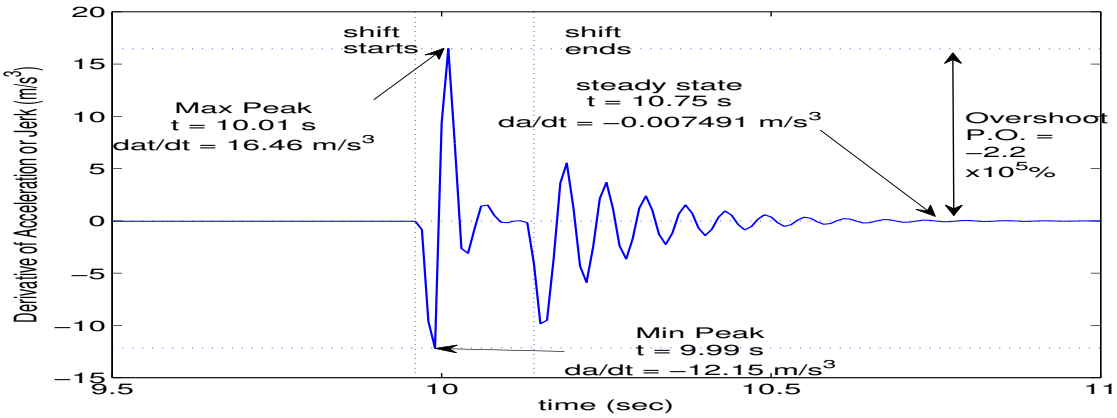

Figure 6.16. Closed–Loop Derivative of Acceleration or Jerk during 2^{nd}–3^{rd} Upshift.

reference angular speed is ω_{S1}, the speed of sun–1, and the desired speed is zero. This means the error signal for the PID controller for this shift is

$$e_{34}(t) = -\omega_{S1} \tag{6.6}$$

The PID controller, with this error input, generates the desired pressure profile for the hydro-electric solenoid valve of clutch C_4.

The PID gains are tuned based on the simulation results of the velocity, the acceleration, the jerk and the output shaft torque. Increasing K_P results in smaller speed error. K_P is set to be 1. Gain K_P is increased until excessive oscillation is seen in both speed and torque plots, which indicate poor shift quality. However, in 3–4 upshift increasing K_P results in the worse shift. Instead, the gain is reduced from 1 by decimals which results in some improvements. The re-tuning of the gains is repeated until a satisfactory change of the pressure in the torque phase is observed as shown in Fig. 6.17. Adding K_I eliminates the steady state error, but worsens the transient response with high overshoot and slow settling time. Adding K_D improves the transient response by reducing overshoot and achieves tracking the desired speed. K_I and K_D are used to shape the pressure profile as shown in Fig. 6.17, since K_P

only can not eliminate the steady-state error. Gains K_I and K_D are initially started as 1 and increased gradually until acceptable results are obtained. The final values of the gains are given in Table 6.1, which result in satisfactory shift response. A comparison is made between the open loop pressure profiles as illustrated in Fig. 5.59 with the closed loop pressure profile in Fig. 6.17. Fig. 6.17 shows that the control pressure is built up in the beginning of the torque phase to about 140 kPa. In the inertia phase, the pressure slightly drops before it increases to about 300 kPa when the clutch is locked up to prevent the clutch slipping. This pressure profile generated by the PID controller leads to a good shift quality. The open loop response has high overshoot and oscillation at the sun–1 speed as illustrated in Fig. 5.83. Once the PID controller is used to generate the pressure profile, Fig. 6.18 shows that the overshoot and oscillation are eliminated significantly. Fig. 6.18 shows that the speed of sun–1 is successfully reduced to match the transmission case without any unacceptable transient. Note that the steady-state error is reduced to zero after two rotating elements are matched. The friction torque at clutch C_4 applied to sun–1 is controlled to have small overshoot and oscillation. The open loop response has high overshoot and oscillation as shown in Fig. 5.87. Compared with the open loop response, PID controller, as shown in Fig. 6.19, almost completely eliminates the overshoot and oscillation. The output torque of the planetary gear sets also has low overshoot and oscillation, as shown in Fig. 6.20. Recall from Fig. 5.86 that the open loop response has higher overshoot and oscillation. In the closed loop response, the vehicle acceleration and jerk show small overshoot and oscillation, as seen in Figs. 6.21 and 6.22, respectively, in comparison to the open loop response with high overshoot and oscillation as can be seen in Figs. 5.88 and 5.89. Maximum Average Power is 0.0016 in both the open loop and closed loop control. Vibration Dose Value (VDV) is reduced from 0.3979 in the open loop to 0.3753 in the closed loop control. MAP and

VDV do not change much because, at high gear ratio such as 4^{th} gear, the turbine torque, which is the input torque to the planetary gear sets, is converted to lower torque while the turbine speed is converted to a higher speed. Table 6.4 summarizes the shift characteristics of the closed–loop response compared with the open–loop and clearly demonstrates the improvements in shift quality with the employment of the PID controller.

Table 6.4. Comparison of 3–4 Upshift Characteristics between the Open–Loop and Closed–Loop Simulations

	open	closed	percent reduction
Sun–1 speed			
overshoot	none	none	
frequency (cycle/shift duration)	none	none	
Clutch Torque at clutch C_4			
overshoot	124%	60%	51.61%
frequency (cycle/shift duration)	15	10	33.33%
Output Torque			
overshoot	86.27%	50.28%	41.71%
frequency (cycle/shift duration)	20	15	25%
Acceleration			
overshoot	134.37%	78.47%	41.6%
frequency (cycle/shift duration)	19	15	21%
Jerk			
overshoot	4.82×10^5%	1.06×10^5%	78%
frequency (cycle/shift duration)	20	20	0%
Max. Average Power (MAP)	0.0016	0.0016	0%
VDV	0.3979	0.3753	6%

6.1.4 4–3 downshift

A 4–3 downshift requires the disengagement of clutch C_4 since the one–way clutch C_3 will be automatically engaged in the third gear, as listed in Table 4.1. Once

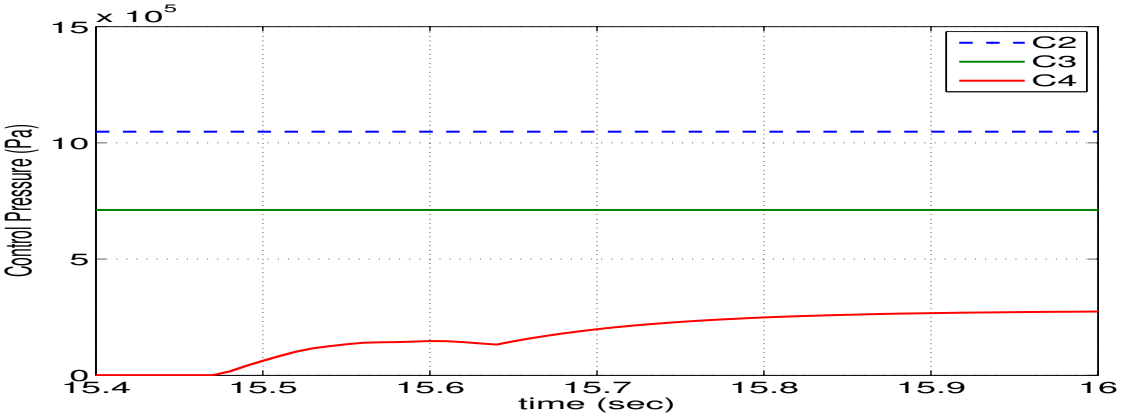

Figure 6.17. Closed–Loop Control Pressure Profile for 3^{rd}–4^{th} Upshift.

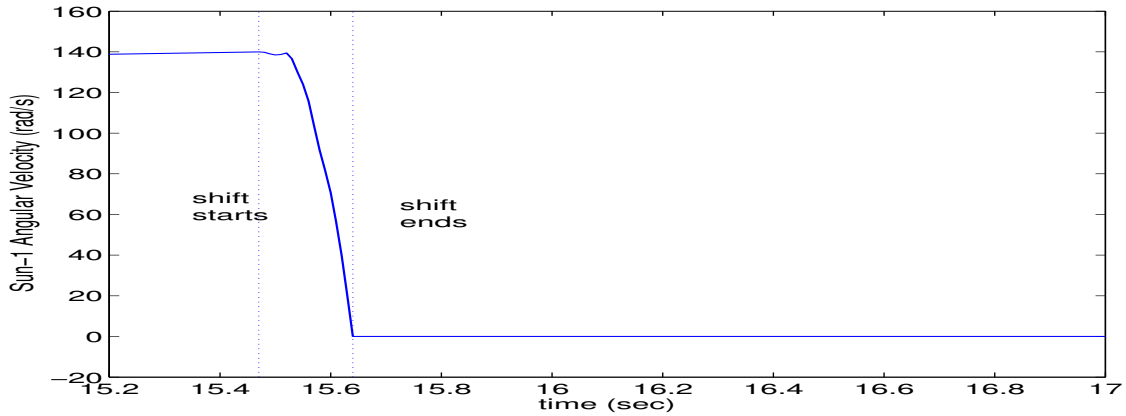

Figure 6.18. Closed–Loop Speed Results for 3^{rd}–4^{th} Upshift.

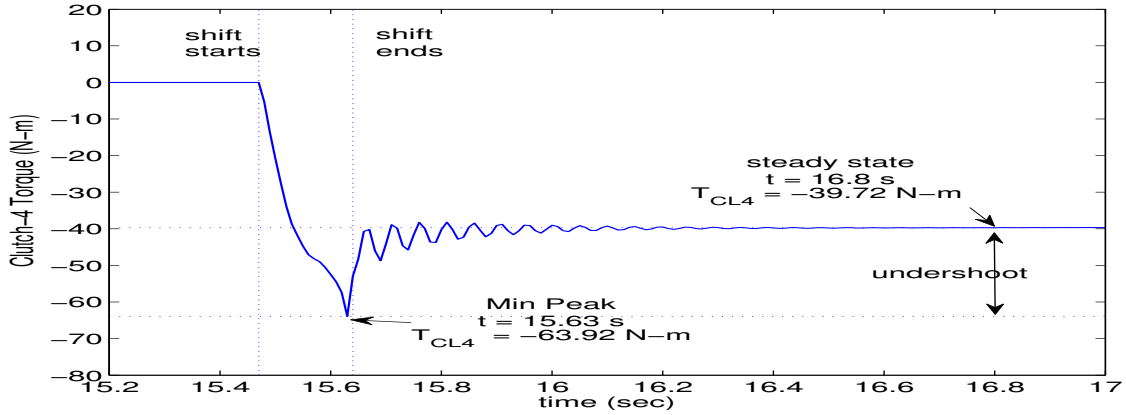

Figure 6.19. Closed–Loop Friction Torque at Clutch C_4 during 3^{rd}–4^{th} Upshift.

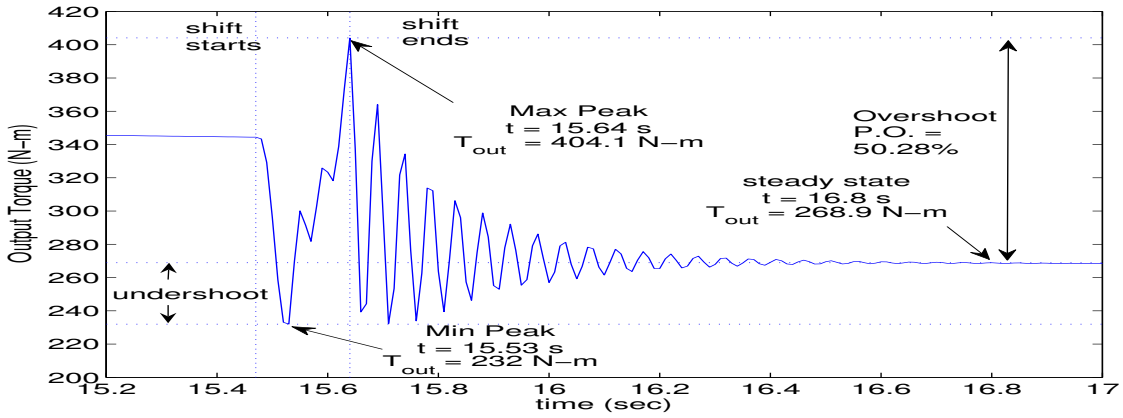

Figure 6.20. Closed–Loop Output Torque during 3^{rd}–4^{th} Upshift.

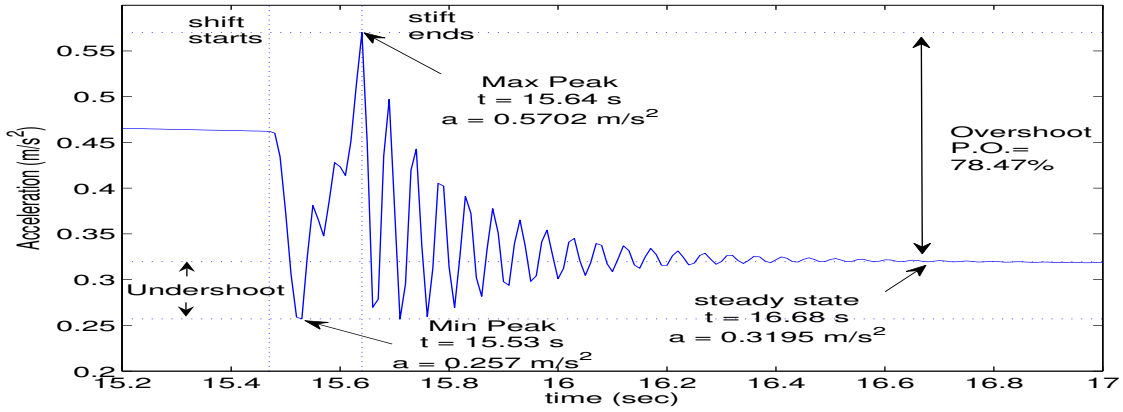

Figure 6.21. Closed–Loop Vehicle Acceleration during 3^{rd}–4^{th} Upshift.

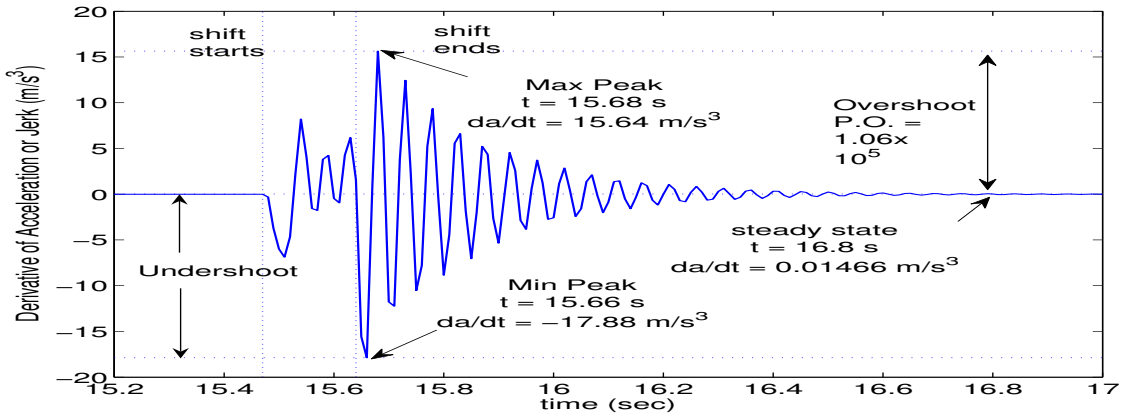

Figure 6.22. Closed–Loop Derivative of Acceleration or Jerk during 3^{rd}–4^{th} Upshift.

disengaged, clutch C_3 will let the sun–1 of the front planetary gear set spin with the turbine. Thus, the reference angular speed is ω_{S1}, the speed of sun–1 and the desired speed is the turbine speed. This means the error signal for the PID controller for this shift is

$$e_{43}(t) = \omega_t - \omega_{S1} \tag{6.7}$$

The PID controller, with this error input, generates the desired pressure profile for the hydro-electric solenoid valve of clutch C_4.

The PID gains are tuned based on the simulation results of the velocity, the acceleration, the jerk and the output shaft torque. Increasing K_P results in smaller speed error. K_P is set to be 1. Gain K_P is increased until excessive oscillation is seen in both speed and torque plots, which indicate poor shift quality. Then, the gains are reduced by half. The re-tuning of the gains is repeated until a satisfactory change of the pressure in the torque phase is observed as shown in Fig. 6.23. Adding K_I eliminates the steady state error, but worsens the transient response with high overshoot and slow settling time. Adding K_D improves the transient response by reducing overshoot and achieves tracking the desired speed. K_I and K_D are used to shape the pressure profile as shown in Fig. 6.23, since increasing K_P only can not eliminate the steady-state error. Gains K_I and K_D are initially started as 1 and increased gradually until acceptable results are obtained. The final values of the gains are given in Table 6.1, which result in satisfactory shift response. The closed loop pressure profile is illustrated in Fig. 6.23. Fig. 6.23 shows that the control pressure on clutch C_4 is reduced from 300 kPa in the beginning of the torque phase to about 40 kPa. In the inertia phase, the pressure rapidly drops to 0 kPa and the clutch is completely disengaged. This pressure profile generated by the PID controller leads to a good shift quality. Once the PID controller is used to generate the pressure profile,

Fig. 6.24 shows that the overshoot and oscillation are eliminated significantly. Fig. 6.24 shows that the speed of sun–1 is successfully raised to match the turbine speed without any unacceptable transient. Note that the steady-state error is reduced to zero after two rotating elements are matched. The friction torques at clutch C_4 applied to sun–1 is controlled to have small overshoot and oscillation, as shown in Fig. 6.25. The output torque of the planetary gear sets also has low overshoot and oscillation, as shown in Fig. 6.26. In the closed loop response, the vehicle acceleration and jerk show small overshoot and oscillation, as seen in Figs. 6.27 and 6.28, respectively. Maximum Average Power is 0.0017. Vibration Dose Value (VDV) is 1.4557.

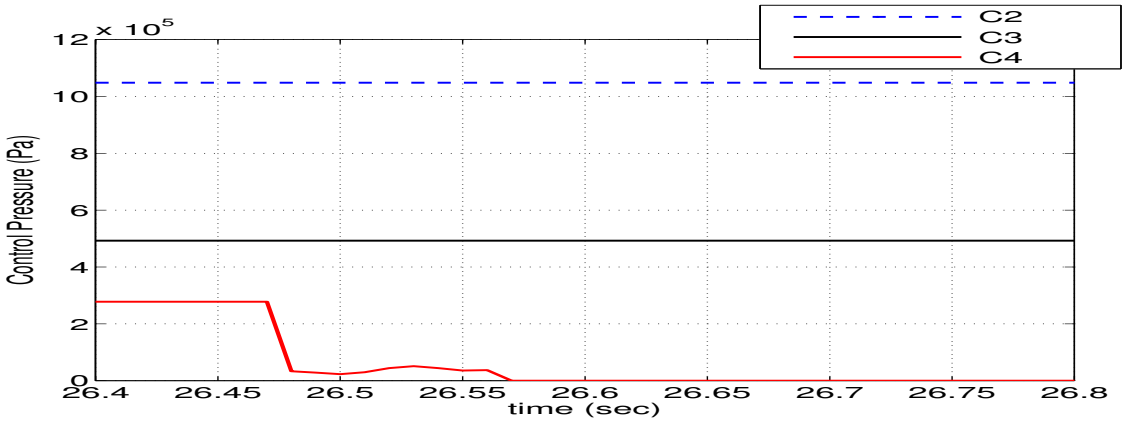

Figure 6.23. Closed–Loop Control Pressure Profile for 4^{th}–3^{nd} downshift.

6.1.5 3–2 downshift

A 3–2 downshift requires the engagement of clutch B_{12} and the disengagement of band C_3, as listed in Table 4.1. Once engaged, band B_{12} will stop the sun of the rear planetary gear set. Thus, the reference angular speed is ω_{S2}, the speed of sun–2,

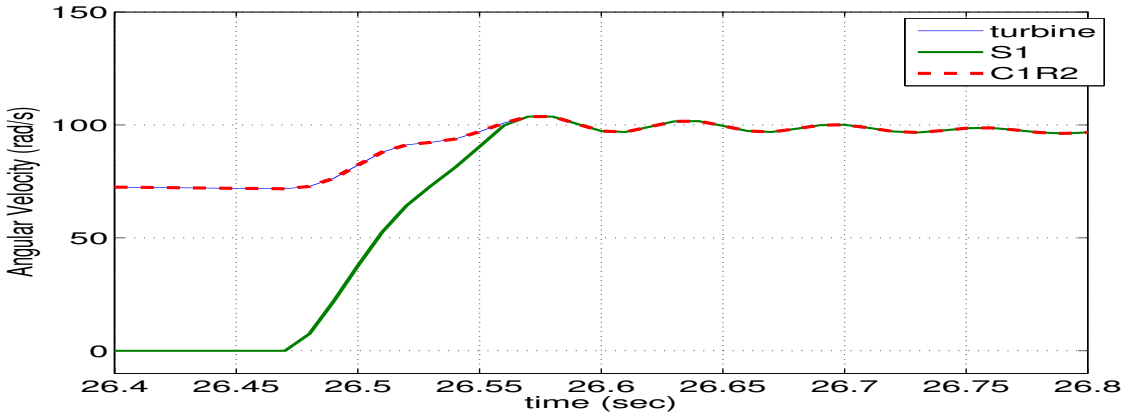

Figure 6.24. Closed–Loop Speed Results for 4^{st}–3^{nd} downshift.

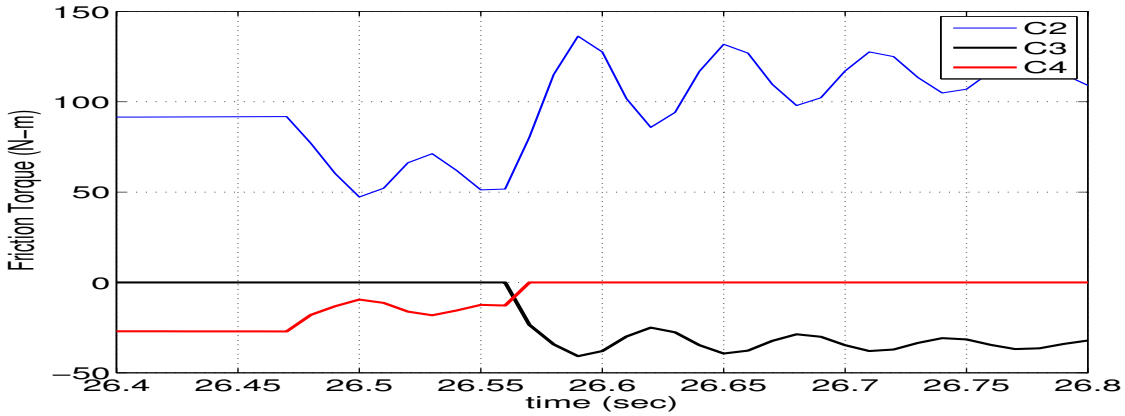

Figure 6.25. Closed–Loop Friction Torque at Clutch/Band during 4^{th}–3^{rd} downshift.

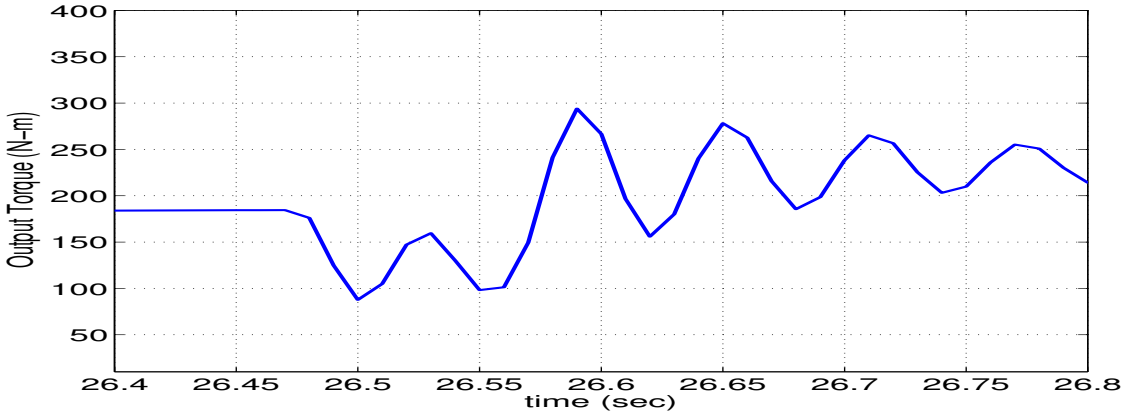

Figure 6.26. Closed–Loop Output Torque during 4^{th}–3^{rd} downshift.

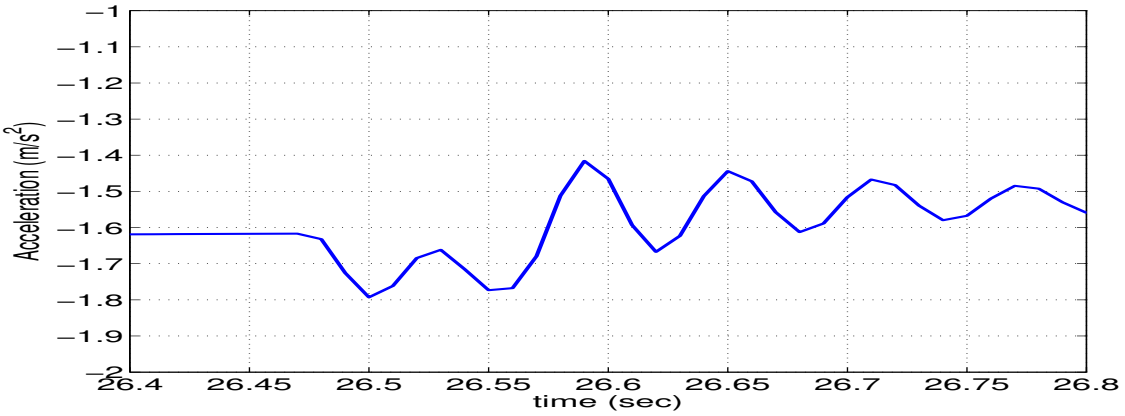

Figure 6.27. Closed–Loop Vehicle Acceleration during 4^{th}–3^{rd} downshift.

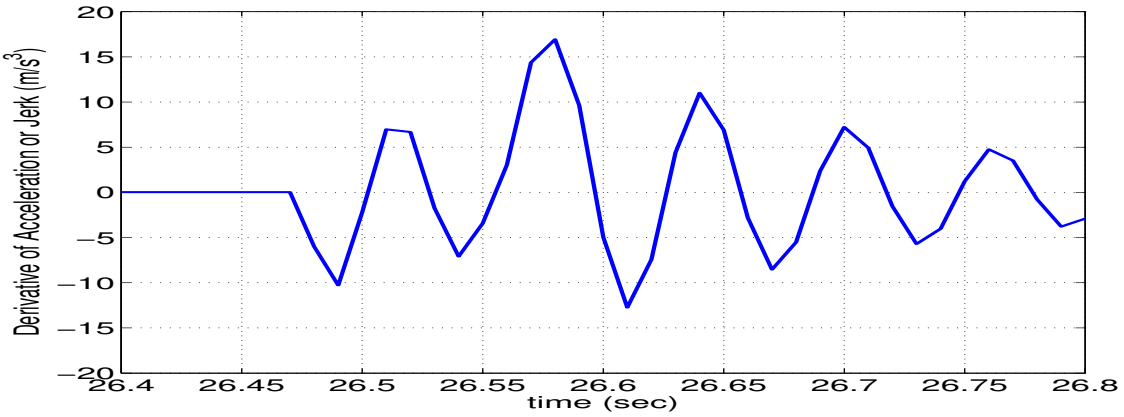

Figure 6.28. Closed–Loop Derivative of Acceleration or Jerk during 4^{th}–3^{rd} downshift.

and the desired speed is zero. This means the error signal for the PID controller of band B_{12} is

$$e_{32,B12}(t) = \omega_{case} - \omega_{S2} \tag{6.8}$$

Clutch C_3 will disconnect the sun of the front planetary gear set from the transmission case. Thus, the reference angular speed is ω_{S1}, the speed of sun–1, and the desired speed is the turbine speed times 1.863, which is the ratio of the sun–1 speed over the turbine speed in the second gear. This means the error signal for the PID controller for clutch C_3 is

$$e_{32,C3}(t) = 1.863 \cdot \omega_t - \omega_{S1} \tag{6.9}$$

The PID controllers, with these error inputs, generate the desired pressure profiles for the hydro-electric solenoid valves of band B_{12} and clutch C_3.

The PID gains are tuned based on the simulation results of the velocity, the acceleration, the jerk and the output shaft torque. The similar tuning procedure is used to tune the PID for 3–2 downshift. First, K_P is set to be 1 for both C_3 and B_{12}. Gains K_P are increased until excessive oscillation is seen in both speed and torque plots, which indicate poor shift quality. Then, the gains should be reduced by half. However, increasing K_P results in the worse oscillation. Instead, reducing K_P from 1 by decimals can give the better results. The re-tuning of the gains is repeated until the pressure profile in Fig. 6.29 are obtained. The control pressure is built up in the beginning of the torque phase for band B_{12} while clutch C_3 pressure is reduced significantly. Adding K_I eliminates the steady state error, but worsens the transient response with high overshoot and slow settling time. Finally, adding K_D improves the transient response by reducing overshoot and achieves tracking the desired speed. K_I and K_D are used to shape the pressure profile as shown in Fig. 6.29, since K_P only can not eliminate the steady-state error. Gains K_I and K_D are initially started as 1 and increased gradually until acceptable results are obtained. The final values of the gains are given in Table 6.1, which result in satisfactory shift response. The closed loop pressure profiles is illustrated in Fig. 6.29. Fig. 6.29 shows that the control pressure on band B_{12} is built up in the beginning of the torque phase to about 130 kPa. In the inertia phase, the pressure increases to about 900 kPa where the clutch is locked up to prevent the clutch slipping. The control pressure on clutch C_3 is reduced to zero at the end of the inertia phase. These pressure profiles generated by the PID controllers leads to a good shift quality. Once the PID controllers are used to generate the pressure profiles, Fig. 6.30 shows that the overshoot and oscillation are eliminated significantly. Fig. 6.30 shows that sun–2 is successfully stopped without

any unacceptable transient. Also, the speed of sun–1 is raised to match its desired speed without any unacceptable transient. Note that the steady-state error is reduced to zero after two rotating elements are matched. The friction torque at band B_{12} applied to sun–2 and the friction torque at clutch C_3 applied to sun–1 are controlled to have small overshoot and oscillation, as shown in Fig. 6.31. The output torque of the planetary gear sets also has low overshoot and oscillation, as shown in Fig. 6.32. In the closed loop response, the vehicle acceleration and jerk show small overshoot and oscillation, as seen in Figs. 6.33 and 6.34, respectively. Maximum Average Power is 0.0032 and Vibration Dose Value (VDV) is 1.4273.

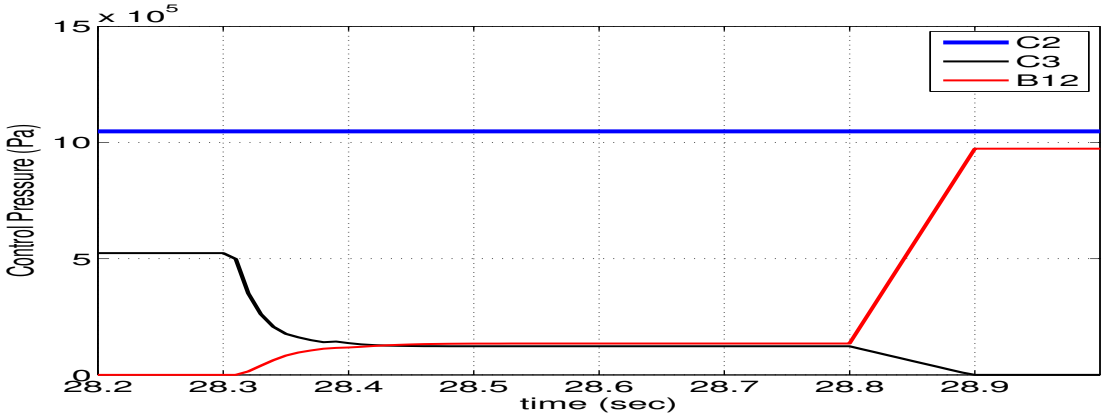

Figure 6.29. Closed–Loop Control Pressure Profile for 3^{rd}–2^{nd} downshift.

6.1.6 2–1 downshift

A 2–1 upshift requires the disengagement of clutch C_2 since the one–way clutch C_1 will be automatically engaged in the first gear, as listed in Table 4.1. Once engaged, clutch C_1 will connect the sun of the front planetary gear set to the turbine. Thus,

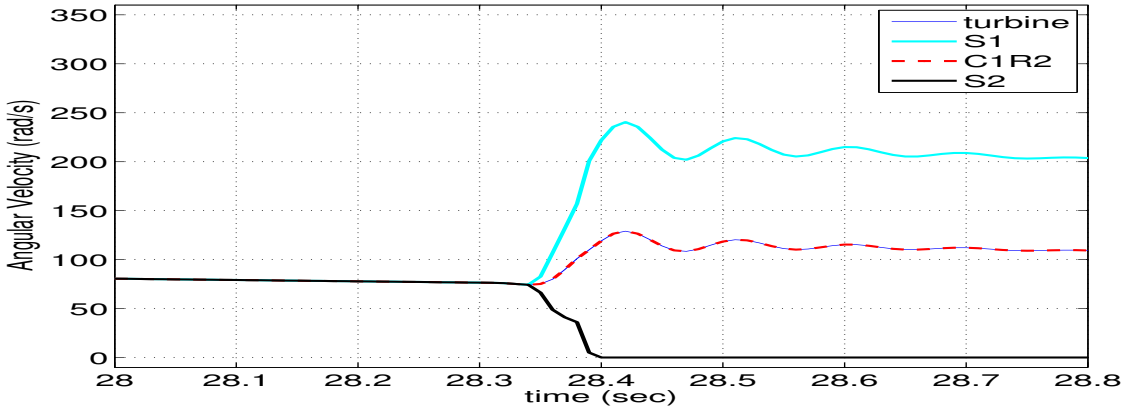

Figure 6.30. Closed–Loop Speed Results for 3^{rd}–2^{nd} downshift.

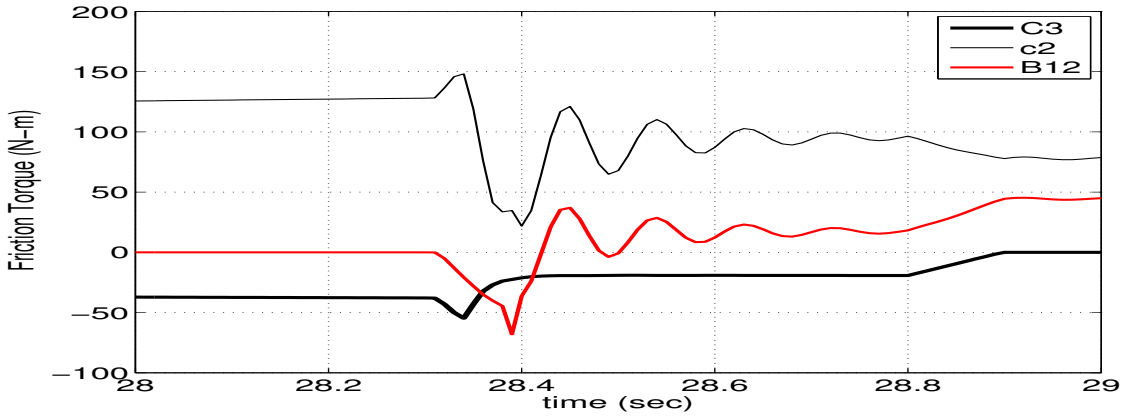

Figure 6.31. Closed–Loop Friction Torque on Clutch/Band during 3^{rd}–2^{nd} Downshift.

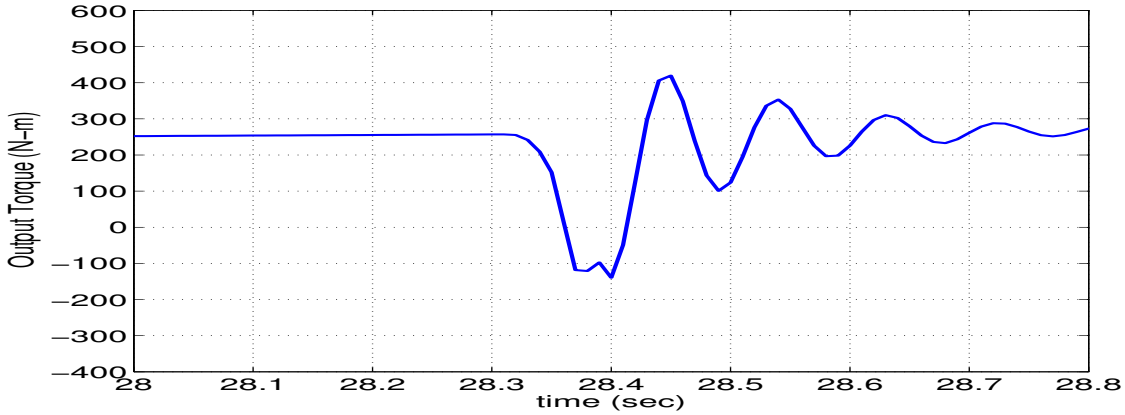

Figure 6.32. Closed–Loop Output Torque during 3^{rd}–2^{nd} downshift.

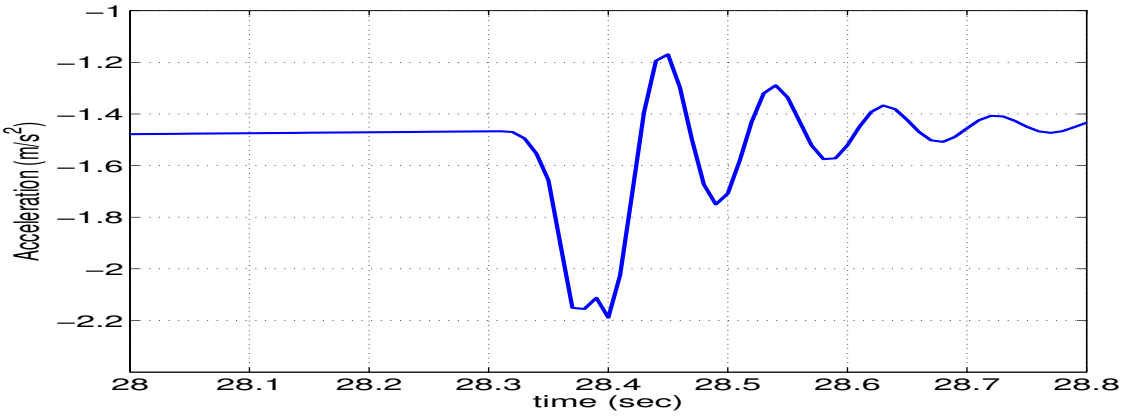

Figure 6.33. Closed–Loop Vehicle Acceleration during 3^{rd}–2^{nd} downshift.

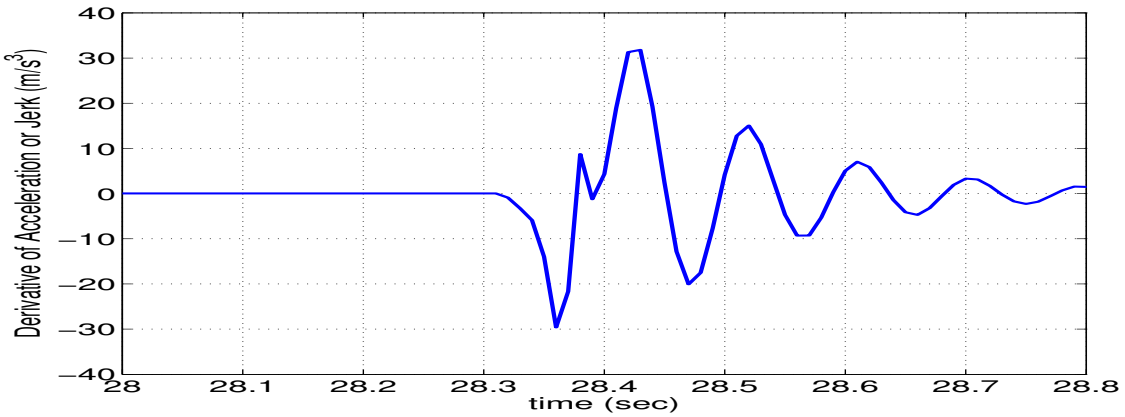

Figure 6.34. Closed–Loop Derivative of Acceleration or Jerk during 3^{rd}–2^{nd} downshift.

the reference angular speed is ω_{S1}, the speed of sun–1 and the desired speed is the turbine speed. This means the error signal for the PID controller for this shift is

$$e_{21}(t) = \omega_t - \omega_{S1} \tag{6.10}$$

The PID controller, with this error input, generates the desired pressure profile for the hydro-electric solenoid valve of clutch C_2.

The PID gains are tuned based on the simulation results of the velocity, the acceleration, the jerk and the output shaft torque. Increasing K_P results in smaller speed error. First, K_P is set to be 1, suggested as the PID tuning method [92].

Gain K_P is increased until excessive oscillation is seen in both speed and torque plots, which indicate poor shift quality. Then, the gains are reduced by half. The re-tuning of the gains is repeated until a satisfactory change of the pressure in the torque phase is observed as shown in Fig. 6.35. Adding K_I eliminates the steady state error, but worsens the transient response with high overshoot and slow settling time. Finally, adding K_D improves the transient response by reducing overshoot and achieves tracking the desired speed. K_I and K_D are used to shape the pressure profile as shown in Fig. 6.35, since increasing K_P only can not eliminate the steady-state error. Gains K_I and K_D are initially started as 1 and increased gradually until acceptable results are obtained. The final values of the gains are given in Table 6.1, which result in satisfactory shift response. Fig. 6.35 shows that the control pressure is reduced in the beginning of the torque phase from about 1000 kPa to 200 kPa. In the inertia phase, the pressure drops to 0 kPa where the clutch is completely disengaged. This pressure profile generated by the PID controller leads to a good shift quality. Once the PID controller is used to generate the pressure profile, Fig. 6.36 shows that the overshoot and oscillation are eliminated significantly. Fig. 6.36 shows that the speed of sun–1 is successfully reduced to match the turbine speed without any unacceptable transient. Note that the steady-state error is reduced to zero after two rotating elements are matched. The friction torque at clutch C_2 applied to carrier–1 is controlled to have small overshoot and oscillation. PID controller, as shown in Fig. 6.37, has small overshoot and oscillation. The output torque of the planetary gear sets also has low overshoot and oscillation, as shown in Fig. 6.38. In the closed loop response, the vehicle acceleration and jerk show small overshoot and oscillation, as seen in Figs. 6.39 and 6.40, respectively. Maximum Average Power is 0.0098 and Vibration Dose Value (VDV) is 1.2538.

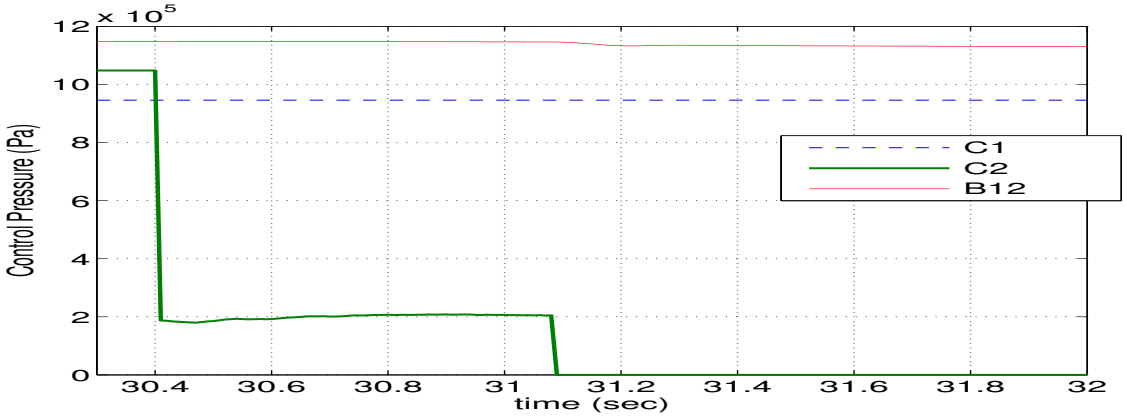

Figure 6.35. Closed–Loop Control Pressure Profile for 2^{nd}–1^{st} downshift.

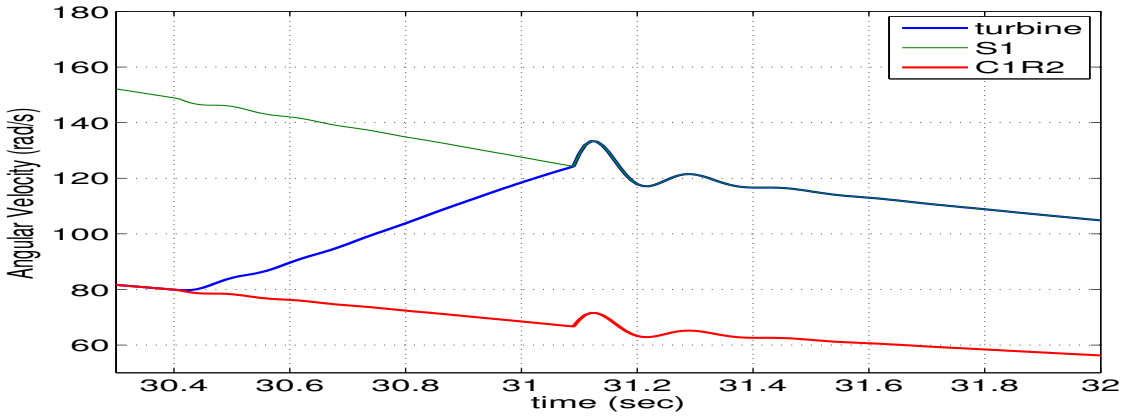

Figure 6.36. Closed–Loop Speed Results for 2^{nd}–1^{st} downshift.

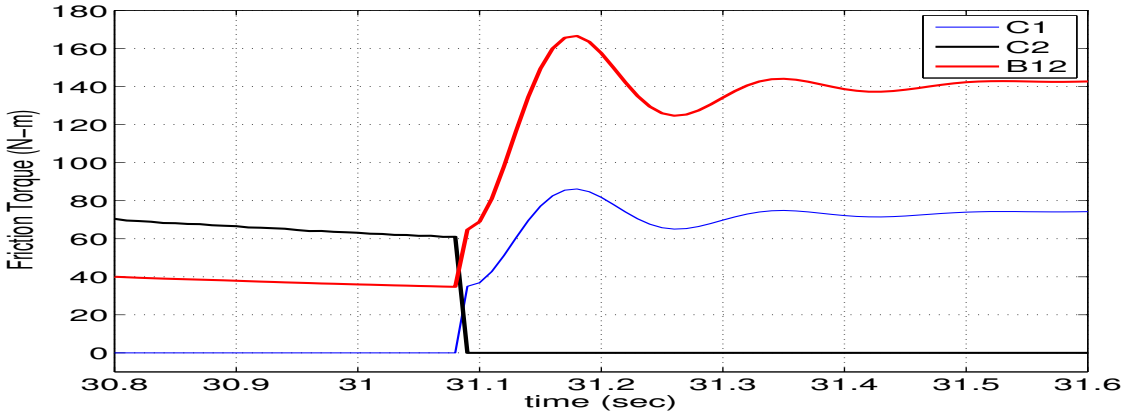

Figure 6.37. Closed–Loop Friction Torque on Clutch/Band during 2^{nd}–1^{st} Downshift.

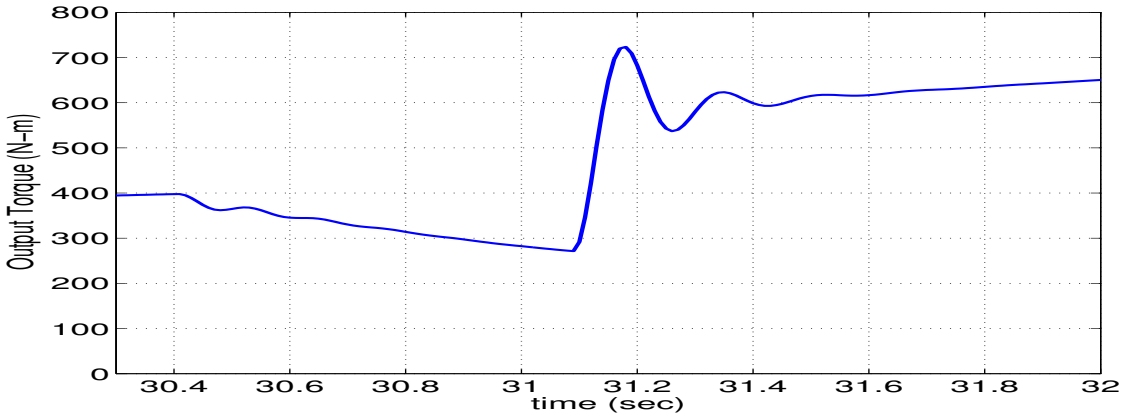

Figure 6.38. Closed–Loop Output Torque during 2^{nd}–1^{st} downshift.

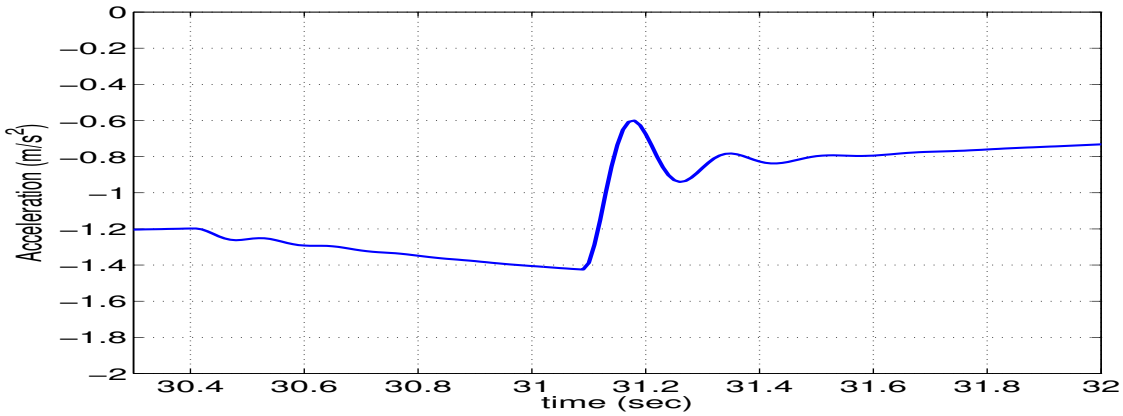

Figure 6.39. Closed–Loop Vehicle Acceleration during 2^{nd}–1^{st} downshift.

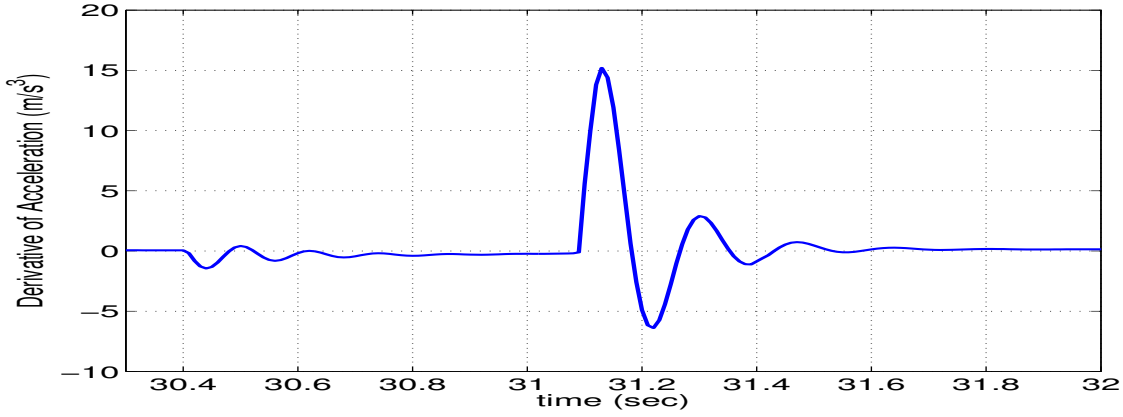

Figure 6.40. Closed–Loop Derivative of Acceleration or Jerk during 2^{nd}–1^{st} downshift.

6.2 Robustness Analysis of PID Controller

The previous section shows that the shift quality can be improved by employing feedback control. This conclusion is based on the simulations of a specific driving condition. One of the important control design requirements is the robustness of the closed–loop system against disturbances and variations of the system characteristics over the operational life of the system. This section is to evaluate the robustness of the PID controller against the variations of the transmission parameters. The robustness of the closed–loop performance is evaluated in terms of the variations of the shift quality metrics while the system characteristics change.

The Monte Carlo method [93, 94] is used to quantify and evaluate the robustness of the closed–lop system against the variations of the friction characteristics in the clutches and bands. The friction coefficient as introduced in Fig. 4.22 is an exponential function of the relative speed with three parameters.

$$\mu = A + B\, exp(-C \cdot \Delta\omega) \tag{6.11}$$

where the nominal valves of A, B and C are 0.0631, 0.0504 and 0.033, respectively. In the open–loop and closed–loop simulations presented in Chapter 5 and this chapter, respectively, the friction coefficient function has its parameters at these nominal values. To model the variation of the friction characteristics, the three parameters are considered to be random variables with normal distribution; their mean values and standard deviations are given in Table 6.5. The standard deviations are selected such that the samples of the random variables have $+/-40\%$ variation of the friction coefficients from their mean values. Such large variations of the friction coefficients are sufficient to represent the degradation of the friction elements throughout the life of a transmission. The robustness of the PID controller is investigated in 1–2 upshift. The 1–2 upshift is simulated 1000 times with the random friction parameters sampled

Table 6.5. Mean and Standard Deviation of Parameter A, B and C

Parameter	**Mean**	**Standard Deviation**
A	0.0631	0.01
B	0.0504	0.01
C	0.033	0.01

independently for each simulations. The histograms of the samples of the parameters, A, B and C are shown in Figs. 6.41, 6.42 and 6.43, respectively. Fig. 6.44 shows the plots of the friction coefficients based on the samples of the parameters. The turbine, sun–1 and carrier–1 speed responses from all the simulations are shown in Fig. 6.45. It is clear from this figure that the shift quality remains consistently good despite the variation in the friction characteristics. After each simulation, four metrics that are used to quantify shift quality are calculated: (i) shift duration, (ii) maximum overshoot in the oncoming friction torque response, (iii) maximum jerk, and (iv) Vibration Dose Value (VDV). Since MAP shows similar trend to that of VDV, only VDV results are given in this section. The histogram plots of these metrics are shown in Figs. 6.46, 6.47, 6.48 and 6.49, respectively. The histograms represent the frequency distribution in the rectangles whose widths represent class intervals and whose areas are proportional to the corresponding frequencies. The width of the interval is equal and obtained by equally spacing the rectangles. In this approach, by using default setting in Matlab, the appearance of the histograms are not like smooth. But they are sufficient to represent the idea of frequency distribution. The shift duration is very likely to be around 0.68, as shown in Fig. 6.46; the shift may take up to 0.71 second with very small likelihood. The maximum clutch C_2 torque is most likely to be around 145 N–m, as shown in Fig. 6.47. There are only a few times the torque exceeding 150 N–m, with a very small probability. The jerk, as shown in Fig. 6.48,

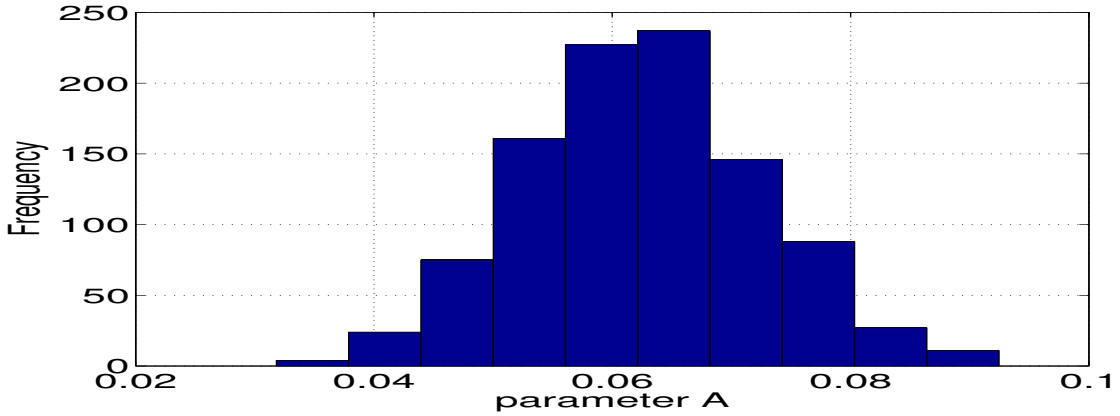

Figure 6.41. Histogram of Parameter A.

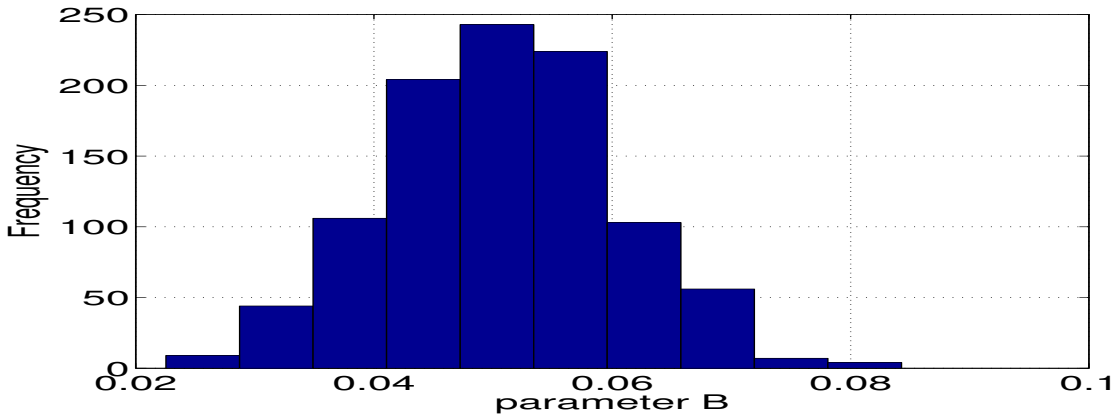

Figure 6.42. Histogram Parameter B.

stays within 8–13 m/s^3, more likely to be around 12 m/s^3. The VDV seems to have a normal–like distribution with its mean at 0.827. These results shown that the PID controller is robust against the variation in shift characteristics and consistently gives a high quality shift.

6.3 Sliding Mode Controller and its Evaluation

This section investigates the feasibility of a nonlinear control design method, Sliding Mode (SM) control. The dynamics of the planetary gear set switches models as the friction model switches between states for the clutches and bands. This makes

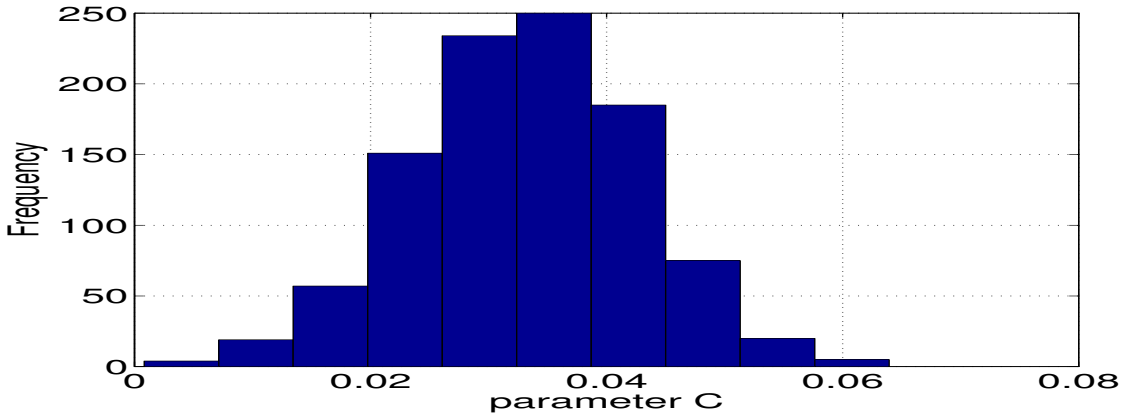

Figure 6.43. Histogram of Parameter C.

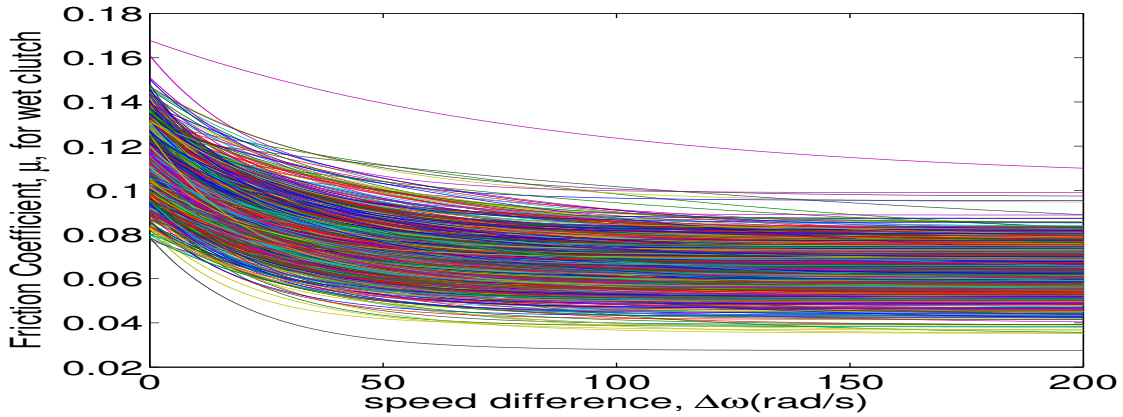

Figure 6.44. Friction Coefficient Variation based on the samples of random A, B and $C4$.

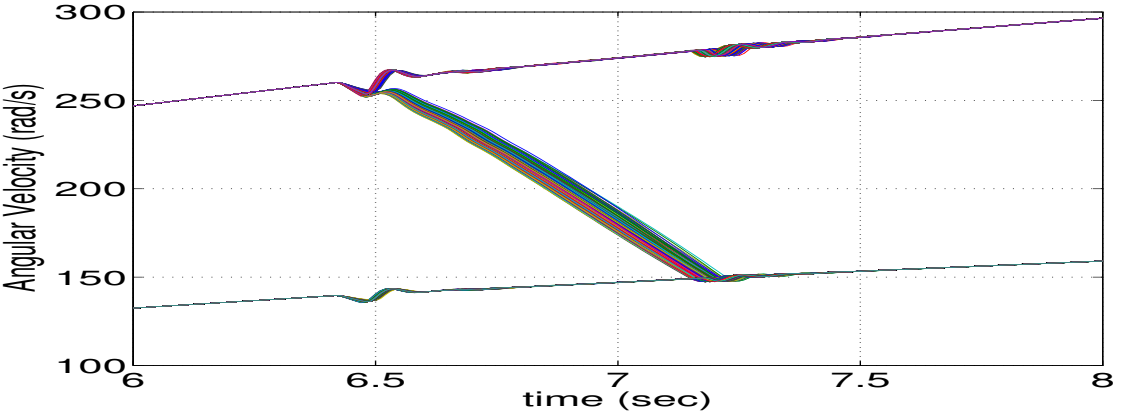

Figure 6.45. Speed Variation during 1^{st}–2^{nd} upshift in the Monte Carlo Simulations.

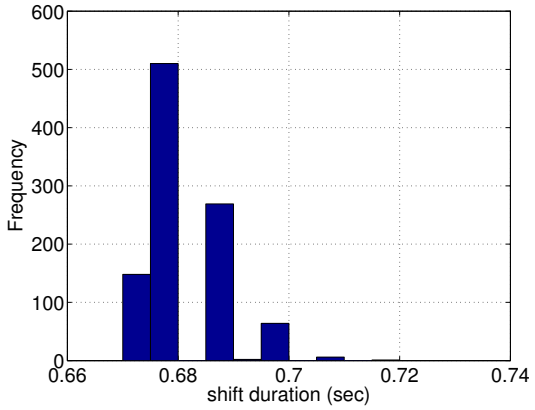

Figure 6.46. Histogram of Shift Duration Variation during 1^{st}–2^{nd} upshift.

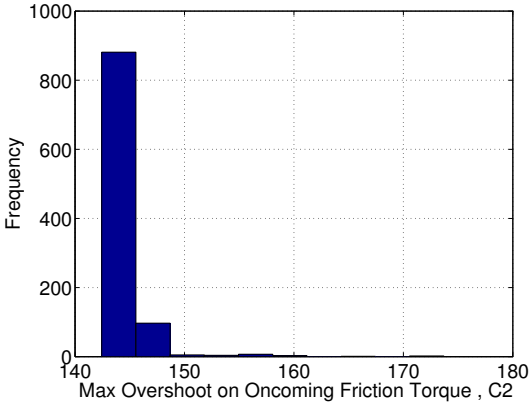

Figure 6.47. Histogram of Oncoming Clutch Torque (C2) Variation during 1^{st}–2^{nd} upshift.

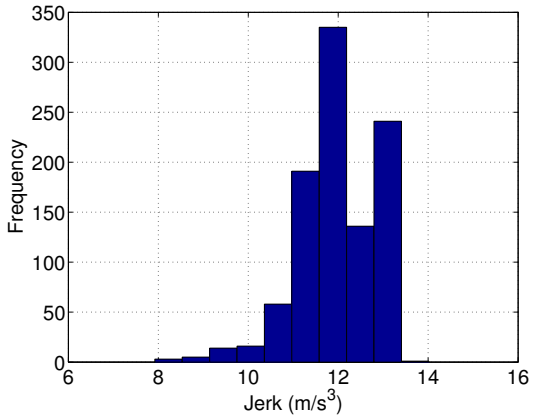

Figure 6.48. Histogram of Jerk Variation during 1^{st}–2^{nd} upshift.

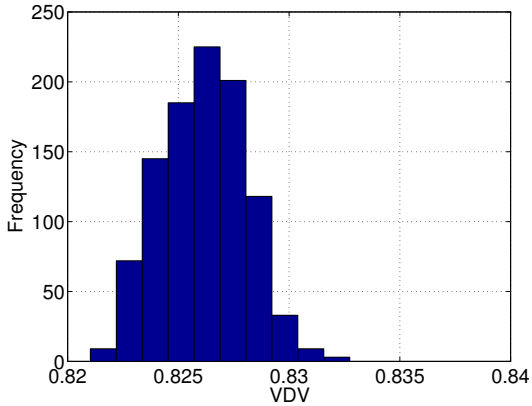

Figure 6.49. Histogram of Vibration Dose Value Variation during 1^{st}–2^{nd} upshift.

SM control very suitable for this inherently nonlinear problem. As depicted in Fig. 6.50, the SM controller takes, as inputs, speed, acceleration and torque measurements as commanded and feedback signals. The SM approach can easily be applied to the problem of transmission control. The parameters of the controller are intuitive to tune. However, the fact that the control law requires torques as feedback signals makes it impractical to implement unless an estimator or observer is used to provide estimates of the required torque signals. In the following sections, the SM approach

is used to design feedback controllers for 1–2 upshift and 3–2 downshift. Their implementations are carried out in simulation with the assumption that torque signals are available for feedback. Then, an attempt to use an observer to estimate the torque signals will be discussed.

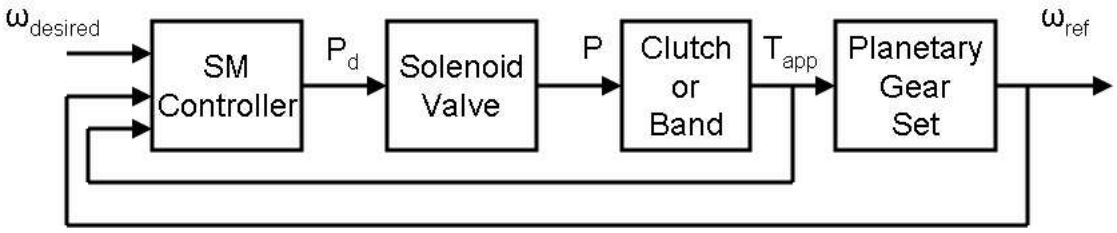

Figure 6.50. Sliding Mode Controller Feedback Loop.

6.3.1 1–2 upshift

As stated earlier in the discussion of 1–2 upshift with PID controller, the engagement of clutch C_2 is controlled since clutch C_1 is a one–way clutch and overruns in the second gear (see Table 4.1). Thus, the purpose of the SM control design is to find applied pressure on clutch C_2. Since the engagement of clutch C_2 connects carrier–1 to the turbine, the SM design, the sliding surface, r, is defined as

$$r = \dot{e} - \lambda e \tag{6.12}$$

where the error, e, between the actual position of carrier–1, θ_2, and desired position of carrier–1, θ_2^d, is

$$e = \theta_2 - \theta_2^d \tag{6.13}$$

and its derivative is

$$\dot{e} = \dot{\theta}_2 - \dot{\theta}_2^d \tag{6.14}$$

The derivative of Eq. (6.12) gives

$$\dot{r} = \ddot{e} - \lambda \dot{e} \tag{6.15}$$

where λ is a strictly positive constant with the unit of 1/sec, which is the slope of sliding surface in the phase plane $(\dot{e}, e)$. From the dynamic model of the coupled planetary gear sets in GM Hydramatic 440 detailed in Chapter 4, Eqs. (4.63) and (4.64), the carrier–1 acceleration, which is ring–2 acceleration, $\ddot{\theta}_2$, is calculated to be

$$\ddot{\theta}_2 = a_1 T_{S_1} + b_1 T_{S_2} + c_1 T_{C_2 R_1} + d_1 T_{C_1 R_2} \tag{6.16}$$

where

$$a_1 = -\frac{B_{21}A_2 + B_{11}A_1}{B_{21}b_{12} - B_{11}B_{22}} \tag{6.17}$$

$$b_1 = \frac{B_{21}A_4 + B_{11}A_5}{B_{21}b_{12} - B_{11}B_{22}} \tag{6.18}$$

$$c_1 = \frac{B_{21}}{B_{21}B_{12} - B_{11}B_{22}} \tag{6.19}$$

$$d_1 = -\frac{B_{11}}{B_{21}B_{12} - B_{11}B_{22}} \ . \tag{6.20}$$

Substituting $\dot{e}$ from Eq. (6.14) and $\ddot{\theta}_2$ from Eq. (6.16) into Eq. (6.15) yields

$$\dot{r} = a_1 T_{S_1} + b_1 T_{S_2} + c_1 T_{C_2 R_1} + d_1 T_{C_1 R_2} - \ddot{\theta}_2^d + \lambda \left(\dot{\theta}_2 - \dot{\theta}_2^d \right) \tag{6.21}$$

As explained in Chapter 4, during 1–2 upshift, the torques of clutch C_1 and band B_{12} are applied on sun–1 and sun–2, respectively. The torque on clutch C_2 is applied to carrier–1. Thus, the applied torques in Eq. (6.21) on the pair of carrier–1 and ring–2, sun–1, and sun–2 are T_{C_2} (clutch C_2 torque), T_{C_1} (clutch C_1 torque), and $T_{B_{12}}$ (band B_{12} torque), respectively. The pair of carrier–2 and ring–1 is connected to the final drive, which implies $T_{C_2 R1}$ is calculated from the output shaft torque. Since 1–2 upshift connects carrier–1 & ring–2 to the turbine, the desires speed, $\dot{\theta}_2^d$

and acceleration, $\ddot{\theta}_2^d$ are set to the speed, ω_t and acceleration, $\dot{\omega}_t$ of the turbine. The best approximation of a continuous control clutch torque, T_{C_2}, that will lead to $r = 0$ is selected to be

$$T_{C_2} = \frac{1}{d_1}\left\{-a_1 T_{C_1} - b_1 T_{B_{12}} - c_1 T_{C_2 R_1} + \dot{\omega}_t - \lambda\left(\dot{\theta}_2 - \dot{\theta}_2^d\right) + v(t)\right\} \tag{6.22}$$

where $v(t)$ can be chosen such that the sliding surface , $r = 0$, is an invariant set [95]. On the surface, $r = 0$, the tracking problem, $\theta_2 = \theta_2^d$ is equivalent to that of remaining on the surface , $r(t) = 0$. Thus, $v(t)$ is chosen as

$$v(t) = -\kappa r \tag{6.23}$$

Substituting Eqs. (6.22) and (6.23) into Eq. (6.21) yields the dynamic of the sliding surface as

$$\dot{r} = -\kappa r \tag{6.24}$$

The solution of Eq. (6.24) is

$$r(t) = exp(-\kappa t) r(0) \tag{6.25}$$

where $r(t)$ goes to zero as time goes to infinity. This implies θ_2^d and $\dot{\theta}_2^d$ are tracked asymptotically. The torque command calculated by the control law is transformed into control pressure command for hydro-electric solenoid valve of clutch C_2 as

$$P_{ctrl,C2,command} = T_{C_2}/(\mu A r n) \tag{6.26}$$

which is processed in the simulation through the same first order transfer function discussed in the previous PID control section. The simulation results show an improved shift as illustrated in Figs. 6.51, 6.52, 6.53 and 6.54. In Fig. 6.51, oscillation and high overshoot in speed response during the shift is reduced significantly in comparison with the open loop response. Fig. 6.52 shows that the high oscillation and

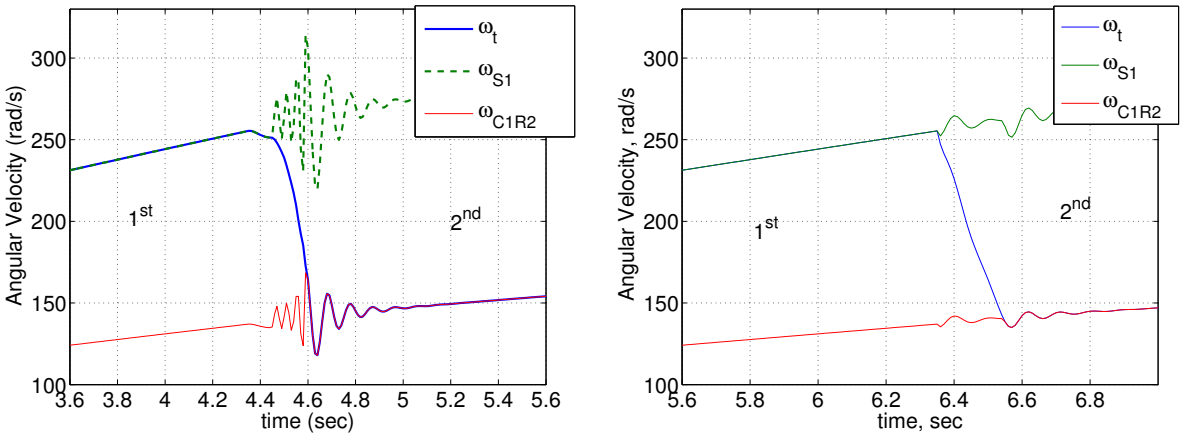

(a) (b)

Figure 6.51. Comparison Velocity Results during 1–2 Upshift between (a) Open Loop and (b) Closed Loop with Sliding Mode Controller.

magnitude in the acceleration of the open loop control is reduced about 50% with the SM control used. Similar improvements are also observed in Figs. 6.53 and 6.54.

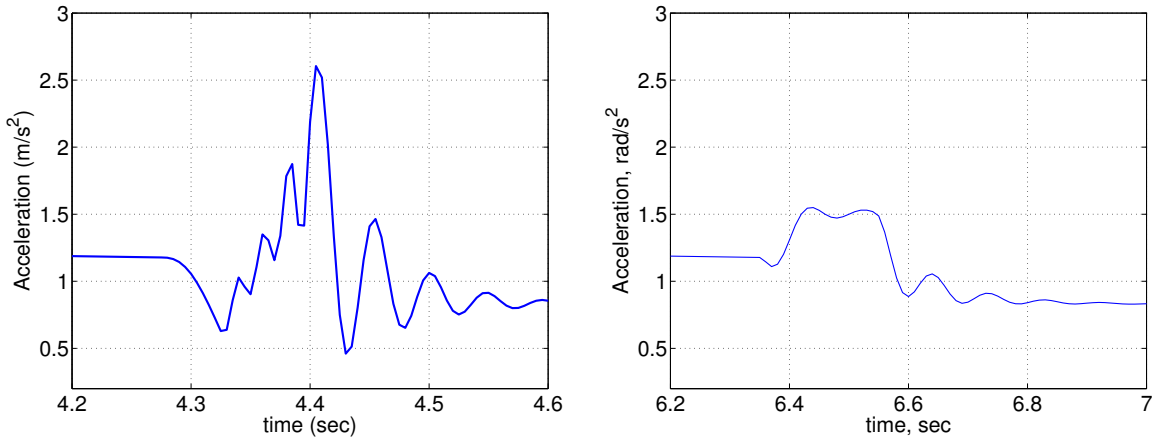

(a) (b)

Figure 6.52. Comparison Acceleration Results during 1–2 Upshift between (a) Open Loop and (b) Closed Loop with Sliding Mode Controller.

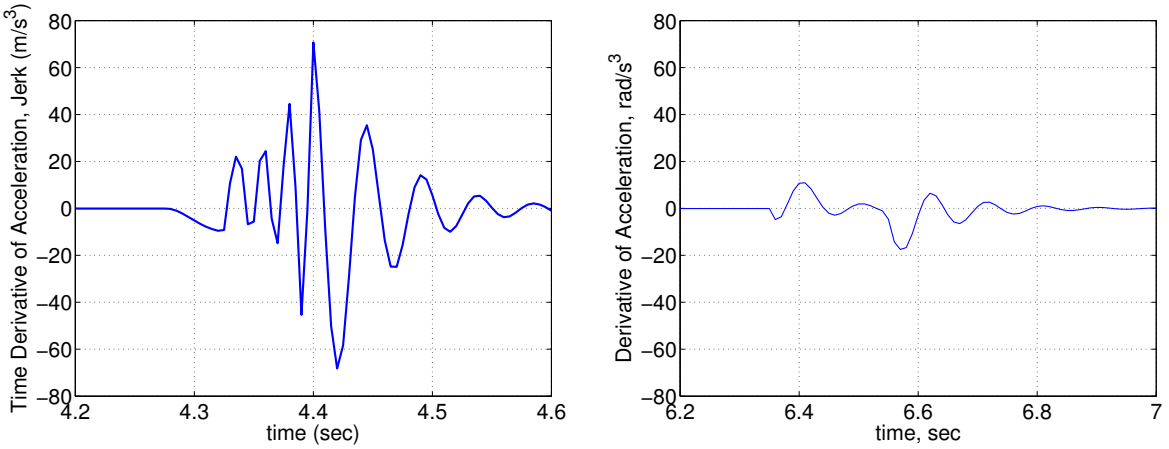

(a) (b)

Figure 6.53. Comparison Jerking Results during 1–2 Upshift between (a) Open Loop and (b) Closed Loop with Sliding Mode Controller.

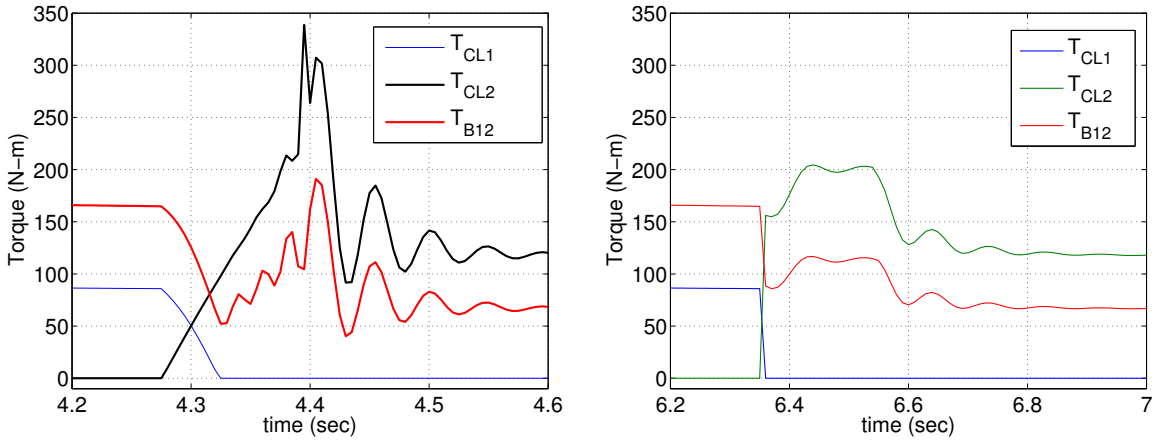

(a) (b)

Figure 6.54. Comparison Clutch Torque Results for 1–2 Upshift between (a) Open Loop and (b) Closed Loop with Sliding Mode Controller.

6.3.2 3–2 downshift

For a 3–2 downshift, clutch C_3 should be released while band B_{12} is engaged (see Table 4.1). This is a swap shift since one friction element needs releasing while another one engaging simultaneously. Such a shift is very challenging to control since engagement and releasing of two friction elements should be coordinated.

See from Fig. 4.1 that clutch C_3 connects sun–1 to the turbine in 3^{rd} gear. When clutch C_3 is released for 2^{nd} gear, sun–1 spins faster than the turbine speed; the ratio of the sun–1 speed over the turbine speed is 1.863. Thus, the desired speed of sun–1 for 3–2 downshift is set to be the turbine speed multiplied by 1.863. Similarly, Fig. 4.1 shows that band B_{12} is to stop sun–2. Thus, the desired speed of sun–2 for 3–2 downshift is zero. Because of the coordination of two friction elements for 3–2 swap shift, two sliding surface should be defined.

The sliding surface for clutch C_3, r_1, is defined as

$$r_1 = \dot{e}_1 - \lambda_1 e_1 \tag{6.27}$$

where the error, e_1, is between the actual position of sun–1, α_1, and desired position of sun–1, α_1^d,

$$e_1 = \alpha_1 - \alpha_1^d \tag{6.28}$$

and its derivative is

$$\dot{e}_1 = \dot{\alpha}_1 - \dot{\alpha}_1^d \tag{6.29}$$

For band B_{12}, the sliding surface, r_2, is defined as

$$r_2 = \dot{e}_2 - \lambda_1 e_2 \tag{6.30}$$

where the error, e_2, is between the actual position of sun–2, α_2, and desired position of sun–2, α_2^d,

$$e_2 = \alpha_2 - \alpha_2^d, \tag{6.31}$$

and its derivative is

$$\dot{e}_2 = \dot{\alpha}_2 - \dot{\alpha}_2^d \tag{6.32}$$

The derivative of Eq. (6.27) is

$$\dot{r}_1 = \ddot{e}_1 - \lambda_1 \dot{e}_1. \tag{6.33}$$

The derivative of Eq. (6.30) is

$$\dot{r}_2 = \ddot{e}_2 - \lambda_2 \dot{e}_2. \tag{6.34}$$

where λ_1 and λ_2 are strictly positive constants with the unit of 1/sec, which are the slopes of sliding surfaces r_1 and r_2, respectively.

The speed and acceleration of sun–1 can be calculated from those of carrier–1 & ring–2 and carrier–2 & ring–1 as formulated in Eq. (4.40). The acceleration of carrier–1 & ring–2 is already formulated in Eq. (6.16). Similarly, the acceleration of carrier–2 & ring–1 is formulated, from Eqs. (4.63) and (4.64), as

$$\ddot{\theta}_1 = a_2 T_{S_1} + b_2 T_{S_2} + c_2 T_{C_2 R_1} + d_2 T_{C_1 R_2} \tag{6.35}$$

where

$$a_2 = -\frac{B_{22}A_2 + B_{12}A_1}{B_{11}B_{22} - B_{21}B_{12}} \tag{6.36}$$

$$b_2 = \frac{B_{22}A_4 + B_{12}A_5}{B_{11}B_{22} - B_{21}B_{12}} \tag{6.37}$$

$$c_2 = \frac{B_{22}}{B_{11}B_{22} - B_{21}B_{12}} \tag{6.38}$$

$$d_2 = -\frac{B_{12}}{B_{11}B_{22} - B_{21}B_{12}} \tag{6.39}$$

Now substitute $\dot{e}$ from Eqs. (6.29) and its derivative into Eq. (6.33). Recall from Eq. (4.40) that, $\dot{\alpha}_1 = A_1\dot{\theta}_2 - A_2\dot{\theta}_1$, which implies that $\ddot{\alpha}_1 = A_1\ddot{\theta}_2 - A_2\ddot{\theta}_1$. As stated earlier, the desire speed and acceleration for the sun–1 are $\dot{\alpha}_1^d = 1.863\,\omega_t$ and $\ddot{\alpha}_1^d = 1.863\,\dot{\omega}_t$, respectively. During 3–2 downshift, the turbine and carrier–1 are connected by clutch C_2. This implies that the angular velocity and acceleration of both turbine and carrier–1 are the same, $\omega_t = \dot{\theta}_2$ and $\dot{\omega}_t = \ddot{\theta}_2$. As a result of these steps, Eq. (6.33) is rewritten as

$$\dot{r}_1 = A_1\dot{\omega}_t - A_2\ddot{\theta}_1 - 1.863\,\dot{\omega}_t + \lambda_1\left(\dot{\alpha}_1 - 1.863\,\omega_t\right) \tag{6.40}$$

which, after rearranged, becomes

$$\dot{r}_1 = (A_1 - 1.863)\,\dot{\omega}_t - A_2\ddot{\theta}_1 + \lambda_1\,(\dot{\alpha}_1 - 1.863\,\omega_t) \tag{6.41}$$

The angular dynamics of the turbine can give an expression for the turbine acceleration as,

$$\dot{\omega}_t = \frac{1}{I_t}(T_t + T_{C_1} + T_{C_2} + T_{C_3}) \tag{6.42}$$

which is the same as Eq. (4.124). Since clutch C_1 is disenegaged/overrunning during 3–2 shift, T_{C_1}. This implies

$$\dot{\omega}_t = \frac{1}{I_t}(T_t + T_{C_2} + T_{C_3}) \tag{6.43}$$

Substituting $\dot{\omega}_t$ from this equation

$$\dot{r}_1 = (A_1 - 1.863)\frac{T_t - T_{C_2} - T_{C_3}}{T_t} - A_2\ddot{\theta}_1 + \lambda_1\,(\dot{\alpha}_1 - 1.863\omega_t) \tag{6.44}$$

The best approximation of a continuous control law for clutch C_3 that would achieve $r = 0$ is selected to be

$$T_{C_3} = T_t - T_{C_2} + \frac{I_t}{(A_1 - 1.863)}\left[-A_2\ddot{\theta}_1 + \lambda_1(\dot{\alpha}_1 - 1.863\omega_t) - v_1(t)\right] \tag{6.45}$$

where $v_1(t)$ can be chosen such that the sliding surface , $r_1 = 0$, is an invariant set [95]. On the surface, $r_1 = 0$, the tracking problem, $\alpha_1 = \alpha_1^d$ is equivalent to that of remaining on the surface, $r_1(t) = 0$. Thus, $v_1(t)$ is chosen as

$$v_1(t) = -\kappa_1 r_1 \tag{6.46}$$

which implies

$$v_1(t) = -\kappa_1(\dot{\alpha}_1 - 1.863\,\omega_t) - \kappa_1\lambda_1(\alpha_1 - 1.863\,\theta_t) \tag{6.47}$$

Substituting Eqs. (6.45) and (6.46) into Eq. (6.44), leads to the dynamic of the sliding surface, r_1, as

$$\dot{r}_1 = -\kappa_1 r_1 \tag{6.48}$$

The solution of Eq. (6.48) is

$$r_1(t) = exp(-\kappa_1 t) r_1(0). \tag{6.49}$$

which implies that $r_1(t)$ goes to to zero as time goes to infinity. This implies α_1^d and $\dot{\alpha}_1^d$ are asymptotically tracked.

Similarly, the SM controller for band B_{12} is derived as follows. First, $\dot{e}_2$ from Eqs. (6.32) and its derivative are substituted into Eq. (6.34). Recall from Eq. (4.42) that $\dot{\alpha}_2 = A_4\dot{\theta}_1 - A_5\dot{\theta}_2$ and $\ddot{\alpha}_2 = A_4\ddot{\theta}_1 - A_5\ddot{\theta}_2$. And the desire velocity and acceleration for the sun–2 are $\dot{\alpha}_2^d = 0$ and $\ddot{\alpha}_2^d = 0$. Further, during 3–2 downshift, the turbine and carrier–1 are connected by clutch C_2. This implies that the angular velocity and acceleration of both turbine and carrier–1 are equal, $\omega_t = \dot{\theta}_2$ and $\dot{\omega}_t = \ddot{\theta}_2$. Thus, Eq. (6.34) is rewritten as

$$\dot{r}_2 = A_4\ddot{\theta}_1 - A_5\dot{\omega}_t + \lambda_2\left(\dot{\alpha}_2\right) \tag{6.50}$$

which is rearranged to become

$$\dot{r}_2 = A_4\left(a_2 T_{S_1} + b_2 T_{S_2} + c_2 T_{C_2R_1} + d_2 T_{C_1R_2}\right) - A_5\dot{\omega}_t + \lambda_2\left(\dot{\alpha}_2\right) \tag{6.51}$$

Note that the torque at carrier–1, sun–1 and sun–2 are the friction torque at clutch C_2, clutch C_3 and band B_{12}, respectively, $T_{C1R2} = T_{C_2}$, $T_{S1} = T_{C_3}$ and $T_{S2} = T_{B_{12}}$. The best approximation of a continuous control law for band–12 that would achieve $r = 0$ is selected to be

$$T_{B_{12}} = \frac{-1}{b_2}\left(a_2 T_{C_3} + c_2 T_{C_2R_1} + d_2 T_{C_2}\right) + \frac{1}{b_2 A_4}\left[A_5\dot{\omega}_t - \lambda_2(\dot{\alpha}_2) + v_2(t)\right] \tag{6.52}$$

where $v_2(t)$ can be chosen such that the sliding surface, $r_2 = 0$, is an invariant set [95]. On the surface, $r_2 = 0$, the tracking problem, $\alpha_2 = \alpha_2^d$ is equivalent to that of remaining on the surface , $r_2(t) = 0$. Thus, $v_2(t)$ is chosen as

$$v_2(t) = -\kappa_2 r_2 \tag{6.53}$$

which implies

$$v_2(t) = -\kappa_2 \dot{\alpha}_2 - \kappa_2 \lambda_2 \alpha_2 \tag{6.54}$$

Substituting Eqs. (6.52) and (6.53) into Eq. (6.51) gives the dynamic of the sliding surface, r_2, as

$$\dot{r}_2 = -\kappa_2 r_2 \tag{6.55}$$

with the solution

$$r_2(t) = exp(-\kappa_2 t) r_2(0) \tag{6.56}$$

which implies that $r_2(t)$ goes to zero as time goes to infinity. This implies that α_2^d and $\dot{\alpha}_2^d$ are asymptotically tracked. Finally, the control laws for torques are transformed into control pressure command, $P_{ctrl,command}$, for hydro-electric solenoid valves as

$$P_{ctrl,C3,command} = T_{C_3}/(\mu A r n) \tag{6.57}$$

$$P_{ctrl,B12,command} = T_{B_{12}}/[A\ r\ n\ (\exp^{\mu\alpha} - 1)] \tag{6.58}$$

The simulation results in Fig. 6.55 show the control pressure profiles generated by the SM control laws. The simulation results show the improvements in shift quality in Figs. 6.56–6.60. Fig. 6.56 shows that the speeds of sun–1 and sun–2 have only small oscillations and overshoot. The friction torque at clutch C_3 and band B_{12} are shown in Fig. 6.57 with small oscillation. There is a drop in the friction torque due to gear change to the low gear. The output torque also has a drop during the shift as shown in Fig. 6.58, since the gear is changed down to a lower gear. Figs. 6.59 and 6.60 show that the high oscillation and overshoot in the acceleration and jerk observed in the open loop simulation are reduced to a satisfactory level.

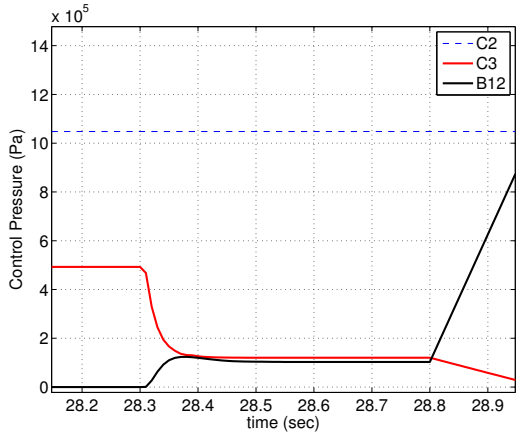

Figure 6.55. Control Pressure Profile during 3^{rd}–2^{nd} Downshift Closed Loop with Sliding Mode.

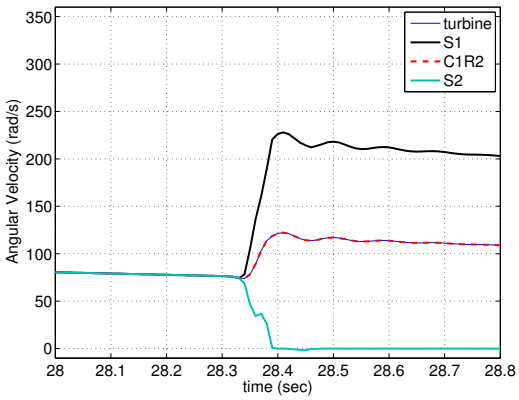

Figure 6.56. Velocity during 3^{rd}–2^{nd} Downshift Closed Loop with Sliding Mode Controller.

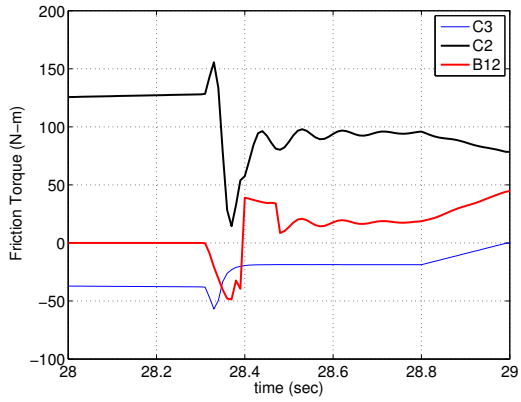

Figure 6.57. Friction Torque on Clutch/Band during 3^{rd}–2^{nd} Downshift Closed Loop with Sliding Mode Controller.

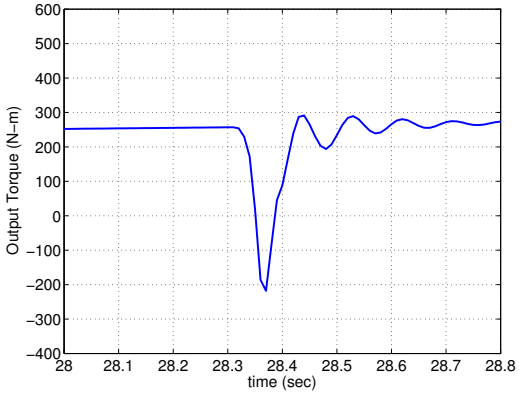

Figure 6.58. Output Torque in the Final Drive Shaft during 3^{rd}–2^{nd} Downshift Closed Loop with Sliding Mode Controller.

6.4 Observer Design

The sliding mode controller developed in the previous section requires the information of torque as feedback signals. Since the clutch/band torques cannot be measured, estimation of such signals are needed for a practical implementation of the sliding mode controller. In this section, the design and implementation of an

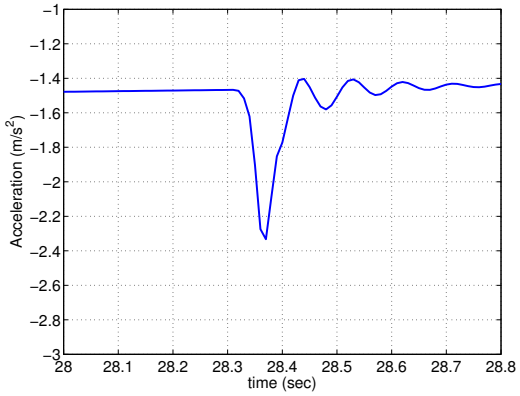

Figure 6.59. Acceleration during 3^{rd}–2^{nd} Downshift Closed Loop with Sliding Mode Controller.

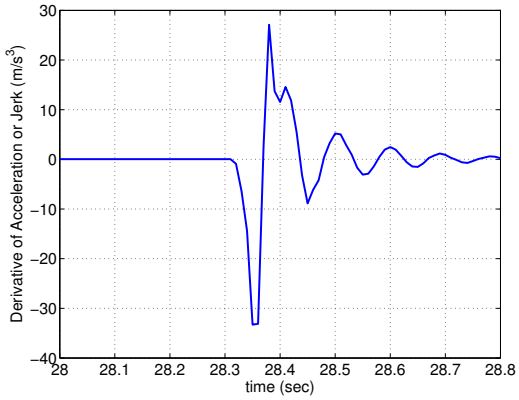

Figure 6.60. Comparison Jerking during 3^{rd}–2^{nd} Downshift Closed Loop with Sliding Mode Controller.

observer in simulation are attempted. This is to investigate whether the sliding mode controller provided with the torque estimated by an observer is practical.

6.4.1 Review of Thau Observer or Lipschitz Observer

Some nonlinear systems can be represented in a special state space form as

$$\dot{x} = Ax + f(x) + Bu \tag{6.59}$$

$$y = Cx \tag{6.60}$$

where A, B and C are known state, input and output matrices, respectively, $f(x)$ is a known nonlinear function, u is a known input, y is the measured outputs. If (A, C) is observable, there exits a matrix K such that the eigenvalues of $A_0 = A - KC$ are in the left half of the complex plane. Then, a Thau observer can be constructed as

$$\dot{\hat{x}} = A\hat{x} + f(\hat{x}) + Bu + K(y - \hat{y}) \tag{6.61}$$

$$y = C\hat{x} \tag{6.62}$$

The observer error between the estimated state, $\hat{x}$, and the actual state, x, is

$$e = \hat{x} - x \tag{6.63}$$

whose derivative results in

$$\dot{e} = (A - KC)e + f(\hat{x}) - f(x) \tag{6.64}$$

$$\dot{e} = A_0 e + f(\hat{x}) - f(x) \tag{6.65}$$

Since A_0 is stable for any given positive definite matrix Q, there exists a unique positive definite matrix P, such that the following Lyapunov equation is satisfied

$$A_0^T P + P A_0 = -2Q \tag{6.66}$$

If K is selected such that A_0 leads to the solution of the Lyapunov equation that satisfies

$$\frac{\lambda_{min}(Q)}{\| P \|} > L \tag{6.67}$$

where L is the Lipchitz constant

$$\| f(x_1) - f(x_2) \| \leq L \| x_1 - x_2 \| \tag{6.68}$$

for any x_1 and x_2, then the Thau nonlinear observer is asymptotically stable.

6.4.2 Application of Thau Observer to System with friction

The brief overview of the Thau nonlinear observer in the preceding section cannot be directly applied to the problem of shift dynamics. This is because the shift dynamics model has torque signals as inputs, which are generated by the friction elements and cannot be measured. Thus, a modified form of the Thau observer is used for estimating torque inputs. This approach uses the fact that the clutch and band torques depend on the states of the planetary gear system in addition to the known/measured applied pressure. Expressing the friction torque as an unknown nonlinear function of the states in Eq. (6.59) leads to

$$\dot{x} = Ax + f_1(x) \tag{6.69}$$

$$y = Cx \tag{6.70}$$

where A, C are known matrices, y is a known signal and $f_1(x)$ is an unknown function. If (A, C) is observable, there exits a matrix K such that the eigenvalues of $A_0 = A - KC$ are in the left half of the complex plane. Then, the nonlinear observer is formulated as

$$\dot{\hat{x}} = A\hat{x} + f_2(\hat{x}) + K(y - \hat{y}) \tag{6.71}$$

$$y = C\hat{x} \tag{6.72}$$

where a known function f_2 is used to approximate the unknown function, f_1. The observer error between the estimated state and the measured state is

$$e = \hat{x} - x \tag{6.73}$$

whose its derivative results in

$$\dot{e} = (A - KC)e + f_2(\hat{x}) - f_1(x) = A_0 e + f_2(\hat{x}) - f_1(x) \tag{6.74}$$

Since A_0 is stable for any given positive definite matrix Q, there exists a unique positive definite P, such that the following Lyapunov equation is satisfied

$$A_0^T P + P A_0 = -2Q \tag{6.75}$$

If K is selected such that A_0 can make the solution of the Lyapunov equation satisfy

$$\frac{\lambda_{min}(Q)}{\| P \|} > L \tag{6.76}$$

where L is the Lipchitz constant

$$\| f_2(\hat{x}) - f_1(x) \| \leq L \| \hat{x} - x \| \tag{6.77}$$

for any $\hat{x}$ and x, then the Thau nonlinear observer is asymptotically stable.

This Thau observer is evaluated in a closed–loop simulation with the sliding mode controller developed in the preceding section. This is to study whether the torque signals can be estimated. To take into account the fact that an actual friction characteristics of a clutch/band are not accurately known, the friction approximation function, $f_2(x)$, is intentionally chosen to be simpler that the friction model used in the simulation of the transmission dynamics. In the transmission model, the relatively complex and more accurate Wood friction model (see Section 4.5) is used. On the other hand, the observer uses the simple classical friction model as $f_2(\hat{x})$. Recall that the simple friction model has a zero relative–speed range defined as speed tolerance. Fig. 6.61 shows the measured sun–1 and carrier–1 speeds, their estimation by the Thau observer. During the 1–2 upshift, clutch C_2 is engaged by the sliding mode controller. The estimated states can track the actual states with small error in the first gear. During and after 1–2 upshift, the error tends to be larger due to the lack of convergence in the estimated friction torques, which are the inputs to the observer system. In Figures 6.62, 6.63 and 6.64, the estimated friction torques in clutch C_1, clutch C_2 and band B_{12} are shown, respectively. Since the approximation friction function, f_2, used in the observer is simple friction model with error in the relative zero velocity region, it can not estimate the actual friction properly. In this simulation, the sliding mode controller uses the actual torque signals. The observer is not run in the feedback loop. This simulation experiment shows that the Thau observer cannot properly estimate the torques. This implies that the sliding model controller with this observer is not feasible.

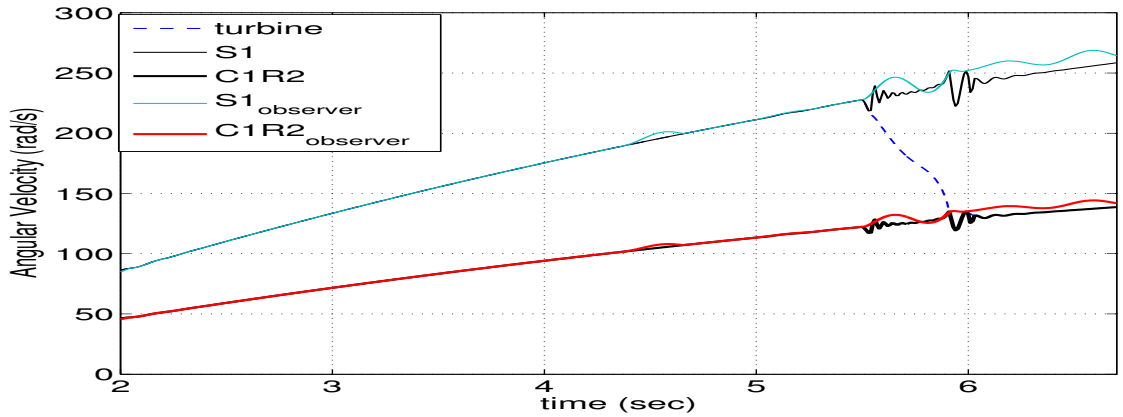

Figure 6.61. Actual and Estimated Angular Velocities during 1^{st}–2^{nd} Upshift with SM Controller.

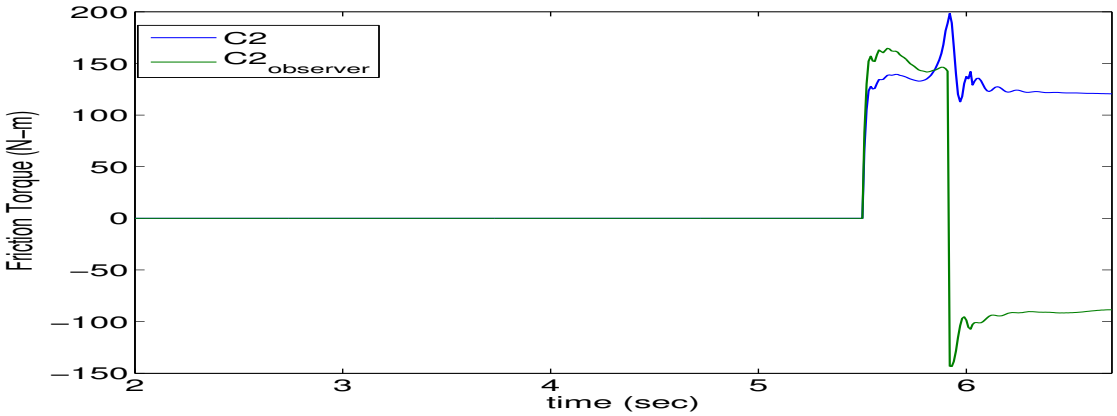

Figure 6.62. Estimated Friction Torque Clutch C_1 during 1^{st}–2^{nd} Upshift with SM Controller.

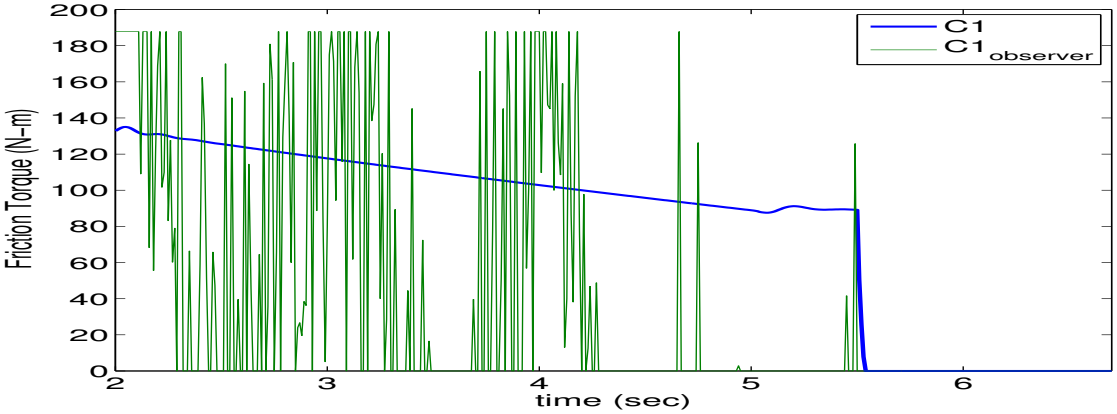

Figure 6.63. Estimated Friction Torque Clutch C_2 during 1^{st}–2^{nd} Upshift with SM Controller.

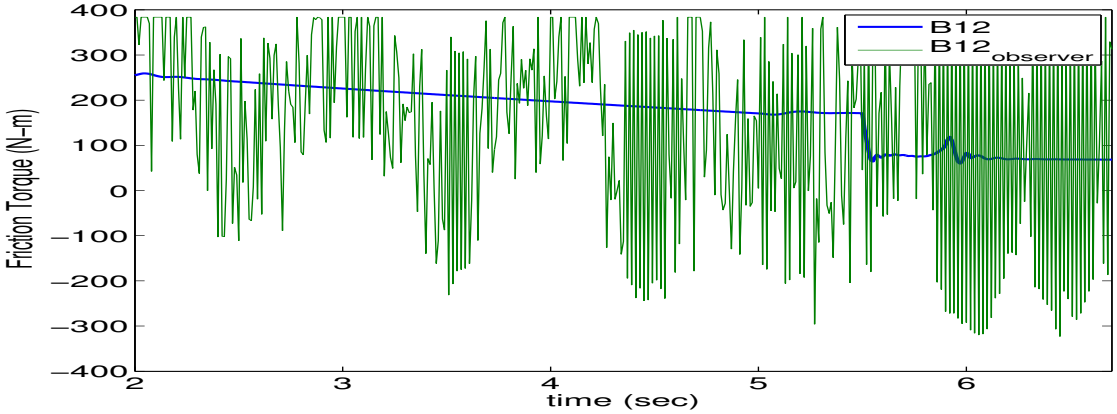

Figure 6.64. Estimated Friction Torque Band B_{12} during 1^{st}–2^{nd} Upshift with SM Controller.

CHAPTER 7

CONCLUSION AND FUTURE WORKS

7.1 Conclusion

This dissertation presents the modeling and control of an automatic transmission with planetary gear sets for shift quality. The mathematical model of the planetary gear sets is developed using a Lagrange method. The main advantage of the Lagrange method is that the equations of motion can be derived without computing the reaction/contact forces and torques. In the derivation, it is assumed that no backlash occurs between gear meshing, gears and shafts are rigid, and friction between the gears is negligible. It is shown that the Lagrange method provides a systematic and direct approach. The derived equations are used to study shift dynamics behavior. There is no need to switch from a set of equations to another during a shift as the equations derived are valid in all gears and shifts. Additionally, the transmission model is integrated with all the other powertrain subsystems, representing the engine, torque converter, hydraulic subsystem, final drive gear and vehicle dynamics.

The development of the friction model for friction elements in an automatic transmission is a major challenge in properly modeling shift dynamics. With an improper friction model, the stick–slip events in clutch/band cannot be adequately modeled, which leads to error in accurately simulating shift dynamics. Wood static and dynamic friction model, which has three modes (in–motion, captured and accelerating, and captured and static), is shown to successfully represent the clutches and bands in shift dynamics simulation. This modeling approach increases the fidelity of

the shift dynamics without compromising the simulation speed and numerical accuracy.

Various metrics used to measure or quantify shift quality are (i) shift duration, (ii) transient response of clutch/band torques in terms of maximum overshoot, (iii) transient response of the output torque, acceleration of the vehicle, (iv) the derivative of the acceleration or jerk, (v) maximum average power, and (vi) vibration dose value. It is shown that open–loop control of a shift requires a tedious calibration of the applied pressure of the clutches and/or bands. On the other hand, feedback control of a shift can lead to a high quality shift in the sense of any of the metrics without the need of calibration. The biggest obstacle to practical implementation of feedback control is to have fast enough hydraulic systems that can provide the applied pressure profile demanded by the controller. Traditional hydraulic actuation systems are not capable of providing such a pressure profile. However, there are new actuation technologies such as electro–hydraulic actuators that can potentially provide fast pressure regulations on clutches and bands. Simulation results demonstrated that PID control approach can be successfully used to feedback control all the up– and down–shift of a specific transmission. A separate PID controller is developed for each shift. The PID controllers use speed measurements as feedback signals and generate pressure profiles for the electro–hydraulic actuation systems of the clutches and/or bands involved. Simulation results shown that high quality shifts are obtained in terms of all the metrics for shift quality. A Monte Carlo simulation experiment proves the robustness of the PID controllers against the variation of the friction characteristics of the clutches and bands. Further, a nonlinear control design approach, sliding mode control, is investigated. While this controller can also provide high quality shifts, the fact that this controller requires torque measurements in addition to speed measurements makes it impractical to implement. An attempt to estimate the torque inputs

using an observer proves unsuccessful without the perfect knowledge of the friction characteristics.

7.2 Future Work

The current planetary gear model does not consider backlash, damping and friction between the gears. The effects of this assumption on shift dynamics should be investigated. If any significant effect is noticed, methods to account for these aspects should be developed. While the friction models developed and used in this research seem to be adequate for studying shift dynamics, methods to improve simulation speed without compromising the fidelity should be investigated. The desired angular speeds used to generate the error signals for the PID controllers are applied as step inputs to trigger shifts. Different desired speed profiles should be investigated to further improve shift quality. New technologies for fast pressure response on clutches and bands are essential for successful implementation of feedback control. This topic should be thoroughly investigated; detailed models for such electro–hydraulic actuation systems should be developed and integrated into the simulation environment. More systematic control design methods can also be studied that considers the shift quality metrics, not only tuning and evaluation of the controllers but also during the design phase of the controllers. The methods developed in this research for shift quality of automatic transmission can be utilized in other applications where planetary gears are used.

REFERENCES

[1] G. Lechner and H. Naunheiimer, *Automotive Transmission: Fundmentals, Selection, Design, and Application*. NY: Springer, 1999.

[2] R. N. Jazar, *Vehicle Dynamics: Theory and Application*. NY: Springer, 2008.

[3] D. Cho, "Nonlinear control methods for automotive powertrain systems," Ph.D. dissertation, Department of Mechanical Engineering, MIT, December 1987.

[4] J. K. Runde, "Modeling and control of an automotive transmission," Master's thesis, Department of Mechanical Engineering, MIT, February 1986.

[5] Q. Zheng, "Modeling and control of powertrains with stepped automatic transmissions," Ph.D. dissertation, The Ohio State University, 1999.

[6] W. H. Wilkinson, "Four ways to calculate planetary gear trains," *Machine Design*, pp. pp.155–159, January 7 1960.

[7] H. L. Benford and M. B. Leising, "The lever analogy: A new tool in transmission analysis," *SAE Technical Paper Series*, no. 810102, 1981.

[8] J. H. Glover, "Planetary gear systems," *Product engineering*, pp. 59–68, January 1964.

[9] ——, "Planetary gear systems," *Product engineering*, pp. 72–79, September 1965.

[10] J. Wojnarowski, "The graph method of determining the loads in complex gear trains," *Mechanism and Machine Theory*, vol. 11, pp. 103–121, 1976.

[11] J. Wojnarowski and A. Lidwin, "The application of signal flow graphs - the kinematic analysis of planetary gear trains," *Mechanism and Machine Theory*, vol. 10, pp. 17–31, 1975.

[12] J. E. Shigley and J. J. Uicker, *Theory of machines and mechanisms.* New York: McGraw-Hill, 1980.

[13] D. Smith, "Analysis of epicyclic gear trains via the vector loop approach," in *Sixth Applied Mechanism Conference*, no. 10, 1979.

[14] D. Gibson and S. Kramer, "Symbolic notation and kinematic equations of motion of the twenty-two basic spur planetary gear trains," *ASME Journal of Mechanisms, Transmission, and Automation in Design*, vol. 106, pp. 333–340, 1984.

[15] R. J. Willis, "On the kinematics of the closed epicyclic differential gears," *ASME Journal of Mechanical Design*, vol. 104, pp. 712–723, October 1982.

[16] R. R. Allen, "Multiport models for the kinematic and dynamics analysis of gear power transmissions," *Journal of Mechanical Design*, vol. 101, pp. 258–267, April 1979.

[17] D. Hrovat and W. E. Tobler, "Bond graph modeling of automotive powertrains," *Journal of the Franklin Institute*, vol. 328, no. 5/6, pp. 623–662, May/June 1991.

[18] O. K. Kelley, "The design of planetary gear trains," in *SAE Annual Meeting*, vol. 67, Detroit, USA, January 14 1959, pp. 495–508.

[19] A. D. Deutschman, W. J. Michels, and C. E. Wilson, *Machine Design: Theory and Practice.* Macmillan Publishing Co., Inc., 1975.

[20] C. H. Pan and J. J. Moskwa, "Dynamic modeling and simulation of the ford aod automobile transmission," in *SAE TECHNICAL PAPER SERIES*, no. 950899. SAE, new Developments in Transmission and Driveline Design (SP-1087).

[21] C. H. Pan, "Powertrain modeling and engine torque estimation using nonlinear observers," Ph.D. dissertation, The University of Wisconsin-Madison, May 1995.

[22] F. Freudenstein and A. T. Yang, "Kinematics and static of coupled epicyclic spur-gear trains," *Mechanism and Machine Theory*, vol. 7, pp. 263–275, 1972.

[23] E. Pennestri and F. Freundenstein, "A systematic approach to power-flow and static-force analysis in epicyclic gear trains," *ASME Cams, Gears, Robot, and Mechanism Design*, vol. DE-Vol. 26, pp. 63–70, 1990.

[24] D. J. Sanger, "The determination of power flow in multiple-path transmission system," *Mechanism and Machine Theory*, vol. 7, pp. 103–109, 1972.

[25] L. W. Tsai, "An algorithm for the kinematic analysis of epicyclic gear trains," in *Ninth Applied Mechanisms Conference*, Kansas city, MO, USA, 1985.

[26] ——, *Modern Kinematics*. New York, USA: John Wiley and Sons, New York, 1993, ch. 6.

[27] A. Kahraman, H. Ligata, K. Kienzle, and D. M. Zini, "A kinematics and power flow analysis methodology for automatic transmission planetary gear trains," *ASME Journal of Mechanical Design*, vol. 126, pp. 1071–1081, November 2004.

[28] P. Samanuhut and A. Dogan, "Dynamics equations of planetary gear sets for shift quality by lagrange method," in *2008 ASME Dynamic Systems and Control Conference*, DSCD of ASME International. MI: ASME, 2008.

[29] J. Chen, D. Z. Chen, and L. W. Tsai, "A systematic methodology for the dynamic analysis of articulated gear-mechanisms," in *Proceedings of the Japan-U.S.A. Symposium on Flexible Automation*, vol. 1. Kyoto, Japan: ASME, July 9-13 1990, pp. 273–278.

[30] F. S. Jeffrey, "Generalized powertrain modeling using euler-lagrange equations," Ph.D. dissertation, The University of Wisconsin-Madison, December 1992.

[31] R. F. Morais and F. G. Dedini, "Dynamics of transmissions using epicyclic gear trains," *SAE Technical Paper*, no. 2001-01-3903, 2001.

[32] A. Kahraman, "Free torsional vibration characteristics of compound planetary gear sets," *Mechanism and Mechine Theory*, vol. 36, pp. 953–971, 2001.

[33] S. Watechagit, "Modeling and estimation for stepped automatic transmission with clutch–to–clutch shift technology," Ph.D. dissertation, The Ohio State University, 2004.

[34] B. K. Powell, "A simulation model of an internal combustion engine–dynamometer system," in *Proc. of Summer Computer Simulation Conference*, July 1978, pp. 464–473.

[35] ——, "A dynamic model for automotive engine control analysis," in *Proc. of IEEE Conf. on Decision and Control*, 1979, pp. 120–126.

[36] D. J. Dobner, "Dynamic engine models for control development – part i: Non–linear and linear model formulation," *International Journal of Vehical Design*, pp. 54–74, 1983.

[37] J. J. Moskwa and J. K. Hedrick, "Automotive engine modeling for real time control application," in *Proceeding of American Control Conference*, June 1987, pp. 341–346.

[38] J. J. Moskwa, "Automotive engine modeling for real time control," Ph.D. dissertation, The Department of Mechanical Engineering, MIT, 1988.

[39] J. D. Powell, "A review of ic engine models for control system design," in *Proc. of Int. Fed. of Auto. Control*, Munich, July 1987, pp. 235–240.

[40] L. Guzzella and C. H. Onder, *Introduction to Modeling and Control of Internal Combustion Engine Systems*. NY: Springer.

[41] P. Zeng and D. N. Assanis, "The development of a computer–based teaching tool for internal combustion engine courses," in *Proceeding of International Mechanical Engineering Congress, IMECE*. Anaheim, CA: ASME, Nov 13–19 2004, pp. 1–7.

[42] J. B. Heywood, *Internal Combustion Engine Fundamentals*. McGraw-Hill, 1988.

[43] A. K. Oppenheim, *Dynamics of Combustion Systems*, 2nd ed. NY: Springer, 2008.

[44] A. J. Kotwicki, "Dynamic models for torque converter equipped vehicles," *SAE Technical Paper*, no. 820393, 1982.

[45] SAE, *Design parctices: passenger car automatic transmission*, 3rd ed. PA: SAE, 1988, vol. 5.

[46] W. L. Husselbee, *Automatic Transmissions Fundamentals and Services*. NJ: Prentice Hall, 1986.

[47] B. Armstrong-Heloury, P. Dupont, and C. C. de Wit, "A survey of models, analysis tools and compensation methods for the control of machines with friction," *Automatica*, vol. 30, no. 7, pp. 1083–1138, September 1994.

[48] D. Karnopp, "Computer simulation of stick–slip friction in mechanical dynamic systems," *ASME Journal of Dynamic Systems, Measurement, and Control*, vol. 107, pp. 100–3, March 1985.

[49] D. A. Haessig and B. Friedland, "On the modeling and simulation of friction," *ASME Journal of Dynamic Systems, Measurement, and Control*, vol. 113, pp. 354–362, September 1991.

[50] J. Deur, J. Asgari, and D. Hrovat, "Modeling of an automative planetary gear set based on karnopp model for clutch friction," in *Proceeding of IMECE 2003 ASME International Mechanical Engineering Congress*, vol. 2. Washington, D.C.: ASME, November 2003, pp. 903–910.

[51] P. Dahl, "Solid friction damping of spacecraft oscillations," *AIAA Guidance and Control Conference*, 1975.

[52] P. R. Dahl, "Solid friction damping of mechanical vibrations," *AIAA Journal*, vol. 14, no. 12, pp. 1675–1682, 1976.

[53] C. C. de Wit, H. Olsson, K. J. Astrom, and P. Lischinsky, "A new model for control of system with friction," *IEEE Transactions on Automatic Control*, vol. 40, no. 3, pp. 419–425, March 1995.

[54] M. Gafvert, "Comparisons of two dynamic friction models," *Proceedings of the 1997 IEEE International Conference on Control Applications*, pp. 386–391, October 1997.

[55] C. W. Gear and O. Osterby, "Solving ordinary differential equations with discontinuities," *ACM Transactions on Mathematical Software*, vol. 10, no. 1, pp. 23–44, March 1984.

[56] F. E. Cellier and E. Kofman, *Continuous System Simulation*. NY: Springer, 2006.

[57] A. K. Tugcu, K. V. Hebbale, A. A. Alexandridis, and A. M. Karmel, "Modeling and simulation of the powertrain dynamics of vehicles equipped with automatic transmission," in *Proceedings of Symposium on Simulation of Ground Vehicles and Transportation Systems*, vol. 2. Anaheim: ASME, December 1986, pp. 39–61.

[58] A. M. Karmel, "Dynamic modeling and analysis of the hydraulic system of automotive transmissions," in *Proceeding of the American Control Conference*, June 1986, pp. 273–278.

[59] Y. Wang, M. Kraska, and W. Ortmann, "Dynamic modeling of a variable force solenoid and a clutch for hydraulic control in vehicle transmission system," in *Proceeding of the American Control Conference*, June 2001, pp. 1789–1793.

[60] Z. Sun and K. Hebbale, "Challenges and opportunities in automotive transmission control," in *Proceeding of the American Control Conference*, June 2005, pp. 3284–3289.

[61] L. F. Schawab, "Development of a shift quality metric for an automatic transmission," *SAE Technical Paper*, no. 941009, 1994.

[62] K. Horste, "Object measurement of automatic transmission shift feel using vibration dose value," *SAE Technical Paper*, no. 951373, 1995.

[63] F. J. Winchell and W. D. Route, *Design parctices: passenger car automatic transmission*. PA: SAE, 1988, vol. 5, ch. Ratio Changing the Passenger Car Automatic Transmission, pp. 79–105.

[64] M. Shinohara, T. Shibayama, K. Ohtsuka, and H. Yoshizumi, "Nissan electronically controlled four speed automatic transmission," in *SAE TECHNICAL PAPER SERIES 890530*, 1989.

[65] K. R. Butts, K. V. Hebbale, and K. W. Wang, "Acceleration–based control of power–on clutch–to–clutch upshift in an automatic transmission," 1992.

[66] K. R. Butts and K. V. Hebbale, "Acceleration–based control of power–on downshift in an automatic transmission," 1992.

[67] A. Yoon, P. Khargonekar, and K. Hebbale, "Design of computer experimentals for open-loop control and robustness analysis of clutch-to-clutch shifts in automatic transmission," in *Proceeding of the American Control Conference*. NM: AACC, June 1997, pp. 3359–3364.

[68] K. Hebbale and C.-K. Kao, "Adaptive control of shifts in automatic transmissions," in *Proceedings of the Symposium on Advanced Automotive Technologies*, vol. DSC-Vol.56. San Francisco, California: ASME International Mechanical Engineering Congress and Exposition, 1995, pp. 171–182.

[69] K. V. Hebbale and Y. A. Ghoneim, "A speed and acceleration estimation algorithm for powertrain control," in *Proceedings of the 1991 American Control Conference*, Boston, MA, 1991.

[70] H. Taniguchi and Y. Ando, "Analysis of a new automatic transmission control system for lexus ls400," in *Automotive Transmission Advancements*, no. 910639. 1991 International Congress and Exhibition, 1991.

[71] D. Hrovat and W. F. Power, *IEEE Control System Magazine*. IEEE, 1988, ch. Computer Control Systems for Automotive Power Trains, pp. 3–10.

[72] S. Bai, R. L. Moses, T. Schanz, and M. J. Gorman, "Development of a new clutch–to–clutch shift control technology," in *Transmission and Driveline Systems Symposium 2002*, no. 2002–01–1252. SAE 2002 World Congress and Exhibition, 2002.

[73] T. Minowa, T. Ochi, H. Kuroiwa, and K.-Z. Liu, "Smooth gear shift control technology for clutch–to–clutch shifting," in *Transmission and Driveline Systems Symposium 1999*, no. 1999–01–1054, International Congress and Exposition. SAE, 1999.

[74] Y. Yamamoto, M. Nishida, K. Suzuki, M. Saitou, H. Tsutsui, and S. Kozaki, "New five–speed automatic transmission for fwd vehicle," in *Transmission and Driveline Systems Symposium 2001*, no. 2002–01–0871. SAE 2001 World Congress, 2001.

[75] H. Tsutsui, T. Hisano, A. Suzuki, M. Hijikata, M. Taguchi, and K. Kojima, "Electro–hydraulic control system for aisin aw new 6–speed automatic transmission," in *Transmission and Driveline Systems Symposium 2004*, no. 2004–01–1638. SAE 2004 World Congress, 2004.

[76] J. Segers, *Analysis Techniques for Racecar Data Acquisition*. PA: SAE, 2008.

[77] J. Baumann, D. D. Torkzadeh, A. Ramstein, U. Kiencke, and T. Schlegl, "Model-based predictive anti-jerk control," *Control Engineering Practice*, vol. 14, pp. 259–266, 2006.

[78] D. G. Luenberger, "Introduction to observer," *IEEE Transaction on Automatic Control*, vol. AC-16, no. 6, pp. 596–602, December 1971.

[79] F. E. Thau, "Observing the state of non-linear dynamic system," *International Journal of Control*, vol. 17, no. 3, pp. 471–479, 1973.

[80] H.-S. Jeong and K.-I. Lee, "Friction coefficient, torque estimation, smooth shift control law for an automatic power transmission," *KSME International Journal*, vol. 14, no. 5, pp. 508–517, 2000.

[81] D. T. Greenwood, *Principles of Dynamics*. NJ: Prentice Hall, 1988.

[82] B.-H. Cho, G.-H. Jung, J.-W. Hur, and K.-I. Lee, "Modeling of proportional control solenoid valve for automatic transmission using system identification theory," *SAE Technical Paper*, no. 1999–01–1061, 1999.

[83] G. S. Lee, H. J. Sung, H. C. Kim, and H. W. Lee, "Flow force analysis of a variable force solenoid valve for automatic transmissions," *ASME Journal of Fluids Engineering*, vol. 132, pp. 031 103–1–031 103–7, March 2010.

[84] P. Cui, R. T. Burton, and P. R. Ukrainetz, "Development of a high speed on/off valve," *SAE Technical Paper*, no. 911815, 1991.

[85] A. J. Turner and K. Ramsay, "Review and developement of electromechanical actuators for improved transmission control and efficiency," *SAE Technical Paper*, no. 2004–01–1322, 2004.

[86] T. G. Duclos, "Design of devices using electrorheological fluids," *SAE Technical Paper*, no. 881134, 1988.

[87] Y. Sakai, "The ecvt electro continunously variable transmission," *SAE Technical Paper*, no. 880481, 1988.

[88] W. J. and M. G., "Magnetorheological fluid devices: Principles, characteristics and applications in mechanical engineering," *Proceeding of IMechE, Part L: Journal of Materials: Design and Applications*, vol. 215, pp. 165–174, 2001.

[89] R. L. Woods, "Woods static and dynamic friction model," 2009, personal Communication.

[90] J. Deur, J. Asgari, D. Hrovat, and P. Kovac, "Modeling and analysis of automatic transmission engagement dynamic-linear case," *ASME Journal of Dynamic Systems, Measurement, and Control*, vol. 128, pp. 263–277, June 2006.

[91] *Matlab and Simulink Release Notes for R2011 a.* MA: The Mathworks, inc, 2011.

[92] F. Haugen, *PID Control.* Trondheim: Tapir Academic Press, 2004.

[93] I. M. Sobol, *A Primer for the Monte Carlo Method.* Ann Arbor: CRC Press, Inc., 1994.

[94] A. Leon-Garcia, *Probability and Random Processes for Electrical Engineering.* NY: Addison-Wesley Publishing Company, Inc., 1993.

[95] J.-J. E. Slotine and W. Li, *Applied Nonlinear Control.* New Jersey: Prentice-Hall, 1991.

BIOGRAPHICAL STATEMENT

Patinya Samanuhut earned his Bachelor of Engineering in Mechanical Engineering from Kasetsart University, Bangkok, Thailand. Following this, he worked in HVAC, plumbing and fire protection system design and construction for a couple of years before coming to the University of Texas at Arlington. He received his Master of Engineering in Mechanical Engineering from UTA. He returned to Thailand to work as a lecturer and researcher at Kasetsart University Sakon Nakorn Campus. He received a scholarship from Royal Thai Government for his doctoral studies. He returned to UTA to pursue his Ph.D in Mechanical Engineering in Control System and Design. His research focuses on dynamics system modeling and control. The main objective of his research is to implement the system modeling and control theory to a vehicle transmission to improve its performance. He will return to teach and conduct researches at Ubon Ratchathani University in Thailand.